Karst Geology of Aguijan and Tinian, CNMI
Cave Inventory and Structural Analysis of Development

Kevin W. Stafford, John E. Mylroie & John W. Jenson

Department of Geosciences
Mississippi State University
Mississippi State, MS 39762

Water and Environmental Research Institute of the Western Pacific
University of Guam
Mangilao, Guam 96923

Technical Report No. 106

Water & Environmental Research Institute of the Western Pacific
University of Guam

September, 2004

WERI
WATER AND ENERGY RESEARCH INSTITUTE
OF THE WESTERN PACIFIC
UNIVERSITY OF GUAM

Karst Geology of Aguijan and Tinian, CNMI
Cave Inventory and
Structural Analysis of Development

Kevin W. Stafford, John E. Mylroie
& John W. Jenson

Department of Geosciences
Mississippi State University
Mississippi State, MS 39762

Water and Environmental Research Institute
of the Western Pacific
University of Guam
Mangilao, Guam 96923

Technical Report No. 106

Water & Environmental Research Institute
of the Western Pacific
University of Guam

September, 2004

THE WATER RESOURCES RESEARCH INSTITUTE PROGRAM OF THE US GEOLOGICAL SURVEY, AWARD NO. 01HQPA0010, SUPPORTED THE WORK REPORTED HERE. THE CONTENT OF THIS REPORT DOES NOT NECESSARILY REFLECT THE VIEWS AND POLICIES OF THE DEPPARTMENT OF THE INTERIOR, NOR DOES THE MENTION OF TRADE NAMES OR COMMERCIAL PRODUCTS CONSTITUTE THEIR ENDORSEMENT BY THE UNITED STATES GOVERNMENT.

ABSTRACT

Tinian and Aguijan, Commonwealth of the Northern Mariana Islands (CNMI), are volcanic, back arc islands in the western Pacific formed by Pacific Plate subduction under the Philippine Plate. The islands are composed of Eocene volcanic cores mantled by Plio-Pleistocene carbonate facies and raised Holocene beach and reef deposits. The entire sequence has been tectonically uplifted and contains high-angle normal faults, while isostatic subsidence and scarp failures overprint tectonic brittle failure features.

A cave and karst inventory on Tinian and Aguijan surveyed 114 features and is believed to adequately represent the megaporosity (cave) development. Two distinct cave classes were identified: mixing zone caves (flank margin caves and banana holes) and fissure caves. Most mixing zone caves were located in or near scarps and coastlines, often at similar elevations to nearby caves. Fissure caves were located in regions of brittle failure, forming linear features with narrow widths. Three previous sea-level positions were identified based on horizons of mixing zone caves. Seventeen freshwater discharge sites and four allogenic recharge sites were identified on Tinian.

Kolmogorov-Smirnov statistical analyses and rose diagram comparisons of orientation trends found significant similarities between megaporosity and geologic structure (brittle failure) on Tinian. Analyses of small regions showed distinct relations between brittle deformation and megaporosity, while at larger scales similarities became less obvious due to the complex geologic history and physiography of the island. Based on similarities in populations of orientation trends, fissure cave development is primarily controlled by brittle failure deformation with development along faults, fractures, and joints, while mixing zone cave development is primarily controlled by fresh-water lens position but significantly influenced by brittle failure deformation.

Tinian and Aguijan do not fit neatly into one classification of the Carbonate Island Karst Model. Regions of Tinian best fit the Simple, Carbonate-Cover and Composite Island Karst Models, but none easily fit the entire island. Aguijan must be classified as a Simple Carbonate Island because no geologic data has proved the presence of non-carbonate rocks interfering with the fresh-water lens, however it is probable that Aguijan does contain basement rocks that extend above sea-level as on other carbonate islands in the Marianas.

PREFACE

WERI (Water and Environmental Institute of the Western Pacific) Tech Report #96 was published as a preliminary assessment of the karst development and water resources of Tinian and Rota, CNMI (Commonwealth of the Northern Mariana Islands), based on a field reconnaissance conducted on the islands in June 2002. Since that time, work in the CNMI has focused on the Islands of Aguijan, Rota and Tinian with a primary emphasis on the cave and karst inventories of these islands, which can be used to evaluate the hydrolgeologic evolution of the islands.

The work presented in this study provides a detailed cave and karst inventory of the Islands of Aguijan and Tinian, CNMI with an analysis of structural controls on cave and karst development on the island of Tinian. The authors conducted this work as thesis research at Mississippi State University in conjunction with the University of Guam, while the US Geological Survey, through the National Institutes for Water Resources Research program, award no. 01HQGR0134, funded fieldwork. The data and findings in this report were originally published as a master's thesis by Kevin Stafford, titled: *Structural Controls on Megaporosity in Eogenetic Carbonate Rocks: Tinian, CNMI*. Ultimately, the work presented herein was made possible through the support of the Municipality of Tinian and Aguijan through: Tinian Mayors Office, CNMI Department of Land and Natural Resources, CNMI Department of Historical Preservation, Commonwealth Utilities Corporation, and Northern Marianas College.

Due to the large volume of data in this report, the appendices (Appendix A: Color Figures; Appendix B: Cave and Karst Inventory; Appendix C: Orientation Data; and Appendix D: Statistical Comparisons) are published as *.pdf* files in the attached CD or can be downloaded from the WERI website (www.uog.edu/weri). These appendices include color images of significant features, detailed maps of the inventoried karst features on Aguijan and Tinian, diagrams representing the structural geology of Tinian, and data matrices of statistical analyses.

Additional research continues in the Mariana Islands, in order to further answer questions about the karst geology and water resources of the islands. A similar study to the work reported herein is currently underway by the authors and master's thesis research by T. Montgomery Keel at Mississippi State University. Ultimately this study and future studies will be used to evaluate the fresh-water lens development on carbonate islands, which can be used to better manage the water resources of these communities.

CONTENTS

CONTENTS (cont.)

LIST OF TABLES

LIST OF FIGURES

LIST OF FIGURES (cont.)

LIST OF FIGURES (cont.)

LIST OF FIGURES (cont.)

LIST OF FIGURES (cont.)

KARST GEOLOGY OF AGUIJAN AND TINIAN, CNMI
Cave Inventory and Structural Analysis of Development

INTRODUCTION

This study has three primary objectives: 1) conduct a cave and karst inventory on Tinian and Aguijan, because no inventory existed, 2) investigate the cave and karst development on Tinian to determine if influences on mega-porosity development are associated with brittle deformation in eogenetic rocks, and 3) evaluate of the islands of Tinian and Aguijan in relation to the Carbonate Island Karst Model (Jenson et al., 2002; Mylroie and Jenson, 2002), in order to further advance the understanding of eogenetic karst development on carbonate islands.

The Tinian municipality of the Commonwealth of the Northern Mariana Islands (CNMI) governs Tinian and Aguijan. The Mariana Islands are a volcanic, back arc island chain in the western Pacific formed by Pacific Plate subduction under the Philippine Plate along the Mariana Trench. Aguijan covers 7.2 square kilometers and Tinian covers 102 square kilometers. A geologic study was conducted on Tinian in 1960 (Doan et al., 1960), which described the island as an Eocene volcanic core mantled by Plio-Pleistocene coralliferous and algal carbonate facies and raised Holocene beach and reef deposits. The entire sequence has been uplifted and contains high-angle normal faults produced from arc tectonism. Tinian has experienced greater than 100 meters of uplift since the Pleistocene, with an estimated 1.8 meters of uplift in the Holocene (Dickenson, 1999). Aguijan has only been studied briefly (Tayama, 1936) and no geologic map has been produced for the island; however, it is presumed to have a depositional and tectonic history similar to Tinian based on its proximity (~9 kilometers southwest of Tinian).

The Carbonate Island Karst Model predicts cave and karst development in eogenetic limestone (Jenson et al., 2002; Mylroie and Jenson, 2002; Mylroie and Jenson, 2001). It provides a fundamental and systematic framework for describing hydrogeologic karst evolution in young carbonate rocks, by incorporating the effects of mixing zone dissolution, glacio-eustacy, tectonism, and lithologic variations. In this model distinctive cave morphologies develop as eogenetic karst. These distinctive morphologies include flank margin caves, banana holes, pit caves, and stream caves. Traditionally, the affects of structural and lithologic controls on eogenetic karst development have been greatly overlooked because the original model was developed to describe features observed in the structurally and lithologically simple islands of the Bahamas (Mylroie and Carew, 1995a).

Structural control of karst development is common in continental settings, where the rock exhibits low porosity and is highly fractured (Klimchouk and Ford, 2000). Eogenetic karst is generally associated with caves formed by mixing zone dissolution, primarily independent of structural controls, in rocks that have never been buried beyond the range of meteoric diagenesis and retain high primary and syngenetic porosities. Recently, Jenson and coworkers (2002) recognized the importance of structural and lithologic controls on carbonate island karst and modified the Carbonate Island Karst Model to account for the effects of deformation and lithology on dissolution that occurs on carbonate islands that are or were tectonically active and/or have intricate interfingering of carbonate and non-carbonate rocks.

The cave and karst inventory of this study was conducted in two intensive field seasons based on information gathered during a reconnaissance survey in June 2002

(Stafford et al., 2002). During fieldwork, caves and karst features were documented, surveyed and classified by cave type. Sites of fresh-water discharge and allogenic recharge were located. Orientations of brittle failure structures were measured. After fieldwork was complete, maps were produced of the cave and karst features that were surveyed. Maps of features on Tinian were analyzed to determine cave orientation. The cave orientation data was compared to fault orientations, scarp orientations, and coastline orientations for similarity. Data comparisons were evaluated as independent data pairs both visually (rose diagrams) and statistically (Kolmogorov-Smirnov 2-sample test). Using similar techniques, Nelson (1988) and Barlow and Ogden (1992) have shown that continental, telogenetic karst development is related to the orientations of regional faults, fractures, and lineaments, implying that cave development is primarily controlled by brittle deformation.

Evaluation of the cave and karst features on Tinian and Aguijan allows them to be evaluated with the Carbonate Island Karst Model. However, the lack of previous geologic studies on Aguijan and the complex tectonic history of Tinian do not allow for simple classification of these islands.

LITERATURE REVIEW

GEOGRAPHICAL AND GEOLOGICAL SETTING

The Mariana Islands are located in the western Pacific Ocean and comprise a total of 17 islands (Figure 1). Guam is the largest and southern-most island in the Marianas and the only one that is not politically affiliated with the Commonwealth of the Northern Mariana Islands (CNMI). The relative position of the islands north of Guam in order of increasing distance is: Rota, Aguijan, Tinian, Saipan and Medinilla, which are carbonate islands. The remainder of the island chain is volcanic (Cloud et al., 1956). Tinian is located approximately 3000 kilometers east of Asia, approximately 180 kilometers north, northwest of Guam, and approximately 10 kilometers south of Saipan, while Aguijan is located approximately 9 kilometers southwest of Tinian. Tinian (Latitude: 15.01^{o}N, Longitude: 145.62^{o}E) has a surface area of 102 square kilometers with 51.2 kilometers of coastline and a maximum elevation of 187 meters (Figure 2). Aguijan (Latitude: 14.85^{o}N, Longitude: 145.57^{o}E) has a surface area of 7.2 square kilometers with 12.4 kilometers of coastline and a maximum elevation of 157 meters (Figure 3). Both islands have wet-dry tropical climates with a distinct rainy season (July-September) and dry season (February-March). Annual rainfall averages 200 centimeters and temperature ranges from 20 ^{o} to 32^{o} Celsius (Gingerich and Yeatts, 2000; Butler, 1992; Tracey et al., 1964; Doan et al., 1960; Cloud et al., 1956).

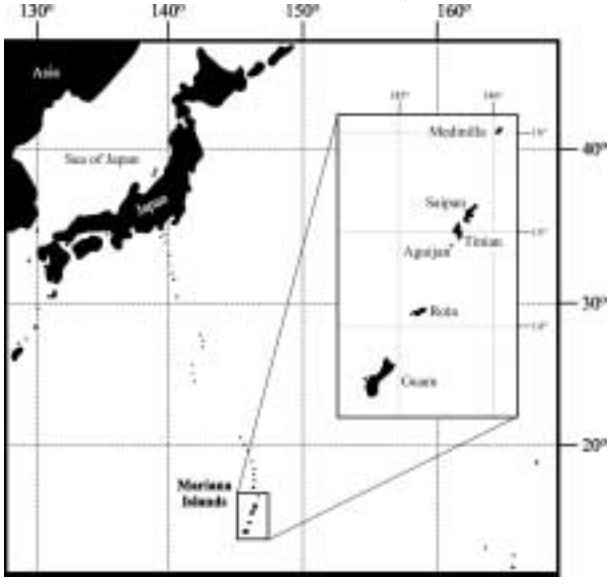

Figure 1: Location map of carbonate islands in the Marianas.

The Mariana Ridge, on which the islands of Tinian and Aguijan are located, is formed along a volcanic arc located approximately 160 kilometers west of the Mariana Trench, which is the world's deepest trench with a maximum depth of 11,035 meters (Gross, 1982). This subduction zone is created at the convergence of the Pacific Plate to the east and the Philippine Plate to the west. The Mariana Islands are situated on an older island arc that is separated by the Mariana Trough from the younger Mariana West Ridge, approximately 300 kilometers to the west, which is developing in the Mariana back-arc basin. This shift in ridge development was initiated by a change in Pacific Plate subduction geometry approximately 43 million years ago (mya) (Dickinson, 1999; Mink and Vacher, 1997; Reagan and Miejer, 1984).

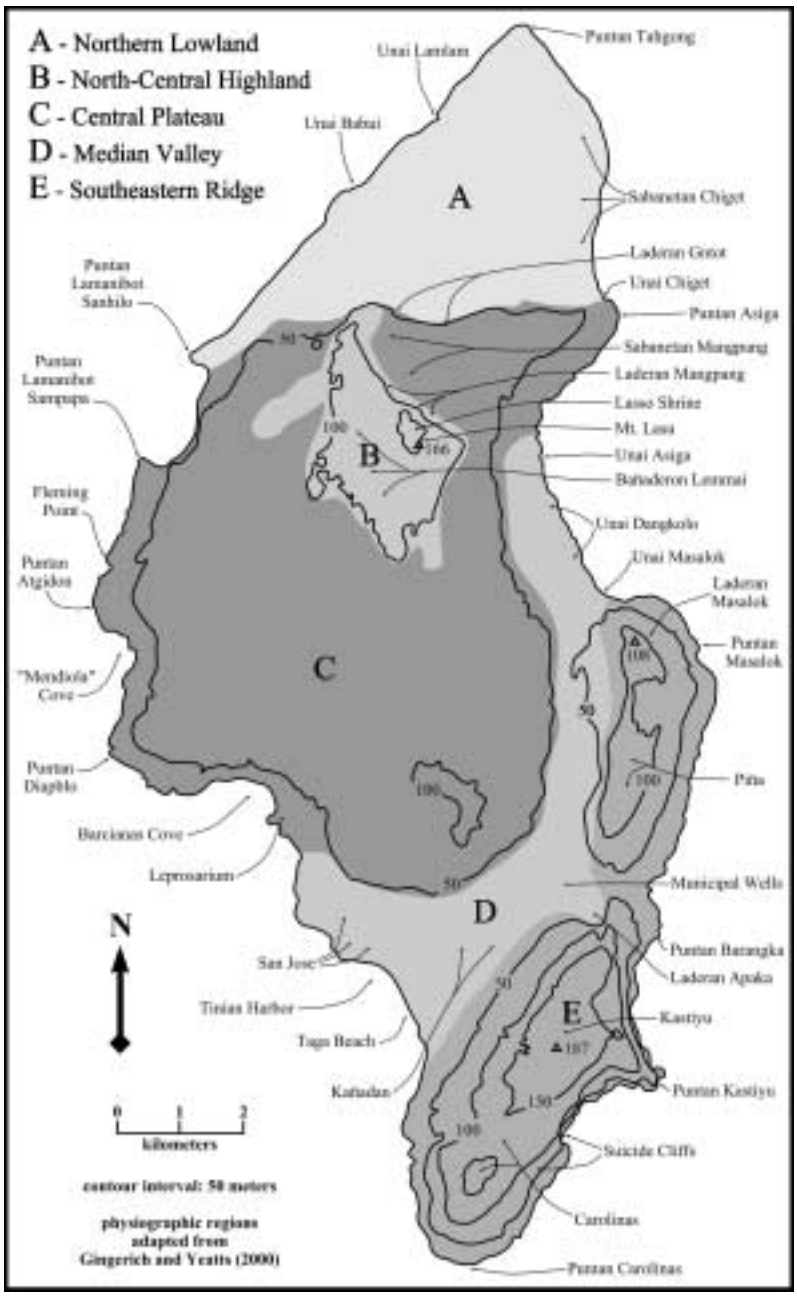

Figure 2: Physiographic map of Tinian, CNMI, with important features and locations identified (adapted from Doan et al., 1960).

Doan and coworkers (1960) used topography and spatial relationships to divide Tinian into five physiographic regions: Northern Lowland, North-Central Highland, Central Plateau, Median Valley and Southeastern Ridge (Figure 2). The Northern Lowland comprises the broad, flat, nearly horizontal surface that slopes gently upward from the west coast to Sabanettan Chiget. Located above the Central plateau and midway between the east and west coasts is the North-Central Highland, which contains the highest point (162 meters) in northern Tinian at Mount Lasu. The Central Plateau includes the central portion of the island and is isolated by steep slopes and bounding scarps associated with north-south faults. In the south and east-central regions, the Median Valley expresses little relief, but forms a broad depression bounded by faults. The Southeastern Ridge, which

includes Kastiyu, the highest point on Tinian (187 meters), is developed on two principal fault blocks (Doan et al., 1960).

Because little geologic work has been performed on Aguijan (Butler, 1992; Tayama, 1936), the following physiographic provinces are proposed based on the classification system used on Rota, which exhibits a similar terraced topography (Sugiwara, 1934): Upper Terrace, defined by elevations greater than 100 meters, which form a broad, relatively flat plateau and reaches a maximum elevation of 157 meters; Middle Terrace, defined by elevations between 50 and 100 meters, which is nearly absent on the northern side of the island and best developed on the southeastern side; and Lower Terrace, defined by elevations less than 50 meters, which includes the steep cliffs that form the coastline and the lowest bench. This classification is proposed here, in order to establish a distinction between karst development located in different regions on Aguijan (Figure 3).

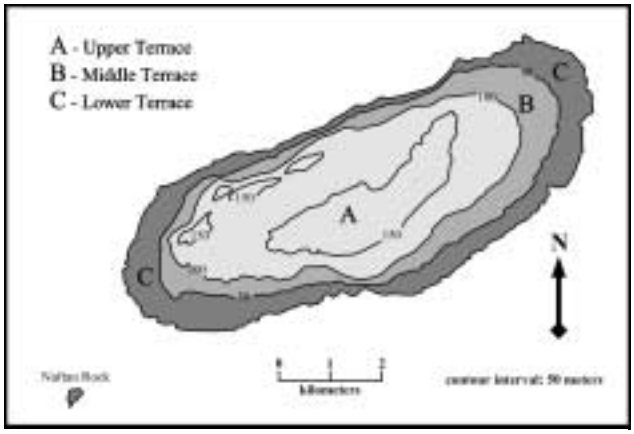

Figure 3: Physiographic map of Aguijan.

The geology of Tinian was described by Doan and coworkers (1960) and remains the most detailed geologic study for the island. Tinian is composed of volcanic tuffs and breccias covered with coralline and algal limestone (Figure 4). The igneous rocks (Tinian pyroclastic) comprise less than three square kilometers and retain only relict structures and textures because of extensive weathering. Based on the presence of foraminifera within the sediments, the

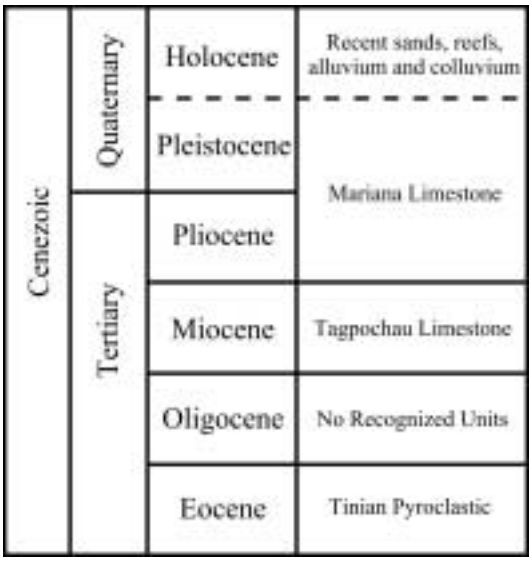

Figure 4: Geology section (adapted from Doan et al., 1960).

pyroclastics were probably ejected from a submerged vent. The limestone units are subdivided into two formations: Tagpochau Limestone and Mariana Limestone. The Tagpochau Limestone covers 16% of surface area of Tinian and is early Miocene in age. The formation is composed of three contemporaneously deposited facies: detrital (Tt), argillaceous (Tta), and sandy (Tts). The detrital facies comprises the majority of the formation and is composed primarily of fragments of biogenic calcium carbonate with calcite cement. The other two facies comprise only a small portion of the Tagpochau Limestone. The Mariana Limestone covers 83% of the surface area of Tinian and was deposited in Pliocene and Pleistocene time. The formation was subdivided based upon the presence of constructional or detrital compositions into seven facies: constructional coralliferous facies (Qtmcc), constructional algal facies (QTmca), detrital coralliferous facies (QTmc), detrital shelly facies (QTms), detrital *Halimeda* facies (QTmh), detrital argillaceous facies (QTmu), and detrital undifferentiated facies (QTmu). Overlying these deposits in coastal regions are Holocene limestones, developing sands and gravels, and reefs (Siegrest, 1988; Doan

et al., 1960; Burke, 1953). Recent fieldwork indicates that late Pleistocene limestones may also overlie the Mariana Limestone, because some limestone present in coastal areas appears to correspond with oxygen isotope stage 5e, suggesting that Mariana Limestone deposition does not extend to the Pleistocene/Holocene boundary (Stafford et al., 2002).

While no detailed study of the geology of Aguijan has been conducted, the same classification for rock units used on Tinian will be applied, based on its close proximity, until future work produces a more detailed geologic map of Aguijan. In addition, it is presumed that Aguijan is similar to other islands in the southern Marianas, in that a non-carbonate core of pyroclastic rocks exists beneath the exposed carbonate rocks that crop out, while the development of three distinct terrace levels on Aguijan suggests a similar tectonic history (Stafford et al., in press; Doan et al., 1960; Sugiwara, 1934).

HISTORICAL SETTING

The Mariana Islands were first settled by the Chamorro people around 1500 B.C.E. (before common error). In 1521, Ferdinand Magellan, discovered the Marianas and named them *Islas de los Ladrones* (Islands of the Thieves), which were then renamed *Islas de las Marianas* (Islands of the Marianas) in the early 1600's after Maria Ana of Austria, the widow of the Spain's king, Phillip the IV. The islands remained in Spanish control for almost four centuries, during which time much migration by indigenous people from the Caroline Islands occurred. In 1899, after Spain's loss of the Spanish-American war, the Spanish controlled islands of Micronesia (Mariana Islands, Caroline Islands and Palau) where sold to Germany. During German control, the northern Marianas greatly developed agricultural and fishing economies by immigrating additional Carolinian people from Chuuk and Yap, as well as Japanese people from nearby islands like Okinawa, who developed a lucrative agricultural trade market of copra and sugar cane. German control lasted until World War One (Hunt and Wheeler, 2000).

In 1914 Japan took control of the Mariana Islands at the start of World War One. After the war, Japan's control as administrator was recognized by the League of Nations and remained so until World War Two. During the Japanese occupation, vast tracts of land were cleared of coconut trees and tropical forest, so that the extensive sugar cane plantations could be developed covering 58% (Bormann, 1992) to 90% (McClure, 1977) of the land area. In 1944, United States military forces secured the islands in some of the bloodiest battles of World War Two. Tinian became instrumental in America's Pacific war campaign. The northern third of the island was developed into a large airbase named North Field, consisting of four major runways. During full operation, this was the largest and busiest airfield in the world with two B-29's taking off simultaneously every 45 seconds on mission days. From North Field, the two atomic bombs, Fat Man and Little Boy, were assembled and loaded into the B-29 bombers Enola Gay and Bock's Car for drops on Hiroshima and Nagasaki, respectively (McClure, 1977).

In 1947, the United Nations gave the United States trusteeship over the Mariana Islands, which continued until the 1970's. In 1970 discussion began between the Marianas and the United States over the termination of the trustee agreement, which led to a plebiscite in 1975, which negotiated a covenant with the Unites States. The *Covenant to Establish a Commonwealth of the Northern Marianas Islands in Political Union with the United States of America* negotiated an agreement where the citizens of the Northern Mariana Islands became self-governing as a Commonwealth, while Guam remained a United States territory. The covenant enabled the Commonwealth of the Northern Mariana Islands (CNMI) to retain the benefits of U.S. citizenship, excluding the right to vote in U.S. presidential elections, which ensured continued economic support. In exchange,

the U.S. was given lease of 75 square kilometers of land in the Northern Mariana Islands, including over two thirds of Tinian (Hunt and Wheeler, 2000).

Today, Tinian and Aguijan are governed by a single municipality as part of the Commonwealth of the Northern Mariana Islands (CNMI). Aguijan is uninhabited and Tinian hosts a population of approximately 2000 individuals. While the majority of the Tinian remains under U.S. military control, small farms and tourism, including scuba diving and casinos, provide commerce (Bormann, 1992).

CARBONATE ISLAND KARST

This study enables the studies in karst geology and hydrology performed on Guam (Mylroie et al., 2001) and in the Caribbean and Atlantic (Frank et al., 1998; Mylroie and Carew, 1995a; Mylroie et al., 1995a) to be applied and evaluated to different settings. A primary objective of investigation on Tinian is to advance the understanding of the karst hydrology of carbonate islands, while refining the general Carbonate Island Karst Model (CIKM). The Carbonate Island Karst Model has been designed as the definitive model for the hydrologic development of island karst. Modern carbonate islands are unique due to extensive interaction between fresh and saline groundwater within young, porous rock, which produces a unique geologic and hydrologic history that is different than that in continental settings (Vacher and Mylroie, 2002; Mylroie and Jenson, 2002; Mylroie et al., 2001; Mylroie and Vacher, 1999, and references therein).

Karst forming in marine conditions on carbonate coasts and islands can be explained by the Carbonate Island Karst Model (Figure 5) (Stafford et al., 2003; Jenson et al., 2002; Mylroie and Jenson, 2002; Mylroie and Jenson, 2001). Its main aspects are:

1. The fresh water/salt water boundary creates mixing dissolution, and produces organic-trapping horizons at both the upper and lower boundaries of the fresh-water lens.
2. Glacio-eustacy has moved the fresh-water lens up and down through a vertical range of over 100 m in the Quaternary.
3. Local tectonics can overprint the glacio-eustatic sea level events, adding complexity to the record.
4. Carbonate islands can be divided into four categories based on basement/sea level relationships:
   i. Simple carbonate islands (no non-carbonate rocks).
   ii. Carbonate cover islands (non-carbonate rocks beneath a carbonate veneer).
   iii. Composite islands (carbonate and non-carbonate rocks exposed on the surface).
   iv. Complex islands (faulting and facies interfingering create complex carbonate/non-carbonate relationships).
5. The karst is eogenetic, *i.e.*, it has developed in carbonate rocks that are young and have never been buried below the range of meteoric diagenesis.

Carbonate islands described by the Carbonate Island Karst Model are composed of young limestones and are heavily influenced by meteoric waters and mixing-zone dissolution, creating an environment for eogenetic karst to develop because of their close proximity to the site of deposition. Vacher and Mylroie (2002, p. 183) define eogenetic karst as "the land surface evolving on, and the pore system developing in, rocks undergoing eogenetic, meteoric diagenesis." Eogenetic carbonate rocks are diagenetically young and have not undergone extensive cementation and compaction, as opposed to telogenetic carbonate rocks that are diagenetically mature, have been buried below the range of meteoric diagenesis, and are currently

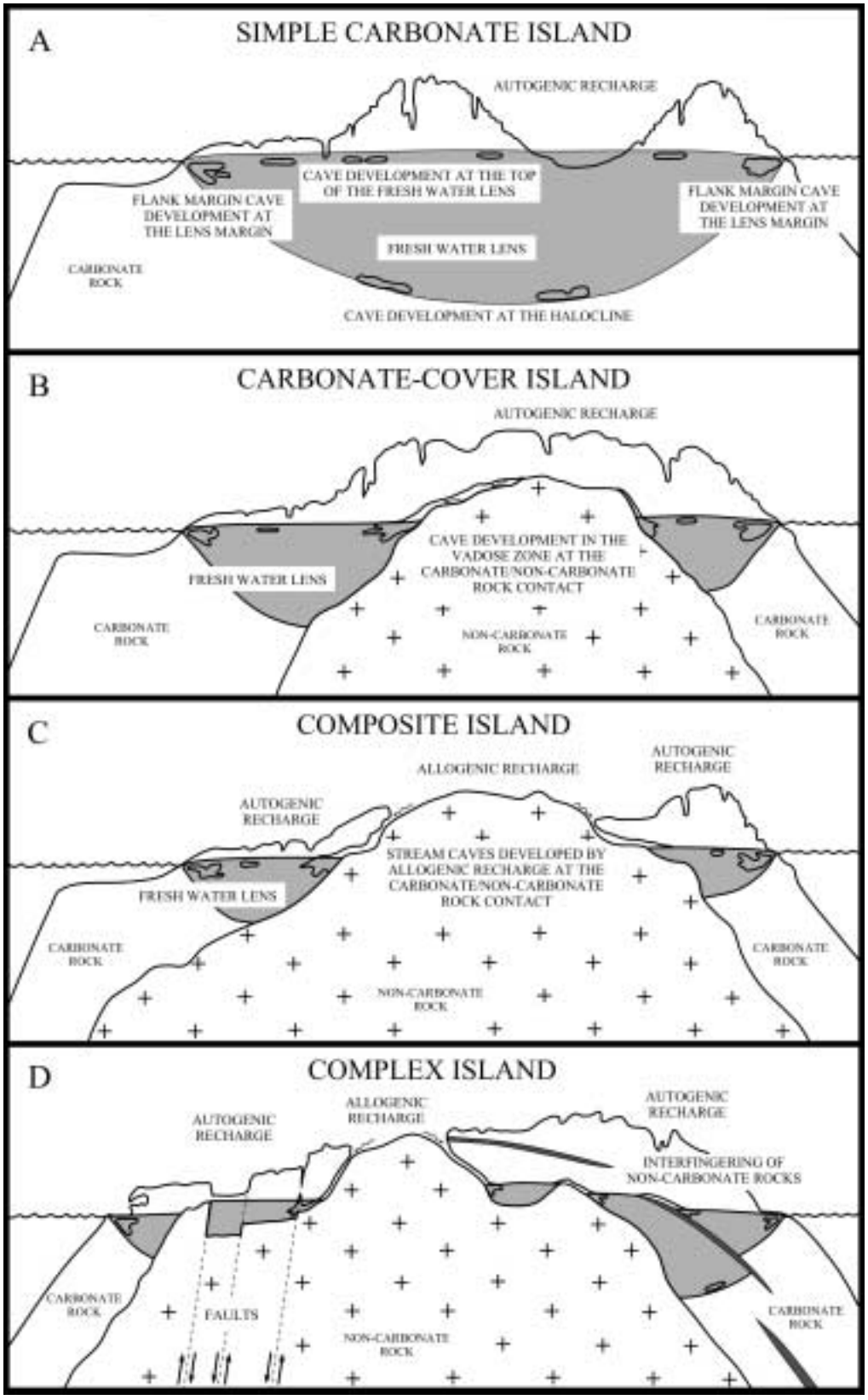

Figure 5: Carbonate Island Karst Model (CIKM) (adapted from Mylroie et al., 2001).

exposed at the earth surface by tectonic uplift and erosion of overlying strata (Klimchouk and Ford, 2000). Typically, small carbonate islands are the sites of eogenetic karst undergoing meteoric diagenesis, however, it is not possible to state that carbonate islands develop solely eogenetic karst and continental settings develop solely telogenetic karst, because fresh-water / sea-water interaction and a fresh-water lens affected by glacio-eustacy are also required for the formation of carbonate island karst, as defined by the Carbonate Island Karst Model (Jenson et al., 2002; Mylroie and Jenson, 2002).

Eogenetic karst development occurs on islands such as Bermuda, the Bahamas, and the Marianas, as well as in continental settings such as the Biscayne aquifer of Florida, where the carbonate rocks are young. Telogenetic karst development occurs on islands such as Gotland (Sweden) and Kephallenia (Greece), as well as in continental settings such as Kentucky (United States) and England (Great Britain), where the rocks are of appreciable age and have been buried beyond the range of meteoric diagenesis (Vacher and Mylroie, 2002). Because eogenetic karst and island karst are not necessarily synonymous, a distinction should be made between *island karst* and *karst on islands*. *Island karst* occurs in specific environments that must include three basic parameters: 1) interaction of fresh-water and sea-water, which produces mixing zone dissolution, 2) a fresh-water lens that was affected by glacioeustatic changes in the Quaternary, and 3) karst that is eogenetic. *Karst on islands* may exhibit some of the characteristics of *island karst*, but these islands are not true *island karst* unless all three basic parameters are present. Islands like Jamaica and Puerto Rico have karst landforms (e.g. cockpits and mogotes) in their interior that are developed in rocks of appreciable age and that are not influenced by glacio-eustacy or fresh-water / salt-water interaction. This makes the karst landforms *karst on islands*. True *island karst* occurs on islands like the Bahamas, where the rock is diagenetically young, fresh-water interacts extensively with the salt-water, and the fresh-water lens has been significantly affected by glacio-eustacy. Therefore, islands that have telogenetic karst, are removed from the affects of glacio-eustacy, and/or do not exhibit mixing zone dissolution should have karst landforms and features reported as *karst on islands*, while islands that exhibit eogenetic karst, are affected by glacio-eustacy, and exhibit mixing zone dissolution should have karst landforms and features reported as *island karst* (Vacher and Mylroie, 2002).

In eogenetic rocks that have not undergone compaction and cementation, the rocks tend to initially exhibit high matrix porosity and moderate permeability, but can develop secondary vuggy porosity as a result of meteoric and fresh-water diagenesis. The matrix porosity will generally decrease with age as secondary cementation infills the pore space, while permeability increases as preferential flow develops extensive horizontal flow routes. Over time, the bulk porosity remains the same or decreases, but the vertical hydraulic conductivity of the rock decreases while the horizontal hydraulic conductivity increases (Vacher and Mylroie, 2002). Due to the proximity of eogenetic karst to marine waters in island settings, it is highly susceptible to changes in sea level, which results in the migration of the fresh-water lens and flow routes in response to glacioeustatic and tectonic changes.

The four conceptual model classifications of carbonate islands are based on island composition (Figure 5). *Simple carbonate islands* are composed of only carbonate rocks at the surface and to a depth below the base of the fresh-water lens (Figure 5A). The Bahama Islands are a good example. *Carbonate cover islands* are composed of only carbonate rocks at the surface, but have non-carbonate rocks that interact with the fresh-water lens without being exposed at the surface (Figure 5B). Bermuda is a good example. Carbonate

cover and simple carbonate islands can easily shift from one form to the other as a result of changes in relative sea level (Figure 6). *Composite islands* are composed of both non-carbonate and carbonate rocks on the surface (Figure 5C). Barbados is a good example. These three island types represent a classification scheme where the two end member environments are islands completely composed of carbonate rocks at one end and islands completely devoid of carbonate rocks at the other end, with intermediate compositions described by the model (Figure 6). The fourth type are *complex islands*, which are characterized as having complex geologies as a result of faulting, the interfingering of different lithologies, and the presence of both carbonate and non-carbonate rocks (Figure 5D). Guam and Saipan are excellent examples (Jenson et al., 2002; Mylroie et al., 2001).

In traditional continental settings, structural and lithologic controls have been recognized as having a significant influence on karst development. Klimchouk and Ford (2000, p. 57) state: "Bedding planes, joints, and faults are planar breaks that serve as the principal structural guides for groundwater flow in almost all karstified rocks." In island karst settings the significance of structural and lithologic controls have often been overlooked because of the dominant role of mixing-zone dissolution in the hydrogeologic system and because the original models for island karst were developed on simple carbonate islands in the Bahamas. Jenson and coworkers (2002) and Mylroie and coworkers (2001) have recently recognized the importance of structural and lithologic controls on carbonate island karst by modifying the CIKM with the addition of the fourth type, the complex island. This addition enables the effects of deformation

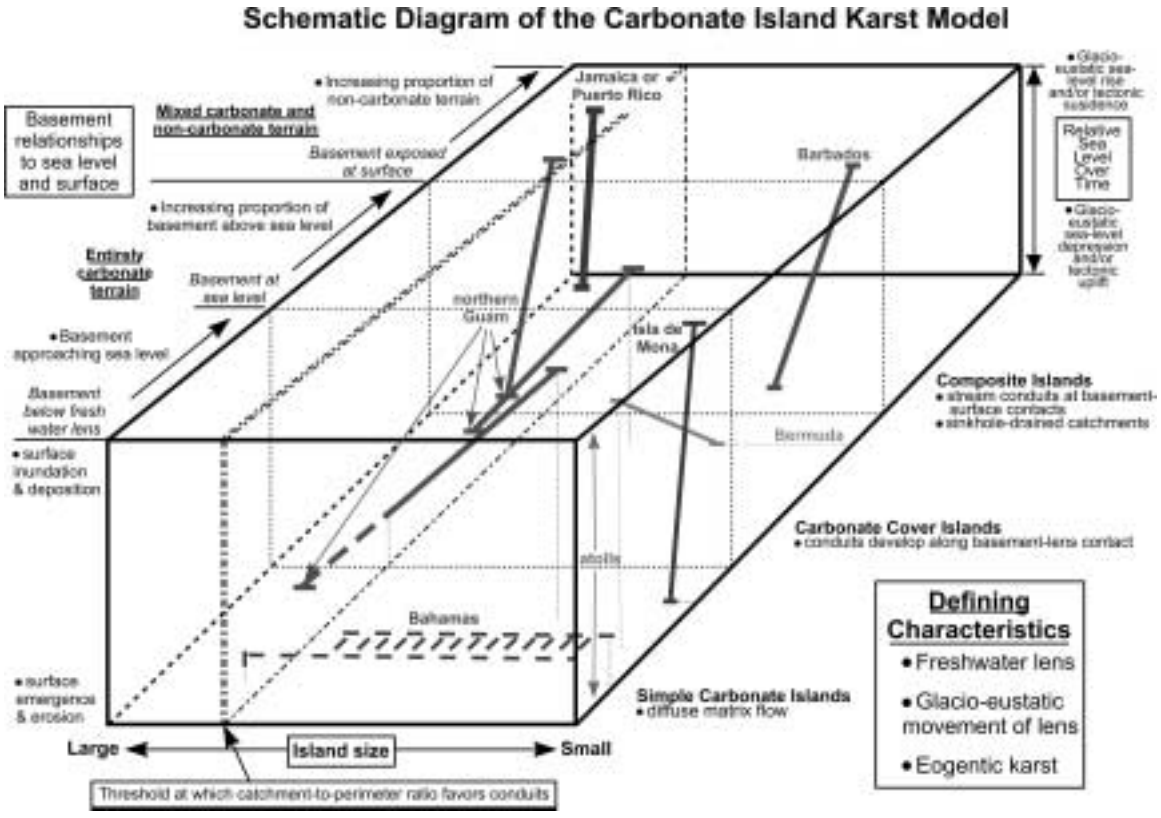

Figure 6: Schematic diagram illustrating the relationship between island size, basement relationships to sea level and surface, and relative sea level for simple, carbonate-cover, and composite islands within the Carbonate Island Karst Model (CIKM) (Mylroie and Jenson, 2001, Fig.2, p. 54).

and lithology to be accounted for on carbonate islands that are or were tectonically active and/or have intricate interfingering of carbonate and non-carbonate rocks.

Lithologic controls include variations in rock composition between rock formations and within the same rock formation, where beds subdivide the unit. Variations may include grain size, grain origin, grain sorting, and chemical composition. These variations provide routes for preferential dissolution within beds and formations of favorable composition, while less favorable beds and formations may restrict dissolution and fluid movement (Klimchouk and Ford, 2000; Sasowsky and White, 1994; Palmer, 1991; White, 1988).

Structural controls include both brittle and ductile deformation. Ductile deformation results in the folding of rock bodies, which adds to the complexity of lithologic controls. Brittle deformation includes joints, fractures, and faults, which are often found in tectonically active, carbonate islands where uplift and subsidence create complex geology. Fractures are surfaces where the rock has been broken, occur over a range of centimeters to meters and fall into several categories, including: extension – relative rock motion is perpendicular to the surface; shear – relative motion is parallel to the surface; and oblique – relative motion is a both parallel and perpendicular to the surface. Joints are specific types of fractures, which show only minor extension (Twiss and Moores, 1992). Fractures reported on Tinian and Aguijan are primarily associated with gravity slides resulting from bank margin or cliff margin failure along steep scarps. Joints reported occur inland of the bank margin/cliff margin fractures, possibly as a result of rock expansion from a decrease in lateral pressure from the scarp failure or as unloading structures associated with isostatic subsidence, and perpendicular to coastlines, which may be associated with coastal erosion or regional faulting (Stafford et al., 2002). Faults are surfaces or narrow zones that show relative displacement similar to fractures, but over larger regions and generally associated with regional tectonics (Twiss and Moores, 1992). Faulting is reported throughout Tinian, including the boundaries between the Southeastern Ridge and the Median Valley and between the Central Plateau and the Northern Lowland, where fault blocks moved independently during island emergence (Doan et al., 1960).

Joints, fractures, and faults generally enhance fluid movement, but may also restrict it. Enhanced flow can occur along planar features that provide a surface for fluid movement both laterally and vertically across lithologic boundaries, creating greater connectivity within the subsurface. Restricted flow can result if recrystallization (slickensides) or secondary infilling (caliche dikes) develop along the planar surface, creating a barrier for fluid movement. Flow restriction may also occur if faulting results in the offsetting of different rock units, which produces contacts between carbonate and non-carbonate rocks that did not previously exist (Klimchouk and Ford, 2000; Sasowsky and White, 1994; Palmer, 1991; White, 1988).

KARST FEATURES

Karst features on Tinian can be classified into four broad categories; epikarst, closed depressions, caves, and discharge features. Identification, classification, and spatial distribution of different karst morphologies provide a basis for understanding the hydrology of the region.

Epikarst

Epikarst is the zone of dissolutional sculpturing (karren) that is present on the surface and upper few meters of bedrock in carbonate regions. Karren has been described as minor solutional forms, which range from millimeters to meters in scale (White, 1988). In general, epikarst is independent of environmental setting; however, in coastal regions, where salt spray

is in active contact with carbonate rocks, an environment is created for the production of biokarst (Viles, 1988) or phytokarst (Folk et al., 1973); however, the biological affects are often overstated (Mylroie and Carew, 1995b). The surface of the karren in eogenetic karst is generally extremely rough and may not support extensive soil profiles because soil-forming material is in short supply. Taborosi and coworkers (in press) have recently reported additional karren morphologies on eogenetic karst on Guam. In the Mariana Limestone on Guam most weathered surfaces are extremely jagged and reminiscent of biokarst or phytokarst and is attributed to a polygenetic origin that includes mixing dissolution from rainwater mixed with salt spray, salt weathering, dissolution by meteoric waters, and biological weathering (Taborosi et al., in press). However, other karren morphologies are also present, which include more rounded karren in inland regions and dissolution along brittle failure planes producing enlarged vertical and horizontal joints as wells as solution pans (kaminetzas) (Taborosi et al., in press). Carbonate rocks on most islands generally have little insoluble material to produce soils, suggesting that the insoluble material is exclusively of eolian origin. The soils that are present are generally piped downward into voids and dissolutional cavities within the karst system. Eogenetic karst regions have specific vegetation types because of the limited development of soils, which affects infiltration rates of water entering the karst system based on soil thickness, composition and its presence, absence or modification (human development). Beneath karren, dissolutional bedrock debris, and soil, which comprise the surficial epikarst, the remainder of the epikarst zone is composed of solutional fissures, holes, and shallow small cavities in the bedrock (Mylroie et al., 2001). Epikarst contributes water to the deep vadose zone as diffuse flow and through the integration of flow paths created by cavities and fissures in the lower epikarst. This integrated flow can effectively bypass the deep vadose zone via fractures and pits and supply water directly to the phreatic zone (Mylroie et al., 1999). Epikarst development and extent is a primary controlling factor on the quantity of water that enters phreatic storage via vadose paths and it is possible that it may serve as a location of significant water storage (Jocson et al., 2002; Jocson et al., 1999; and Jenson et al., 1997). Epikarst on Tinian appears identical to that seen on Guam and Saipan (Taborosi, 2000).

Individuals involved in the development of land in karst regions dominated by epikarst should be aware that any modifications to the land surface and epikarst would alter the drainage dynamics of the area. Ponding basins may actually exhibit lower infiltration rates because of high sediment loads. Runoff events and soil erosion may also increase as a result of the modification of the natural landscape (Mylroie and Carew, 1997).

Closed Depressions

In carbonate island environments, closed depressions can be classified into three general categories: dissolution, natural construction, and human modification. These different types can be extremely hard to differentiate based on appearance and it is possible that the features may have been any or all of the three classification types at some point in their development. In carbonate islands, dissolutional depressions are generally small to moderate in size as a result of their young age and the nature of autogenic recharge. However, in areas where non-carbonate rocks are exposed at the surface, streams can develop that provide allogenic recharge to the karst system, possibly forming large depressions as are seen on Guam (Mylroie et al., 2001; Taborosi, 2000). Natural construction depressions are those that formed at the time the rocks were deposited or are the result of subsequent deformational processes. Mylroie and coworkers (2001) report that natural construction depressions are the most common form on simple carbonate

islands, and anthropogenic depressions (e.g. quarries, landfills, artificial drainage ponds, and storage ponds) are often constructed in these pre-existing features (Mylroie et al., 1999).

Tinian exhibits areas where dissolution-type closed depressions are formed. Dissolution depressions have been seen at the contacts between exposed volcanic outcrops and carbonate outcrops (Stafford et al., 2002). On Tinian, four exposures of volcanic rocks are recorded near Sabanettan Mangpang, Bañaderon Lemmai, and Laderan Apaka. At the three northern locations (two at Sabanettan Mangpang and one at Bañaderon Lemmai), there are closed depressions in the limestone outcrops, which show allogenic streams descending into them from the volcanic outcrops. An initial field investigation of Bañaderon Lemmai has shown that these features are similar to those seen on Guam and are providing point source recharge into the karst system (Stafford et al., 2002). In the south-central region near Laderan Apaka, volcanic outcrops are exposed on a north-facing cliff. To the north of the outcrops, a large closed depression (Sisonyan Makpo) exists in which the Municipal Wells are located (United States Department of the Interior Geological Survey, 1983), which may be a natural construction feature formed by complex faulting on the island, based on its location between the two prominent ridges (Kastiyu/Carolinas and Piña) of the Southeastern Ridge and the low-lying Median Valley. Weathering of volcanic rocks and talus accumulation may be partially armoring the slopes of the cliff and the closed depression, increasing recharge to the closed depression and possibly leading to lateral corrosion of the closed depression.

Throughout Tinian, human-modified depressions are also commonly reported (United States Department of the Interior Geological Survey, 1983) and may represent modified constructional depressions similar to those reported on other carbonate islands (Mylroie et al., 1999). These include modern and ancient quarries (latte stone), borrow pits, refuse disposal sites, artificial drainage ponds in residential areas, and features associated with World War Two (bomb pits, defensive positions, etc.). Initial field investigations have revealed that significant natural depressions are found in association with volcanic outcrop exposures. The large closed depressions seen elsewhere are probably natural construction features or features produced by human modification, possibly to pre-existing natural depressions, of the land surface (Stafford et al., 2002).

Caves

Caves are natural openings in the earth that can be characterized based on their size, shape, length and overall geometry (White, 1988). Solution caves, which have been formed by the dissolution of bedrock by circulating groundwater, are present throughout the islands of Tinian and Aguijan. Solution caves on carbonate islands can be grouped into various categories. In the Mariana Islands, five distinct cave types have been documented: banana hole, flank margin cave, fissure cave, pit cave, and stream cave (Figure 7). In some areas, it is difficult to discern the exact origin and original extent of some caves, because of the extensive modification of some features for Japanese military purposes during World War Two (Taborosi and Jenson, 2002). In addition to human modification, horizontal notches cut into cliff faces create an additional classification problem. Traditionally these have been identified as bioerosion notches, but may also form by lateral corrosion and cliff retreat, or they may be the remnants of flank margin caves (Mylroie et al., 1999). Accurate classification of karst features is integral to interpreting the hydrogeology of island karst.

Banana holes (Figure 7) are shallow, small chambers that formed at the top of the fresh-water lens. They are isolated features and exhibit a morphology with a width to depth ratio greater than one (Harris et al., 1995). On Tinian no feature has been currently identified as a definite banana

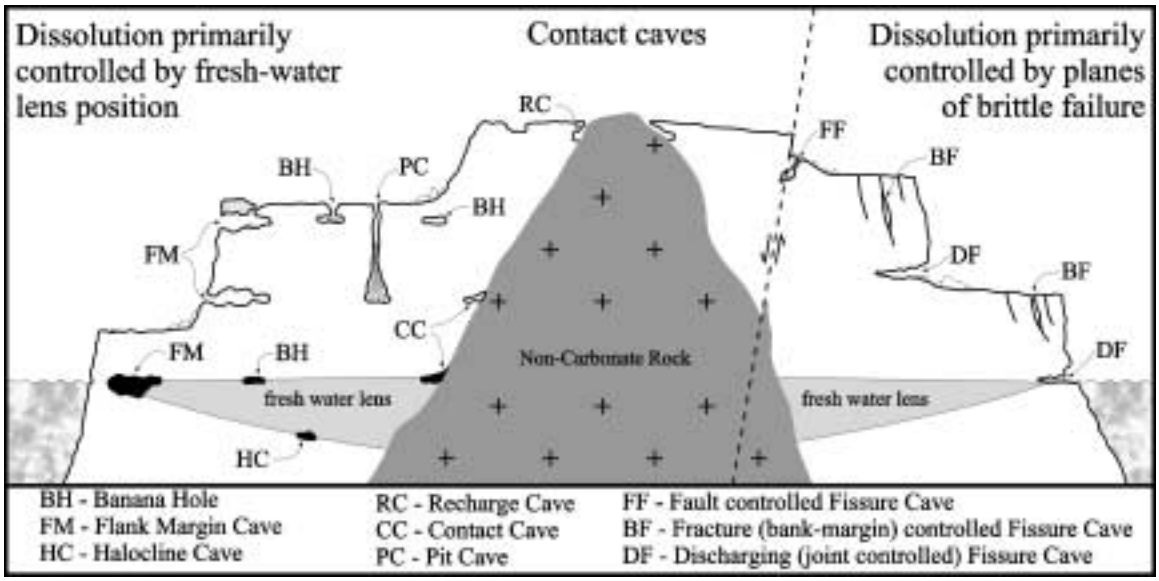

Figure 7: Conceptual model of cave types that form in eogenetic rocks on carbonate islands.

hole. A feature located several hundred meters to the northwest of the Lasso Shrine appears to have a complex history that could be explained as the stacking of two or more banana hole features vertically on one another as sea level fluctuated. Later collapse by upward stoping could then form the collapsed areas seen in the lower levels of this feature (Stafford et al., 2002).

Flank margin caves (Figure 7) are formed in the distal margin of the freshwater lens where thinning of the lens and mixing of fresh and saline waters creates dissolutionally aggressive phreatic waters (Mylroie et al., 1995a) and are the most common morphology type that has been reported on Tinian (Stafford et al., 2003, 2002). Flank margin caves exhibit globular morphologies with a wide range of sizes that may be connected, but often remain as isolated chambers. Flank margin caves can be used as indicators of previous sea-level stillstands and have potential as tools for evaluating differential rates of uplift in tectonically active carbonate islands (Carew and Mylroie, 1995; Mylroie et al., 1995a,b). Flank margin caves may collapse in coastal regions to form coves and caletas, which retain only remnants of the original cave morphology (Back et al., 1984). Further complicating the morphology and identification of flank margin caves are bioerosion notches formed by wave erosion and invertebrate borings at sea level during stillstands (Mylroie and Carew, 1991).

Flank margin caves have been reported at various locations. The most significant flank margin cave development is in the Suicide Cliffs on the southern end of Tinian, were numerous entrances can be seen inland from the road on the southern coastal terrace. These caves are located approximately 50 meters upslope from the lower terrace and are developed along a consistent horizon that is believed to reflect a past sea-level stillstand. Along the northern edge of the Southeastern Ridge, near Laderan Apaka, a series of flank margin caves are located, which are less extensive due to more complete erosion and slope retreat. Near Lasso Shrine on northern Tinian, a series of modified flank margin caves are located in the eastern cliffs. Along the east coast, flank margin caves that are at various stages of erosion due to cliff retreat and coastal erosion are present near Unai Masalok and Unai Dangkolo. At Unai Dangkolo, the largest flank margin cave documented on Tinian is located approximately 200 meters inland. This cave

is breached on the surface by ceiling collapse and can only be entered from above via a 10-meter descent. The cave consists of several large chambers that intersect, creating a complex system that is laterally extensive covering and area greater than 1300 square meters with cave passages developed around a central chamber approximately 15 meters tall and 35 meters in diameter (Stafford et al., 2002).

Fissure caves (Figure 7) are developed along joints, fractures, or faults, in which preferential flow along the planar surface has resulted in enhanced dissolution rates (White, 1988). Three basic types of fissure caves have been identified, based on their morphology and spatial relationship to the island. At the coastal edge, development perpendicular to the coastline has been reported, which in several cases has resulted in caves that often discharge freshwater and penetrate inland up to 30 meters as tubular passages with distinct joints located in their ceilings. The second type has formed as fractures parallel to the coastline or scarps as a result of cliff-margin or bank-margin failure. These fractures may reach the water table where they can affect the flow dynamics of the lens by locally distorting the lens or by providing vadose routes that intercept the normal diffuse flow in the phreatic zone (Mylroie et al., 1995c; Aby, 1994). Dissolutionally enhanced fractures have produced caves over 40 meters deep on Tinian. The third type occur where dissolution along a fault plane, in conjunction with collapse, has formed caves, which tend to develop at moderate to steep angles along the dip of the fault, and the caves extend laterally along the strike of the fault. All three types of fissure caves are hydrologically important because they provide vadose fast flow routes for water through the subsurface, either as recharge or discharge features and may distort the local lens morphology and flow dynamics (Stafford et al., in press; Stafford et al., 2002).

Pit caves (Figure 7) are vertical shafts that have developed by the dissolution of descending meteoric waters and have a depth to width ratio greater than one. Pit caves often develop as a series of shafts with connecting lateral sections, act as vadose fast-flow routes for water entering the subsurface, and effectively drain the epikarst (Mylroie and Carew, 1995a). Although common in certain settings (Harris et al., 1995; Mylroie and Carew, 1995a), only one pit cave has been reported on Tinian. It is located 10 meters from the cliff edge on the south coast, where it connects to a low-level bench just above sea level. It is approximately 25 meters deep with an entrance width of 3 meters, but due to its location and near-direct connection to the ocean, it has little effect on aquifer recharge. However, its presence indicates the possibility of other similar features in the area, which may be covered at the surface by collapse and at shallow depths could be open, acting as vadose fast flow routes (Stafford et al., 2002).

Stream caves (recharge caves, Figure 7), hydrologically active caves that are fed by allogenic water, have been documented in regions were contacts between carbonate and non-carbonate rocks occur. Meteoric water is unable to infiltrate efficiently into the volcanic rocks, and forms surface streams, which channel water to the outcrop periphery where it descends into the carbonate rocks as point source allogenic recharge (Mylroie et al., 2001).

Tinian volcanic rocks outcrop in four regions and closed depressions are associated with the periphery of each of these outcrops. Due to time and logistics, only one of these features, located to the east of the largest outcrop at Bañaderon Lemmai, was investigated in June 2002 (Stafford et al., 2002). This site contains a large sinkhole that appears to be armored with volcanic sediments that restrict infiltration, but on the eastern edge, a small cave is present that shows evidence of allogenic recharge during rain events (Stafford et al., 2002). It is expected that other closed depressions associated with these volcanic outcrops will exhibit similar features formed

by dissolution at the non-carbonate/carbonate contact, with variations dependant on sediment infilling and the volume of allogenic recharge that is received.

Discharge Features

Discharge volume and types vary greatly on carbonate islands and spatially within the same island. Three general categories of discharge features can be defined: seeps, springs, and submarine freshwater vents. Of these types, seeps represent diffuse discharge, while the other types represent focused discharge points. Seeps occur extensively in coastal areas where calcareous sand covers the bedrock and disperses emerging water over a large area. Springs are locations in which water emerges from the bedrock along preferential flow paths generally defined by bedding planes or fractures along coastlines. Springs may be laterally extensive if controlled by bedding planes or they may be restricted to a single point discharge if controlled by fractures. Submarine freshwater vents are areas where freshwater discharge occurs below tidal level along the island periphery (Jocson et al., 2002; Mylroie et al., 1999).

Seeps and springs have been documented in coastal regions on Tinian. Minor seeps are present at Unai Dangkolo and Unai Masalok on Tinian, while springs have been documented in various coastal areas. On Tinian, fracture caves were reported along the west coast near Unai Masalok where freshwater could be observed mixing with salt water and discharging from solutionally widened bedding planes that extend approximately 30 meters inland (Stafford et al, 2002). Submarine freshwater vents are not reported for Tinian and Aguijan, but features are expected to exist that are similar to those that have been reported from Guam (Mylroie et al., 2001; Jenson et al., 1997), where freshwater discharges below sea level.

WATER RESOURCES

Fresh-water is partitioned in a lens above salt-water and is affected by the presence of non-carbonate rocks interacting with the fresh-water lens. Basal water occurs where the fresh-water lens is directly underlain by sea-water, while parabasal water occurs where the fresh-water lens is directly underlain by non-carbonate, basement rocks (Figure 8; Mink and Vacher, 1997). Basal waters develop a lens thickness defined by the Ghyben-Herzberg Principle:

$$Z = [(\rho_f)/(\rho_s - \rho_f)]h,$$

where Z is the depth of the fresh-water lens below sea level, h is the height of the lens above sea level, and ρ_f and ρ_s are the densities of fresh-water and salt-water respectively (Figure 8; White, 1988; Raeisi and Mylroie, 1995). The fresh-water/salt-water lens thickens as the fresh-water head depresses the interface below sea level, relative to the density difference in the two waters:

$$Z = \alpha h,$$

where $\alpha = (\rho_f)/(\rho_s - \rho_f)$. With ρ_f = 1:00 g/cm^3 and ρ_s = 1.025 g/cm^3, $\alpha = 40$; therefore, for every one meter or foot of fresh-water head, the fresh-water/salt-water interface is depressed 40 meters or feet (1:40 ratio) (White, 1988; Raeisi and Mylroie, 1995).

Island environments have limited water resources and specific problems because of the morphology of the fresh-water lens (water with a chloride concentration <250 mg/L (Gingerich and Yeatts, 2000)). Because of the limited extent of island aquifers and the characteristics of eogenetic karst, island aquifers are extremely susceptible to contamination. Contamination from the surface can include: human and animal wastes, fertilizers, detergents, pesticides, herbicides, petroleum spills, and solvent spills. Subsurface contamination can occur from salt-water

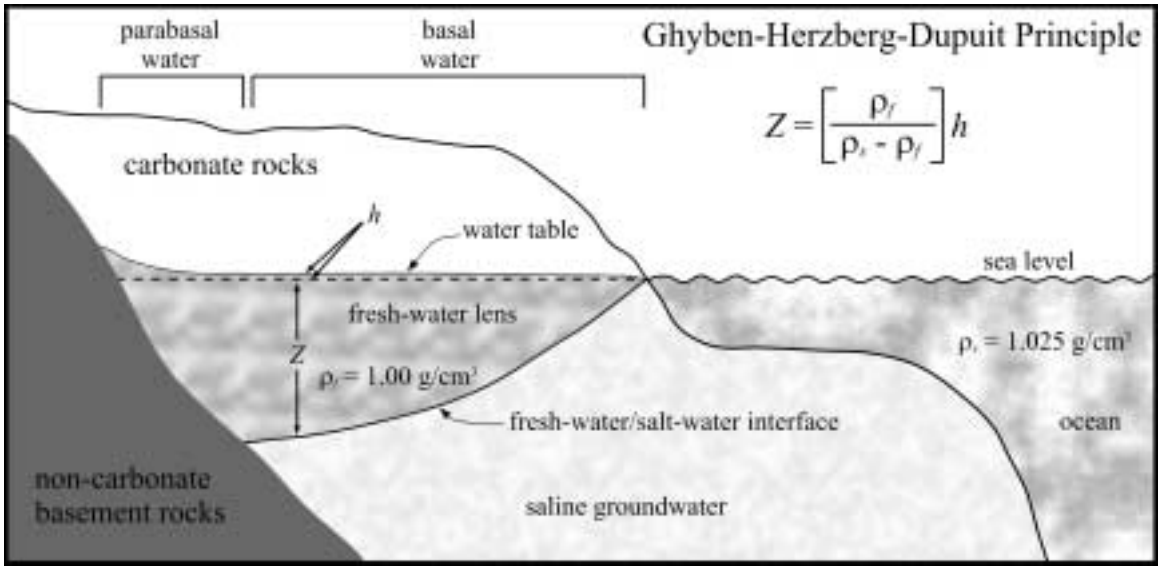

Figure 8: Model showing the fresh-water lens morphology showing the location of basal and parabasal waters and the Ghyben-Herzberg principle (adapted from Mink and Vacher, 1997 and Raeisi and Mylroie, 1995).

intrusion, where over pumping produces a cone-of-depression in the lens, which then up-cones salt-water into the fresh-water lens at a one to forty ratio. Because of the ratio of up-coned water to lens thickness above sea level, a small decrease in the lens thickness above sea level will create a large cone of depression at depth in basal waters (Gingerich and Yeatts, 2000; Mylroie and Carew, 1997). When non-carbonate rocks extend into or through the freshwater lens, basement rocks restrict upconing of parabasal water because salt-water does not directly underlie fresh-water. Therefore, it is important for island communities to effectively manage their water resources in order to continue to produce potable water, by limiting water extraction at specific sites and by utilizing zones of parabasal groundwater (Mink and Vacher, 1997).

In the 1995 census, 2,631 people were listed as living on Tinian primarily in the Median Valley and parts of the adjacent Central Plateau, which comprises 25% of the total island surface area. This limited region of population is partially the result of the United States control of the northern third of the island, the Northern Lowland, for military purposes, while other regions are less accessible due to terrain. Of the inhabited region, 60% is an undeveloped, public, rural area. The remaining 40% of this region is composed of residential and commercial lots that include a casino resort, small businesses, farming, grazing and housing. The residential and commercial lots provide the largest concerns for contamination from surface spills and biological waste disposal. Tinian currently has no sewer facility, instead human waste is disposed of through septic and seepage tanks, leaching fields or holding tanks, which may not be adequate for preventing groundwater contamination, because of the thin soil profile and rapid infiltration rates associated with eogenetic, carbonate rocks. Other sources of contamination include the airport, several quarries and a solid waste disposal dump, which provide paths for direct recharge into the aquifer by bypassing the soil surface and epikarst, which have been removed (Gingerich and Yeatts, 2000; Bormann, 1992).

On Tinian, USGS investigations show that the maximum lens thickness is approximately 12 meters (40 feet) in the

center of the Median Valley, with slight thinning near the Municipal Well and Marpi Marsh (Gingerich and Yeatts, 2000). The Municipal Well (a Maui-type, infiltration well) supplies the majority of the islands water needs at a rate of approximately 4.5 x 10^6 liters/day (~1.2 Mgal/day). Today water produced from the Municipal well has a chloride concentration of 180 mg/L, which is 100 mg/L greater than when the well was constructed in 1945. The USGS monitored the aquifer thickness in relation to rain events in the wet season of 1993 and reported an aquifer thickening of 90-150 cm (3-5 ft), while reports in the dry season of 1994 showed an aquifer thinning of 30-60 cm (1-2 ft). These results revealed that annual fluctuations are minor and lens thickness is dependent more upon long-term rainfall patterns instead of annual fluctuations, for maintaining overall morphology (Gingerich and Yeatts, 2000). This stable lens morphology indicates that contamination problems have the potential to produce long term effects due to long residence time for water within the aquifer.

With the stable fresh-water lens morphology on Tinian, the location and identification of karst features becomes important for preventing groundwater contamination. Understanding the spatial distribution and extent of fissure caves, pit caves, and recharge features, which can transport contaminants rapidly to the lens, may enable government planners to regulate activities near sensitive areas. Similarly, identified discharge features can be used as sampling points for monitoring possible groundwater contamination. Identification of allogenic recharge may be used to predict regions where parabasal waters may be thicker due to increased recharge, such that salt-water intrusion risks from water extraction may be reduced. Spatial distributions of flank margin and banana hole caves may provide insight into the diffuse flow characteristics of previous fresh-water lenses, making it possible to better evaluate current lens morphology. If positive correlations do exist between brittle deformation and megaporosity, then regional structure may provide insights into groundwater behavior.

STUDY METHODOLOGY

This study had three objectives. It was initially developed to inventory, survey, and classify the cave and karst features on Tinian and Aguijan, because no such database existed for the islands. In addition to the inventory, this study was developed to evaluate whether or not a statistical comparison could be made between megaporosity and zones of brittle failure in eogenetic rocks on carbonate islands, using data collected from the island of Tinian where basic geologic studies have been conducted (Doan et al., 1960). The study was conducted in five major phases, in order to reach the two objectives: 1) initial site investigation, 2) data collection, 3) data reduction, 4) statistical comparison of data, and 5) small-scale test site evaluation. Results from the two primary objectives of the study were used to evaluate the islands of Tinian and Aguijan in relation to the Carbonate Island Karst Model.

INITIAL SITE INVESTIGATION

The initial site investigation included a reconnaissance of Tinian and analysis of the physiography and geology of the island. The reconnaissance was conducted in June 2002 (Stafford et al., 2002) and provided basic information about the cultural, physical and logistical aspects of Tinian, while establishing relationships with local government bodies that would be crucial for in-depth studies on the island. During this reconnaissance areas that were reported by island residents as having significant cave development were visited, including, but not limited to: Suicide Cliffs, Unai Dangkolo,

and Mount Lasu. This initial site investigation demonstrated that most known caves, reported by local residents and hunters, occur predominantly along scarps, coastlines, and closed depressions, which agreed with previous investigations on carbonate islands (Stafford et al., 2002; Mylroie et al., 1999).

After the initial reconnaissance, the islands geography and geology were analyzed with a geographical information system (GIS) that was produced for the island using ArcView 3.2 (ESRI, 2000). A digital elevation model (DEM) was created for the island using spatial data transfer standard (SDTS) compliant raster data with 10-meter postings produced by the National Mapping Program of the United States Geological Survey (USGS, 2001a,b,c,d,e), which provides greater resolution than the 1:25,000 topographic map produced by the USGS (USGS, 1983). The DEM was then overlain with a scanned geology map produced by Doan and coworkers (1960). It was geo-referenced using Image Analyst (ESRI, 2000) in order to scale and align the geology map with DEM, then all igneous outcrops and faults were manually digitized in order to create shape files of these features. The DEM and digitized geologic features were then used as the basic dataset needed to delineate prominent scarps and closed depressions on the island.

Scarps were defined as any change in slope greater than twenty degrees, which enabled the identification of all major scarps in the island interior and coastline (Figure 19, Appendix A). Because of the DEM cell size, smaller scarps that might contain cave entrances were excluded; however, it did not eliminate investigations of smaller coastal scarps because coastlines were identified as sites of cave development during the initial reconnaissance. Closed depressions were defined as regions that were lower than the surrounding topography on all sides. Only closed depressions greater than 10 meters in diameter could be identified based on the limitations of the DEM grid size. The closed depressions where analyzed in relation to outcrops of igneous rock. The closed depressions that were found to be proximal to the igneous outcrops were identified as locations of possible allogenic recharge developed by dissolution, while the closed depressions that were distal to the igneous outcrops probably had non-dissolutional (i.e. constructional or human modified) origin (Figure 20, Appendix A).

The reconnaissance and GIS investigation of Tinian provided a framework for fieldwork and data collection on Tinian. Because there is little published geology on Aguijan and a reconnaissance visit was not possible, no detailed fieldwork plan could be developed. However, this project extended the cave and karst inventory to Aguijan when the opportunity for access to the island was available.

DATA COLLECTION

Two types of data were collected during fieldwork: 1) cave and karst surveys, and 2) structural orientations of zones of brittle failure. These two datasets were collected over the course of two intensive field seasons (December 10, 2002 to January 07, 2003 and May 04, 2003 to June 1, 2003) and provided the database for analysis and correlation in this study. During the course of fieldwork, coastal and scarp investigations were limited to regions that could be accessed within an acceptable risk level that would not greatly endanger safety.

Cave and karst surveys were conducted on Aguijan and Tinian based on the initial site investigation and additional reports provided by local residents during the course of fieldwork. This fieldwork focused on known caves, coastlines, scarps, and closed depressions. Caves were surveyed in accordance with current international standards for cave cartography and mapping established by the National Speleological Society (NSS) (Dasher, 1994) and the Association for Mexican Cave Studies (AMCS) (Sprouse and Russell, 1980). Individual surveys were conducted using a Suunto compass, Suunto inclinometer, and fiberglass tape, in association with a field

sketch recorded by experienced project sketchers. Caves and other karst features, including discharge and recharge features, which did not warrant survey, were photo-documented and recorded. Discharge volumes on discharge features were estimated (minimal discharge and significant discharge), because coastal conditions did not allow for measurements of salinity and temperature to be taken at most sites.

During fieldwork, features were classified by cave type based on their appearance in accordance with the Carbonate Island Karst Model. The feature types included: banana hole, discharge cave/feature, fissure cave, flank margin cave, recharge cave/feature, and pit cave. When satellite coverage permitted, Universal Transverse Mercator System (UTM) coordinates and elevation were recorded with the global positioning system (GPS), in order to establish accurate location information for the feature. When satellite coverage was not possible, because of vegetation or topography, cave locations were identified on 1:25,000 USGS topographic maps (USGS, 1983), which were then used to determine UTM coordinates and elevation for features.

Structural orientations of planes of brittle failure were measured using a Suunto compass during fieldwork on Tinian. Aguijan was excluded from this phase of data collection, because no published geologic map for the island exists and available time on the island was limited. Orientations were taken in areas where a joint or fracture could be observed in the bedrock and was not obscured by karren or phytokarst development. Orientations were only taken where the joint or fracture continued over a distance of several meters, cut through more than one bedding plane or several meters of bedrock, and in areas where the bedrock appeared to be *in situ*.

DATA REDUCTION

Data reduction included five phases: 1) survey data reduction and production of maps of the cave and karst features surveyed on Aguijan and Tinian, 2) analysis of cave maps and delineation of primary cave orientations and cave segment orientations for features on Tinian, 3) analysis of faults and joints reported by Doan and coworkers (1960), 4) analysis of scarp and coastline orientations on Tinian, and 5) orientation data reduction and production of rose diagrams for structural and cave orientations on Tinian.

Data from surveyed cave and karst features was reduced using the software package WALLS (McKenzie, 2002), which enables compass, inclinometer and tape measurements taken during surveys to be plotted with corrections for minor loop closure errors and regional magnetic declination. The corrected line plots for each cave were then used as a basis for drafting spatially correct final maps of the features using Corel Xara 2.0 (Xara, 1997). Final cartographic products were created by overlaying field sketch notes and corrected line plots. The field sketch notes were scaled and rubber-banded to match the corrected line plots, then features recorded on the field sketch notes were manually digitized using standard cave symbology established by the NSS and AMCS (Figure 21, Appendix A; Sprouse and Russell, 1980) in order to create accurate maps of the cave and karst features inventoried.

These maps were used to delineate primary cave orientations and segment orientations for features surveyed on Tinian, using two methods: 1) apparent trends and 2) entrance oriented trends. Cave orientations have been used in previous studies in continental settings to correlate cave and karst development with regional structure (Nelson, 1988; Barlow and Ogden, 1982), where the orientations of individual cave segments that have a consistent trend are measured and compared against regional brittle failure features to determine if a correlation between the two populations exist.

Using the apparent trend method, all Tinian cave maps were analyzed individually and a primary axis was defined

through the cave based on the maximum length of the cave and the location of the breached entrance. Cave segments were then defined by the orientation of individual chambers, passages, and wall characteristics such as large pockets and chamber alcoves (Figures 9 and 10). This technique is highly subjective, but was used because of its similarity to studies in caves where passages tend to be linear (Nelson, 1988; Barlow and Ogden, 1982). The primary and segment cave trends were then measured and compiled. The segment cave trends were length-weighted into 5 and 10-meter increments, such that each 5 or 10-meter section of cave segment was counted as an individual orientation measurement in order to give greater significance to longer segment trends during data analysis (Nelson, 1988; Barlow and Ogden, 1982). Two segment lengths were used to form two sets of data that would reduce the subjectivity of the parameters that were used to define segment length, such that smaller cave sections would be included in the 5-meter segment data, while only larger cave sections would be included in the 10-meter segment data.

The entrance width trend method of delineating cave orientations was developed and performed in an attempt to reduce the subjectivity in data reduction for flank margin and banana hole type caves, which tend to form globular or elliptical chambers instead of the more linear passages seen in fissure caves. Using the entrance orientation method, up to three orientations were measured for flank margin and banana hole type cave maps on Tinian (Figure 11). In this technique, the orientation of the entrances to caves that were entered horizontally was measured. Next a maximum penetration measurement was calculated near perpendicular to the entrance ($90^o \pm 15^o$ from the entrance orientation). In caves that had been breached by ceiling collapse and were entered vertically, no entrance orientation was measured, but the penetration measurement was defined as the longest dimension of the cave. Based on the

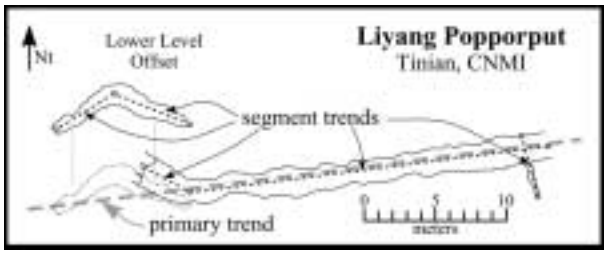

Figure 9: Example of primary and segment orientation trends measured using the apparent trend method for a typical fissure cave.

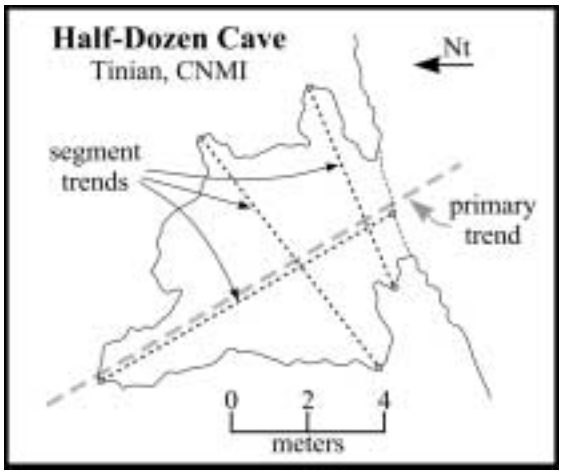

Figure 10: Example of primary and segment orientation trends measured using the apparent trend method for a typical mixing zone cave.

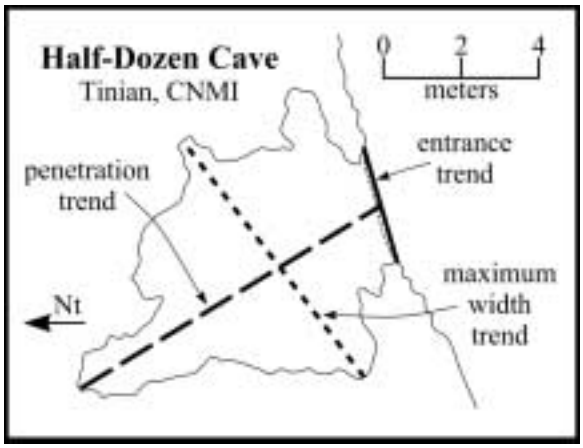

Figure 11: Example of entrance, maximum width, and penetration trends measured using the entrance width trend method for a typical mixing zone cave.

penetration measurement, a maximum width was measured near perpendicular to the penetration orientation ($90^o \pm 15^o$ from the penetration orientation). In cases where the cave entrance was the maximum width, the same measurement was reported for both entrance width and the maximum width. These measurements were then compiled as primary entrance width, penetration length, and maximum width orientations and corresponding segment orientations that were length-weighted in 5 and 10-meter segments similar to the cave segments defined in the apparent method.

Faults and joints reported by Doan and coworkers (1960) were measured for length and orientation. The data for faults was length-weighted by 50 and 100-meter segments in order to apply greater significance to faults that extended over greater distances. Two segment lengths were used in order to reduce the subjectivity in selecting segment lengths, such that shorter lengths would be included in the 50-meter segment data and only longer segments would be included in the 100-meter segment data. These two segment lengths were defined because they are proportional to the segment definition used for cave passages, but measured at a scale that is one order of magnitude greater, because 5 and 10-meter lengths could not be accurately measured from the geology reported by Doan and coworkers (1960). Similarly, all scarps that were identified during the initial site investigation and all coastlines were divided into linear segments in order to eliminate the effects of minor variations in coastal erosion and mass wasting. The linear segments were measured for orientation and length; with length weighted, 50 and 100-meter segments applied to both scarp and coastline orientations as was defined for fault segments, because the DEM cell size does not allow for accurate measurements less than 10 meters.

In the final phase of data reduction, all orientation measurements were reduced to produce rose diagrams using the software package GEOrient 9.2 (Holcombe, 2003), using five-degree orientation sectors in order to be able to visually compare the orientation patterns of caves, zones of brittle failure, scarps, and coastlines. Rose diagrams were produced for each type of orientation data in each of the five physiographic provinces of Tinian (Central Plateau, Median Valley, Northern Lowland, North-Central Plateau, and Southeastern Ridge) and for the entire island of Tinian (Tinian Composite). These rose diagrams include the following types:

1. fault orientations
2. fault, 5-meter segment orientations
3. fault, 10-meter segment orientations
4. joint orientations
5. orientations of fractures measured during fieldwork
6. inland scarp orientations
7. inland scarp, 5-meter segment orientations
8. inland scarp, 10-meter segment orientations
9. coastal scarp orientations
10. coastal scarp, 5-meter segment orientations
11. coastal scarp,10-meter segment orientations
12. all scarps orientations
13. all scarps, 5-meter segment orientations
14. all scarps, 10-meter segment orientations
15. coastline orientations
16. coastline, 5-meter segment orientations
17. coastline, 10-meter segment orientations
18. fissure cave orientations
19. fissure cave, 5-meter segment orientations
20. fissure cave, 10-meter segment orientations
21. mixing zone cave orientations
22. mixing zone cave, 5-meter segment orientations
23. mixing zone cave, 10-meter segment orientations
24. all cave types orientations
25. all cave types, 5-meter segment orientations
26. all cave types, 10-meter segment orientations
27. mixing zone cave penetration orientations
28. mixing zone cave penetration, 5-meter segment orientations
29. mixing zone cave penetration, 10-meter segment orientations

30. mixing zone cave entrance width orientations
31. mixing zone cave entrance width, 5-meter segment orientations
32. mixing zone cave entrance width, 10-meter segment orientations
33. mixing zone cave maximum width orientations
34. mixing zone cave maximum width, 5-meter segment orientations
35. mixing zone cave maximum width, 10-meter segment orientations

STATISTICAL COMPARSION OF DATA

Statistical comparisons were calculated in order to determine if different populations of orientation data were similar within each of the five physiographic provinces of Tinian and the entire island of Tinian. The comparisons were calculated in order to determine if there is a significant relationship between: 1) brittle deformation of eogenetic rocks and the development of eogenetic karst; 2) scarp orientations and the development of eogenetic karst; and 3) coastline orientations and the development of eogenetic karst.

Statistical comparisons were conducted using the Kolmogorov-Smirnov 2-sample test (Burt and Barber, 1996; Till, 1974; Miller and Kahn, 1962), which performs a non-parametric test on two independent sample populations to determine if they represent similar populations or population distributions. During the statistical comparison phase, several populations of orientations were evaluated, which correspond to the 35 orientation types that were used to produce rose diagrams during the data reduction phase. Each of the 35 orientation types was evaluated for correlation with:

1. fault orientations
2. fault, 5-meter segment orientations
3. fault, 10-meter segment orientations
4. joint orientations
5. orientations of fractures measured during fieldwork
6. inland scarp orientations
7. inland scarp, 5-meter segment orientations
8. inland scarp, 10-meter segment orientations
9. coastal scarp orientations
10. coastal scarp, 5-meter segment orientations
11. coastal scarp, 10-meter segment orientations
12. all scarps orientations
13. all scarps, 5-meter segment orientations
14. all scarps, 10-meter segment orientations
15. coastline orientations
16. coastline, 5-meter segment orientations
17. coastline, 10-meter segment orientations

These correlations were performed in order to test three different null hypotheses (H_0):

$H_0(1)$: Regional brittle deformation and karst development represent significantly different populations or population distributions and develop independently.

$H_0(2)$: Regional scarp positions and karst development represent significantly different populations or population distributions and develop independently.

$H_0(3)$: Regional coastline positions and karst development represent significantly different populations or population distributions and develop independently.

The first null hypothesis ($H_0(1)$) was formulated in order to determine if there is a relationship between brittle deformation and karst development on Tinian, while the second and third null hypotheses ($H_0(2$ and $3)$) were formulated to determine if there is a relationship between karst development and coastlines or scarps, where the edge of the paleo fresh-water lens would be expected based on the Carbonate Island Karst Model (Mylroie and Vacher, 1999). Because of the wide variation in orientations of the data in

this study, a high significance level ($P \leq 0.01$) was used to ensure that the populations or population distributions that were compared represented significantly similar datasets. If the first null hypothesis is rejected, then the regional populations of joints, fractures, and faults are similar to the regional karst development and a positive relationship between the two populations can be inferred. If the second null hypothesis is rejected, then the regional populations of scarp orientations are similar to the regional karst development and a positive relationship between the two populations can be inferred. If the third null hypothesis is rejected, then the regional populations of coastline orientations are similar to the regional karst development and a positive relationship between the two populations can be inferred.

SMALL-SCALE TEST SITE EVALUATION

In addition to the analyses performed for the five physiographic provinces and the island of Tinian, smaller-scale test sites were analyzed to determine if any relationships existed at various scales: 1) island scale, 2) province scale, and 3) site scale. Because of the wide distribution of cave and karst features, one square kilometer test sites were chosen for additional analyses. In order to compare the results of analyses from test sites with the larger regions of Tinian, five parameters where required to exist within the one square kilometer boundary, including: 1) three or more surveyed features, 2) both fissure and mixing zone caves, 3) coastline, 4) faults reported by Doan and coworkers (1960), and 5) fracture orientations measured during fieldwork.

The requirements for choosing small-scale test sites required the completion of fieldwork and the cave and karst inventory of this study. Once the inventory stage was complete, three test sites were chosen for analysis (Figure 22, Appendix A): Carolinas Limestone Forest, Puntan Diapblo, and Unai Dangkolo. At each of these sites, statistical comparisons were evaluated using the Kolmogorov-Smirnov 2-sample test, with the same 35 parameters evaluated for each of the physiographic provinces and the entire island of Tinian.

STUDY RESULTS

CAVE AND KARST INVENTORY

The mapping portion of cave and karst inventory surveyed 114 caves or cave complexes (green areas, Figure 23, Appendix A; Appendix B): 26 on Aguijan and 88 on Tinian. The features were classified by morphology type and grouped by physiographic province they were found in (Table 1, Appendix B; Table 2, Appendix B). On Aguijan, the cave survey produced maps of 1 banana hole, 5 fissure caves, and 20 flank margin caves. On Tinian, the cave survey produced maps of 3 banana holes, 5 discharge features, 12 fissure caves, 65 flank margin caves, 1 pit cave, and 2 recharge features; however, 4 of the discharge features were also classified as fissure caves, making a total of 16 fissure caves. Mixing zone type caves (banana hole and flank margin type caves) were the most prominent cave types found during the inventory (81% on Aguijan; 77% on Tinian). While Tinian exhibited a larger diversity and quantity of caves, the ratio of fissure caves to mixing zone caves on both islands was 0.24 (0.235 for Aguijan; 0.238 for Tinian), with fissure caves accounting for almost 20% of the caves recorded.

A total of seventeen locations were found on Tinian, which exhibited fresh-water discharge (Figure 24, Appendix A). Most of these features were identified by schlieren mixing at the coastline, but only five of them were associated with cave development and surveyed. Fresh-water discharge observed at Unai Dangkolo, Unai

Masalok and Taga Beach appeared as diffuse discharge through carbonate sand beach deposits, while the discharge at other sites appeared as focused discharge along fractures and bedding planes. The two discharge features that exhibited the greatest discharge were located on the east and west coasts of the island at Gecko Cave and Barcinas Cove, respectively.

Investigation of closed depressions identified four definite regions of allogenic recharge in the North-Central Highland, with small caves associated with two of them (Lasu Recharge Cave and West Lasu Depression Cave). The presence of accumulated detritus and the lack of sediment coatings on the feature walls is evidence that recharge is rapid and that water does not pond at these features during recharge events. The other two recharge features (North and South Lemmai Recharge Features) covered larger areas, contained contacts between carbonate and non-carbonate rocks, and showed vegetative evidence of water ponding within the closed depressions prior to entering the subsurface (Figure 25, Appendix A). Ponded water was present in portions of South Lemmai Recharge Feature when investigated (Figure 26, Appendix A).

The other sixteen closed depressions identified during the initial site investigation that were not confirmed as allogenic recharge features were also investigated (Figure 27, Appendix A), either physically or through communication with local residents. Five closed depressions were identified as quarries or borrow pits, eight were identified as natural constructional features, and three appear to be recharge features. Four of the modified closed depressions (quarries and borrow pits) showed evidence of excavation in the past, while the quarry located near Barcinas Cove is being actively excavated today (Figure 28, Appendix A). The eight natural construction features showed no evidence of excavation or allogenic recharge; however, Hagoi in the Northern Lowland is less than 2 meters above mean sea-level and contained fresh-water at the time of survey (Figure 29, Appendix A), while the largest closed depression on the island (Sisonyan Makpo) is less than 3 meters above mean sea-level at its lowest elevation and is the site of the islands primary municipal well (Makpo Wells). The three unconfirmed recharge features are located north of Mount Lasu near small outcrops of non-carbonate rocks, but due to their small size and dense vegetation in the area, a positive confirmation could not be made.

CAVE ORIENTATIONS

The two methods of cave orientation analysis (apparent trend and entrance width trend) were applied to orientation data for mapped caves on Tinian. Aguijan was excluded from this analysis because no geologic map has been published for the area, which would compliment the cave orientation data when comparing cave and karst development to brittle failure features. Each cave was analyzed separately, including those that occurred on maps where a complex or series of caves were surveyed together as one map, making it possible to have several datasets of orientation measurements for some cave maps. Using the apparent trend method all fissure caves and mixing zone caves (flank margin and banana hole type caves) were analyzed for primary orientation and segment orientations. The single pit cave and two recharge caves were excluded from all datasets except composite cave types (all cave types) because of their small sample size. Using the entrance trend method, the mixing zone caves were analyzed for entrance width, penetration length and maximum width, while fissure caves, the single pit cave and the two recharge caves were excluded. The fissure caves were excluded from the entrance width trend method because they are linear features with distinct segment orientations similar to telogenetic caves (Nelson, 1988; Barlow and Ogden, 1982), while the single pit cave and two recharge caves were excluded again because of their small sample size.

The apparent trend method was applied because of its similarity to previous studies (Nelson, 1988; Barlow and Ogden, 1982). Apparent trend analysis of fissure caves analysis yielded 18 primary cave orientations (Table 3, Appendix C): 5 in the Central Plateau; 5 in the Median Valley; 0 in the North-Central Highland; 1 in the Northern Lowland; and 7 in the Southeastern Ridge. Fissure cave segment analysis using the apparent trend method yielded 147 orientations with 297 five-meter segments and 135 ten-meter segments (Table 4, Appendix C):

- Central Plateau: 15 orientations, 24 five-meter segments and 12 ten-meter segments
- Median Valley: 69 orientations, 100 five-meter segments and 44 ten-meter segments
- North-Central Highland: 0 orientations and segments
- Northern Lowland: 2 orientations, 2 five-meter segments and 2 ten-meter segments
- Southeastern Ridge: 61 orientations, 171 five-meter segments and 77 ten-meter segments

Apparent trend analysis of mixing zone caves yielded 128 primary orientations (Table 5, Appendix C): 46 in the Central Plateau; 27 in the Median Valley; 8 in the North-Central Highland; 1 in the Northern Lowland; and 46 in the Southeastern Ridge. Mixing zone cave segment analysis yielded 388 orientations with 980 five-meter segments and 480 ten-meter segments (Table 6, Appendix C):

- Central Plateau: 123 orientations, 302 five-meter segments and 122 ten-meter segments
- Median Valley: 126 orientations, 424 five-meter segments and 212 ten-meter segments
- North-Central Highland: 20 orientations, 30 five-meter segments and 9 ten-meter segments
- Northern Lowland: 4 orientations, 11 five-meter segments and 9 ten-meter segments
- Southeastern Ridge: 115 orientations, 213 five-meter segments and 128 ten-meter

The entrance width trend method was performed in order to reduce the subjectivity of orientation measurements that exist in the apparent trend method. Measurements used in the entrance width trend method included entrance width, penetration length, and maximum width, with 10 caves excluded from the entrance width analysis because their entrances were entered vertically as a result of ceiling collapse. Entrance width analysis using the entrance trend method yielded 107 entrance widths with 324 five-meter segments and 163 ten-meter segments (Table 7, Appendix C):

- Central Plateau: 40 orientations, 105 five-meter segments and 59 ten-meter segments
- Median Valley: 20 orientations, 89 five-meter segments and 43 ten-meter segments
- North-Central Highland: 5 orientations, 11 five-meter segments and 6 ten-meter segments
- Northern Lowland: 1 orientation, 22 five-meter segments and 11 ten-meter segments
- Southeastern Ridge: 42 orientations, 97 five-meter segments and 44 ten-meter segments

Penetration length analysis using the entrance trend method produced 118 orientations with 369 five-meter segments and 190 ten-meter segments (Table 8, Appendix C):

- Central Plateau: 42 orientations, 116 five-meter segments and 54 ten-meter segments
- Median Valley: 26 orientations, 116 five-meter segments and 67 ten-meter segments
- North-Central Highland: 6 orientations, 15 five-meter segments and 6 ten-meter segments
- Northern Lowland: 1 orientation, 16 five-meter segments and 8 ten-meter segments

- Southeastern Ridge: 43 orientations, 106 five-meter segments and 55 ten-meter segments

Maximum width analysis using the entrance trend method yielded 118 orientations with 407 five-meter segments and 208 ten-meter segments (Table 9, Appendix C):

- Central Plateau: 42 orientations, 140 five-meter segments and 72 ten-meter segments
- Median Valley: 26 orientations, 116 five-meter segments and 60 ten-meter segments
- North-Central Highland: 6 orientations, 13 five-meter segments and 7 ten-meter segments
- Northern Lowland: 1 orientation, 22 five-meter segments and 11 ten-meter segments
- Southeastern Ridge: 43 orientations, 116 five-meter segments and 58 ten-meter segments

BRITTLE DEFORMATION

Analysis of the data from the geologic survey conducted by Doan and coworkers (1960) identified 313 faults (Figure 30, Appendix A) and 112 joints on Tinian. The data reported by Doan and coworkers (1960) was divided by physiographic province and measured separately, with faults that occurred at the boundary between two physiographic provinces not being reported, because Doan and coworkers (1960) defined the five physiographic provinces based on high-angle faults that divided the island into distinct regions. The measurements for each of the faults were length weighted to produce a total of 3322 fifty-meter segments and 1661 one hundred-meter segments with segments rounded to the nearest 50 and 100-meter increment. This process produced 39 orientations with 358 fifty-meter segments and 179 one hundred-meter segments in the boundary areas separating different physiographic provinces (Table 10, Appendix C), which included:

- Central Plateau: 94 orientations, 944 fifty-meter segments and 472 one hundred-meter segments
- Median Valley: 50 orientations, 686 fifty-meter segments and 343 ten-meter segments
- Northern Lowland: 22 orientations, 324 fifty-meter orientations and 162 ten-meter segments
- North-Central Highland: 43 orientations, 394 fifty-meter segments and 197 one hundred-meter segments
- Southeastern Ridge: 65 orientations, 618 fifty-meter segments and 309 one hundred-meter segments

Joint data reported by Doan and coworkers (1960) produced 38 orientations in the Central Plateau, 25 orientations in the Median Valley, 0 orientations in the North-Central Highland, 16 orientations in the Northern Lowland, and 33 orientations in the Southeastern Ridge (Table 11, Appendix C).

Measurements of planes of brittle failure measured during fieldwork yielded 345 orientations for the island of Tinian (Table 12, Appendix C). Because of dense vegetation, soil cover, and the criteria used for orientation sampling, the orientations measurements were primarily limited to coastal areas where exposed bedrock could be observed. However, measurements were attained in all regions accept the North-Central Highland, which has no coastline. Measurements included 103 orientations in the Central Plateau, 106 orientations in the Median Valley, 86 orientations in the Northern Lowland, and 50 orientations in the Southeastern Ridge.

SCARPS AND COASTLINES

Analysis of scarps based on 20-degree slopes derived from the ten-meter posting DEM provided the basis for scarp orientations on Tinian (Figure 19, Appendix A). Scarps were divided into inland scarps and coastal scarps and measured, resulting in a total of 154 inland scarp orientations with 725 fifty-meter segments and 379 one hundred-meter segments and 147 coastal

scarp orientations with 539 fifty-meter segments and 266 one hundred-meter segments (Tables 13 and 14, Appendix C). The measurements were grouped by the physiographic province for both the inland and coastal scarps for data analysis. Inland scarp orientations included (Table 13, Appendix C):

- Central Plateau: 27 orientations, 126 fifty-meter segments and 68 one hundred-meter segments
- Median Valley: 12 orientations, 46 fifty-meter segments and 24 one hundred-meter segments
- North-Central Highland: 30 orientations, 150 fifty-meter segments and 79 one hundred-meter segments
- Northern Lowland: 0 orientations
- Southeastern Ridge: 85 orientations, 403 fifty-meter segments and 208 ten-meter segments

Coastal scarp orientations included (Table 14; Appendix C):

- Central Plateau: 65 orientations, 539 fifty-meter segments and 101 ten-meter segments
- Median Valley: 3 orientations, 10 fifty-meter segments and 5 one hundred-meter segments
- North-Central Highland: 0 orientations
- Northern Lowland: 0 orientations
- Southeastern Ridge: 79 orientations, 320 fifty-meter segments and 160 one hundred-meter segments

Coastline orientations were measured at the 0 elevation contour on the DEM for Tinian. Coastlines were measured similar to island scarps, producing 251 orientations with 945 fifty-meter segments and 501 one hundred-meter segments for the island (Table 15, Appendix C), which yielded 50.1 kilometers of coastline segments, closely approximating the 51.2 kilometers of coastline that exist (Doan et al., 1960). The coastline measurements were grouped by the appropriate physiographic province, with:

- Central Plateau: 84 orientations, 250 fifty-meter segments and 134 one hundred-meter segments
- Median Valley: 48 orientations, 169 fifty-meter segments and 94 one hundred-meter segments
- Northern Lowland: 40 orientations, 206 fifty-meter segments and 113 one hundred-meter segments
- Southeastern Ridge: 79 orientations, 320 fifty-meter segments and 160 one hundred-meter segments

The North-Central Plateau is surrounded on all sides by other physiographic provinces and has no coastline.

ROSE DIAGRAMS

Rose diagrams were plotted for each of the 35 parameters investigated in this study, with diagrams corresponding to each of the physiographic provinces and the entire island of Tinian (Appendix C). The data was visually analyzed to determine if any similar populations or population distributions existed between independent parameters within the same region. The orientation data showed a wide range of variability, while some datasets contained no orientations or only one orientation trend, which eliminated them from the comparison. The rose diagrams for the Central Plateau and the Northern Lowland showed no distinct similarities, while the diagrams for the entire island of Tinian, Median Valley, North-Central Highland, and Southeastern Ridge showed few distinct similarities.

The data for the entire island of Tinian (Tinian Composite) showed similarity in four parameter comparisons:

1. inland scarp orientations and 10-meter segment orientations of mixing zone cave entrance widths
2. 50-meter segment orientations of inland scarps and 10-meter segment orientations of mixing zone cave entrance widths
3. 100-meter segment orientations of inland scarps and 10-meter segment orientations of mixing zone cave entrance widths

4. 100-meter segment orientations of coastal scarps and mixing zone entrance width orientations

The data for the Median Valley showed similarity in three parameter comparisons:

1. orientations of fractures measured in the field and 5-meter segment orientations of mixing zone cave entrance widths
2. orientations of fractures measured in the field and 10-meter segment orientations of mixing zone cave entrance widths
3. composite scarp orientations and mixing zone cave entrance width orientations

The data for the North-Central Highland showed similarity in three parameter comparisons:

1. inland scarp orientations and composite cave primary orientations
2. inland scarp orientations and mixing zone cave primary orientations
3. composite scarp orientations and composite cave primary orientations

The data for the Southeastern Ridge showed similarity in 13 parameter comparisons:

1. fault orientations and composite cave primary orientations
2. fault orientations and 10-meter segment orientations of mixing zone cave penetrations
3. 50-meter segment orientations of faults and composite cave primary orientations
4. 50-meter segment orientations of faults and 5-meter segment orientations of mixing zone cave penetrations
5. 50-meter segment orientations of faults and 10-meter segment orientations of mixing zone cave penetrations
6. 100-meter segment orientations of faults and composite cave primary orientations
7. 100-meter segment orientations of faults and 5-meter segment orientations of mixing zone cave penetrations
8. 100-meter segment orientations of faults and 10-meter segment orientations of mixing zone cave penetrations
9. orientations of fractures measured in the field and 10-meter segment orientations of mixing zone caves
10. 50-meter segment orientations of inland scarps and 10-meter segment orientations of mixing zone cave entrance widths
11. 100-meter segment orientations of inland scarps and 10-meter segment orientations of mixing zone cave entrance widths
12. coastal scarp orientations and 5-meter segment orientations of mixing zone cave maximum widths
13. coastline orientations and 5-meter segment orientations of mixing zone cave maximum widths

STATISTICAL COMPARISON

Orientation datasets were compared for population similarities or population distribution similarity by performing non-parametric tests on independent samples for each of the physiographic regions and the island of Tinian. Populations or population distributions were considered similar if the significance level between two independent samples was less than 0.01 ($P \leq 0.01$) when compared using the Kolmogrov-Smirnov 2-sample test. The data showed a high degree of similarity with results varying for each province and the island of Tinian.

Tinian Composite

Statistical comparisons for the entire island of Tinian showed similarity for 266 (60.2 %) pairs of independent data. Joints and fracture orientations measured in the field were similar to the faults, while segment datasets showed similarity to all segment lengths in 37 dataset comparisons (Table 16; Appendix D):

1. faults and inland scarps
2. faults and all scarps
3. faults and coastlines
4. faults and all cave types
5. faults and fissure caves
6. faults and mixing zone caves
7. faults and mixing zone cave penetrations
8. faults and mixing zone cave entrance widths
9. faults and mixing zone cave maximum widths
10. inland scarps and all cave types
11. inland scarps and fissure caves
12. inland scarps and mixing zone caves

13. inland scarps and mixing zone cave penetrations
14. inland scarps and maximum cave widths
15. coastal scarps and all cave types
16. coastal scarps and fissure caves
17. inland scarps and mixing zone caves
18. inland scarps and mixing zone cave penetrations
19. inland scarps and mixing zone cave entrance widths
20. inland scarps and mixing zone cave maximum widths
21. coastal scarps and all cave types
22. coastal scarps and fissure caves
23. coastal scarps and mixing zone caves
24. coastal scarps and mixing zone cave penetrations
25. coastal scarps and mixing zone cave entrance widths
26. coastal scarps and mixing zone cave maximum widths
27. all scarps and coastlines
28. all scarps and all cave types
29. all scarps and fissure caves
30. all scarps and mixing zone caves
31. all scarps and mixing zone cave penetrations
32. all scarps and mixing zone cave entrance widths
33. all scarps and mixing zone cave maximum widths
34. coastlines and all cave types
35. coastlines and fissure caves
36. coastlines and mixing zone caves
37. coastlines and mixing zone cave penetration

Central Plateau

Statistical comparisons for the Central Plateau showed similarity for 199 (45.0 %) pairs of independent data. Joints and fracture orientations measured in the field are similar to the faults, while the segment datasets showed similarity for all segment lengths in 19 dataset comparisons (Table 17, Appendix D):

1. faults and inland scarps
2. faults and coastal scarps
3. faults and all scarps
4. faults and all cave types
5. faults and fissure caves
6. faults and mixing zone caves
7. faults and mixing zone cave penetrations
8. faults and mixing zone cave entrance widths
9. faults and mixing zone cave maximum widths
10. inland scarps and coastal scarps
11. inland scarps and all scarps
12. inland scarps and all cave types
13. coastal scarps and all cave types
14. coastal scarps and mixing zone caves
15. coastal scarps and mixing zone cave entrance widths
16. all scarps and mixing zone cave entrance widths
17. coastlines and all cave types
18. coastlines and mixing zone caves
19. coastlines and mixing zone cave entrance widths

Northern Lowland

Statistical comparisons for the Northern Lowland showed similarity for 72 (52.9 %) pairs of independent data. Although only 72 datasets showed similarity, this is more than half of the total comparisons for the province, because data was limited for this region. Analysis of the DEM produced no scarps and the cave and karst inventory only mapped two features (Rogue Cave and Unai Lamlam) in the Northern Lowland. Joints and fracture orientations measured in the field were similar, while segment datasets showed similarity for all segment lengths in eight dataset comparisons (Table 18, Appendix D):

1. faults and all cave types
2. faults and mixing zone cave penetrations
3. faults and mixing zone cave entrance widths
4. faults and mixing zone cave maximum widths
5. coastlines and all cave types
6. coastlines and mixing zone cave penetrations
7. coastlines and mixing zone cave entrance widths
8. coastlines and mixing zone maximum widths

North-Central Highland

Statistical comparisons for the North-Central Highland showed similarity for 12

(7.0 %) pairs of independent data. This province showed the least similarity between orientations datasets for all segment lengths; however, data were limited for the region. Because this province is completely surrounded by other provinces, no coastal scarps or coastlines exist for this province. Additionally, structural data were limited to the faults reported by Doan and coworkers (1960) and no fissure caves were located in this region during fieldwork. Segment datasets showed similarity in only two dataset comparisons (Table 19, Appendix D):

1. faults and inland scarps
2. faults and all cave types

Median Valley

Statistical comparisons for the Median Valley showed similarity for 189 (42.8 %) pairs of independent data. Joints and fractures measured during fieldwork were not similar to the faults for this province, but segment datasets showed similarity for all segment lengths in 27 dataset comparisons (Table 20, Appendix D):

1. faults and inland scarps
2. faults and all scarps
3. faults and all coastlines
4. faults and all cave types
5. faults and mixing zone caves
6. faults and mixing zone cave penetrations
7. faults and mixing zone cave entrance widths
8. faults and mixing zone cave maximum widths
9. inland scarps and coastal scarps
10. inland scarps and coastlines
11. inland scarps and all cave types
12. inland scarps and mixing zone caves
13. inland scarps and mixing zone cave penetrations
14. inland scarps and mixing zone cave entrance widths
15. inland scarps and mixing zone cave maximum widths
16. all scarps and all coastlines
17. all scarps and all cave types
18. all scarps and mixing zone caves
19. all scarps and mixing zone cave penetrations
20. all scarps and mixing zone cave entrance widths
21. all scarps and mixing zone cave maximum widths
22. coastlines and all cave types
23. coastlines and fissure caves
24. coastlines and mixing zone cave types
25. coastlines and mixing zone cave penetrations
26. coastlines and mixing zone cave entrance widths
27. coastlines and mixing zone maximum widths

Southeastern Ridge

Statistical comparisons for the Southeastern Ridge showed similarity for 236 (53.4 %) pairs of independent data. Joints and fractures measured during fieldwork were not similar to the faults for this province, but segment datasets showed similarity for all segment lengths in 23 dataset comparisons (Table 21, Appendix D):

1. faults and all cave types
2. faults and fissure caves
3. faults and mixing zone cave penetrations
4. faults and mixing zone cave entrance widths
5. faults and mixing zone cave maximum widths
6. inland scarps and all cave types
7. inland scarps and fissure caves
8. inland scarps and mixing zone cave penetrations
9. inland scarps and mixing zone cave entrance widths
10. inland scarps and mixing zone cave maximum widths
11. coastal scarps and all cave types
12. coastal scarps and fissure caves
13. coastal scarps and mixing zone cave penetrations
14. coastal scarps and mixing zone cave entrance widths
15. all scarps and all cave types
16. all scarps and fissure caves
17. all scarps and mixing zone cave penetrations
18. all scarps and mixing zone cave entrance widths
19. all scarps and mixing zone cave maximum widths

20. coastlines and all cave types
21. coastlines and fissure caves
22. coastlines and mixing zone cave penetrations
23. coastlines and mixing zone cave entrance widths

SMALL-SCALE TEST SITES

Three one square kilometer tests sites (Figure 22, Appendix A; Carolinas Limestone Forest, Puntan Diapblo, and Unai Dangkolo) were analyzed separately to determine if orientation data from independent populations showed similarity at a smaller scale. Statistical comparisons were made for each of the three test sites using the same criteria as was used for the province and island scale comparisons. As in the larger scale orientation comparisons, datasets were considered to represent similar populations or population distributions if they showed a significance level less than 0.01 ($P \leq 0.01$) when compared using the Kolmogrov-Smirnov 2-sample test. The results of the comparisons for the test sites showed less similarity than the data evaluated over larger regions, but did show significant similarity.

Carolinas Limestone Forest

Statistical comparisons for the Carolinas Limestone Forest test site showed similarity for 64 (18.7 %) pairs of independent data. The test site included three fissure caves (Carolinas Fracture Cave, Plunder Cave, and Water Cave) and one mixing zone cave (Skip Jack Cave). No joint data was reported for this area, but fracture orientations measured in the field showed similarity to faults. Segment datasets showed similarity for all segment lengths in three dataset comparisons (Table 22, Appendix D):

1. faults and all cave types
2. faults and fissure cave
3. faults and mixing zone cave maximum widths

Puntan Diapblo

Statistical comparisons for the Puntan Diapblo test site showed similarity for 67 (16.4 %) pairs of independent data. The test site included three fissure caves (Death Fracture Complex) and nine mixing zone caves (Cavelet Cave, Dos Sakis Cave Complex, Flamingo Tail Cave Complex, Monica Cave, Orange Cave, and Liyang Diapblo). No joint data was reported for the area, but fracture orientations measured in the field showed similarity to faults, inland scarps, all cave types, fissure caves, mixing zone cave entrance widths, and mixing zone cave maximum widths. Segment datasets showed similarity to all segment lengths in two dataset comparisons (Table 23, Appendix D):

1. faults and inland scarps
2. faults and mixing zone cave penetrations

Unai Dangkolo

Statistical comparisons for the Unai Dangkolo test site showed similarity for 63 (44.7 %) pairs of independent data. The test site included one fissure cave (Dripping Tree Fracture Cave) and five mixing zone caves (Andyland Cave, John's Small Cave, Liyang Dangkolo, North and South Unai Dangkolo). No joint data was reported for the area and no scarps could be resolved from the DEM for the area. Fractures measured in the field showed similarity to the coastline, mixing zone cave penetrations, mixing zone cave entrance widths, and mixing zone cave maximum widths. Segment datasets showed similarity to all segment lengths in seven dataset comparisons (Table 24, Appendix D):

1. faults and coastlines
2. faults and mixing zone cave entrance widths
3. faults and mixng zone cave maximum widths
4. coastline and all cave types
5. coastline and fissure caves
6. coastline and mixing zone caves
7. coastline and mixing zone cave penetrations

DISCUSSION AND CONCLUSIONS

TINIAN CAVE AND KARST INVENTORY

The Tinian cave and karst inventory surveyed eighty-eight caves (Figure 23. Appendix A), located seventeen sites of freshwater discharge (Figure 24, Appendix A), and four allogenic recharge areas (Figure 27, Appendix A). Cave development on Tinian is dominated by mixing zone type caves (flank margin and banana hole type caves), but fissure caves account for twenty percent of the total. Only one pit cave and two recharge caves were identified (see Appendix B for maps and descriptions of individual cave and karst features).

The lack of pit caves and recharge caves suggests that these features are uncommon on Tinian; however, it is possible that more exist and that this is a sampling bias. Tinian experienced intense sugarcane farming during the Japanese occupation and extensive military construction by the U. S. and Japan during and after World War Two. If more of these features existed in the past, it is probable that they were infilled intentionally as part of island development or infilled by soil erosion from deforestation, farming and construction. Although soils may be limited in eogenetic karst environments, it is probable that the soil present will erode more easily as a result of human modification of the land surface.

Mixing zone caves were located in every physiographic province and at elevations from sea level to over 150 meters. Three caves were classified as banana holes because they are small features located shallow in the subsurface and are significantly wider than tall; however, these may represent small flank-margin caves. Most coves represent collapsed flank margin caves that have been breached by coastal processes (Figure 31, Appendix A), with speleothems and remnant cave chambers confirming their origin. One feature located north of Unai Dangkolo (Hidden Beach Cave, Figure 32, Appendix A) confirmed that these were collapsed flank margin caves because it was breached at sea level and contained a carbonate sand floor, but retained several regions of intact ceiling rock. Flank margin caves have a wide range of sizes, from a few square meters to the archetypical Tinian flank margin cave (Liyang Dangkolo, Figure 33, Appendix A) that is over 1,300 square meters. Smaller caves have single chambers and larger caves have central chambers with smaller, interconnected passages extending from them (Figure 12), demonstrating how mixing zone caves become interconnected as they grow in size (Figure 13). Horizons of flank margin cave development (Figure 14) occur at several locations, including Mendiola Cove, the southeastern portion of

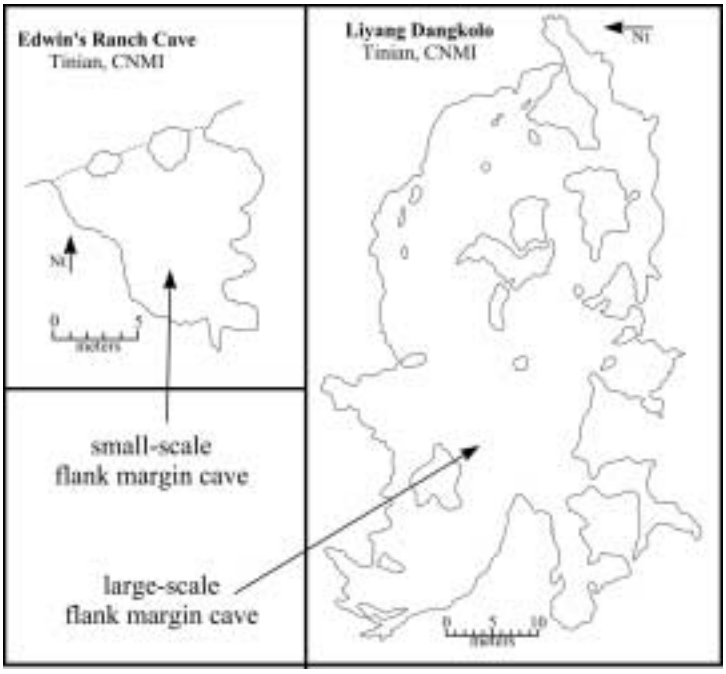

Figure 12: Flank margin caves develop more complicated morphologies as they grow in size as observed on Tinian (note these figures only include bedrock walls and columns in the cave maps).

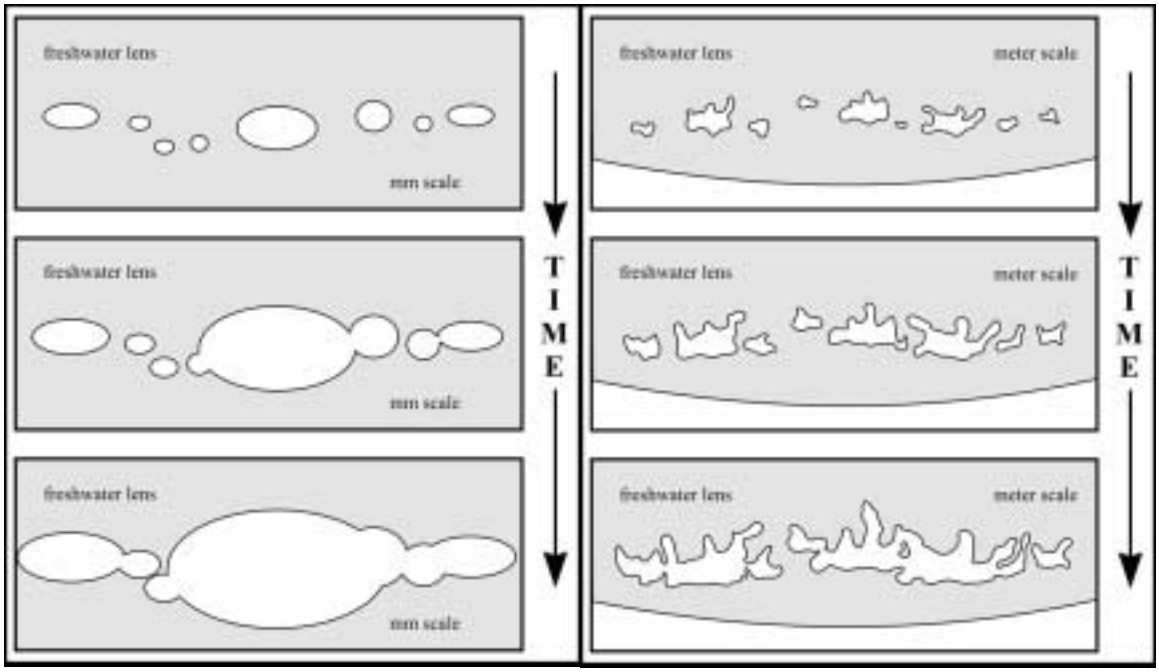

Figure 13: Conceptual model for the growth of flank margin caves. At small scales (vug scale) mixing zone dissolution forms simple ellipse because the rock is locally homogeneous. However, at larger scales (cave scale) inhomogeneities in rock form more complex morphologies with growth as a result of preferential dissolution of the bedrock.

Piña Ridge, Suicide Cliffs, Unai Dangkolo, and Unai Masalok. These horizons indicate at least three previous fresh-water lens positions on Tinian (Figure 34, Appendix A), but complex faulting prevents the direct correlation of horizons of mixing zone development across large regions.

Fissure caves show linear development that appears to be associated with brittle failure (Figure 35, Appendix A). They were located in all physiographic provinces except the North-Central Highland and at elevations ranging from sea level to over 100 meters. These caves can extend to significant depths when located in inland regions and provide fast flow routes for autogenic recharge. The deepest fissure cave (Masalok Fracture Cave) is 42 meters deep and has pools of fresh water at the bottom. Coastal fissure caves generally extend inland at angles near perpendicular to the coastline and frequently have fresh-water discharge associated with them. Other fissure caves (Plunder Cave and Water Cave) form broader, linear, dipping chambers with much collapse and are located near reported faults (Doan et al., 1960). No evidence of offset resulting from faulting could be seen in these caves, either because it does not exist or because extensive flowstone and speleothem development covering the walls obscured it (Figure 36, Appendix A).

Groundwater recharge on Tinian is primarily autogenic. Closed depressions and recharge caves in the North-Central Highland indicate allogenic recharge occurs where volcanic rocks crop out. The small igneous outcrop near the municipal well does not show direct evidence of supplying waters for allogenic recharge, but clays weathered from the volcanic exposure may be armoring the carbonate rock slope below, decreasing the effectiveness of autogenic recharge in these rocks and providing some allogenic recharge to the large closed depression where the municipal well is located. If this is occurring, this allogenic recharge is likely to be minimal because the igneous rocks crop out only on the steep

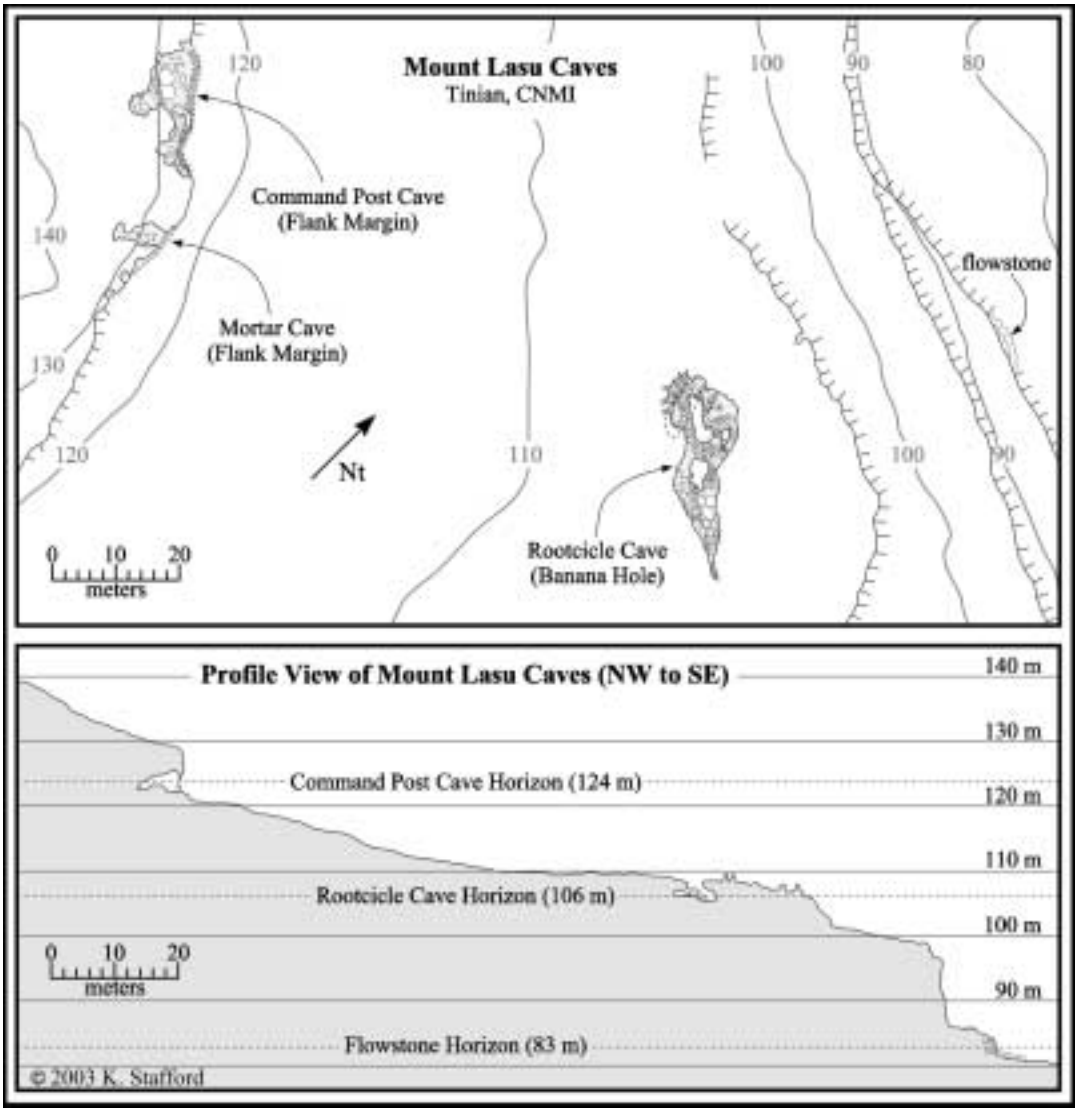

Figure 14: Multiple levels of mixing zone dissolution exist on Tinian with at least three identified in the North-Central Highland near Mount Lasu. However, more probably exist, but island faulting prevents correlation of horizons of development across large regions.

slope over a small area. In addition to the closed depressions that showed evidence of allogenic recharge, five closed depressions were identified as quarries or borrow pits. Although these features have autogenic recharge, recharge rates in these closed depressions is expected to be faster than in other regions of autogenic recharge because the soil cover and surface rock have been removed.

Fresh-water discharge was observed across much of the east and west coast. Much of the coastline could not be investigated due to strong surf; therefore, it is expected that many more discharge sites exist. The discharge sites that were located were generally associated with focused discharge along bedding planes or fractures, indicating that much of the fresh-water discharge is occurring along preferential flow routes, which would be expected to distort the lens morphology regionally. Areas near fissure caves that were discharging fresh-water did not have any

breached flank-margin caves nearby. This may indicate that these features have distorted the fresh-water lens to a great enough degree that the mixing zone caves are not forming in these areas or that they are developing further inland and have not been breached by coastal processes as have other flank margin caves seen along coastlines elsewhere.

AGUIJAN CAVE AND KARST INVENTORY

The cave and karst inventory surveyed 26 features on Aguijan (see Appendix B for maps and descriptions of individual cave and karst features); however, no site of fresh-water discharge was identified because the time was limited on the island and the coastline consists of large scarps that are subject to constant heavy surf. The inventory identified two banana holes, nineteen flank margin caves, five fissure caves, and one problematic cave. According to local guides, these 26 features represent the majority of the caves on Aguijan. The general morphology of Aguijan appears similar to the Carolinas Ridge on Tinian and is expected to have a similar geologic history, although no detailed geologic studies have been conducted on Aguijan to confirm this.

Fissure and mixing zone caves are located at all three terrace levels and on all sides of the island. Boonie Bee Sink may be a small flank margin cave, but because of its general morphology it was classified as a banana hole. The flank margin caves range in size from a few square meters to hundreds of square meters. The fissure caves show three distinct morphologies, which appear to correspond with the morphologies seen on Tinian. Two of the fissure caves (Insect Bat Cave and Toppled Column Cave), located at the edge of the middle terrace, are similar to freshwater discharge caves seen on Tinian and Guam (Taborosi, 2002), but do not discharge freshwater. These two features have been identified as paleo-discharge features (Figure 37, Appendix A).

The one problematic cave (Liyang Atkiya) does not show typical island karst development. It consists of a large entrance chamber, which descends steeply and is floored with breakdown. At the base of this chamber, the walls and floor are coated with a thick coating of dark sediment. The chamber also contains several small pools of water. Extending from the large chamber, a linear passage continues for several hundred meters, while continuing to descend gradually. Old Scallops on the walls of this linear passage indicate that in the past water was flowing upwards from deeper in the cave towards the entrance chamber (Figure 38, Appendix A). The linear passage eventually splits and small mazelike tubes are encountered, which were not completely surveyed. The origin of this feature is problematic because scallops are not normally seen in island karst because of the dominance of mixing zone dissolution. Kalabera Cave on Saipan contains scallops (Jenson et al., 2002), which indicate that water was rising as a lift tube along a lithologic barrier of non-carbonate rocks. However, the lack of evidence of non-carbonate rocks in Liyang Atkiya prevents applying the Kalabera Cave model to this cave. Another investigator sampled black sediments from Liyang Atkiya. Analysis of this material may provide further insight into the origin of this cave.

CONTROLS ON CAVE AND KARST DEVELOPMENT

The second objective of this study is to determine if comparisons of cave development orientation trends to brittle failure trends show similarity that would indicate structural influence on eogenetic karst development or if karst development is related to scarp and coastline positions where the margin of the paleo or current fresh-water lens is expected to be. Cave and karst development in continental settings is significantly influenced by geologic structure and lithology (Klimchouk and Ford, 2000; White, 1988), while island karst is dominated by mixing zone dissolution

with the fresh-water lens position significantly influencing porosity development. Jenson and coworkers (Jenson et al., 2002; Mylroie et al., 2001) have recently recognized the importance of structural and geologic controls on eogenetic, island karst development, but the extent of the influence that geologic structure and lithology have on carbonate island karst development has not been well studied. The morphological difference in fissure caves and mixing zone caves suggests that each class of cave development is dominated by different controls on dissolution. A simple comparison of the length to width ratio for fissure caves and mixing zone caves shows that these two general cave types represent different populations (Figure 15).

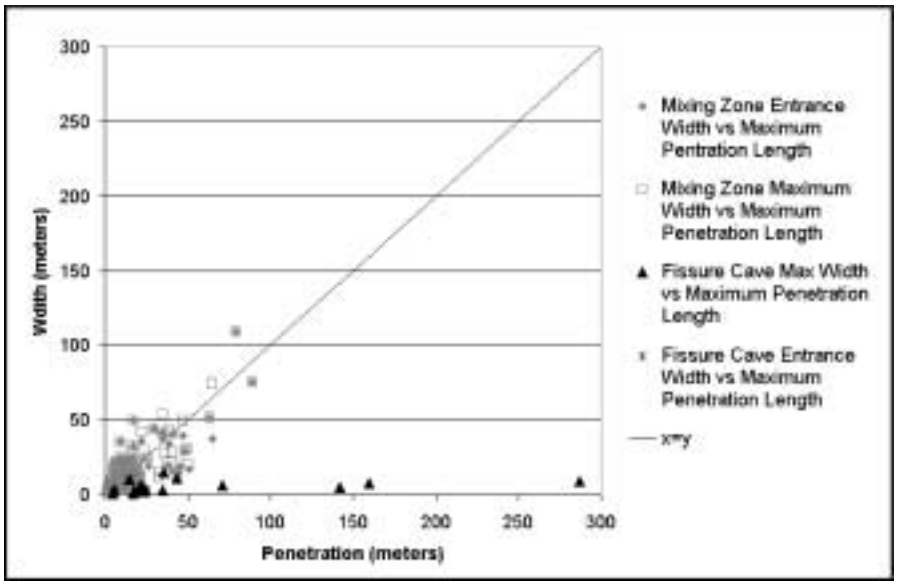

Figure 15: Diagram showing the relationship between cave widths and lengths, which represent two distinct populations for fissure caves and mixing zone caves. Note that as flank margin caves grow in size they have a length to width ratio close to one.

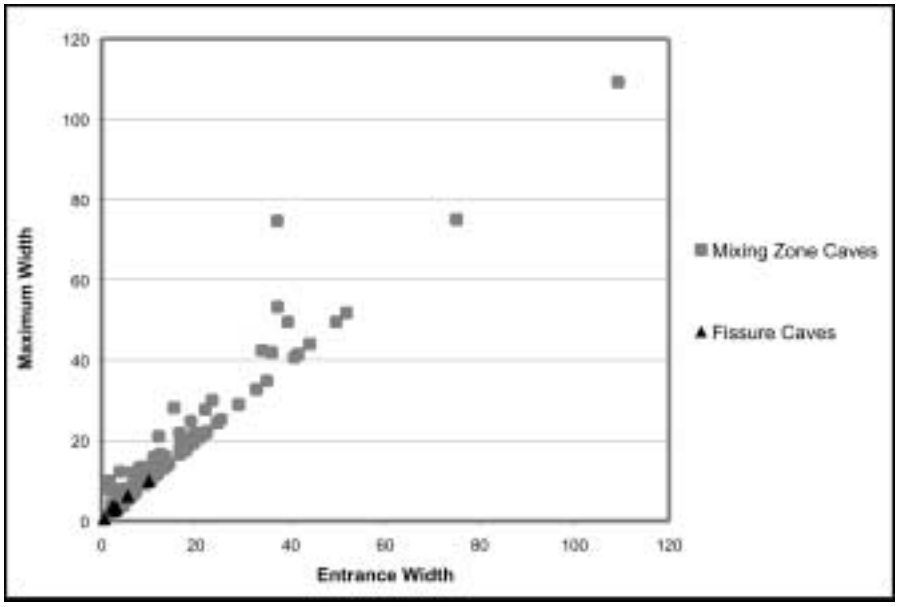

Figure 16: Diagram showing the relationship cave entrance width and cave maximum width. Note that a large portion of the caves plot with a ratio of one, indicating that the entrance width and the maximum width are the same.

This portion of the study was only conducted on data from Tinian, where the geology and structural deformation had been mapped (Doan et al., 1960), because of the focus on the relationship between zones of brittle failure and karst development. Several biases may have been introduced into the data that would affect the results of the comparison of orientation populations. It is inevitable that in the cave and karst

inventory some features were not inventoried because of time constraints in the field, dense vegetation concealing entrances, safety issues, or because the caves must be breached in order to enter and survey them. The methodology used for determining cave orientations was subjective and depended on the accuracy of the cave survey and the parameters used to determine orientations, especially in mixing zone caves that are globular or elliptical. The segment lengths that were used in comparisons had the potential of introducing error using the Kolmogorov-Smirnov 2-sample test (Nelson, 1988; Barlow and Ogden, 1992), therefore two sets of segment data were used for all orientation categories. Data types were only considered to be similar if they showed similarity amongst all segment lengths for those data pairs being compared. The degree of breaching may have biased the data, where collapse, cliff retreat or coastal erosion removed portions of the original cave, leaving an incomplete remnant. If a flank margin cave were modeled as a simple ellipse or if flank margin caves are linear features developed parallel to the cliff, then removal of one half or more of the feature by erosion would make the entrance width and the maximum width of the feature the same. In many cases, it appears that at least 50% of the original flank-margin caves had been removed by cliff retreat (Figure 16). The cell size of the DEM limited the resolution of scarps and coastlines. The measurement of fracture orientations in the field was subject to human error, as were the faults and joints reported by Doan and coworkers (1960), which were based on interpretation of data gathered during fieldwork conducted in the 1950's. All of these biases may have affected the comparison of independent data populations, therefore only data pairs that showed a high degree of similarity ($P \leq 0.01$) were considered to be related.

Comparisons between orientations of brittle failure features, scarp and coastline orientations, and cave primary and segment orientations show a wide range of orientation trends at the island and province scale, but more distinct trends at smaller-scale test sites. This wide range of variability at the larger scales may be the result of the physiographic nature of islands. Coastline and scarp orientation trend datasets show a wide range of orientation trends at large region or entire island scales because of the roughly elliptical shape of islands. Island coastlines have orientation trends between 0^o and 360^o because islands are surrounded on all sides by water, therefore a wide range of orientations exist for coastline orientations at the island scale. Similarly, any ridge that may produce scarps will be roughly elliptical in shape and also show a wide range of orientations. However, trend orientations associated with the long axis of these features will show greater dominance as the length to width ratio increases ($L/W > 1$) for the island and scarps (Figure 17).

The orientations of brittle deformation structures reported by Doan and coworkers

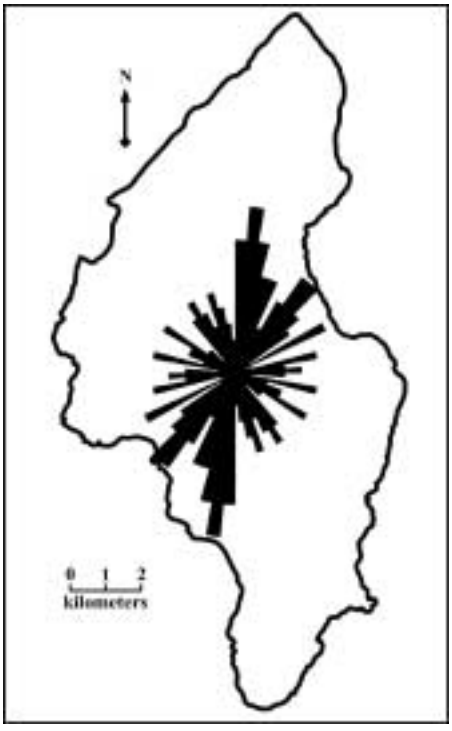

Figure 17: Coastline orientations for Tinian show a wide range of trends because of the elliptical shape of the island. Note that the rose diagram pattern for coastlines resembles the coast outline of Tinian.

(1960) and those measured during fieldwork show a wide range of trends. This is probably the result of Tinian's complex tectonic setting. Tinian is a Paleogene volcanic edifice mantled by younger carbonate rocks with complex, high-angle normal faulting throughout the island. The geomorphology of Tinian is primarily controlled by three factors: 1) the original volcanic depositional regime, 2) the original carbonate depositional regime, and 3) structural deformation primarily in the form of brittle failure. The coastlines of Tinian are primarily erosional, with modern carbonate beach deposits representing less than 5% of the coastline (light blue regions in Figure 39, Appendix A), and strongly influenced by geologic structure. Because of the erosional nature of the coastline and the geomorphology of Tinian, three types of brittle failure are expected to exist (Figure 38): 1) regional faulting associated with island arc tectonism, 2) brittle failure near-parallel to coastlines associated with margin failures, and 3) brittle failure near-perpendicular to coastlines associated with tension release structures that form perpendicular to margin failures (Doan et al., 1960). In addition to the three primary types of brittle failure expected, rock units may also be fractured by passive, isostatic subsidence (>0.05 mm/yr, Dickinson, 1999). The combination of the faulting and fracturing from subsidence and margin failure creates great variability in the orientations of brittle failure features observed on Tinian.

ISLAND SCALE COMPARISONS

At the island scale, comparisons showed 60% similarity in paired, independent samples. This high degree of similarity appears to indicate that the complex nature of brittle deformation and the great variability of coastline and scarp orientations make it impossible to differentiate between relationships at the island scale. The similarity also does not enable the elimination of variables that may not be influencing cave and karst development, because scarps, coastlines, brittle failure features and cave development all show similarities indicating that at large scales the interaction of these variables is too complex to define cause and affect. However, rose diagrams show that, at the island scale, scarps are the only features that show similarity to cave development, suggesting that cave development is primarily controlled by the position of the fresh-water lens if the scarps do represent paleo-coastlines, as predicted in the Carbonate Island Karst Model (Stafford et al., 2003; Jenson et al., 2002; Mylroie and Jenson, 2002; Mylroie and Jenson, 2001).

PROVINCE SCALE COMPARISONS

At the physiographic province scale, fewer independent pairs showed similarity; however, rose diagrams showed more similar pairs. Data for the Northern Lowland and North-Central Highland showed the least degree of similarity in comparisons, which is probably due to a sampling bias of cave and karst features. Only two features were located in the Northern Lowland (one fissure cave and one mixing zone cave) and eight mixing zone caves were located in the North-Central Highland. Therefore, these small sample sizes suggest that these regions do not have enough data to be analyzed with any confidence. The other physiographic provinces produced larger datasets and appeared to have less sampling bias.

The cave inventory of the Central Plateau surveyed 5 fissure caves and 46 mixing zone caves. Rose diagrams show no distinct similarities amongst independent orientation populations. However, statistical analysis of the data showed significant similarity in 45% of the independent sample pairs. Analysis of the data showed similarity between faults, scarps, coastlines, fissure caves and mixing zone caves. This presents the same problem as the island-scale analyses. The Central Plateau, which extends from the east coast to the west coast, exhibited too much variability in the data to determine if brittle failure features,

coastlines or scarps were the dominant control on cave development. The data for the Central Plateau suggests that brittle failure does significantly influence cave development in the region. In the Central Plateau similarity with caves to scarps and coastlines (paleo and modern fresh-water lens) appeared to dominate in all cases except fissure caves, which only showed significant similarity to faults.

The cave inventory of the Median Valley surveyed 5 fissure caves and 27 mixing zone caves. Rose diagrams showed similarities between fractures, scarps, and mixing zone cave entrance widths, suggesting that the breaching of mixing zone caves is associated with scarp failure as expected. Statistical analysis of data showed significant similarity for 43% of the independent data pairs, with similarity between faults, scarps, coastlines and cave development. The only statistical similarity seen for fissure caves was with coastlines. The Median Valley, which extends from the east coast to the west coast, again showed too much variability in the data to determine if brittle failure features, coastlines or scarps were the dominant control on cave development. The similarity between fissure caves segments and coastlines, suggests that the fissure caves in this region are associated with bank-margin failure and not regional faulting; however, the segment data is being highly biased towards one cave (Dripping Tree Fracture Cave) that is significantly longer than the other fissure caves combined.

Seven fissure caves and forty-six mixing zone caves were inventoried on the Southeastern Ridge. Rose diagrams showed more distinct similarities in this province than in others. Fault orientations appeared similar to mixing zone primary orientations and penetrations, while scarps and coastlines showed similarity to mixing zone cave widths. Statistical analysis showed similarities for 53% of the independent data pairs, with similarity between faults, scarps, coastlines and cave development. As in the Central Plateau and Median Valley, the data showed too much variability to determine the dominant control on cave development. However, the data for the Southeastern Ridge suggests that the fissure caves in this region are associated with scarp failures, while mixing zone caves are controlled by a combination of fault and fresh-water lens position. Mixing zone cave penetration shows significant similarity to faults, while mixing zone cave widths are significantly similar to scarps and coastlines. This suggests that mixing zone dissolution at the edge of the fresh-water lens expanded laterally in relation to the edge of the lens and inland in relation to regional fault patterns.

SMALL-SCALE TEST SITE COMPARISONS

The one square kilometer test sites showed a lesser degree of orientation variability than was observed in the larger-scale comparisons. Because these were only test sites used to evaluate whether or not orientation similarities exist at different scales on the island, no rose diagrams were used. Instead, analyses were limited to statistical comparisons. The three test sites chosen for small-scale analyses all contained fissure caves, mixing zone caves, faults, and coastline, and were locations where fractures had been measured in the field.

The Carolinas Limestone Forest test site contained three fissure caves and one mixing zone cave. Data analyses showed similarities for 19% of the independent data pairs. Fractures measured in the field showed significant similarity to regional faults. Segment analyses only showed significant similarity for all segment lengths in three data pairs. The significantly similar segment orientations were all related to regional faults and caves, with faults being similar to fissure caves, mixing zone cave maximum widths and all cave type orientations. This data suggests regional faulting controls fissure caves in this area. The similarities between all cave types and mixing zone caves are not considered reliable because of the small sampling size

of mixing zone caves for this regions, but the do suggest that regional brittle deformation may be affecting mixing zone development.

The Puntan Diapblo test site contained three fissure caves and nine mixing zone caves. Data analyses showed similarities for 16% of the independent data pairs. Fractures measured in the field showed similarity to faults, scarps, fissure caves and mixing zone cave widths. As in the Carolinas Limestone Forest test site, similarity between segment orientations were only seen in relation to faults. Faults were similar to inland scarps and mixing zone cave penetrations, suggesting regional jointing and faulting influence mixing zone cave development. The lack of similarity between faults and the fissure cave development does not mean that these fissure caves are not controlled by brittle deformation. Similarity seen between fractures measured in the field and the fissure caves suggests that these fissure caves are controlled by fractures that are near perpendicular to the coastline and may be related to unloading structures associated with regional isostatic subsidence or tension release features.

The Unai Dangkolo test site contains one fissure cave and five mixing zone caves. Data analyses showed similarities for 45% of the independent data pairs, which appears high. Data for this test site was limited because analyses of the DEM showed that no major scarps exist in this area. Fractures measured during fieldwork and faults both showed similarity to the coastline and mixing zone cave development. Coastline orientations showed similarity to fissure caves and mixing zone caves. This data suggests that mixing zone caves in this area are influenced by both the coastline (edge of the fresh-water lens) and regional faulting. Fissure cave development appears to be completely associated with coastlines, suggesting that Dripping Tree Fracture cave is related to bank-margin failure parallel to the coastline.

STRUCTURAL CONTROL OF CAVES

Eogenetic karst development on Tinian is dominated by mixing zone dissolution; however, brittle deformation appears to have a significant influence. Seventy-seven percent of the caves surveyed on Tinian are mixing zone caves, while only twenty percent are fissure caves. These two groups of caves are significantly different and their developmental controls are different.

Orientations of fissure caves showed significant similarity to zones of brittle failure; however, the type of brittle failure is varied. Independently, orientations of fissure caves show similarities to regional faulting, jointing, coastline and scarp position. The statistical comparisons imply that fissure cave development is controlled by brittle failure that results from island tectonism (high-angle faulting), passive isostatic subsidence (joints), and scarp failure (fractures). Additionally, most fresh-water discharge observed on Tinian was associated with fissure caves or smaller-scale dissolutionally widened bedrock fractures.

Mixing zone caves appear to be primarily controlled by the fresh-water lens position; however, orientation similarities between mixing zone caves and brittle deformation features exist in analyses ranging from the small-scale test areas to the entire island of Tinian. Although the relationships are not consistent from region to region, analyses of the orientation data suggest that brittle deformation does significantly affect mixing zone development.

KARST DEVELOPMENT ON AGUIJAN AND TINIAN

This study indicates that karst development on Tinian is dominated by mixing zone dissolution, but that geologic structure, in the form of brittle deformation, plays a significant role. Significant similarities between independent populations or population distributions confirm that the structural controls on fissure cave development inferred from cave

morphology are correct and that mixing zone caves are being significantly influenced by brittle failure. Based on the presence of at least three zones of mixing zone cave development, it is believed that Tinian and Aguijan have experienced several stable sea-level stillstands that lasted for significant periods. These horizons probably represent previous sea-level stillstands related to glacio-eustacy with constant uplift; however, they may indicate episodic island uplift. Some flank-margin caves are vertically exaggerated; suggesting slow uplift, slow sea level change or a combination of the two at times.

The data indicate that Tinian does not conveniently fit in to any single model for carbonate island karst. The data do not suggest that Tinian is a Complex Carbonate Island because no intricate interfingering of carbonate and non-carbonate facies were identified, although the island does show a high degree of faulting. The high-angle faulting does appear to separate the island into distinct regions and significantly distort the fresh-water lens as indicated by fresh-water discharge sites identified near the boundaries between the Median Valley and Southeastern Ridge and between the Northern Lowland and Central Plateau. The Northern Lowland best fits the Simple Carbonate Island Karst Model, with fresh-water exposed at the surface at Hagoi and no non-carbonate rocks cropping out. The Southeastern Ridge best fits the Carbonate-Cover Island Karst Model, with several areas of mixing zone cave development and non-carbonate rocks that outcrop, but do not show any direct evidence of allogenic recharge. The Central Plateau, North-Central Highland and Median Valley cannot be easily fit into separate models, but together best fit the Composite Island Karst Model with allogenic recharge occurring at the non-carbonate / carbonate rock contacts in the North-Central Highland. Because the central portion of the Tinian best fits the Composite Island Karst Model, the entire island must be classified as this although the northern and southern portions of the island do not represent this model well.

Aguijan can only be classified as a Simple Carbonate Island because only carbonate rocks are known. However, the geomorphology of Aguijan is similar to that of the Southeastern Ridge of Tinian, indicating that it is most likely a Carbonate-Cover Island. Further complicating the interpretation of Aguijan is Liyang Atkiya, which may indicate some complex interaction between carbonate and non-carbonate rocks.

SUMMARY

This study inventoried and surveyed 26 cave and karst features on Aguijan and 88 cave and karst features on Tinian and is believed to have adequately sampled the cave and karst development on the islands, although it is probable that more features exist. Two distinct classes of cave and karst features were identified: mixing zone caves (flank margin and banana hole type caves) and fissure caves (linear caves associated with planes of brittle failure). Most mixing zone caves are located in or near scarps and coastlines, at elevations from sea level to 160 meters, have areas from a few square meters to more than 1300 square meters, and are often at consistent levels with nearby caves. At least three distinct horizons of breached mixing zone caves occur on Tinian, representing previous fresh-water lens positions that have been tectonically uplifted and breached by erosional processes. Fissure caves were located in regions that showed evidence of brittle failure produced from active tectonic uplift, passive isostatic subsidence, or bank margin and smaller scale scarp failure. The fissure caves range in length from a few tens of meters to hundreds of meters and are

relatively narrow. Some of these features reached significant depth. The fissure caves show direct evidence of vadose fast flow routes, which can rapidly transmit fluids more than 40 meters into the subsurface and can distort the fresh-water lens morphology. Although some fissure caves extended over longer distances and to greater depths than the mixing zone caves, mixing zone caves were found to be significantly more abundant (mixing zone cave / fissure caves = 4).

In addition to the karst inventory, fresh-water discharge and allogenic recharge sites were investigated. Along the coastline of Tinian, 17 fresh-water discharge sites were identified, many associated with sea level caves. No active discharge sites were identified on Aguijan because strong surf conditions prevented exploration, but two paleo-discharge sites were identified on the Middle Terrace. Four closed depressions were identified as sites of allogenic recharge on Tinian at contacts between non-carbonate igneous outcrops and carbonate rocks, including two with caves that receive direct recharge. No allogenic recharge sites were identified on Aguijan because only carbonate rocks outcrop on the island.

Orientation data showed that brittle failure features significantly influence karst development on Tinian. At the island scale and regional scale, it is difficult to determine if megaporosity (cave) development is associated with geologic structure or with fresh-water lens position (scarps and coastlines), because of the wide range of data orientations on Tinian, resulting from the island geomorphology and complex tectonic setting. However, similarities between data populations or population distributions suggest that geologic structure does affect karst development. At smaller scales, more direct evidence of structural controls on megaporosity development are seen, probably resulting from the narrower range of orientation data present at these scales because of smaller sample sizes.

Analyses of cave maps in relation to brittle failure and island geomorphology indicates that the interpretations for origin of fissure caves that have been inferred from cave morphology are correct. Fissure cave orientation trends in the vicinity of faulting show significant similarity to faults, implying that the caves formed along preferential flow paths created by faulting. Fissure cave orientation trends near coastlines and scarps show significant similarities to nearby fractures, implying that the caves formed along preferential flow paths created by bank-margin and smaller-scale scarp failure or in relation to tension release structures. Orientations of mixing zone caves show significant similarities to scarps and coastlines, implying that the caves formed in relation to the edge of the fresh-water lens. However, mixing zone caves often show similarities with brittle failure features, suggesting that mixing zone caves are significantly influenced by geologic structure, although mixing zone dissolution along the edge of the fresh-water lens is the dominant controlling factor. Clearly, the interaction between megaporosity development and brittle deformation on carbonate islands is complex, often resulting in features that are primarily controlled by different factors (fresh-water lens position or brittle deformation) developing close to each other (Figure 18).

Tinian and Aguijan show that the Carbonate Island Karst Model cannot be simply applied to entire carbonate islands that occur in complex tectonic settings. In order to apply the Carbonate Island Karst Model to Tinian it must be divided into different regions. The Northern Lowland best fits the Simple Carbonate Island Karst Model. The Southeastern Ridge best fits the Carbonate-Cover Island Karst Model. The North-Central Highland, Central Plateau, and Median Valley cannot be easily separated, but when grouped together best fit the Composite Island Karst Model. Aguijan must be classified as a Simple Carbonate Island because no proof has been found to confirm that the island has a core of non-carbonate rocks that extend above sea

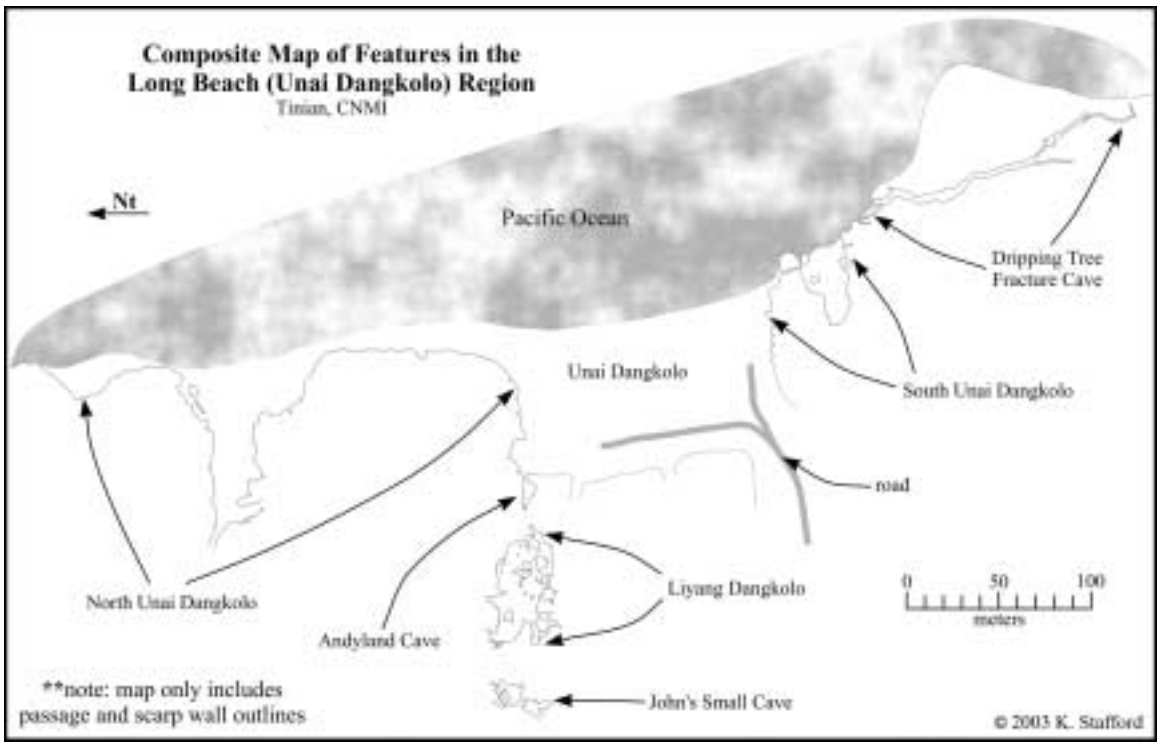

Figure 18: Map of Unai Dangkolo region showing the close proximity of lank margin cave and fissure cave development.

level and partition the fresh-water lens. However, based on Aguijan's similarity with the Southeastern Ridge of Tinian it probably best fits the Carbonate-Cover Island Karst Model.

Geologic investigations on the islands of Tinian and Aguijan have been limited in the past and much remains to be done in future research, which is beyond the scope of this study. The cave and karst inventory surveyed the majority of known cave and karst features on Tinian and Aguijan; however, more features exist which need to be identified and surveyed. Basic geologic mapping is still needed for the island of Aguijan. During this study, the author and other investigators sampled speleothems, paleosols, and cave sediments, which may provide greater insight into the geology and hydrogeology of the Mariana Islands. Future isotope analysis of speleothems and petrographic analysis of paleosols may provide important information about the paleoclimatic history of the region, while future analysis of cave sediments may elucidate the origin of Liyang Atkiya.

REFERENCES CITED

Aby, S.B., 1994. Relation of bank-margin fractures to sea level change, Exuma Islands, Bahamas. Geology, v. 22, pp. 1063-1066

Back, W., Hanshaw, B.B., and Van Driel, J.N., 1984. Chapter 12, Role of groundwater in shaping the Eastern Coastline of the Yucatan Peninsula, Mexico. *in* LaFleur, R.G. (Editor), Groundwater as a Geomorphic Agent, Allen & Unwin, Inc., Boston, pp. 281-293.

Barlow, C.A., and Ogden, A.E., 1992. A statistical comparison of joint, straight cave segment, and photo-lineament orientations. NSS Bulletin, v. 44, pp. 107-110.

Bormann, N.E., 1992. Ground-water resources management on Tinian, CNMI. American Water Resources Association technical publication series, v. 92-1, pp. 35-44.

Burke, H.W., 1953. The Petrography of the Mariana Limestone, Tinian, Mariana Islands. Graduate dissertation, Stanford University, 111 p.

Burt, J.E., and Barber, G.M., 1996. Elementary Statistics for Geographers: Second Edition. The Gulford Press, New York, NY, 640 p.

Butler, B.M, 1992. An Archaeological Survey of Aguiguan (Aguijan), Northern Mariana Islands: Micronesian Archaeological Survey Report Number 29. The Micronesian Archaeological Survey. Division of Historic Preservation, Dept. of Community and Cultural Affairs, Saipan, MP, 260 p.

Carew, J.L., and Mylroie, J.E., 1995. Quaternary tectonic stability of the Bahamian Archipelago: evidence from fossil coral reefs and flank margin caves. Quaternary Science Reviews, v. 14, pp. 145-153.

Cloud, P.E., Jr., Schmidt, R.G., and Burke, H.W., 1956. Geology of Saipan, Mariana Islands, Part 1. General Geology. 280-A, U.S. Geological Survey Professional Paper, U.S. Government Printing Office, Washington, D.C., pp. 126.

Dasher, G.R., 1994. On Station. National Speleological Society, Inc., Huntsville, Alabama, 242 p.

Dickinson, W.R., 1999. Hydro-isostatic and tectonic influences on emergent Holocene paleoshorelines in the Mariana Islands, Western Pacific Ocean. Journal of Coastal Research, v. 16, no. 3, pp. 735-746.

Doan, D.B., Burke, H.W., May, H.G., Stensland, C.H., and Blumenstock, D.I., 1960. Military Geology of Tinian, Mariana Islands. Chief of Engineers, U.S. Army, 149 p.

ESRI, 2000. ArcView GIS 3.2. Environmental Systems Research Institute, Inc., software.

Folk, R.L., Roberts, H.H., and Moore, C.C., 1973. Black phytokarst from Hell, Cayman Islands, British West Indies. Geological Society of America Bulletin, v. 84, pp. 2351-2360.

Frank, E.F., Mylroie, J.E., Troester, J., Alexander, E.C., and Carew, J.L., 1998. Karst development and speleologensis, Isla de Mona, Puerto Rico. Journal of Cave and Karst Studies, v. 60, no. 2, pp. 73-83.

Gingerich, S.B., and Yeatts, D.S., 2000. Ground-Water Resources of Tinian, Commonwealth of the Northern Mariana Islands, Water-resources Investigations Report 00-4068. U.S. Department of the Interior, 2 sheets.

Gross, M.G., 1982. Oceanography: A View of the Earth. Prentice-Hall, Inc., Eaglewood Cliffs, NJ, 498 p.

Harris, J.F., Mylroie, J.E. and Carew, J.L., 1995. Banana holes: Unique karst features of the Bahamas. Carbonates and Evaporites, v. 10, no. 2, pp. 215-224.

Holcombe, R., 2003. GEOrient 9.2. Department of Earth Sciences, University of Queensland, Australia.

http://www.earth.uq.edu.au/~rodh/software/

Hunt, E., and Wheeler, T., 2000. South Pacific. Lonely Planet Publications, Oakland, CA, 928 p.

Jenson, J.W., Jocson, J.M.U., and Siegrist, H.G., 1997. Groundwater discharge styles from an uplifted Pleistocene island karst aquifer, Guam, Mariana Islands. *in* Beck, B.F. and Stephenson, J.B. (Editors), The Engineering Geology of Karst Terraines, Balkema, Springfield, Missouri. pp. 27-32.

Jenson, J.W., Mylroie, J.E., Mylroie, J.R., and Wexel, C., 2002. Revisiting the carbonate island karst model. Geological Society of America Abstracts with Program, v. 34, no. 6, p. 226.

Jocson, J.M.U., Jenson, J.W., and Contractor, D.N., 2002. Recharge and aquifer responses: Northern Guam Lens Aquifer, Guam, Mariana Islands. Journal of Hydrology, v. 260, pp 231-254.

Jocson, J.M.U., Jenson, J.W., and Contractor, D.N., 1999. An Integrated Numerical Modeling Study and Field Investigation of the Northern Guam Lens Aquifer. Technical Report #88, Water and Environmental Research Institute of the Western Pacific, University of Guam, Mangilao, 34 p.

Klimchouk, A., and Ford, D., 2000. Chapter 3.2, Lithologic and structural controls of dissolutional cave development. *in* Klimchouk, A., Ford, D., Palmer, A., and Dreybrodt, W. (Editors), Speleogenesis: Evolution of Karst Aquifers. National Speleological Society, Huntsville, AL, pp. 54-64.

Mink, J.F., and Vacher, H.L., 1997. Hydrogeology of northern Guam. *in* Vacher, H.L., and Quinn, T. (Editors), Geology and Hydrogeology of Carbonate Islands. Developments in Sedimentology 54, Elsevier Science, pp. 743-761.

Miller, R.L., and Kahn, J.S., 1962. Appendix G: The Kolmogorov-Smirnov Statistic. in. Miller, R.L., and Kahn, J.S., Statistical Analysis in the Geological Sciences. John Wiley and Sons, Inc., New York, NY, pp. 464-468.

McClure, G.E., 1977. Tinian, Then and now..: 5th edition. Glenn E. McClure, Universal City, TX, 28 p.

McKenzie, D., 2002. WALLS Project Editor – Beta Version 2.0 B6. http://davidmck.home.texas.net/walls/, shareware software.

Mylroie, J.E., and Carew, J.L., 1997. Land use and carbonate island karst. *in* Beck and Stephenson (Editors), The Engineering and Hydrology of Karst Terranes. Balkema, Rotterdam, pp. 3-12.

Mylroie, J.E., and Carew, J.L., 1995a. Karst development on carbonate islands. *in* Budd, D.A., Harris, P.M., and Staller, A. (Editors), Unconformities and Porosity in Carbonate Strata. American Association of Petroleum Geologists, pp. 55-76.

Mylroie, J.E., and Carew, J.L., 1995b. Geology and karst geomorphology on San Salvador Island, Bahamas. Carbonates and Evaporites, v. 10, no. 2, pp. 193-206.

Mylroie, J.E., and Carew, J.L., 1991. Erosional notches in Bahamian carbonates: bioerosion or groundwater dissolution?. *in* Bain, R.J. (Editor), Proceedings of the Fifth Symposium on the Geology of the Bahamas. Bahamian Field Station, San Salvador, Bahamas, pp. 185-191.

Mylroie, J.E., Carew, J.L., and Vacher, H.L., 1995a. Karst development in the Bahamas and Bermuda. In: Curran, H.A., and White, B. (Editors), Terrestrial and Shallow Marine Geology of the Bahamas and Bermuda, pp. 251-267.

Mylroie, J.E., Carew, J.L., and Moore, A.I., 1995c. Blue hole: definition and genesis. Carbonates and Evaporites, v. 10, no. 2, pp. 225-233.

Mylroie, J.E., and Jenson, J.W., 2002. Karst flow systems in young carbonate islands. *in* Martin, J.B., Wicks, C.M.,

and Sasowsky, I.D. (editors), Hydrogeology and biology of post-Paleozoic carbonate aquifers. Karst Waters Institute Special Publication Number 7, Karst Waters Institute, Inc., Charles Town, WV, pp. 107-110.

Mylroie, J.E., and Jenson, J.W., 2001. The carbonate island karst model applied to Guam. Theoretical and Applied Karstology, v. 13-14, pp. 51-56.

Mylroie, J.E., Jenson, J.W., Jocson, J.M.U., and Lander, M., 1999. Karst Geology and Hydrology of Guam: A Preliminary Report, Technical Report #89. Water and Environmental Institute of the Western Pacific, University of Guam, Mangilao, 32 p.

Mylroie, J.E., Jenson, J.W., Taborosi, D., Jocson, J.M.U., Vann, D., and Wexel, C., 2001. Karst features of Guam in terms of a general model of carbonate island karst. Journal of Cave and Karst Studies, v. 63, no. 1, pp. 9-22.

Mylroie, J.E., Panuska, B.C., Carew, J.L., Frank, E., Taggart, B.E., Troester, J.W., and Carrasquillo, R., 1995b. Development of flank margin caves on San Salvador Island, Bahamas and Isla de Mona, Puerto Rico. *in* Boardman, M. (Editor), Proceedings of the Seventh Symposium on the Geology of the Bahamas. Bahamian Field Station, San Salvador, Bahamas, pp. 49-81.

Mylroie, J. E., and Vacher, H. L., 1999. A conceptual view of carbonate island karst. *in* Palmer, A. N., Palmer, M. V., and Sasowsky, I. D. (Editors), Karst Modeling, Karst Waters Institute Special Publication 5, Karst Waters Institute, Inc., Charles Town, WV, pp. 48-57.

Nelson, J.W., 1988. Structural and Geomorphic Controls of the Karst Hydrogeology of Franklin County, Alabama [MS Thesis]. Mississippi State University, 165 p.

Palmer, A.N., 1991. Origin and morphology of limestone caves. Geological Society of America Bulletin, v. 103, pp. 1-21.

Raeisi, E., and Mylroie, J.E., 1995. Hydrodynamic behavior of caves formed in the fresh-water lens of carbonate islands. Carbonates and Evaporites, v. 10, no. 2, pp. 207-214

Reagan, M.K., and Meijer, A., 1984. Geology and geochemistry of early arc-volcanic rocks from Guam. Geological Society of America Bulletin, v. 95, pp. 701-713.

Sasowsky, I.D., and White, W.B., 1994. The role of stress release fracturing in the development of cavernous porosity in carbonate aquifers. Water Resources Research, v. 30, no. 12, pp. 3523-3530.

Siegrest, H.G., 1988. Miocene reef carbonates of the Mariana Islands. American Association of Petroleum Geologists Bulletin, v. 72, no. 2, p. 248.

Sprouse, P., 1991. Proyecto Espeleologico Purificacion: Standard cave map symbols. The Death Coral Caver, no. 2, p. 37.

Sprouse, P., and Russell, W., 1980. AMCS cave map symbols: AMCS Activities Newsletter, no. 11, pp. 64-67.

Stafford, K.W., Mylroie, J.E., Mylroie, J.R., and Jenson, J.W., 2003. Tinian, CNMI: A carbonate island karst model evaluation. Geological Society of America abstracts with programs, v. 35, no. 1, p. 54.

Stafford, K.W., Mylroie, J.E., and Jenson, J.W., 2002. Karst Geology and Hydrology of Tinian and Rota (Luta), CNMI: Technical Report No. 96. Water and Environmental Institute of the Western Pacific, University of Guam, Mangilao, 31 p.

Stafford, K.W., Mylroie, J.E., Mylroie, J.R., and Jenson, J.W., 2003. Tinian, CNMI: A carbonate island karst model evaluation. Geological Society of America Abstracts and Programs, v. 35, no. 1, p. 3.

Sugiwara, S., 1934. Topography, Geology, and Coral Reefs of Rota Island. Pacific Geological Surveys, Military Branch, United States Geological Survey, 59 p.

Taborosi, D.S., 2000. Karst Features of Guam [MS thesis]. University of Guam, Mangilao, 19 p.

Taborosi, D.S., and Jenson, J.W., 2002. World War II artefacts and wartime use of caves in Guam, Marian Islands. Capra 4, http://www.shef.ac.uk/~capra/4/.

Taborosi, D., Jenson, J.W., and Mylroie, J.E., in press. Karren features in island karst: Guam, Mariana Islands. Zeitschrift fur Geomorphologie.Tayama, R., 1936. Geomorphology, Geology, and Coral Reefs of Tinian Island Together with Aguijan and Naftan Islands. Institute of Geology and Paleontology, Tohoku University, Japan. 72 p.

Till, R., 1974. Chapter 7: Non-Parametric Statistics. in Till, R., Statistical Methods for the Earth Scientist. John Wiley and Sons, Inc., New York, NY, pp. 117-138.

Twiss, R.J., and Moores, E.M., 1992. Structural Geology. W.H. Freeman and Company, U.S., 532 p.

Tracey, J.I., Jr., Schlanger, S.O., Stark, J.T., Doan, D.B., and May, H.G., 1964. General Geology of Guam. 403-A, U.S. Geological Survey Professional Paper, U.S. Government Printing Office, Washington, D.C., 104 p.

United States Department of the Interior Geological Survey, 2001a. 1697184.DEM.SDTS.TAR.GZ. National Mapping program of the U.S. Geological Survey, ftp://sdts.er.usgs.gov/pub/sdts/datasets/raster/dem/

United States Department of the Interior Geological Survey, 2001b. 1697335.DEM.SDTS.TAR.GZ. National Mapping program of the U.S. Geological Survey, ftp://sdts.er.usgs.gov/pub/sdts/datasets/raster/dem/

United States Department of the Interior Geological Survey, 2001c. 1697336.DEM.SDTS.TAR.GZ. National Mapping program of the U.S. Geological Survey, ftp://sdts.er.usgs.gov/pub/sdts/datasets/raster/dem/

United States Department of the Interior Geological Survey, 2001d. 1697337.DEM.SDTS.TAR.GZ. National Mapping program of the U.S. Geological Survey, ftp://sdts.er.usgs.gov/pub/sdts/datasets/raster/dem/

United States Department of the Interior Geological Survey, 2001e. 1697338.DEM.SDTS.TAR.GZ. National Mapping program of the U.S. Geological Survey, ftp://sdts.er.usgs.gov/pub/sdts/datasets/raster/dem/

United States Department of the Interior Geological Survey, 1983. Topographic Map of the Island of Tinian, Commonwealth of the Northern Mariana Islands: U.S. Geological Survey, scale 1:25,000.

Vacher, H.L., and Mylroie, J.E., 2002. Eogenetic karst from the perspective of an equivalent porous medium. Carbonates and Evaporites, v. 17, no. 2, pp. 182-196.

Viles, H. A., 1988. Biogeomorphology. Basil Blackwell, Oxford, United Kingdom, 325 p.

White, W.B., 1988. Geomorphology and Hydrology of Karst Terrains. Oxford University Press, New York, 464 p.

Xara, 1997. CorelXara 2.0. Xara Ltd., Hertfordshire, United Kingdom, http://www.xara.com, software.

APPENDIX A

Color Figures

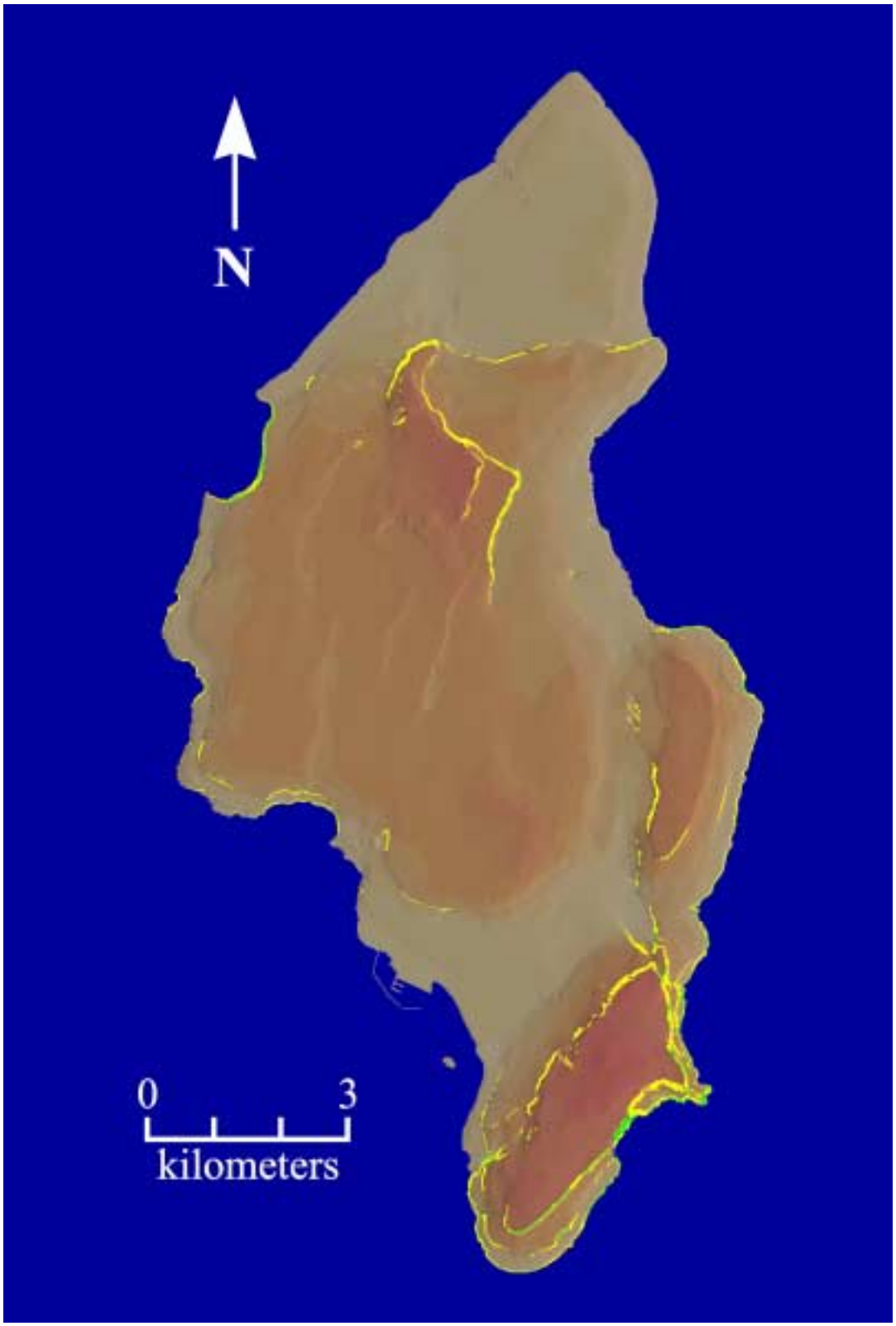

Figure 19: Inland and coastal scarps on Tinian.

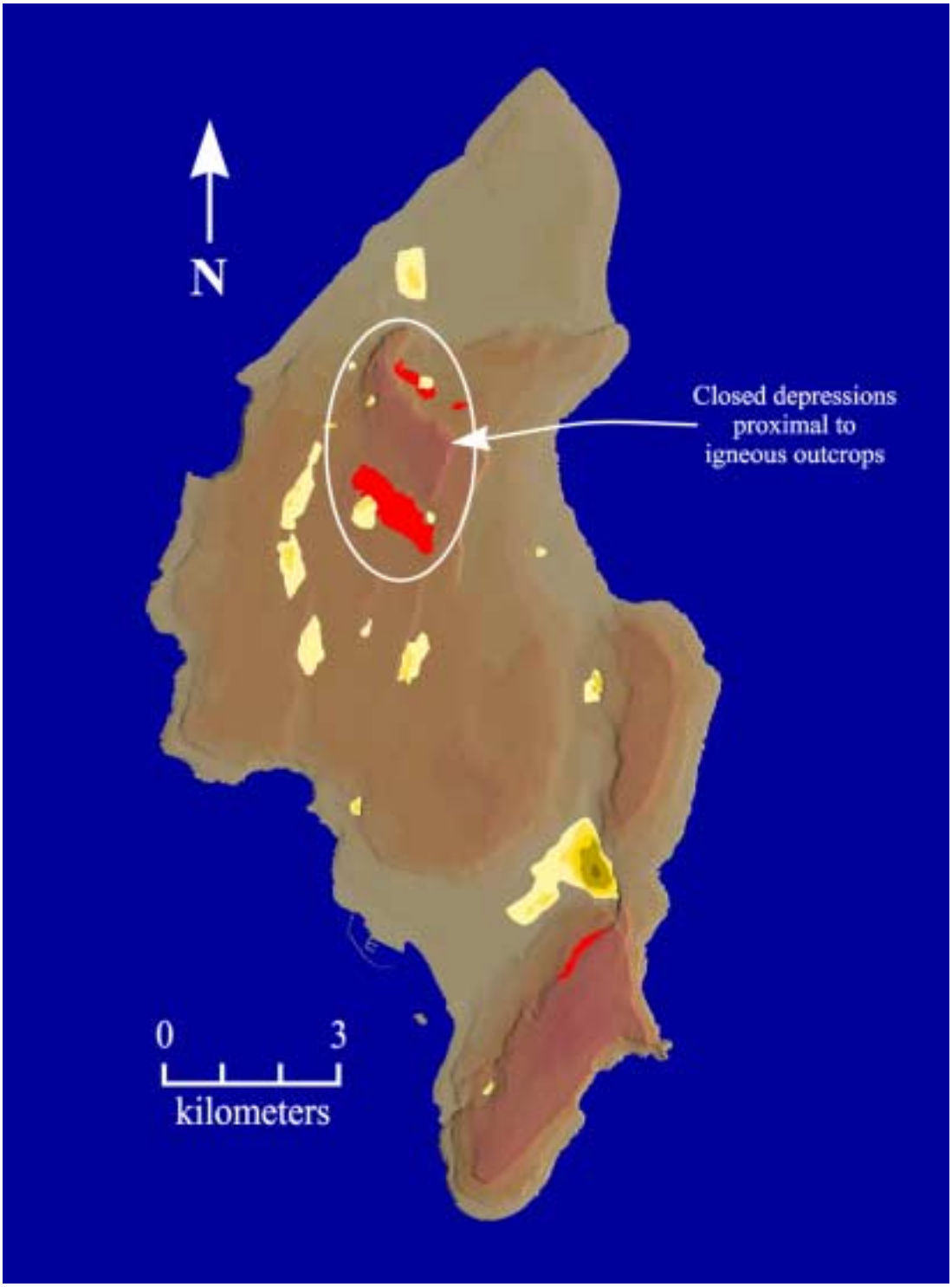

Figure 20: Areas of potential allogenic recharge based on non-carbonate rock outcrops (shown in red) and closed depressions (shown in yellow with darker shades of yellow representing greater depth).

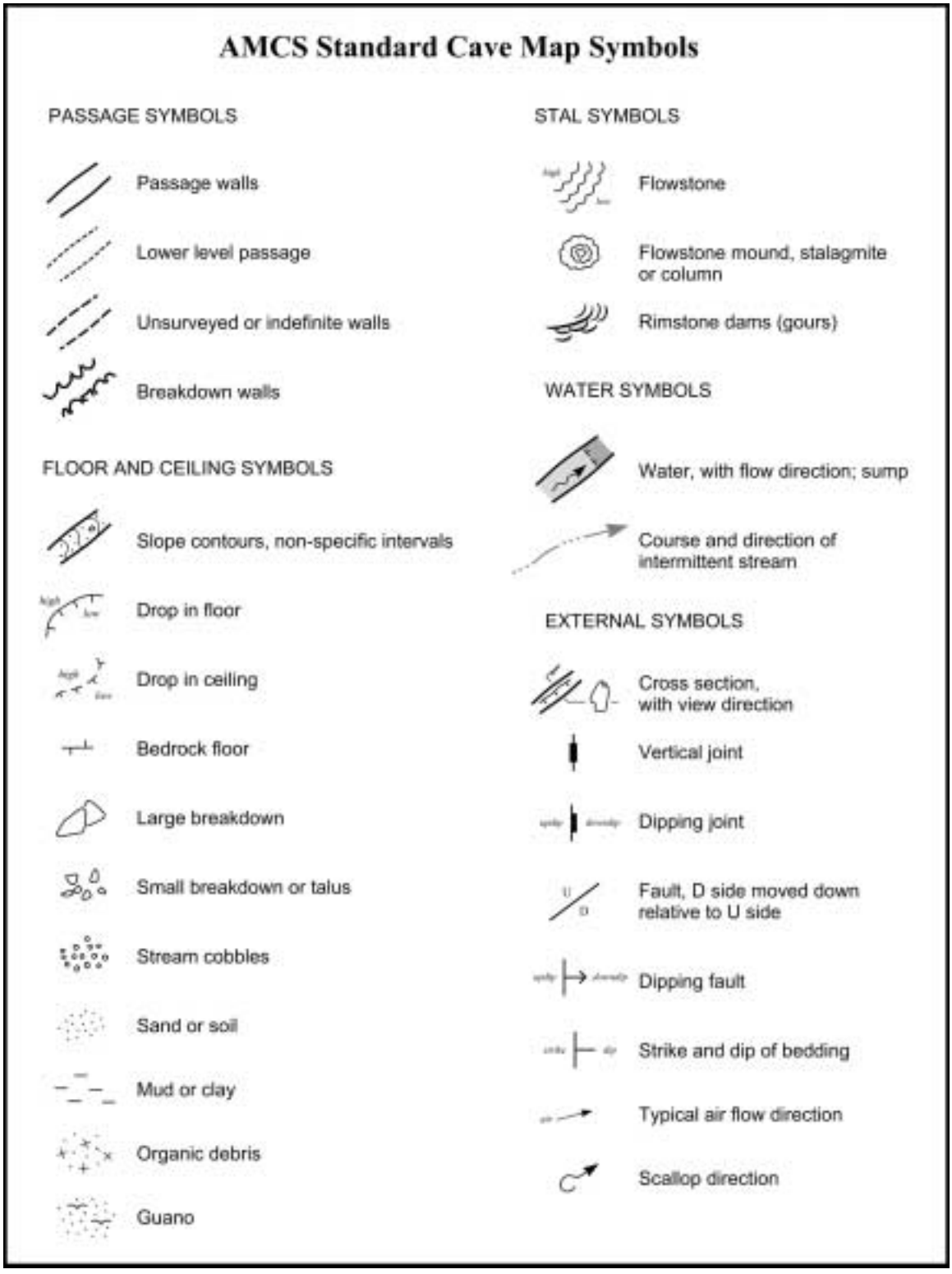

Figure 21: AMCS standard cave symbology (Sprouse, 1991).

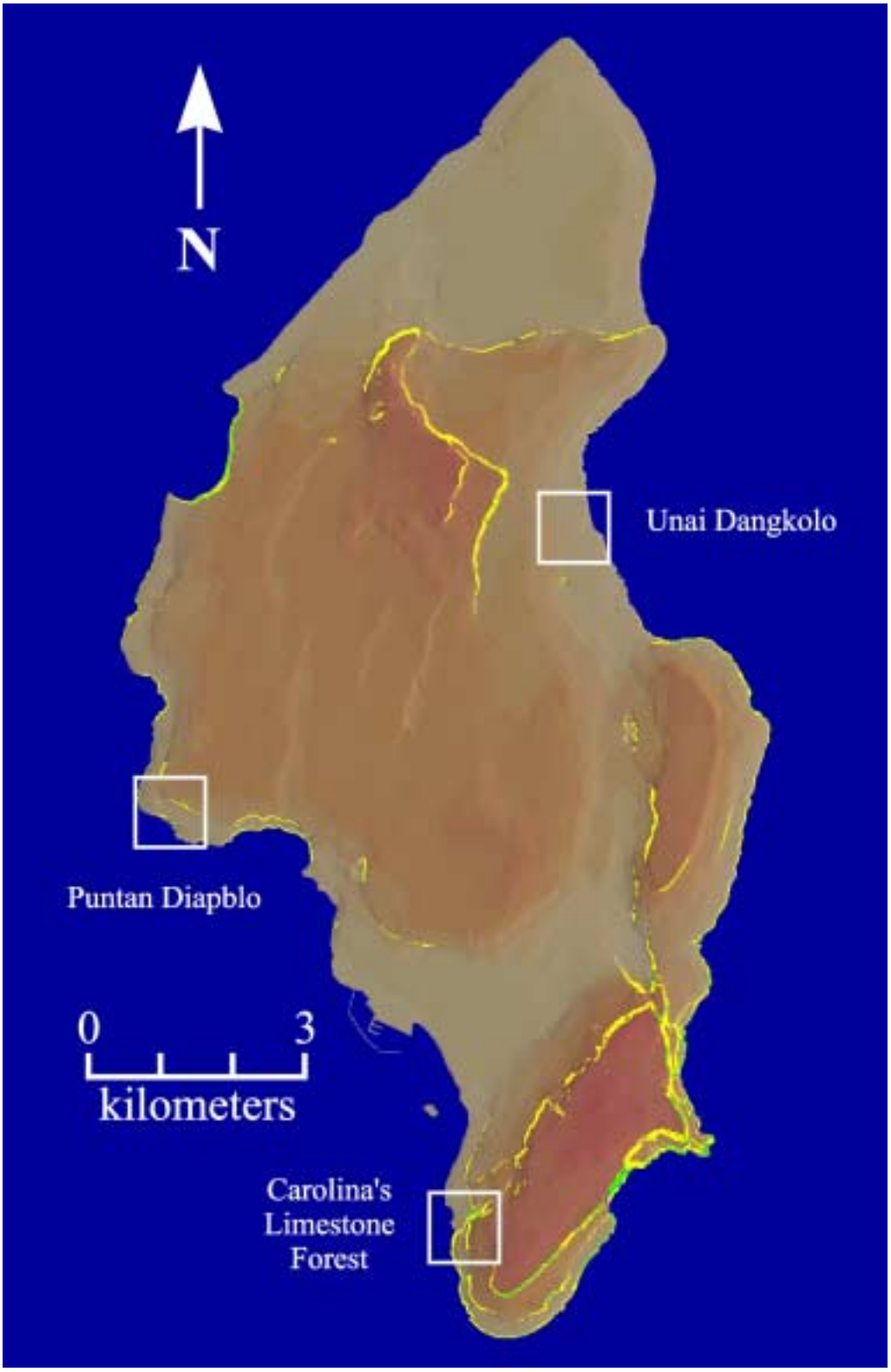

Figure 22: Location of test site areas.

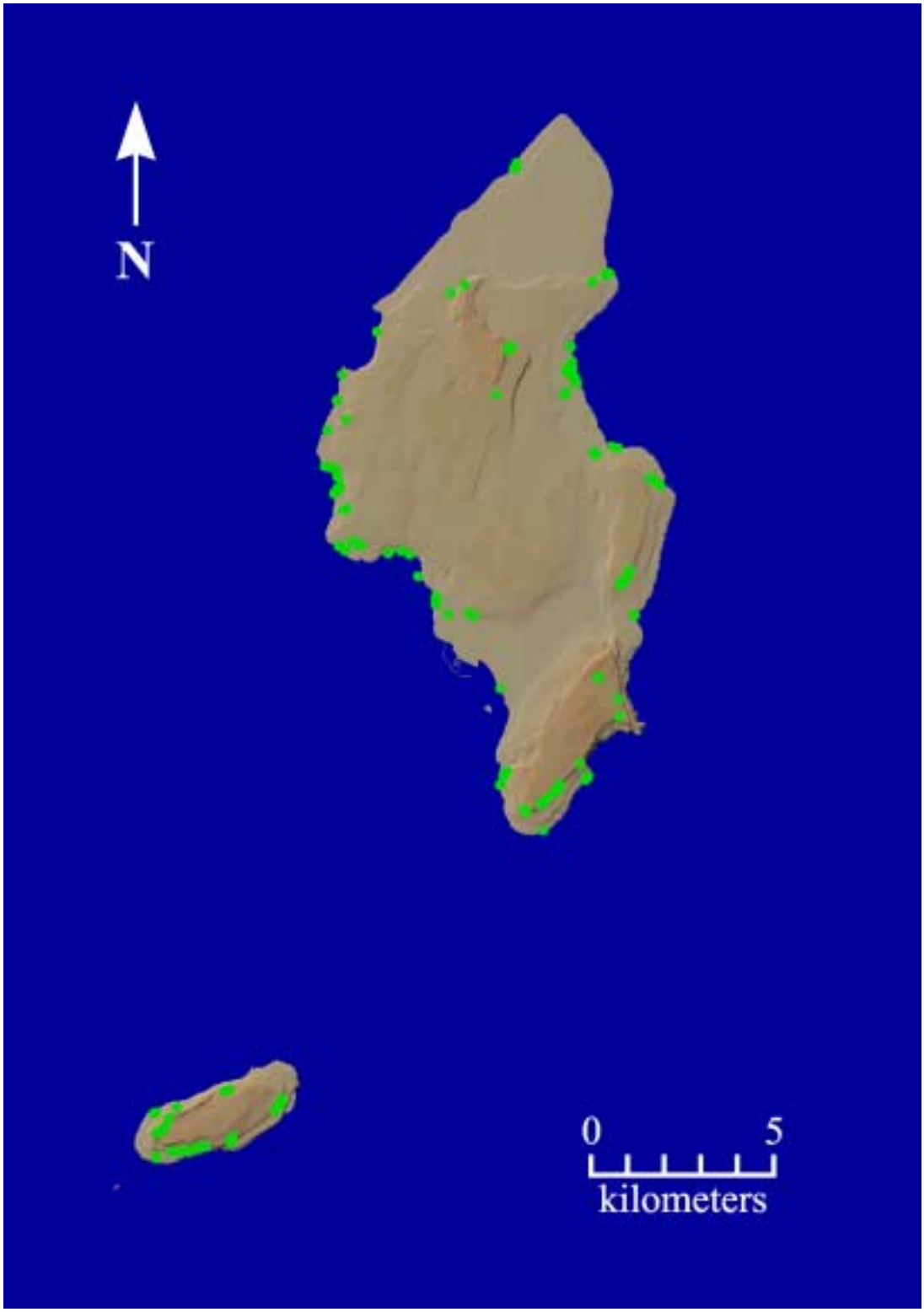

Figure 23: Green areas represent the location of cave and karst features surveyed on Aguijan and Tinian.

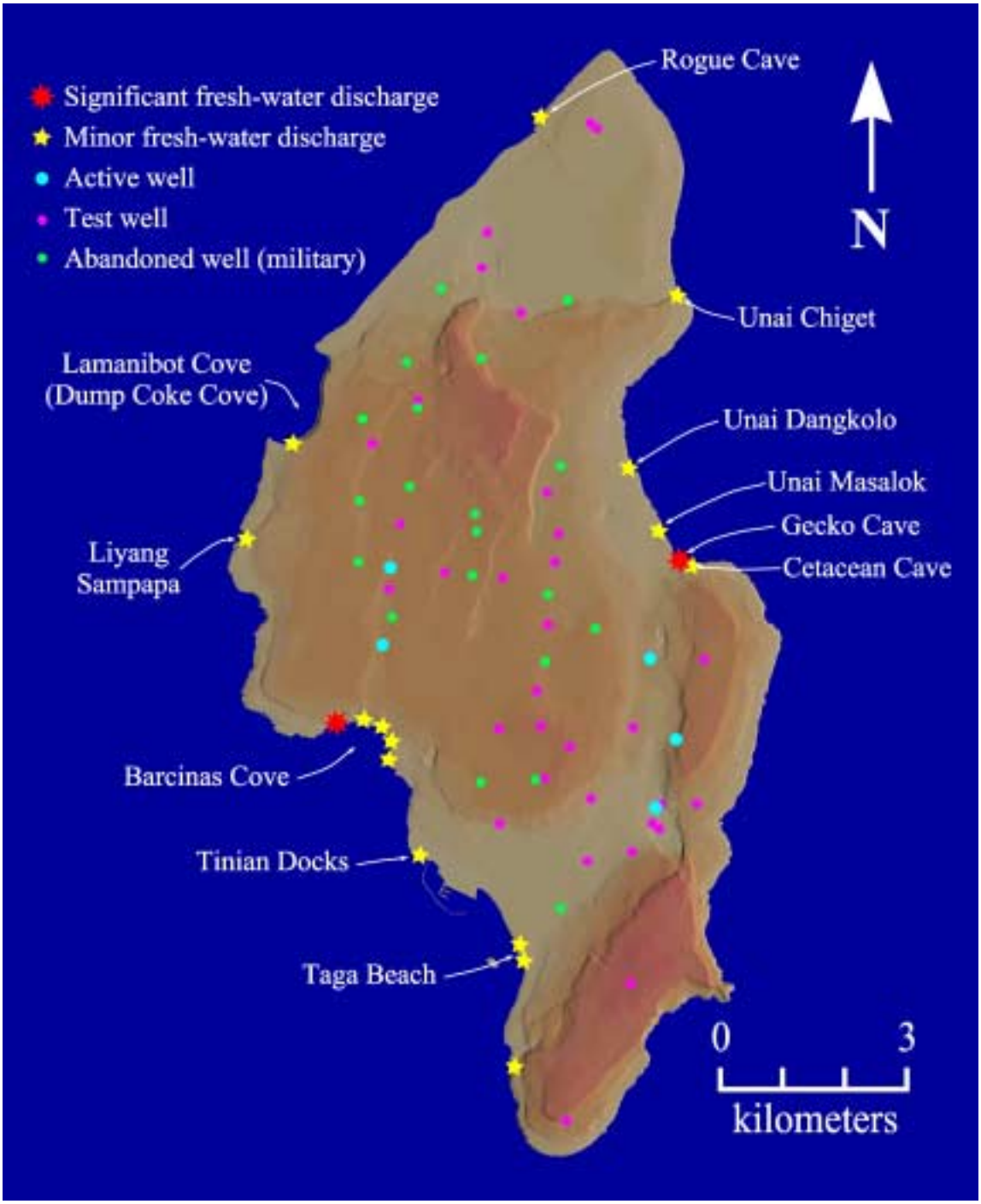

Figure 24: Fresh-water discharge sites located on Tinian

Figure 25: Bamboo growing in the North Lemmai Recharge Feature, with vines coating the scarp that forms the non-carbonate / carbonate contact.

Figure 26: Ponded water in the South Lemmai Recharge.

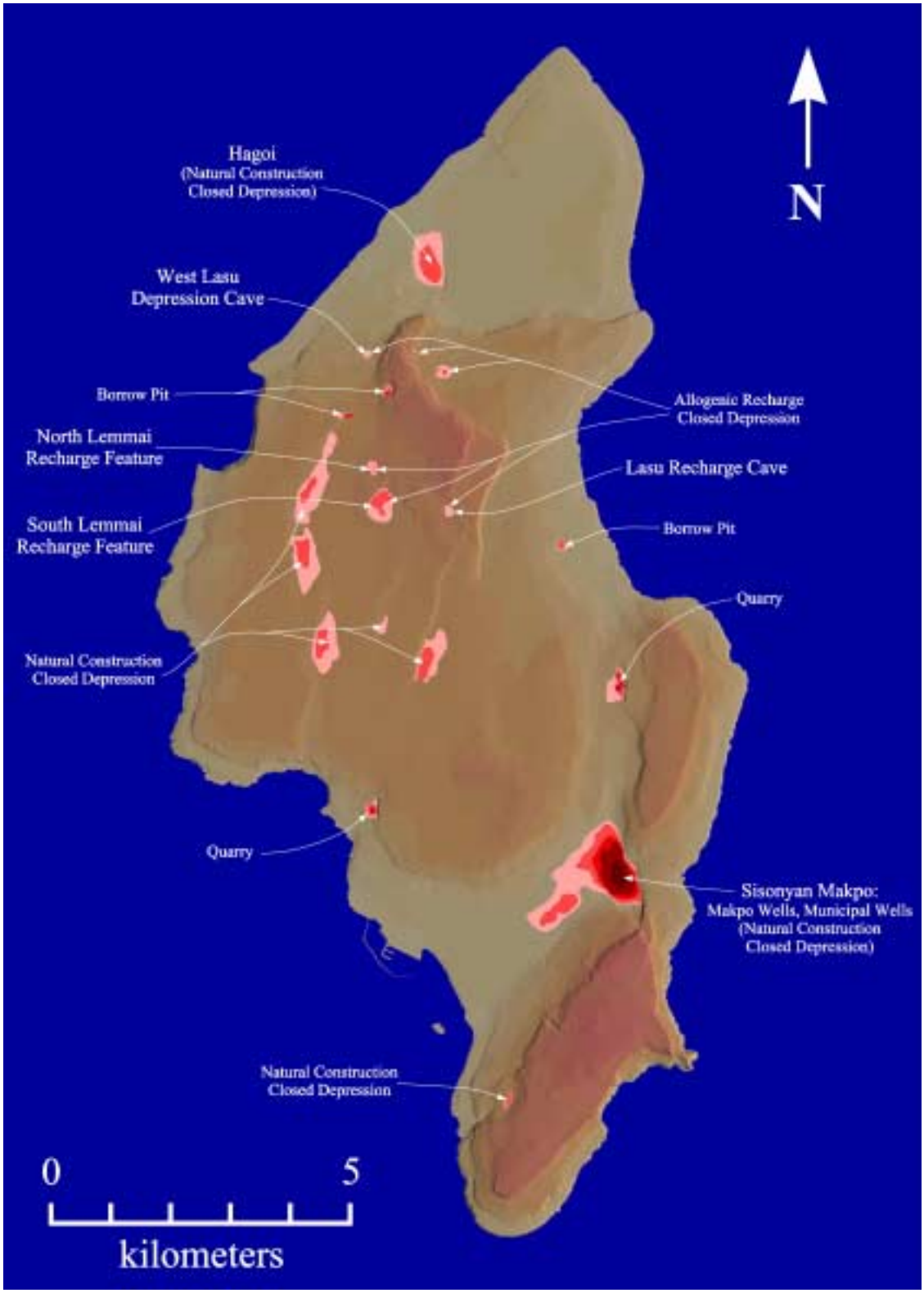

Figure 27: Location of closed depressions on Tinian.

Figure 28: Active quarry on Tinian.

Figure 29: Fresh-water at the land surface (~2 meters above mean sea level) at Hagoi in the Northern Lowland.

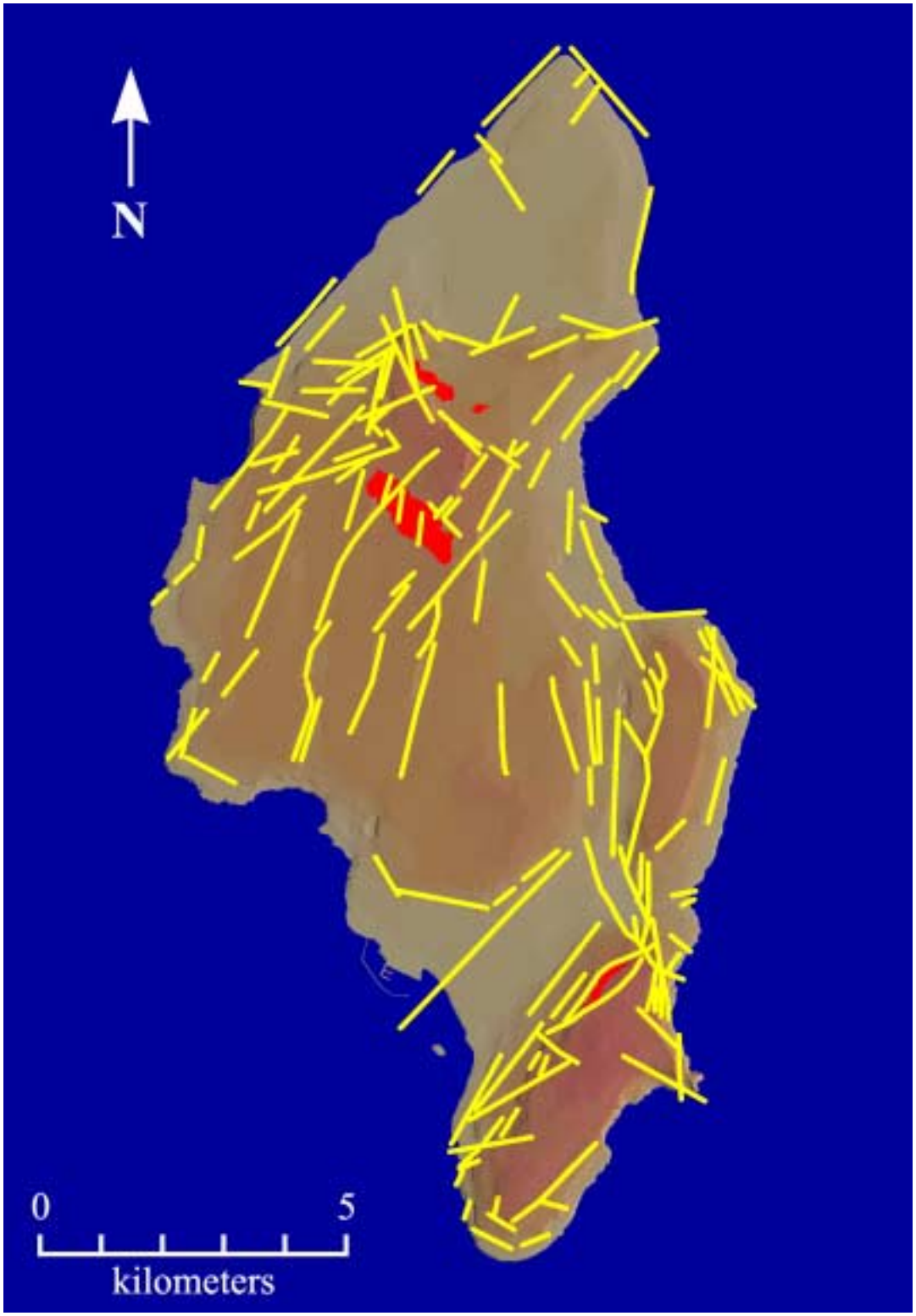

Figure 30: Faults (yellow) and non-carbonate rock outcrops (red) reported by Doan and coworkers (1960).

Figure 31: South Unai Dangkolo represents a typical cove that has formed from collapse and coastal erosion of a large flank margin cave.

Figure 32: Hidden Beach Cave demonstrates well the transition from flank margin cave to cove resulting from coastal erosion.

Figure 33: Typical flank margin cave morphology in one of the passages extending from the main chamber in Unai Dangkolo.

Figure 34: Horizons of flank margin cave development show previous fresh-water lens positions as seen at Suicide Cliffs, Tinian.

Figure 35: Fissure caves form narrow, linear passages that appear to be developed along zones of brittle failure as seen in Carolina's Fracture Cave.

Figure 36: Flowstone deposits on ceilings and walls prevent observation of offsetting of rocks by faulting if it exists (Plunder Cave, Tinian).

Figure 37: Insect Bat Cave on Aguijan represents a paleo-discharge feature.

Figure 38: Scallops on the ceiling and walls of Liyang Atkiya, Aguijan.

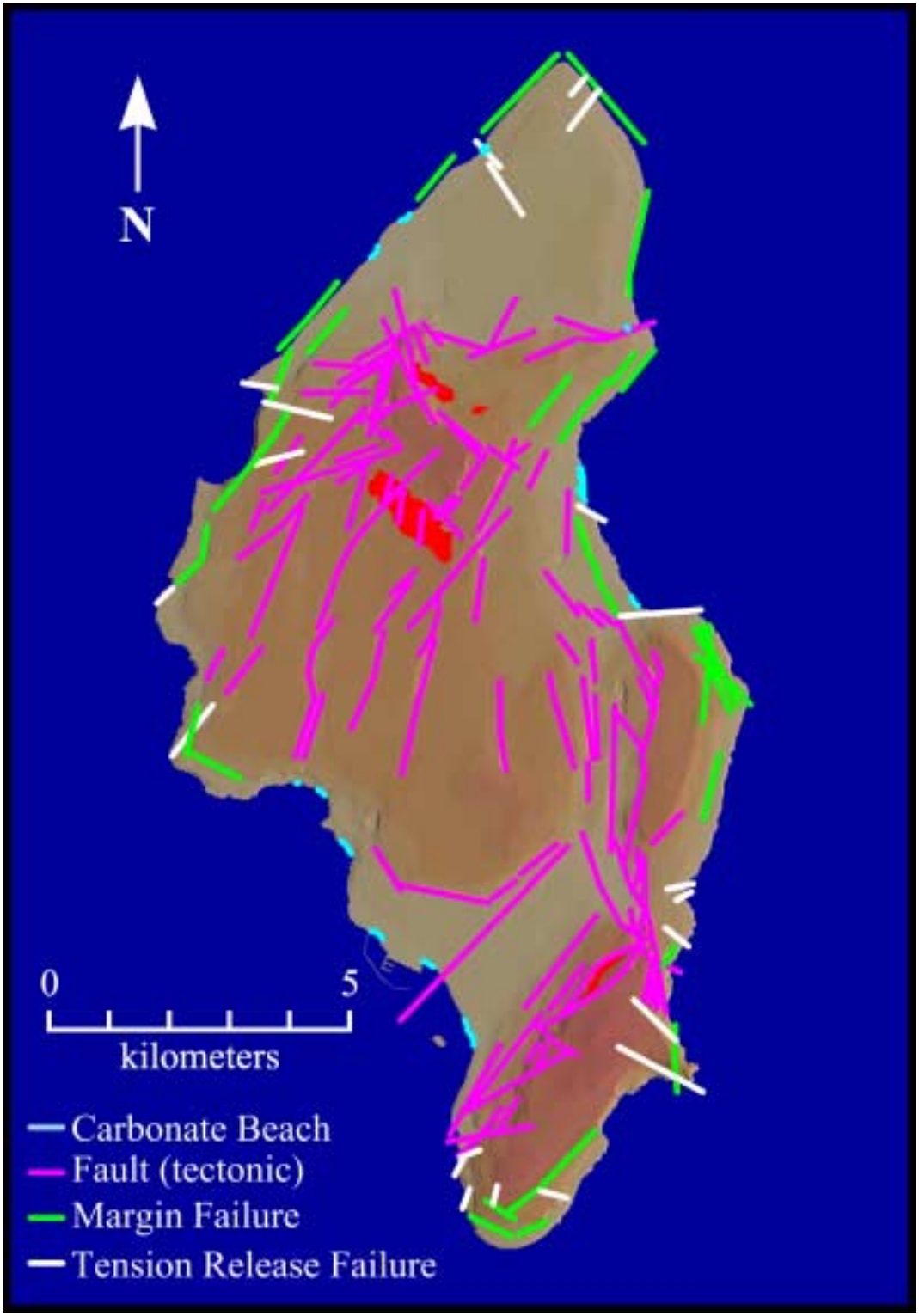

Figure 39: Diagram showing the location of modern carbonate beach deposits (light blue) and primary brittle failure types: tectonic faults (purple), margin failures (green) and tension release failures (white) (adapted from Doan et al., 1960).

APPENDIX B

CAVE AND KARST INVENTORY:

MAPS AND DESCRIPTIONS

The following descriptions are listed in alphabetical order by the feature's name, in order to simplify locating information pertaining to a specific feature. Features on Tinian are summarized in Table 1 and features on Aguijan are summarized in Table 2. Each surveyed feature includes its physiographic location (Figure 1 and 2, Chapter II) with the description and approximate cave locations. All features were surveyed in accordance with the National Speleological Society's protocols (Dasher, 1994) and final maps drafted using the Association for Mexican Cave Studies (AMCS) symbology (Figure 10, Chapter III ; Sprouse and Russell, 1980).

"600 Meter" Fracture System (Southeastern Ridge, Tinian – Figure 40)

The "600 Meter" Fracture System is a high-angle fracture located approximately 500 meters west/northwest of Puntan Masalok in the Mariana Limestone (QTmu), where it trends northwest (~310^{o}) for over 300 meters before the feature becomes obscured by additional surface features and vegetation, however topographic maps for the island confirm that it extends for approximately 600 meters (United States Department of the Interior Geological Survey, 1983). Full Bottle Cave is located in the northwest portion of the fracture system, while Masalok Fracture Cave is located in the southeast portion. Numerous small pocket caves are located in the northeastern scarp wall along the entire length of the feature, however fewer are present in the regions where a southwestern wall is present. Throughout the feature, numerous speleothems are present on the cliff walls and within the small pocket caves, indicating that at some point in the past this feature was roofed. In the middle portions of the feature, where two cliff walls are exposed at the surface, the feature measures over 5 meters wide with a northeastern wall that is approximately 10 meters tall and a southwestern wall that is approximately 3 meters tall. Along the fracture, several less dissolutionally enhanced fractures are intersected at high angles to the primary fracture. In addition, several small collapse areas in the breakdown floor are present, indicating that greater void space is present at depth. This extensive, dissolutionally enhanced fracture system demonstrates the importance of fractures within carbonate islands as routes for the transfer of water into the subsurface.

Almost Cave (Upper Terrace, Aguijan – Figure 41)

Almost cave is a small, breached, flank margin cave located in the northwest region of the Upper Terrace in the Mariana Limestone (QTmu). The cave consists of two levels offset approximately 1 meter with a total width of 3 meters and depth of 1.5 meters. The cave is located 2 meters high on a small scarp with two entrances separated by a bedrock column. The cave has no speleothems and the floor is covered with alluvium.

Andyland Cave (Median Valley, Tinian – Figure 42)

Andyland Cave extends 20 meters inland from the northwest corner of Unai Dangkolo and is developed in the Mariana Limestone (QTmca). It is a flank margin cave consisting of one primary chamber with a maximum height of 3.5 meters and a width of 8 meters. The floor is composed of carbonate beach sand, which may be infilling additional cave passage in the western portions. Andyland Cave is positioned in-line with the northern scarp of Unai Dangkolo and Liyang Dangkolo, with a 10-meter gap separating Andyland Cave from Liyang Dangkolo. Based on carbonate sand observed in eastern portion of Liyang Dangkolo, it is likely that the two caves physically connect but are currently separated by sand accumulation.

Table 1: Cave and karst features surveyed on Tinian, CNMI: UTM location, physiography, cave type and geology.

Cave Name	Easting	Northing	Elevation	Location	Type	Lithology - Formation	Lithology - Facies
"600 Meter" Fracture System	356720	1659760	45	Southeastern Ridge	Fracture	Mariana Limestone	Detrital Undifferentiated Facies
Andyland Cave	354671	1662767	3	Median Valley	Flank Margin	Mariana Limestone	Constructional Algal Facies
Barcinas East Cave	350140	1657850	1	Median Valley	Flank Margin	Mariana Limestone	Detrital Undifferentiated Facies
Barcinas West Cave	349910	1657950	1	Median Valley	Flank Margin	Mariana Limestone	Detrital Undifferentiated Facies
Barely Cave	348420	1659160	50	Central Plateau	Flank Margin	Mariana Limestone	Detrital Undifferentiated Facies
Bee Hooch Cave	355950	1657090	100	Southeastern Ridge	Flank Margin	Mariana Limestone	Detrital Undifferentiated Facies
Body Repel Cave	354190	1661480	125	Southeastern Ridge	Flank Margin	Mariana Limestone	Detrital Undifferentiated Facies
Broken Stal Cave	356190	1657460	100	Southeastern Ridge	Flank Margin	Mariana Limestone	Detrital Undifferentiated Facies
Cannon Cave	349525	1657825	40	Central Plateau	Flank Margin	Mariana Limestone	Detrital Undifferentiated Facies
Carolina's Fracture Cave	352737	1661812	70	Southeastern Ridge	Fracture	Mariana Limestone	Detrital Undifferentiated Facies
Cave Without a Cave	353737	1661037	115	Southeastern Ridge	Flank Margin	Tagpochau Limestone	Detrital Facies
Cave Without a Roof	353087	1661187	120	Southeastern Ridge	Flank Margin	Tagpochau Limestone	Detrital Facies
Cavelet Cave	348340	1658020	3	Central Plateau	Flank Margin	Mariana Limestone	Detrital Undifferentiated Facies
Central Mendiola Cave Complex	348140	1660090	1	Central Plateau	Flank Margin	Mariana Limestone	Detrital Undifferentiated Facies
Cetacean Cave	355820	160780	1	Southeastern Ridge	Discharge	Mariana Limestone	Detrital Undifferentiated Facies
Chigel Fracture	355050	1665187	30	Central Plateau	Fracture	Mariana Limestone	Detrital Undifferentiated Facies
Cobble Cave	347090	1660260	1	Central Plateau	Flank Margin	Mariana Limestone	Detrital Undifferentiated Facies
Coconut Trap Cave	356070	1657260	100	Southeastern Ridge	Flank Margin	Mariana Limestone	Detrital Undifferentiated Facies
Command Post Cave Complex	352540	1663370	130	North-Central Highland	Flank Margin	Mariana Limestone	Constructional Algal Facies
Cowrie Cave	347920	1660280	1	Central Plateau	Flank Margin	Mariana Limestone	Detrital Undifferentiated Facies
CUC Cave	351080	1656260	25	Median Valley	Banana Hole	Mariana Limestone	Constructional Algal Facies
Danko's Misery	355821	1654081	70	Southeastern Ridge	Fracture	Mariana Limestone	Constructional Algal Facies
Death Fracture Complex	348450	1657800	10	Central Plateau	Fracture	Mariana Limestone	Detrital Undifferentiated Facies
Dos Cenotes Cave	347870	1660290	1	Central Plateau	Flank Margin	Mariana Limestone	Detrital Undifferentiated Facies
Dos Sakis Cave Complex	348020	1658160	50	Central Plateau	Flank Margin	Mariana Limestone	Detrital Undifferentiated Facies
Dripping Tree Fracture Cave	354671	1662767	18	Median Valley	Fracture	Mariana Limestone	Constructional Algal Facies
Dump Coke Cave	349260	1663990	5	Central Plateau	Flank Margin	Mariana Limestone	Detrital Undifferentiated Facies
Dynasty Cave	352610	1654230	1	Median Valley	Flank Margin	Mariana Limestone	Detrital Undifferentiated Facies
East Suicide Cliff Cave (Suicide Cliff Cave #1)	354625	1651962	120	Southeastern Ridge	Flank Margin	Mariana Limestone	Detrital Undifferentiated Facies
Edwin's Ranch Cave	348387	1661600	60	Central Plateau	Flank Margin	Mariana Limestone	Constructional Coralliferous Facies
Elevator Cave	354070	1651350	130	Southeastern Ridge	Flank Margin	Mariana Limestone	Detrital Undifferentiated Facies
False Floor Cave	356160	1657400	100	Southeastern Ridge	Flank Margin	Mariana Limestone	Detrital Undifferentiated Facies
Five Bee Cave Complex	354970	1654780	85	Southeastern Ridge	Flank Margin	Mariana Limestone	Detrital Coralliferous Facies
Flamingo Tail Caves	348590	1658250	50	Central Plateau	Flank Margin	Mariana Limestone	Detrital Undifferentiated Facies
Fleming Point Cave	347880	1661230	1	Central Plateau	Flank Margin	Mariana Limestone	Detrital Undifferentiated Facies
Full Bottle Cave	356580	1659880	60	Southeastern Ridge	Fracture	Mariana Limestone	Detrital Undifferentiated Facies
Gecko Cave	355790	1660826	1	Median Valley	Discharge	Mariana Limestone	Detrital Undifferentiated Facies
Half-Dozen Cave	349562	1657960	45	Central Plateau	Flank Margin	Mariana Limestone	Detrital Facies
Headless Tourist Pit	353870	1650033	20	Southeastern Ridge	Pit	Mariana Limestone	Detrital Undifferentiated Facies
Hermit Crab Cave	356130	1657320	100	Southeastern Ridge	Flank Margin	Mariana Limestone	Detrital Undifferentiated Facies
Hidden Beach Cave	354590	1663410	1	Median Valley	Flank Margin	Mariana Limestone	Constructional Algal Facies
John's Small Cave	354260	1662350	20	Median Valley	Flank Margin	Mariana Limestone	Constructional Algal Facies
Lasu Recharge Cave	352225	1662012	100	North-Central Highland	Recharge	Tagpochau Limestone	Detrital Facies

Table 1 (continued): Cave and karst features surveyed on Tinian, CNMI: UTM location, physiography, cave type and geology.

Cave Name	Easting	Northing	Elevation	Location	Type	Lithology - Formation	Lithology - Facies
Leprosy Caves	350587	1656437	1	Median Valley	Flank Margin	Mariana Limestone	Detrital Undifferentiated Facies
Leprosy Discharge Feature	350062	1657025	1	Median Valley	Discharge	Mariana Limestone	Detrital Undifferentiated Facies
Liyang Barangka	356350	1656230	10	Southeastern Ridge	Flank Margin	Mariana Limestone	Detrital Undifferentiated Facies
Liyang Dangkolo	354320	1662360	20	Median Valley	Flank Margin	Mariana Limestone	Constructional Algal Facies
Liyang Diapblo	348230	1658080	1	Central Plateau	Flank Margin	Mariana Limestone	Detrital Undifferentiated Facies
Liyang Gritot	351990	1665450	75	North-Central Highland	Flank Margin	Tagpochau Limestone	Detrital Facies
Liyang Mohlang	355187	1654550	150	Southeastern Ridge	Flank Margin	Tagpochau Limestone	Detrital Facies
Liyang Popporput	355925	1653368	150	Southeastern Ridge	Fracture	Mariana Limestone	Constructional Algal Facies
Liyang Sampapa	348270	1662790	5	Central Plateau	Discharge	Mariana Limestone	Constructional Algal Facies
Liyang Umumu	348300	1659110	30	Central Plateau	Banana Hole	Mariana Limestone	Detrital Undifferentiated Facies
Lower Sucide Cliff Cave Complex	355070	1651820	2	Southeastern Ridge	Flank Margin	Mariana Limestone	Detrital Undifferentiated Facies
Masalok Fracture Cave Complex	354590	1661880	15	Southeastern Ridge	Fracture	Mariana Limestone	Detrital Undifferentiated Facies
Mendiola Arch Cave Complex	348260	1659720	1	Central Plateau	Flank Margin	Mariana Limestone	Detrital Undifferentiated Facies
Metal Door Cave	351710	1665310	80	North-Central Highland	Flank Margin	Tagpochau Limestone	Detrital Facies
Metal Spike Cave Complex	354426	1662341	20	Median Valley	Flank Margin	Mariana Limestone	Constructional Algal Facies
Metal Stretcher Cave	353775	1651075	115	Southeastern Ridge	Flank Margin	Tagpochau Limestone	Detrital Facies
Modified Cave	354212	1651440	100	Southeastern Ridge	Flank Margin	Tagpochau Limestone	Detrital Facies
Monica Wants to be Like Kevin Cave	348710	1658190	50	Central Plateau	Flank Margin	Mariana Limestone	Detrital Undifferentiated Facies
North Unai Dangkolo	354671	1662767	1	Median Valley	Flank Margin	Mariana Limestone	Constructional Algal Facies
Northern Playground Cave	355920	1657120	100	Southeastern Ridge	Flank Margin	Mariana Limestone	Detrital Undifferentiated Facies
Nuestra Senora de Santa Lourdes Cave Complex	351789	1656226	40	Central Plateau	Flank Margin	Mariana Limestone	Detrital Undifferentiated Facies
Orange Cave	348350	1658050	10	Central Plateau	Flank Margin	Mariana Limestone	Detrital Undifferentiated Facies
Pebble Cave	348030	1660240	1	Central Plateau	Flank Margin	Mariana Limestone	Detrital Undifferentiated Facies
Pina Cave Complex	355990	1657170	100	Southeastern Ridge	Flank Margin	Mariana Limestone	Detrital Undifferentiated Facies
Playground Cave	355870	1657070	100	Southeastern Ridge	Flank Margin	Mariana Limestone	Detrital Undifferentiated Facies
Plunder Cave	352712	1651875	30	Median Valley	Fracture	Mariana Limestone	Detrital Undifferentiated Facies
Radio Inactive Cave	354200	1651490	130	Southeastern Ridge	Flank Margin	Mariana Limestone	Detrital Undifferentiated Facies
Red Snapper Cave	348150	1662080	10	Central Plateau	Flank Margin	Mariana Limestone	Detrital Undifferentiated Facies
Rock Hammer Cave	348140	1660000	1	Central Plateau	Flank Margin	Mariana Limestone	Detrital Undifferentiated Facies
Rogue Cave	353090	1668610	1	Northern Lowland	Discharge	Mariana Limestone	Detrital Undifferentiated Facies
Rooticicle Cave	352913	1663561	100	North-Central Highland	Banana Hole	Mariana Limestone	Constructional Algal Facies
Skip Jack Cave	352610	1651560	2	Southeastern Ridge	Flank Margin	Mariana Limestone	Detrital Undifferentiated Facies
Skull Cave Complex	356020	1657170	100	Southeastern Ridge	Flank Margin	Mariana Limestone	Detrital Undifferentiated Facies
Skylight Cave	354190	1651420	130	Southeastern Ridge	Flank Margin	Mariana Limestone	Detrital Undifferentiated Facies
Solitary Cave	355890	1659350	80	Southeastern Ridge	Flank Margin	Mariana Limestone	Detrital Undifferentiated Facies
South Mendiola Cave	348080	1659570	1	Central Plateau	Flank Margin	Mariana Limestone	Constructional Coralliferous Facies
South Unai Dangkolo	354600	1662100	2	Median Valley	Flank Margin	Mariana Limestone	Constructional Algal Facies
Swimming Hole Cave Complex	350960	1656670	10	Median Valley	Flank Margin	Mariana Limestone	Detrital Undifferentiated Facies
Twin Ascent Caves	354237	1651575	120	Southeastern Ridge	Flank Margin	Tagpochau Limestone	Detrital Facies
Unai Chigat	355337	1665312	2	Northern Lowland	Fracture	Mariana Limestone	Constructional Algal Facies
Unai Lamlam	353060	1668500	1	Northern Lowland	Flank Margin	Mariana Limestone	Constructional Coralliferous Facies
Unai Masalok	355212	1660674	5	Median Valley	Flank Margin	Mariana Limestone	Constructional Algal Facies
Water Cave	352687	1651850	25	Median Valley	Fracture	Mariana Limestone	Detrital Undifferentiated Facies
West Lasu Depression Cave	351270	1665220	40	Central Plateau	Recharge	Mariana Limestone	Detrital Undifferentiated Facies
West Suicide Cliff Caves	353187	1650600	115	Southeastern Ridge	Flank Margin	Mariana Limestone	Detrital Undifferentiated Facies

Table 2: Cave and karst features surveyed on Aguijan, CNMI: UTM location, physiography, and cave type.

Cave Name	Easting	Northing	Elevation	Location	Type
Almost Cave	343450	1642170	150	Upper Terrace	Flank Margin
Anvil Cave	343670	1642560	150	Upper Terrace	Fracture
Biting Mosquitoes Cave	343380	1642140	150	Upper Terrace	Flank Margin
Booney Bee Sink	343440	1642140	150	Upper Terrace	Banana Hole
Cabrito Cave	346675	1642675	70	Middle Terrace	Flank Margin
Diamond Cave	344337	1641687	50	Lower Terrace	Flank Margin
Dove Cave	343280	1642560	150	Upper Terrace	Banana Hole
Goat Cave	344538	1641684	55	Lower Terrace	Flank Margin
Goat Island Fracture Cave	343840	1642820	50	Lower Terrace	Fracture
Hollow Column Cave	354260	1662350	50	Lower Terrace	Flank Margin
Insect Bat Cave	343810	1641550	60	Middle Terrace	Fracture
Isotope Cave	343320	1642050	150	Upper Terrace	Flank Margin
Liyang Atkiya	345246	1641755	50	Lower Terrace	Unknown
Liyang Lomuk	345210	1643260	100	Middle Terrace	Flank Margin
Lizard Cave	345140	1643240	100	Middle Terrace	Flank Margin
Natural Arch Cave	344140	1641580	60	Middle Terrace	Flank Margin
Orphan Kids Cave Complex	343198	1641434	50	Lower Terrace	Fracture
Pepper Cave	343230	1642070	150	Upper Terrace	Flank Margin
Scorpion Cave	346680	1642680	70	Middle Terrace	Flank Margin
Screaming Bat Cave	343340	1642110	140	Upper Terrace	Flank Margin
Spider Cave	345070	1643200	100	Middle Terrace	Flank Margin
Swarming Termites Cave	346560	1642740	70	Middle Terrace	Flank Margin
Swiftlet Cave	343180	1642620	15	Lower Terrace	Flank Margin
Toppled Column Cave	343940	1641560	60	Middle Terrace	Fracture
Tridactid Cave Complex	346670	1642670	70	Middle Terrace	Flank Margin
Waypoint Cave	346510	1642660	70	Middle Terrace	Flank Margin

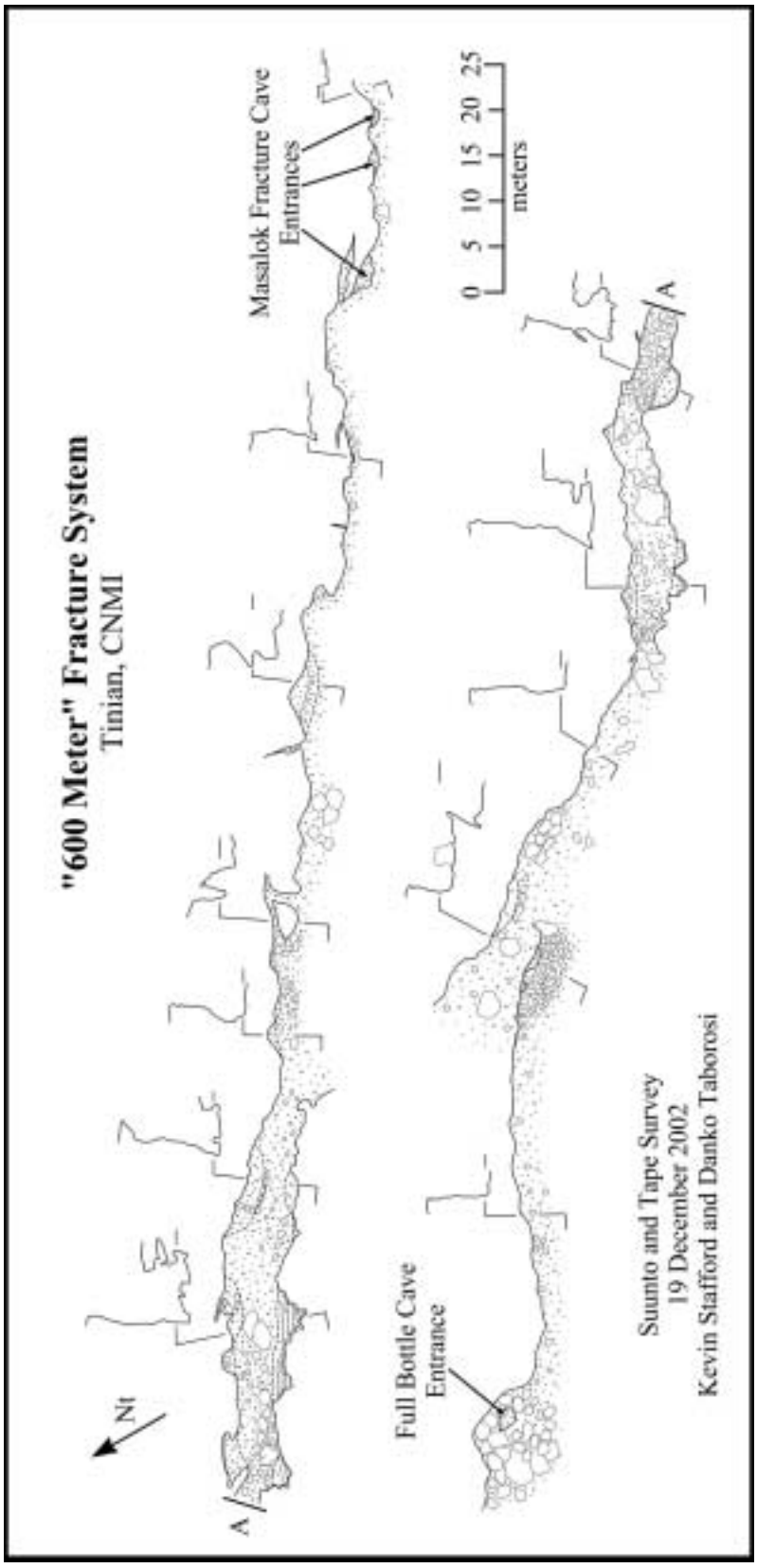

Figure 40: Map of "600 Meter" Fracture System.

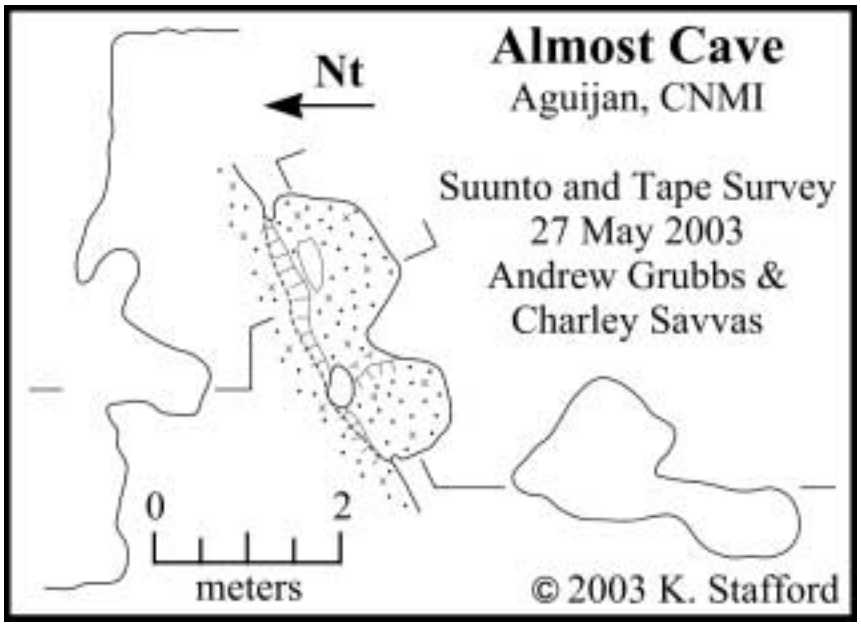

Figure 41: Map of Almost Cave.

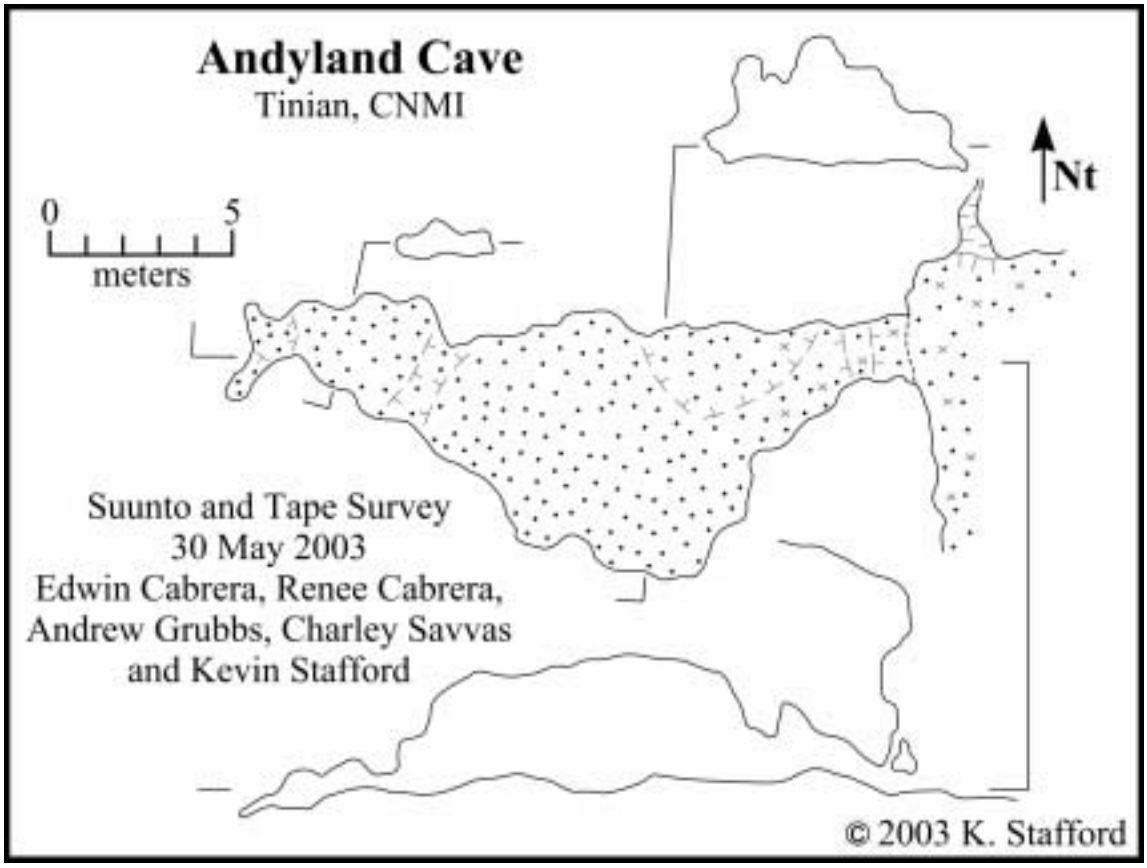

Figure 42: Map of Andyland Cave.

Anvil Cave (Upper Terrace, Aguijan – Figure 43)

Anvil Cave is a fracture cave developed from scarp failure in the northwest region of the Upper Terrace. It is developed in the Mariana Limestone (QTmu) along a fracture strike of 45°. The cave consists of two primary levels. The upper level is partially roofed, 10 meters long and 3 meters wide with a bedrock shelf extending 2 meters to the northwest. The lower level averages 3 meters in width and drops steeply to the northeast over a breakdown floor, with a small breakdown chamber located to the west. The cave continues as a 5 meter wide, 9 meter deep, alluvium floored canyon to the northeast, connecting the Upper and Middle Terraces. The cave contains minor speleothem deposits and is composed primarily of breakdown with enhanced dissolution along the fracture trend and shows evidence of military occupation and modification.

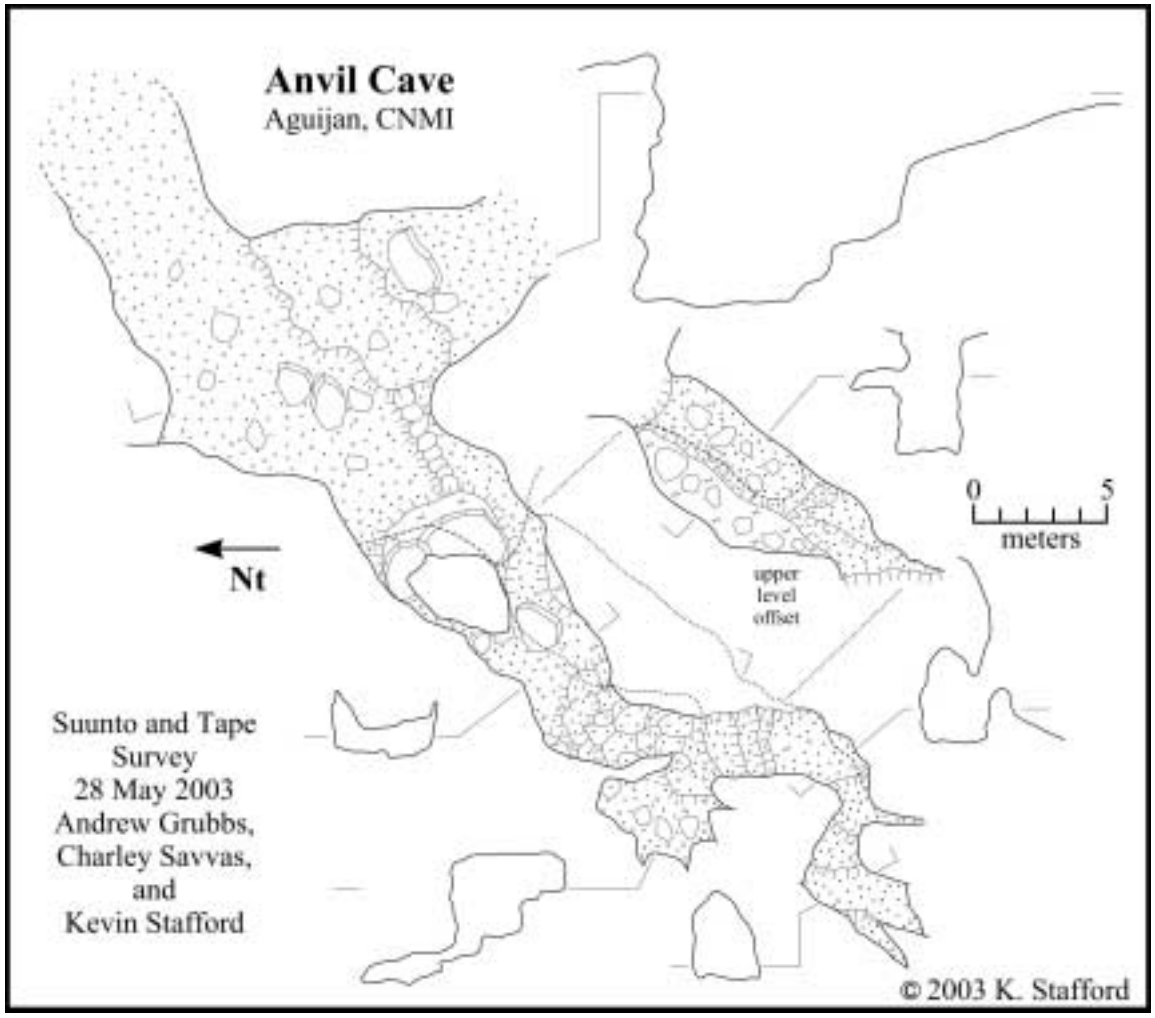

Figure 43: Map of Anvil Cave.

Barcinas East Cave (Median Valley, Tinian – Figure 44)

Barcinas East Cave is a flank margin cave located approximately 200 meters east of Barcinas West Cave on the north side of Barcinas Cove (Turtle Cove) in the Mariana Limestone (QTmu). It is positioned approximately 1 meter above mean sea level with a width of 34 meters, depth of 18 meters and maximum ceiling height of 4 meters. The main cave is separated by 3 bedrock pillars and is influenced by two joints trending north/northeast. The interior of the main

cave is devoid of speleothems and appears to have been severely impacted by intense storm events, producing a flat bedrock floor that is near level with high tide levels. A few meters west of the main cave, a smaller flank margin remnant exists that is partially protected by the rock comprising the main cave, which extends slightly farther seaward.

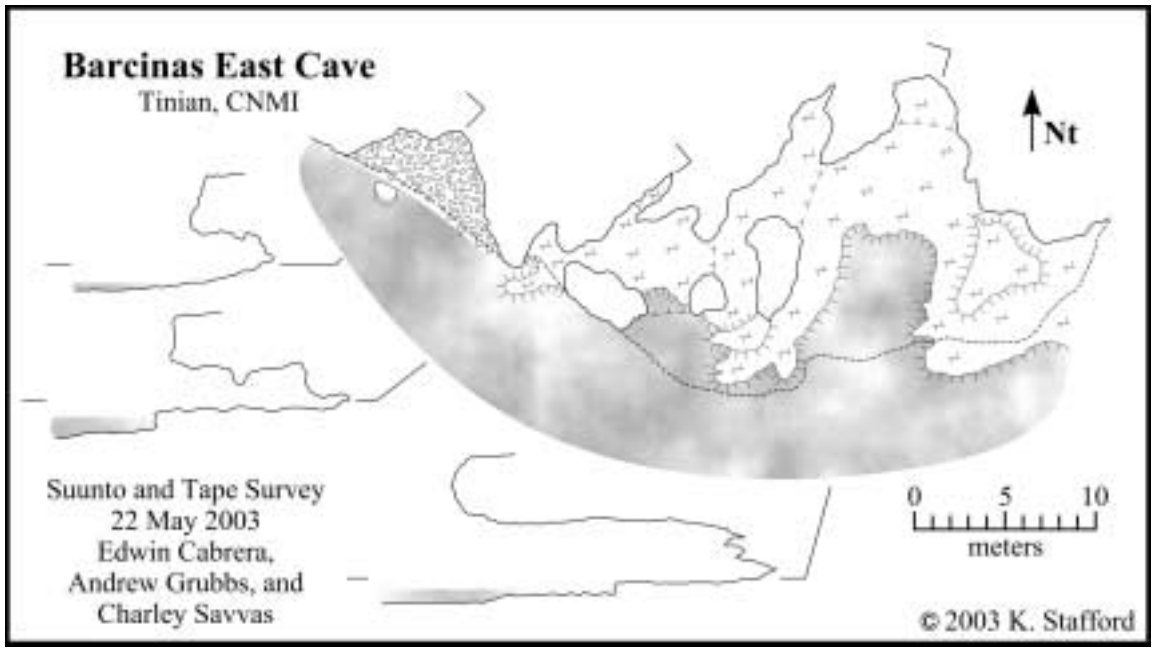

Figure 44: Map of Barcinas East Cave.

Barcinas West Cave (Median Valley, Tinian – Figure 45)

Barcinas West Cave is a flank margin cave located approximately 200 meters west of Barcinas East Cave on the north side of Barcinas Cove (Turtle Cove) in the Mariana Limestone (QTmu). It is a single chamber positioned approximately 1 meter above mean sea level with a width of 22 meters, depth of 15 meters, and maximum ceiling height of 5 meters. A single small column divides the entrance in half, although a large breakdown block in the western portion of entrance gives the appearance of dividing the cave into three entrances. The cave is partially protected from the direct impact of waves by a large resistant bedrock pillar is located approximately 6 meters south of the entrance. Extending 5 meters to the east of the cave is a small passage that is developed along a joint. The cave is devoid of speleothems and the floor is covered with large breakdown blocks and cobbles that have been well rounded by wave action.

Barely Cave (Central Plateau, Tinian – Figure 46)

Barely Cave is a remnant, flank margin cave that is located approximately 600 meters southeast of Puntan Diapblo at sea-level in the Mariana Limestone (QTmu). The cave is 38 meters wide and 18 meters deep and appears to have been severely impacted by intense storm events. The majority of the feature is unroofed, with a partial roof existing on the southeast side of the feature in the region were the cave floor is below sea level. The northern portion of the feature has a bedrock floor, while minor amounts of heavily eroded flowstone exist on the floor of the east-central portion of the cave. Although heavily impacted by coastal processes, the presence of flowstone confirms a spelean origin for the feature.

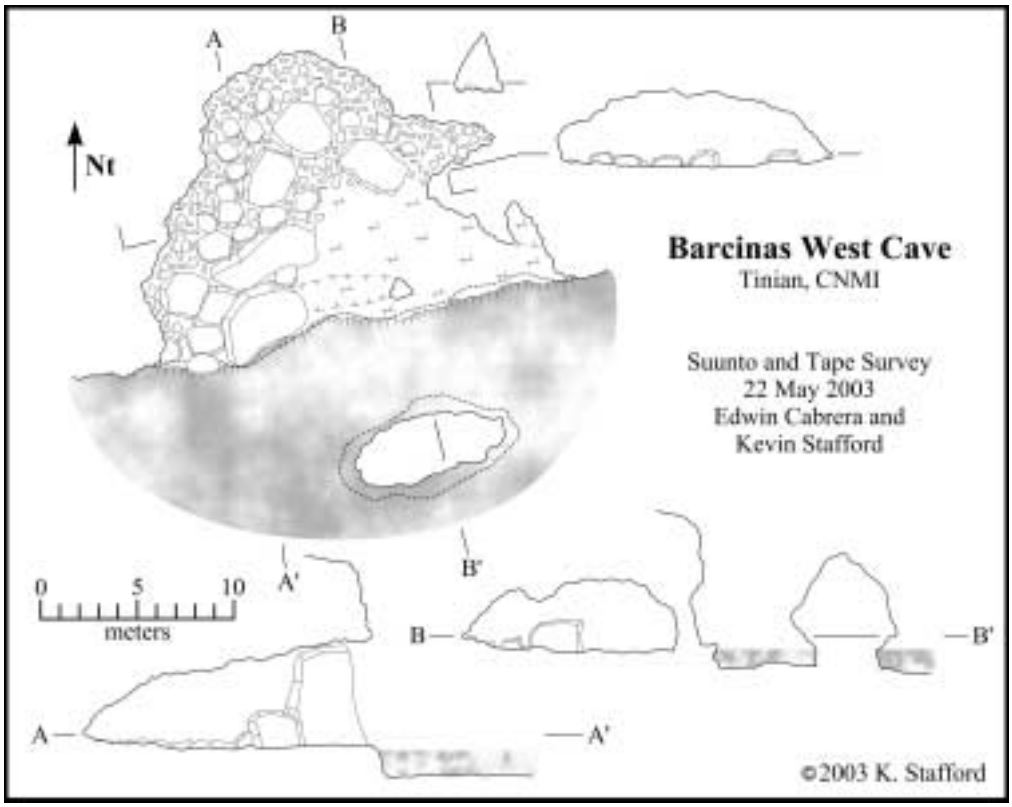

Figure 45: Map of Barcinas West Cave.

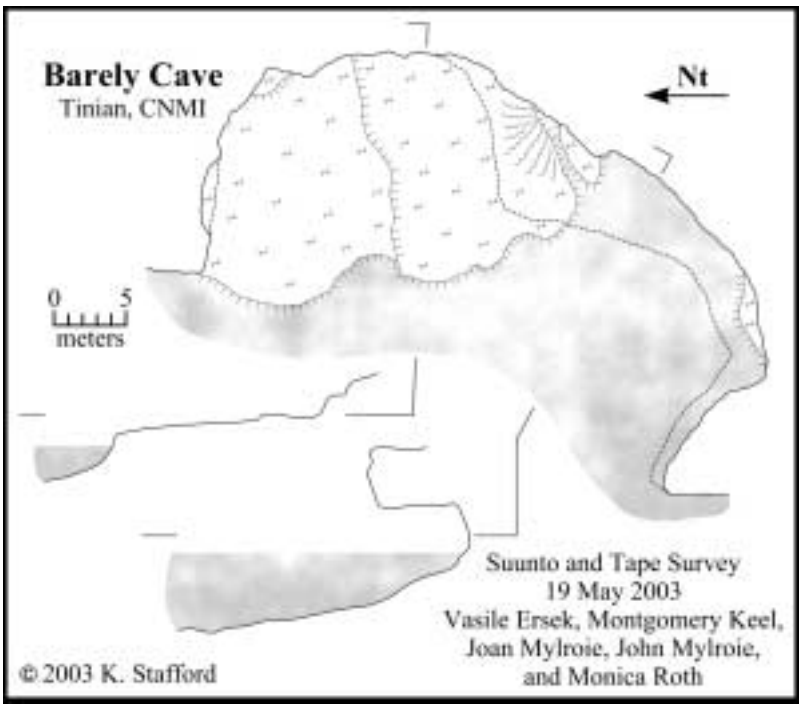

Figure 46: Map of Barely Cave.

Bee Hooch Cave (Southeastern Ridge, Tinian – Figure 47)

Bee Hooch Cave is located along the southeastern scarp of the Piña ridge in the Mariana Limestone (QTmu). It is a flank margin cave breached by cliff retreat with an entrance width of 12 meters, depth of 9 meters and ceiling height of 4.5 meters. The cave has been extensively modified by humans, including the addition of wooden floors that are highly deteriorated in the northwest and northeast portions of the cave. The cave contains minor amounts of flowstone along the walls and has a floor comprised primarily of soil and small breakdown blocks.

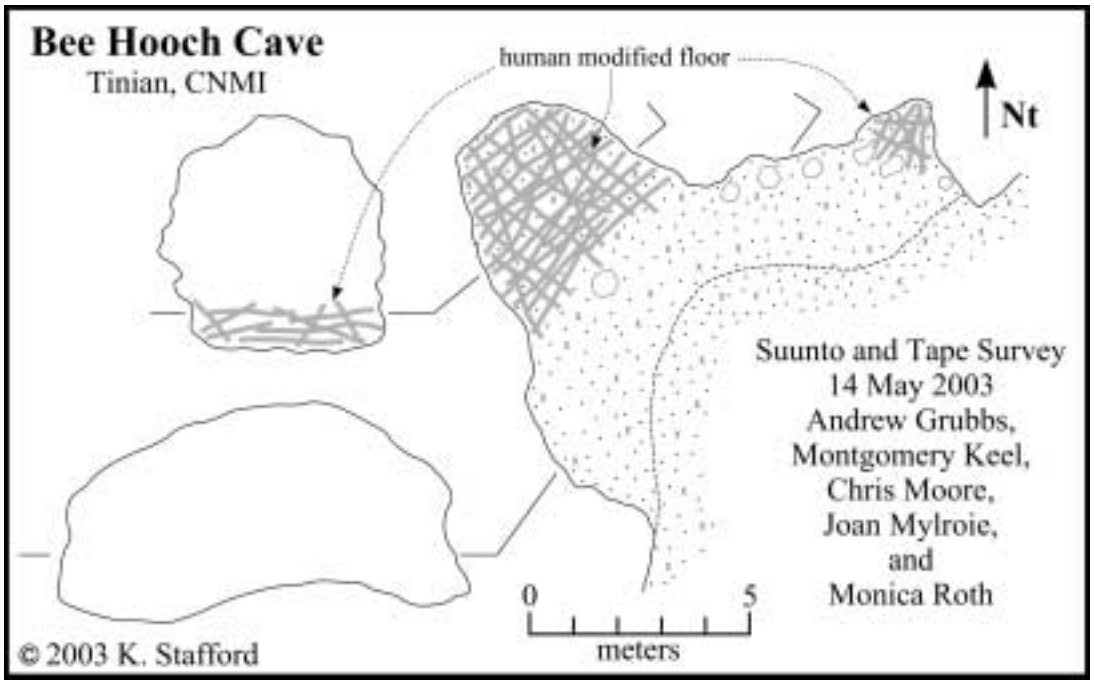

Figure 47: Map of Bee Hooch Cave.

Biting Mosquitoes Cave (Upper Terrace, Aguijan – Figure 48)

Biting Mosquitoes Cave is a small, breached flank margin cave located in the northwest region of the Upper Terrace in the Mariana Limestone (QTmu). It consists of a single chamber 8 meters wide and 10 meters deep with an average ceiling height of 1.5 meters. The floor is primarily composed of alluvium, but speleothem deposits are present in the northwest portion of the cave, forming a large flowstone mound. There is a collapsed, man-made wall in the entrance of the cave.

Body Repel Cave (Southeastern Ridge, Tinian – Figure 49)

Body Repel Cave is a breached, flank margin cave located in the central region of Suicide Cliffs approximately 5 meters below the top of the scarp. It is developed in the Mariana Limestone (QTmu), has a width of 24 meters exposed along the cliff, a depth of 7 meters and maximum ceiling height of 6 meters. This cave remnant represents the inland wall of a larger flank margin chamber that has almost been removed by scarp retreat. The ceiling covers approximately seventy percent of the floor area, which consists of several small terraces.

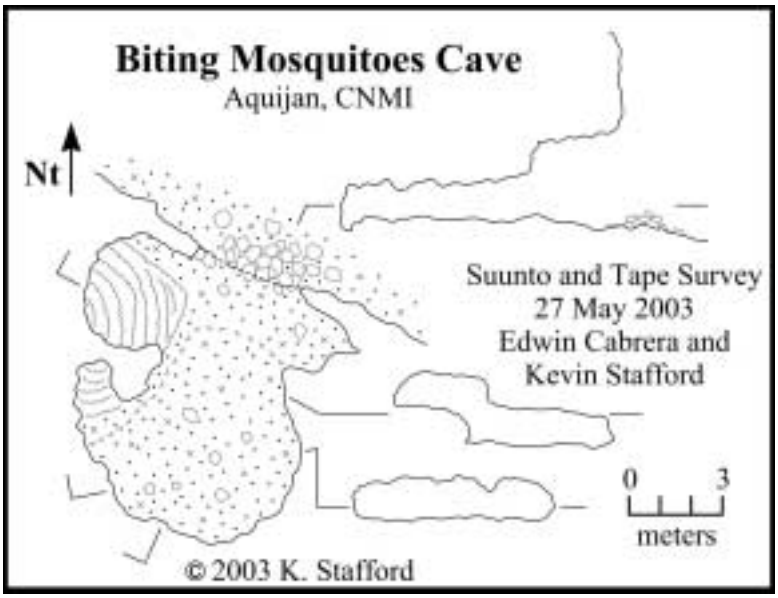

Figure 48: Map of Biting Mosquitoes Cave.

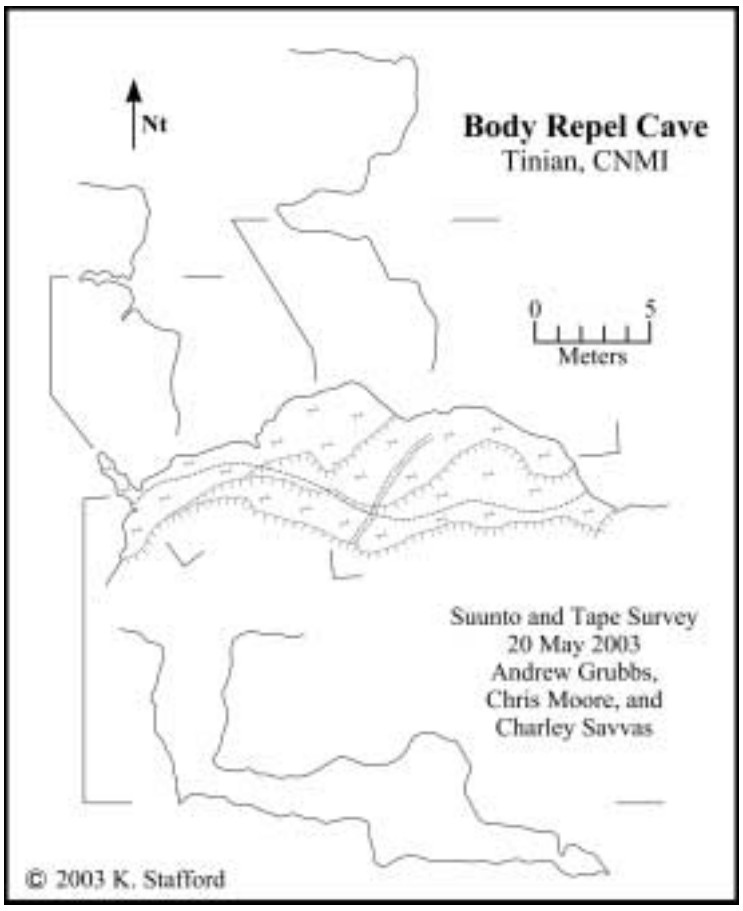

Figure 49: Map of Body Repel Cave.

Booney Bee Sink (Upper Terrace, Aguijan – Figure 50)

Booney Bee Sink is a small banana hole type cave located in the northwest region of the Upper Terrace in the Mariana Limestone (QTmu). It is 1 meter wide, 4 meters long and up to 1 meter tall, with a floor composed of alluvium and a small passage continuing from the southeast corner of the cave. This feature appears to take some local recharge when precipitation exceeds local infiltration rates, but the area affected appears to be limited to a few square meters.

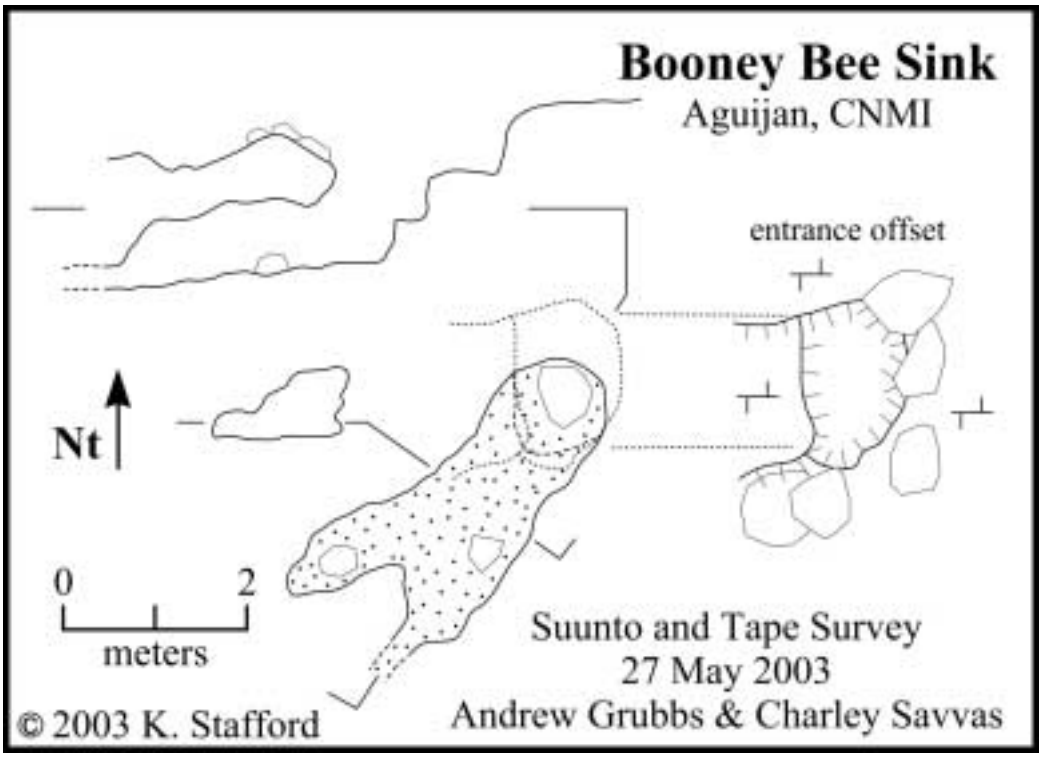

Figure 50: Map of Booney Bee Sink.

Broken Stal Cave (Southeastern Ridge, Tinian – Figure 51)

Broken Stal Cave is located along the southeastern scarp of Piña ridge in the Mariana Limestone (QTmu) and contains limited speleothem deposits except for a single 6-centimeter tall stalagmite in the south-central portion. The main cave remnant is 5 meters wide at the entrance and splits into two smaller passages that join 6 meters inland. The cave is 4 meters tall in the entrance area where the floor is composed of soil and detritus, but the floor is elevated at a 2-meter tall ledge, 1-meter inland from the cave entrance, where the floor becomes bedrock. A 1-meter wide, 2-meter deep bedrock column separates the two passages, while an additional 1 to 2 meters of bedrock separate the main cave from a smaller cave remnant to the south.

Cabrito Cave (Middle Terrace, Aguijan – Figure 52)

Cabrito Cave is a small, breached flank margin cave located in the eastern region of the Middle Terrace in the Mariana Limestone (QTmu). It is 5 meters wide, 2 meters deep and has a maximum height of 2.5 meters. The floor is composed of alluvium in the entrance area and bedrock in the inland portions. The cave contains slightly elevated floor regions in the northern and southern portions, forming a lowered, "trench-like" region in the central portion that is the same elevation as the region near the entrance.

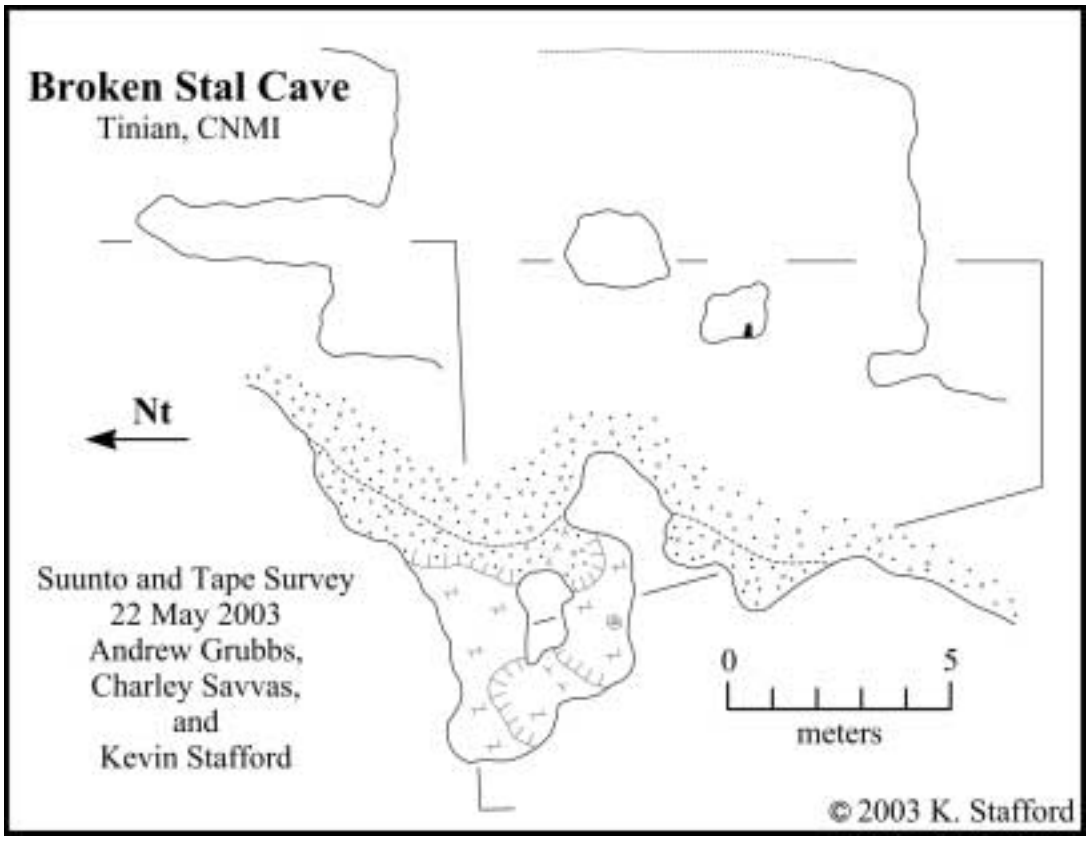

Figure 51: Map of Broken Stal Cave.

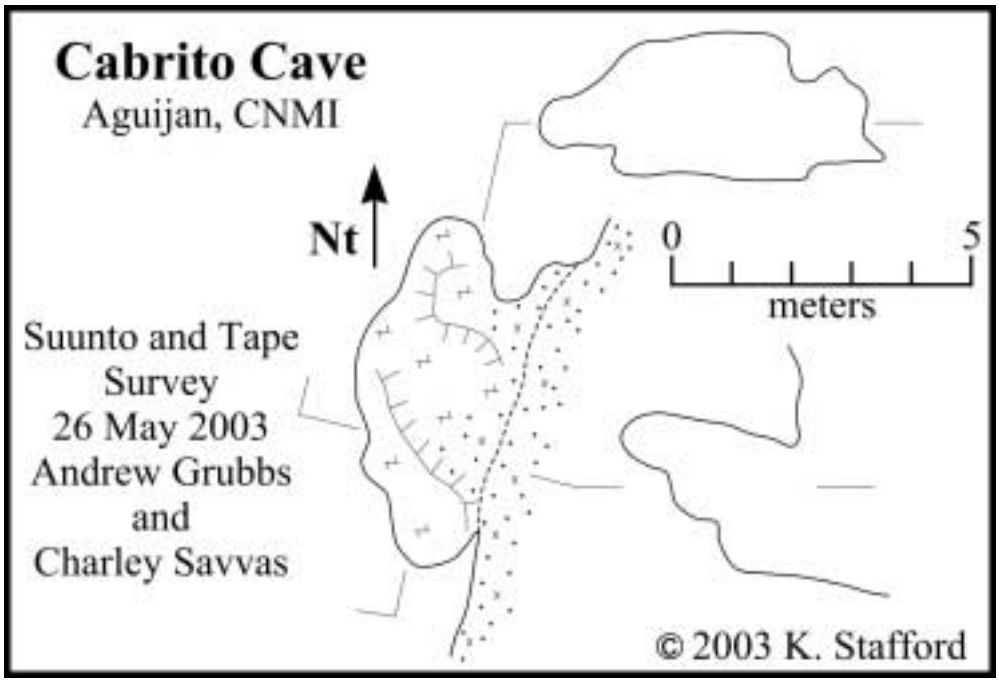

Figure 52: Map of Cabrito Cave.

Cannon Cave (Central Plateau, Tinian – Figure 53)

Cannon Cave is a modified flank margin cave formed in the Mariana Limestone (QTmu). It is located approximately 2 kilometers east of Puntan Diapblo, approximately 300 meters north of the coast. The cave was modified and used as a defensive position by the Japanese during World War II and still contains a 5-meter long, 16-centimeter Japanese gun. The natural chamber is 5 meters by 12 meters with a ceiling height of 5 meters. Extending to the East is a 5-meter long, 1.5-meter square dug, tunnel probably used to store ammunition. This feature appears to have had little modification to the ceiling and the walls of the main chamber, but the floor appears to have had significant modification for use as a defensive position.

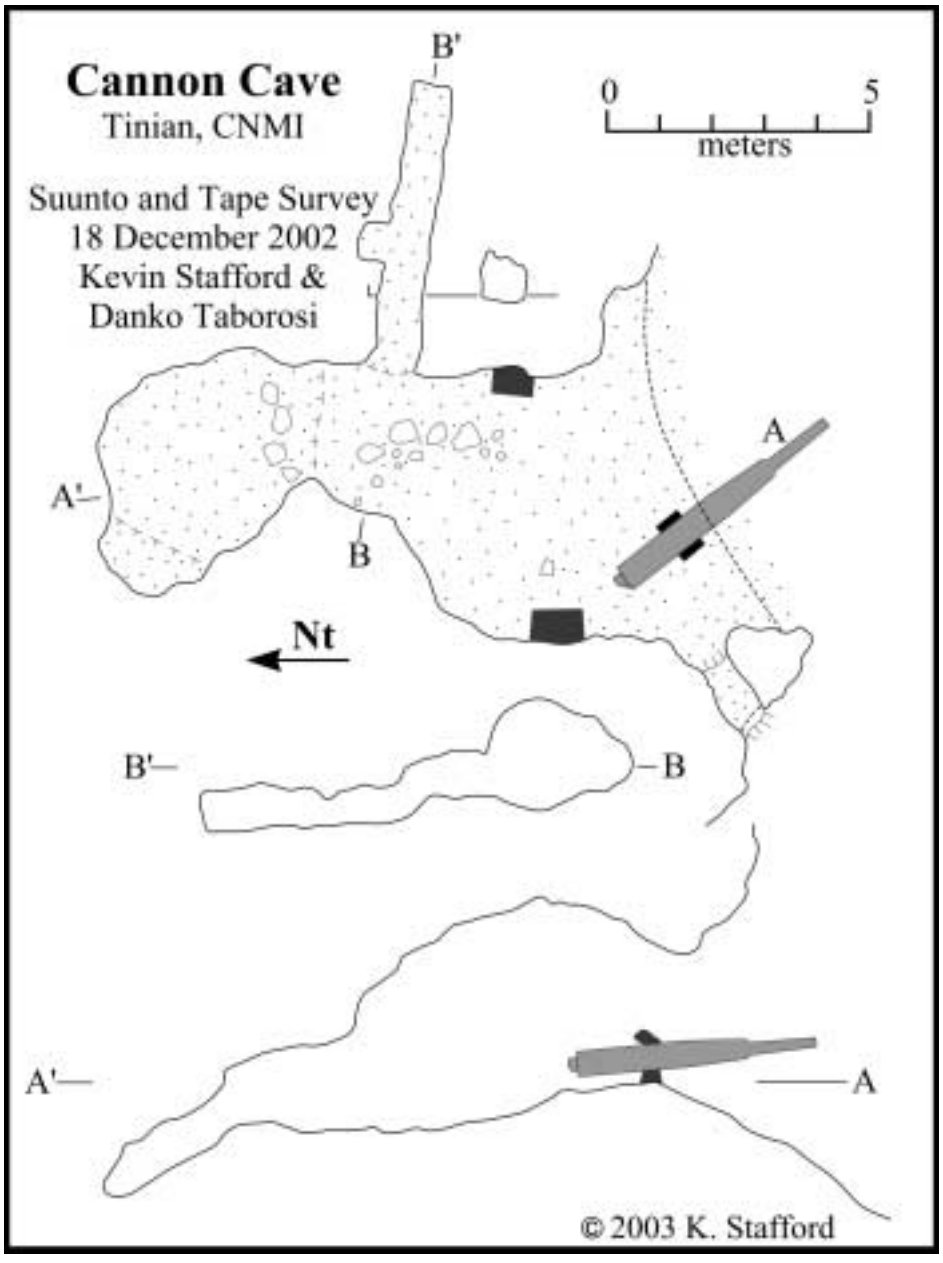

Figure 53: Map of Cannon Cave.

Carolinas Fracture Cave (Southeastern Ridge, Tinian – Figure 54)

Carolinas Fracture Cave is located in Carolinas Limestone Forest, approximately 500 meters east of the ocean and oriented roughly parallel to the cliff margin. This feature is developed in the Mariana Limestone (QTmu) as a result of the dissolutional widening of a fracture created by cliff margin retreat. The feature trends northeast (~50°) and extends for approximately 70 meters, with an average width of 2 meters and maximum depth of 16 meters. Approximately one half of the feature is roofed with large breakdown blocks, comprising the northeastern portion of the feature, which intersects the cliff line that is retreating. The cave shows extensive speleothems covering the walls in the roofed section with lesser amounts in the unroofed portions.

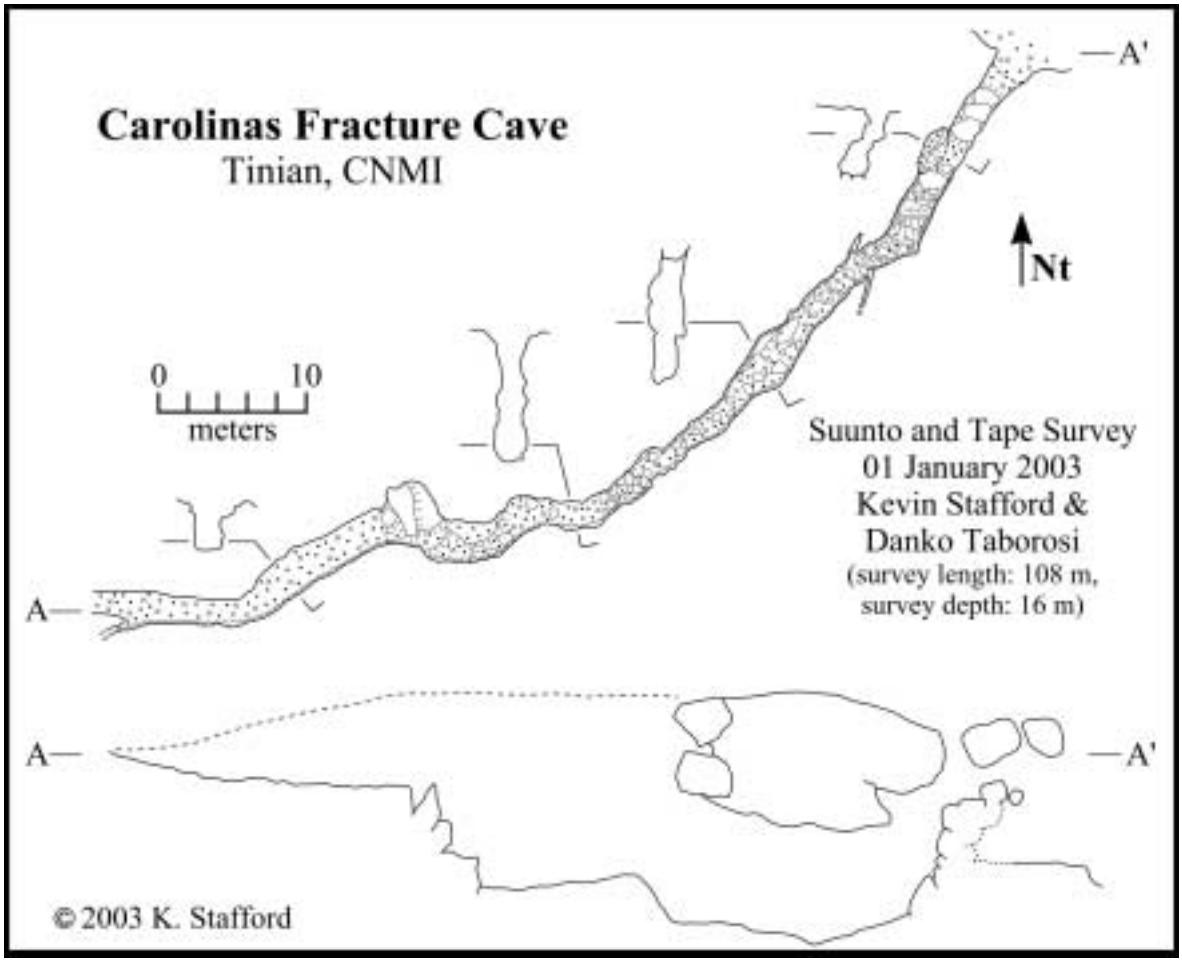

Figure 54: Map of Carolinas Fracture Cave.

Cave Without a Cave (Southeastern Ridge, Tinian – Figure 55)

Cave Without a Cave is an extreme end member of a remnant flank margin cave breached by cliff retreat. It is located in the central portion of Suicide Cliffs, approximately 20 meters above the base of the cliff and is developed in the Tagpochau Limestone (Tt). This feature is 20 meters wide, 5 meters deep, 5 meters tall and apparently represents the most inland wall of a flank margin cave. The cave has undergone extensive erosion, but some minor speleothems are present.

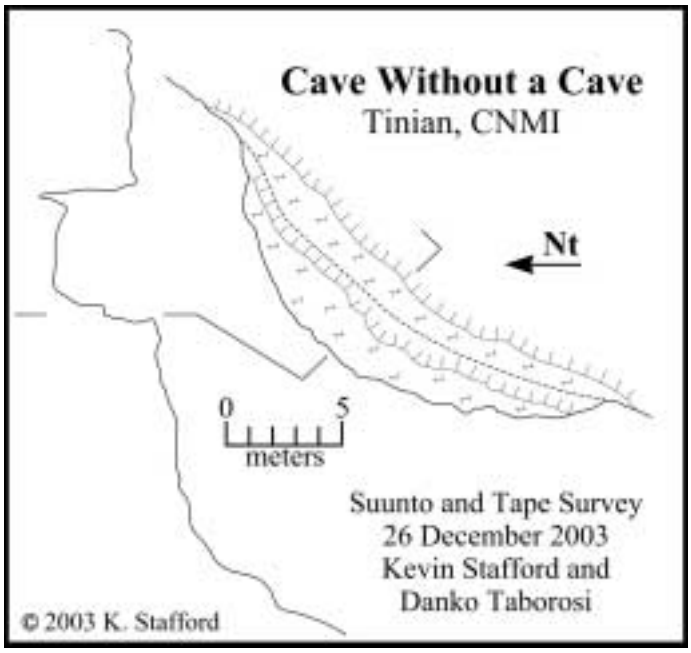

Figure 55: Map of Cave Without a Cave.

Cave Without a Roof (Southeastern Ridge, Tinian – Figure 56)

Cave without a Roof is an intersected flank margin cave located in the central portion of Suicide Cliffs, approximately 25 meters above the base of the cliff, developed in the Tagpochau Limestone (Tt). It is a single, remnant chamber that is 5 meters by 14 meters in size, with a ceiling height of 5 meters. The cave contains only minor speleothems possibly because it has undergone extensive collapse as part of cliff retreat. The roof is missing in most portions of the cave, representing an intermediate stage in the process of cliff retreat where the cave has not only been breached, but the cave roof has been removed by erosional processes.

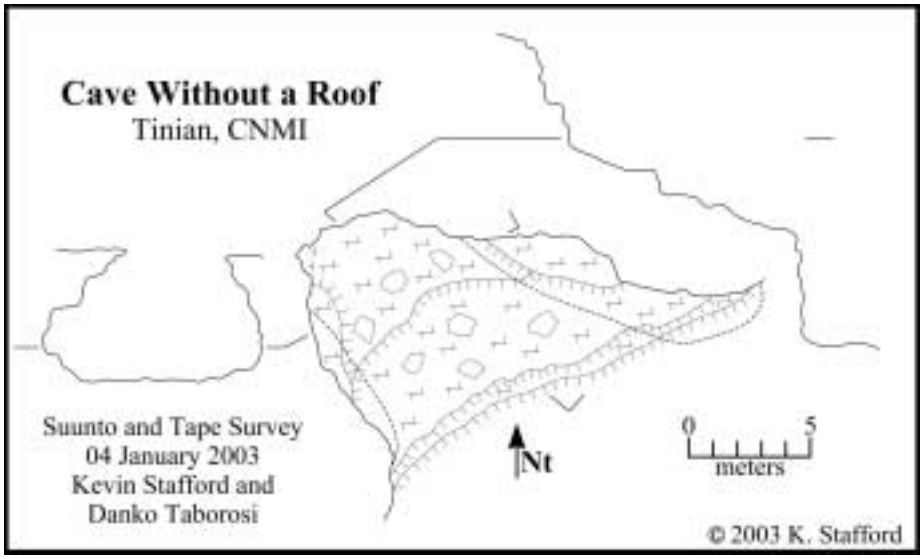

Figure 56: Map of Cave Without a Roof.

Cavelet Cave (Central Plateau, Tinian – Figure 57)

Cavelet Cave is a small, remnant, flank margin cave located approximately 500 meters southeast of Puntan Diapblo. The cave, developed in the Mariana Limestone (QTmu), has an entrance 4 meters wide, extends inland 5 meters, and has an average ceiling height of 1.5 meters. The cave is located 3 meters above sea level and approximately 100 meters inland. The floor is composed of bedrock with small breakdown blocks, while the cave is devoid of speleothems, possibly as a result of intense storm events.

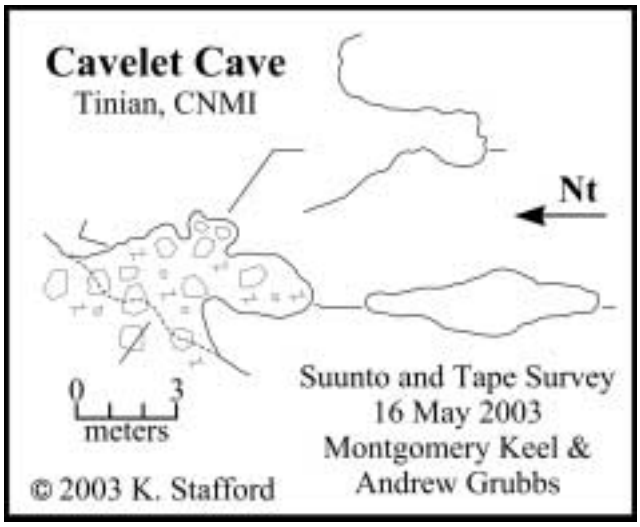

Figure 57: Map of Cavelet Cave.

Central Mendiola Cave Complex (Central Plateau, Tinian – Figure 58)

Central Mendiola Cave Complex is located in the central region of a large cove approximately 800 meters southeast of Puntan Atgidon, which is locally referred to as Mendiola Cove after the landowner. This cave complex is developed in the Mariana Limestone (QTmu) and covers 150 meters of coastline. The breached, flank margin caves extend inland up to 20 meters with and average ceiling height of 4 meters. They are located slightly above mean sea level and primarily contain bedrock floors with weathered breakdown blocks and cobbles. Smaller cave chambers exist at the north and south ends of the surveyed cave complex with the largest chamber located in the central region. The largest chamber has an entrance 50 meters wide and extends inland 15 meters as a single large chamber. There is a sea stack located at its southern margin that may represent a previous bedrock column. To the south of the largest cave, the deepest cave extends inland 20 meters with average width of 8 meters, while to the north of the largest cave a chamber divided by a 2 meter wide, 10 meter long bedrock column extends inland 15 meters. This series of breached, flank margin caves appear to have been connected as a single cave in the past based on the proximity of the individual cave remnants and their corresponding ceiling drip lines.

Cetacean Cave (Southeastern Ridge, Tinian – Figure 59)

Cetacean Cave is located 250 meters southeast of Unai Masalok in the Mariana Limestone (QTmu) near and parallel to a large fault scarp, which trends 85^{o}. The cave is developed along a joint that can be observed in the ceiling, while significant freshwater discharges from the fracture in the floor. The cave extends 25 meter inland with and average width of 3 meters and ceiling height between 2 and 3 meters. The entrance area is partially

Figure 58: Map of Central Mendiola Cave Complex.

obstructed by two large breakdown blocks, while the presence of numerous fishing net floats wedged into the ceiling joint is evidence of intense wave impact. The majority of the cave has a bedrock floor submerged under 0.25 to 0.5 meters of water with some weathered breakdown blocks and cobbles protruding above water level. It appears that the cave formed by freshwater discharging along a fracture, resulting in the headward dissolution of limestone enhanced by the mixing of fresh and salt waters.

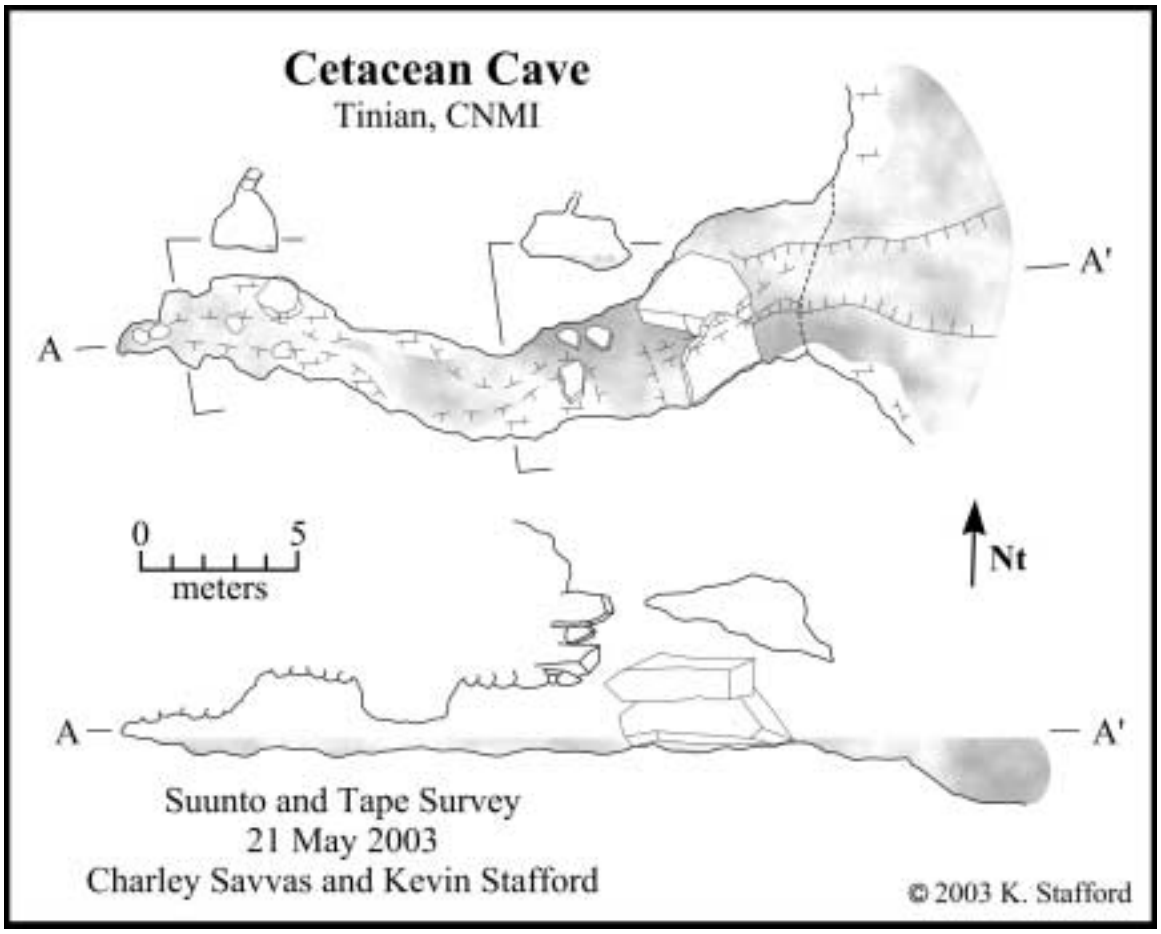

Figure 59: Map of Cetacean Cave.

Chiget Fracture (Central Plateau, Tinian – Figure 60)

Chiget Fracture is located on the southern wall of the Unai Chiget Fault scarp, approximately 500 meters inland. It is developed in the Mariana Limestone (QTmu) and is a dissolutionally widened fracture that is oriented northeast (~50 ^{o}) and intersected by a smaller fracture oriented east/southeast (~105 ^{o}) in the inland portion. The main fracture is approximately 20 meters long, 1.5 meters wide and 15 meters deep. In the inland portion, the fracture is blocked by breakdown, which forms a small roofed portion, but no speleothems are present. The small fracture extends for over 6 meters and is less than 0.5 meters wide. These dissolutionally widened fractures are the result of cliff retreat associated with fracturing at the cliff margin.

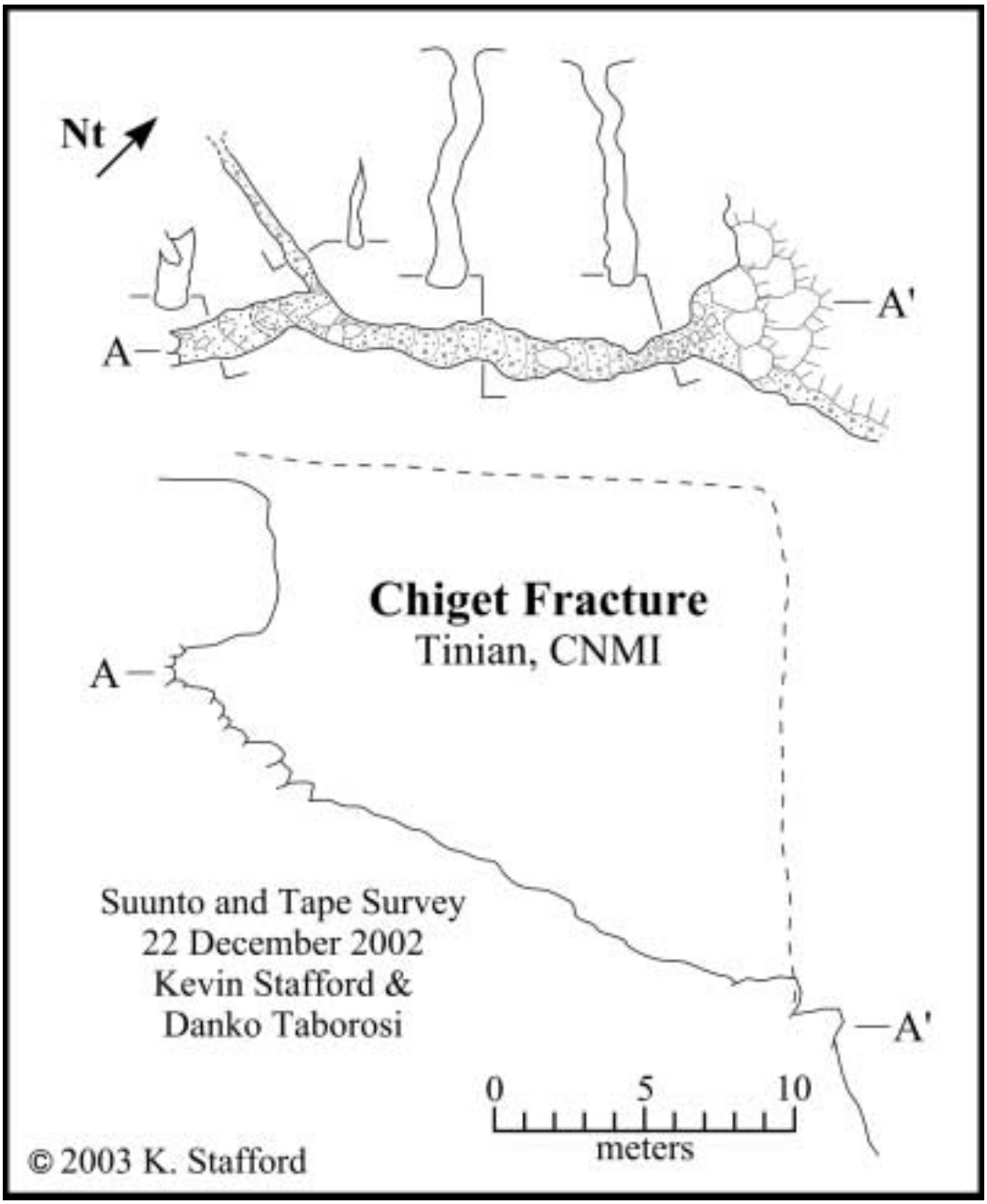

Figure 60: Map of Chiget Fracture.

Cobble Cave (Central Plateau, Tinian – Figure 61)

Cobble Cave is located 650 meters southeast of Puntan Atgidon in the Mariana Limestone (QTmu). It is a flank margin cave remnant located approximately 1 meter above sea level in the northeastern portion of a large cove referred to locally as Mendiola Cove after the landowner. The entrance is 19 meters wide and the cave extends inland 11 meters with an average ceiling height o f 4 meters. The floor is primarily composed of carbonate sand but numerous well-round cobbles and breakdown blocks are scattered around the chamber, some of which appear to be remnants of the original ceiling that extended farther seaward.

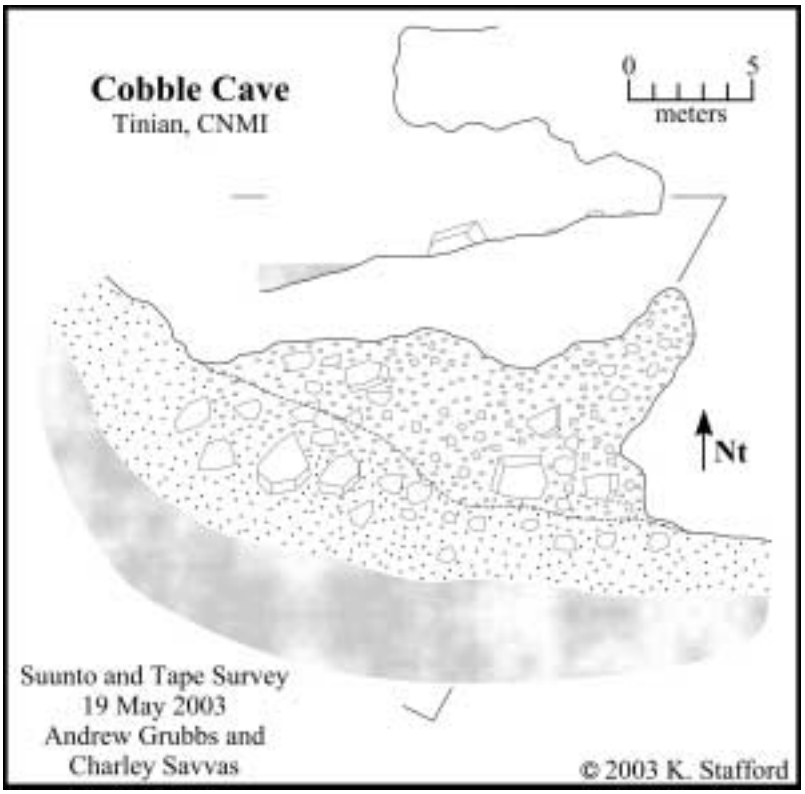

Figure 61: Map of Cobble Cave.

Coconut Trap Cave (Southeastern Ridge, Tinian – Figure 62)

Coconut Trap Cave is located in the southeastern region of the Piña ridge and developed in the Mariana Limestone (QTmu). This small, flank margin cave remnant has an entrance 5 meters wide and extends inland 5 meters with an average ceiling height of 2 meters. The cave has a small flowstone mound that partially separates the entrance area from the inland portions and has a floor composed of soil and detritus.

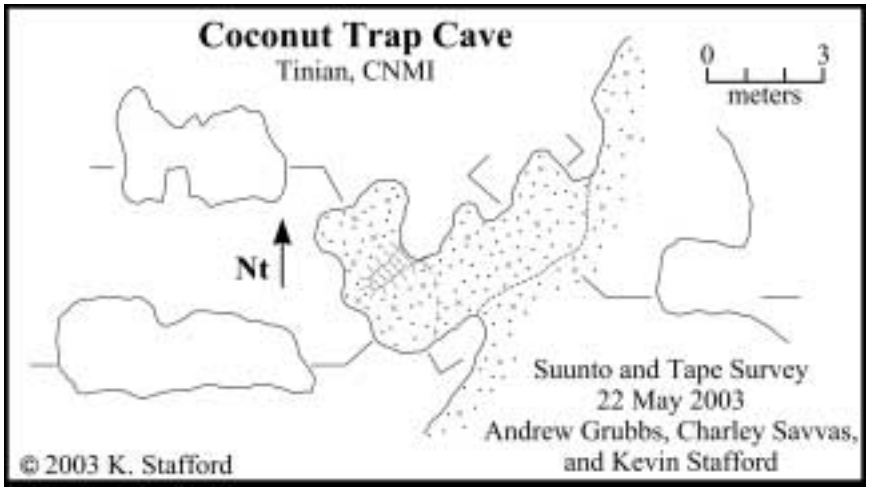

Figure 62: Map of Coconut Trap Cave.

Command Post Cave Complex (North-Central Highland – Figure 63)

The Command Post Cave Complex is located approximately150 meters north/northeast of the Lasso Shrine on Mt. Lasu. These caves, developed in the Mariana Limestone (QTmca) at the base of the cliff, appear to be breached cliff retreat. These caves were highly modified during WWII for use by the Japanese and include such features as large fortified walls across the entrances and excavated cave floors. Although the caves have been highly modified, the walls and ceiling appear to have little modification. The larger cave is approximately 19 meters by 10 meters, while the ceiling rises to 5 meters in regions. The smaller cave is approximately 4 meters by 9 meters with a ceiling height averaging 1.5 meters.

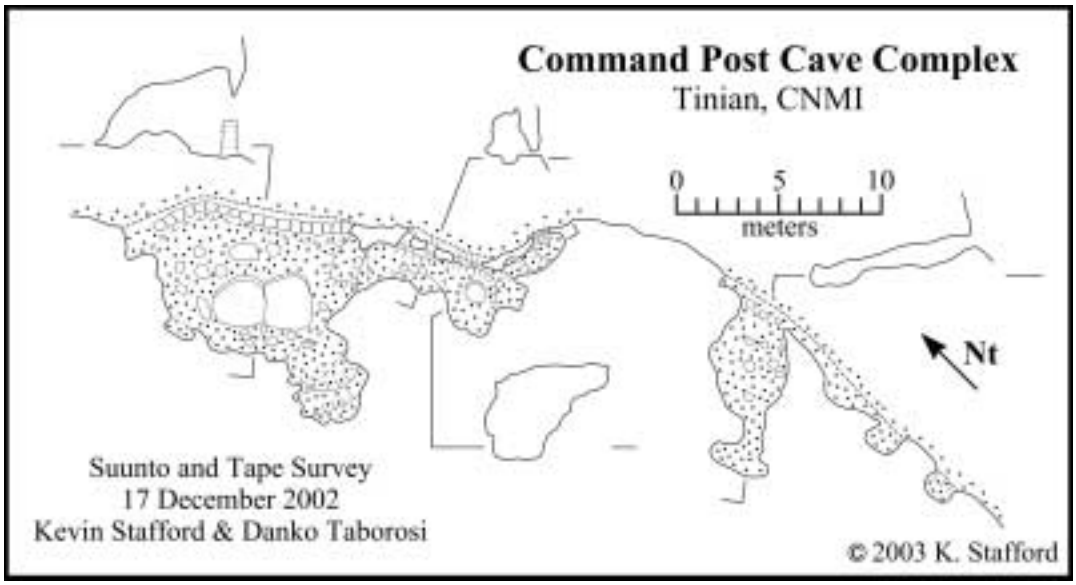

Figure 63: Map of Command Post Cave Complex.

Cowrie Cave (Central Plateau, Tinian – Figure 64)

Cowrie Cave is located approximately 500 meters southeast of Puntan Atgidon on the northern edge of a large cove locally referred to as Mendiola Cove after the landowner. This bedrock floored cave is a breached flank margin cave positioned less than 1 meter above mean sea level. The cave is 8 meters wide and 16 meters deep with a maximum ceiling height of 7 meters. A prominent fracture trends 113°, parallel to the entrance, approximately 5 meters inland and has produced 2 meter deep dissolutional features in the east and west walls of the cave. The cave is named for several large cowries that were living in a small pool of water at the time of survey.

CUC Cave (Median Valley, Tinian – Figure 65)

CUC Cave is a banana hole type cave located 500 meters east of the CUC power plant. It consists of a low broad chamber 8 by 9 meters with an average ceiling height of 1 meter. The cave contains numerous speleothem deposits primarily as stalactites and one 0.5-meter diameter column located in the middle of the feature. The floor is primarily alluvium introduced from two breached entrances; a small entrance located in the northwest corner of the feature and a larger, main entrance located in the northeast corner. The cave is located in dense vegetation on relatively flat land and is easily overlooked; however, the cave does show evidence of human modification including many broken cave formations.

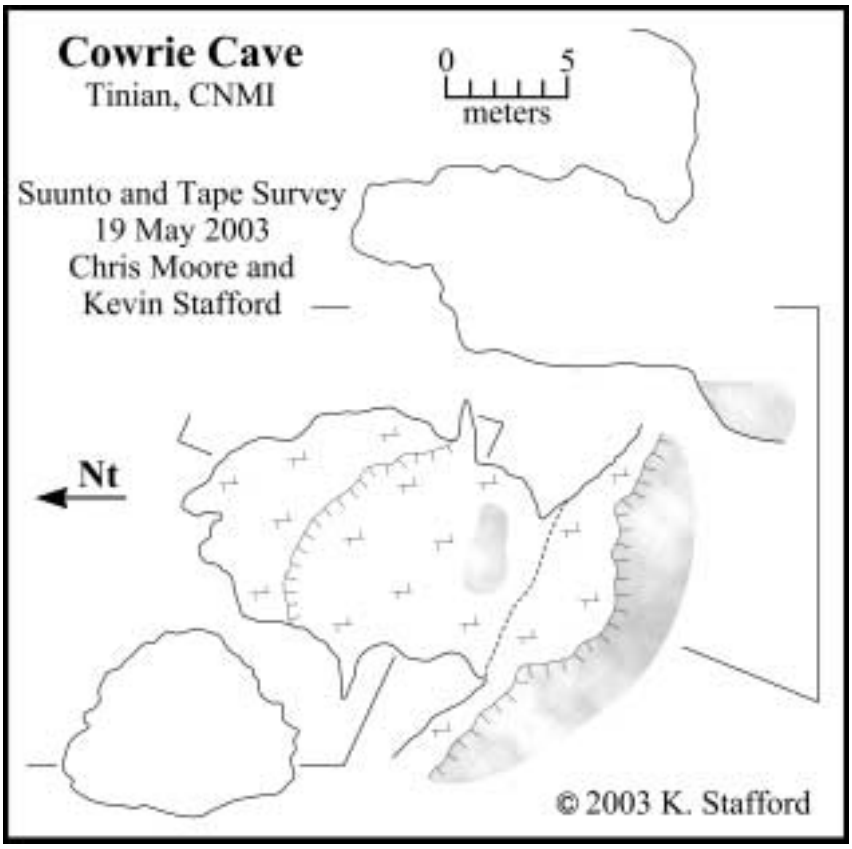

Figure 64: Map of Cowrie Cave.

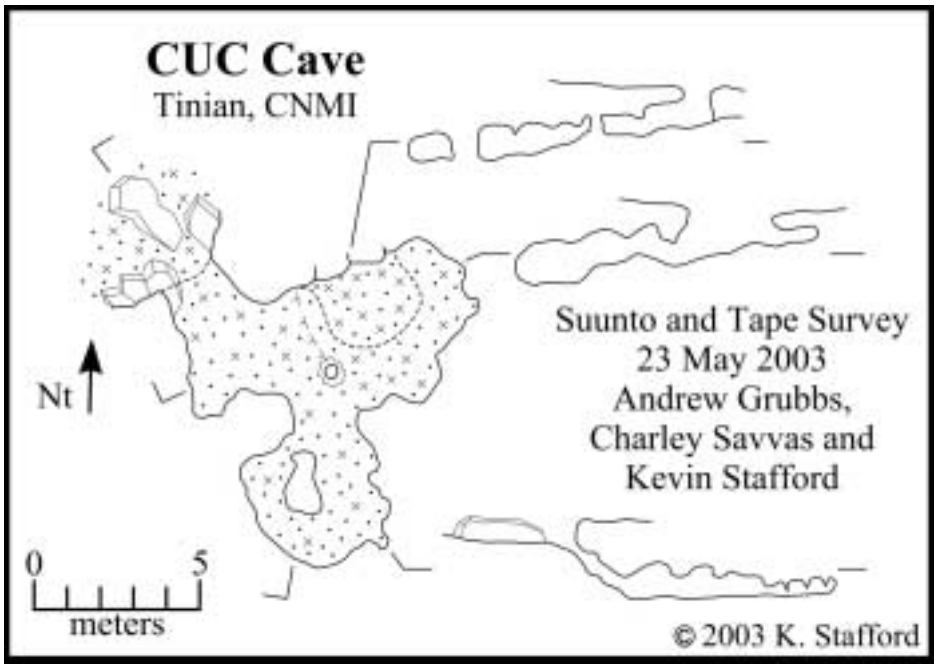

Figure 65: Map of CUC Cave.

Danko's Misery (Southeastern Ridge, Tinian – Figure 66)

Danko's Misery is located approximately 1000 meters southwest of Puntan Barangka along the northeastern cliffs of Carolina's Ridge. It is developed in the Mariana Limestone (QTmca) as a dissolutionally enhanced bank-margin fracture that is oriented northwest at a bearing of 305°. This fracture cave is 24 meters in length, 22 meters deep and has a maximum width of 2 meters. The floor is composed of breakdown, forming three levels that increase in depth to the southwest, which limited exploration. In the general region of Danko's Misery, there are numerous other fractures with the same general orientation, however most of these features are not humanly enterable.

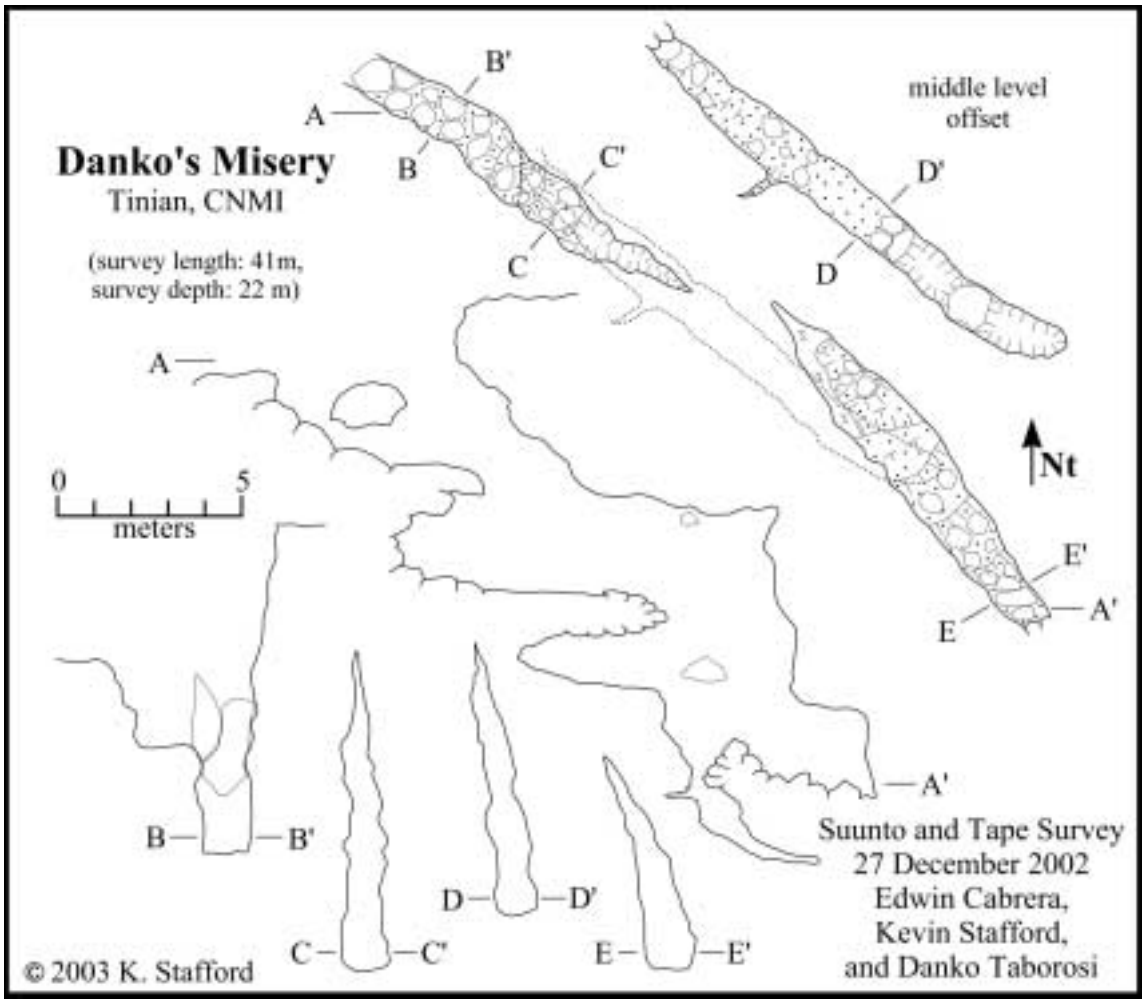

Figure 66: Map of Danko's Misery.

Death Fracture Complex (Central Plateau, Tinian – Figure 67)

The Death Fracture Complex is located along the west coast approximately 900 meters south of Puntan Diapblo in the Mariana Limestone (QTmu). This fracture complex contains three primary features, which extend inland as dissolutionally widened fractures oriented at 53°, 60°, 80°, and 112° with an average depth to sea level of 8 meters. The features are widest near the coastline and decrease in width with distance inland, however all features extend well below sea-level and are severely impacted by normal wave attack, which limited exploration to surface

observations at the time of survey. The features appear to have well-developed ledges at sea level, but the cave then appears to widen below sea level. Because of their similarity to features seen on Guam (No-Can Cave, Taborosi, 2000) and their development along prominent regional fractures, these features are interpreted as structurally controlled, fresh-water discharge features although strong surf conditions, which would surge over 4 meters upwards into the features, prevented physical observation of fresh-water discharge.

Diamond Cave (Lower Terrace, Aguijan – Figure 68)

This flank margin cave remnant is located on the southern side of Aguijan on the lower terrace in Mariana Limestone (QTmu). It extends inland (north) approximately 26 meters as two passages that are connected in the entrance area, where the ceiling height reaches a maximum of 9 meters at the entrance drip line. Extensive speleothems, including large columns, suggest that the cave was closed for period of time and was then breached by retreat of the cliff margin. This feature showed evidence of extensive use by feral goats.

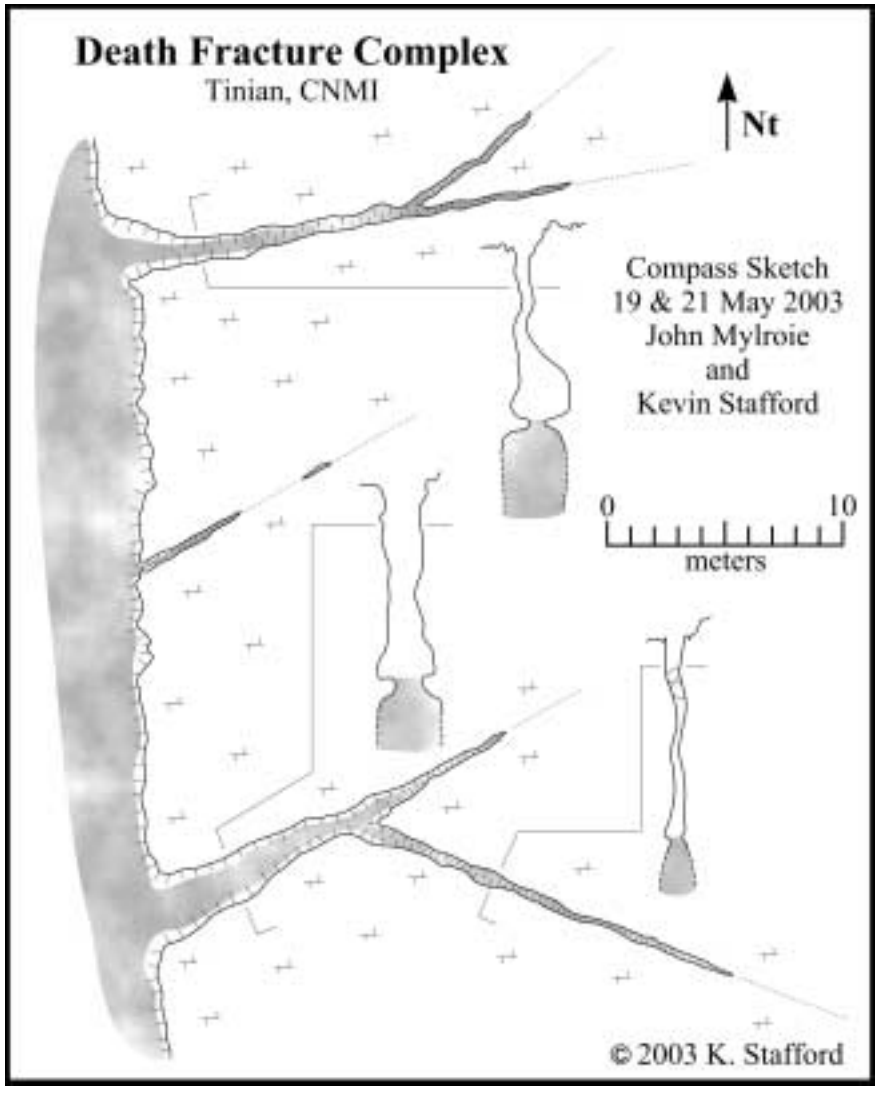

Figure 67: Map of Death Fracture Complex.

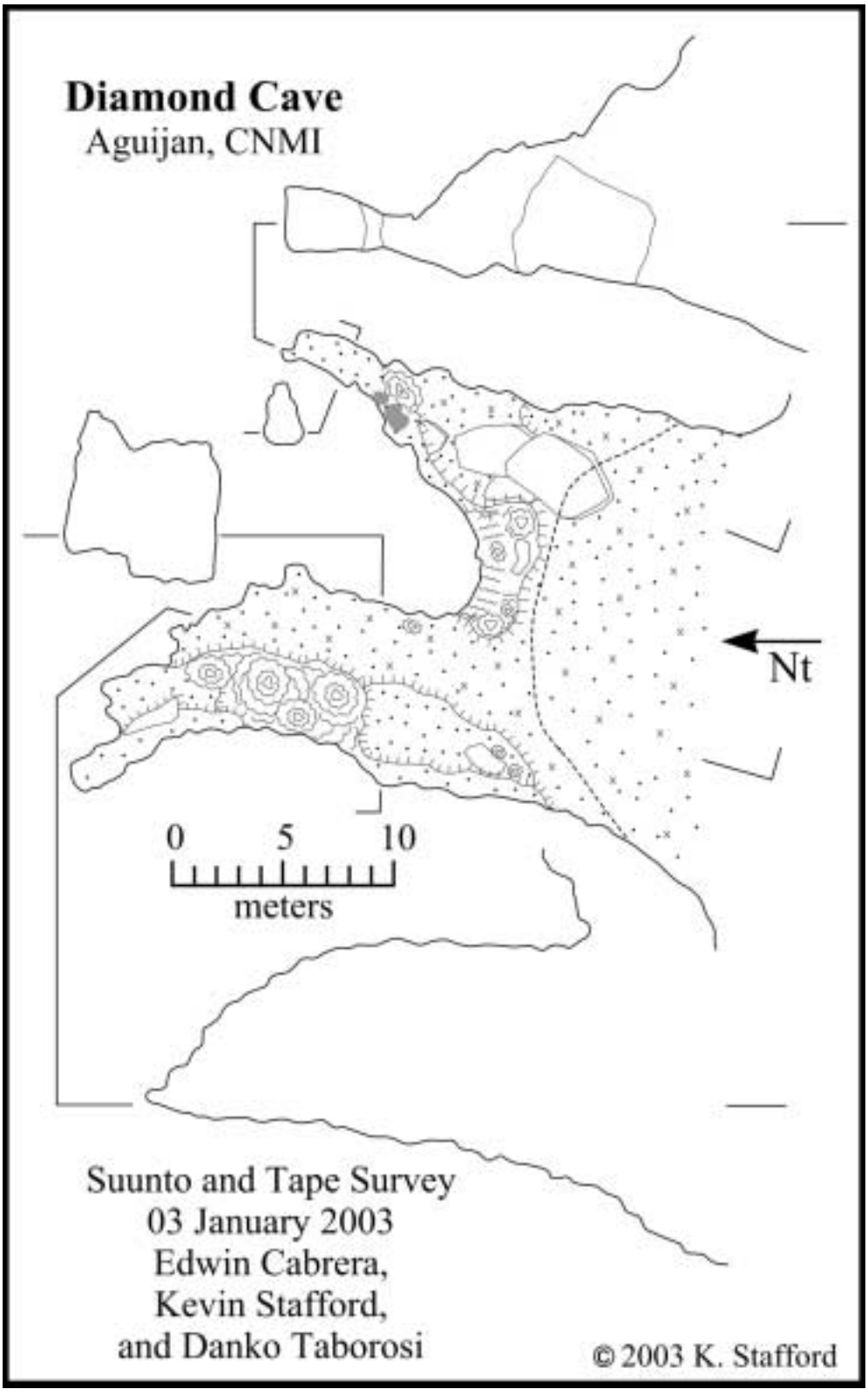

Figure 68: Map of Diamond Cave.

Dos Cenotes Cave (Central Plateau, Tinian – Figure 69)

Dos Cenotes Cave is located approximately 450 meters southeast of Puntan Atgidon in the northwest corner of a large cove locally referred to as Mendiola Cove after the landowner. The 45-meter wide, south facing entrance opens to the ocean and is protected by headlands projecting from the southeast and southwest sides. In the northeast portion, the cave extends inland 15 meters as a terraced chamber with a large bedrock column in the middle. In the northwest portion, the cave extends inland 12 meters with two bedrock columns located near the entrance. From the northwest portion of the cave, a passage averaging 3 meters wide extends to the west for 30 meters where it connects to the surface through a skylight entrance and to the ocean through a submerged passage. The cave primarily contains bedrock floors, but breakdown blocks and minor speleothem deposits are found throughout. The cave is named after two pools of water approximately 3 meters deep, which are located southwest of the main entrance area.

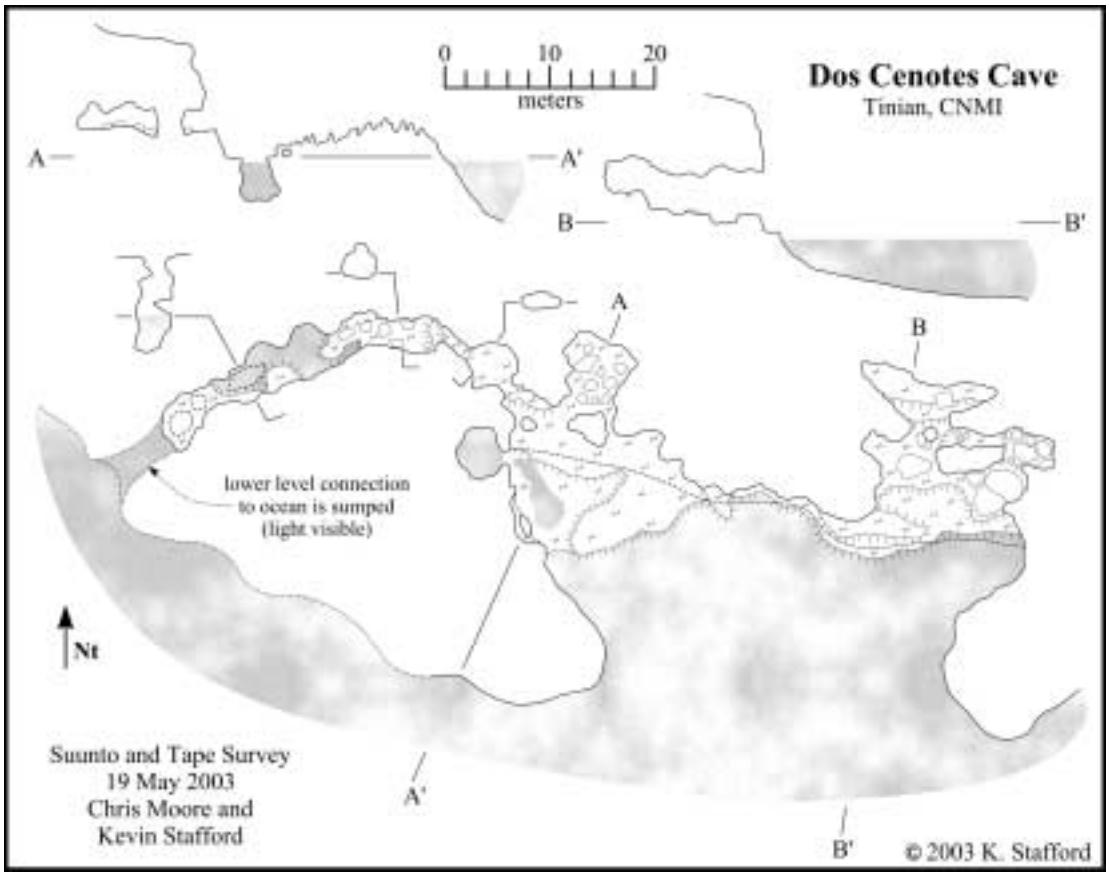

Figure 69: Map of Dos Cenotes Cave.

Dos Sakis Cave Complex (Central Plateau, Tinian – Figure 70)

Dos Sakis Cave Complex consists of five breached, flank margin caves located approximately 1000 meters east of Puntan Diapblo along a 9-meter tall scarp in the Mariana Limestone (QTmu). The caves extend inland a maximum of 5 meters with an average ceiling height of 3 meters. The most western and smallest cave in the complex is slightly elevated on the scarp wall. The two eastern most caves are simple chambers that show minor human modification including a partial rock wall. The two central caves, extend the farthest inland and show greater human modification. The western of the two has a 1-meter wide and 1-meter deep

trench extending from the entrance to the back wall of the cave. The eastern central cave is the largest and has a depression 1 to 1.5 meters deep and almost 5 meters in diameter excavated in the entrance area, while the cave floor rises 2 meters in the inland portion. The caves in this complex have floors primarily of soil and detritus with occasional breakdown blocks and all appear to have been partially to extensively modified by humans.

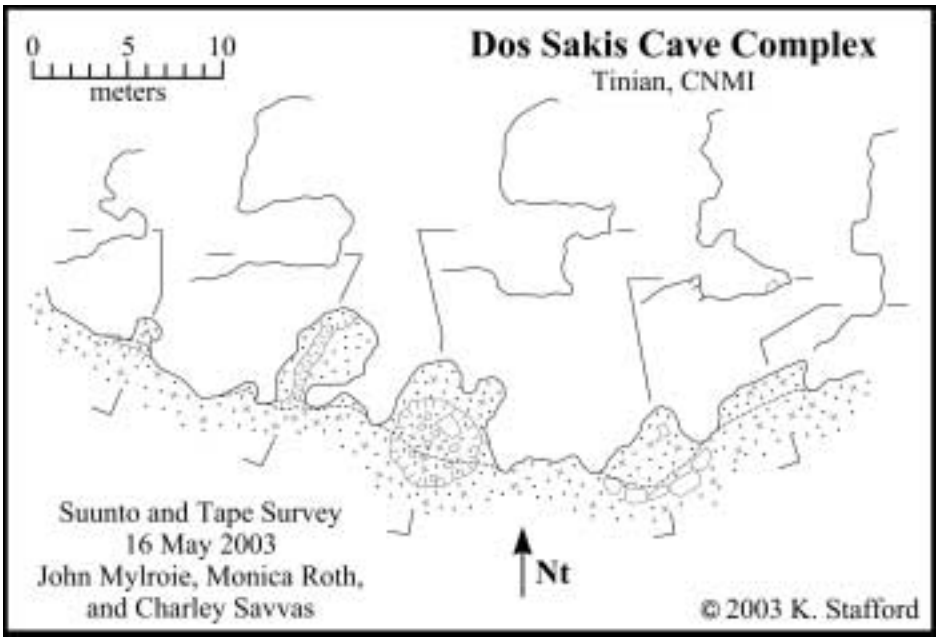

Figure 70: Map of Dos Sakis Cave Complex.

Dove Cave (Upper Terrace, Aguijan – Figure 71)

Dove Cave is a small banana hole type cave located in the northwest portion of the Upper Terrace in the Mariana Limestone (QTmu). It has a maximum width of 6 meters and an average height of 1 meter, with a floor primarily composed of alluvium and detritus. In the northeast portion of the cave, a flowstone mound is present which is 1 meter by 2 meters and rises 0.5 meters above the floor level of the cave. The entrance is located on the southern side of the feature in a region composed of breakdown blocks, which partially conceal the entrance.

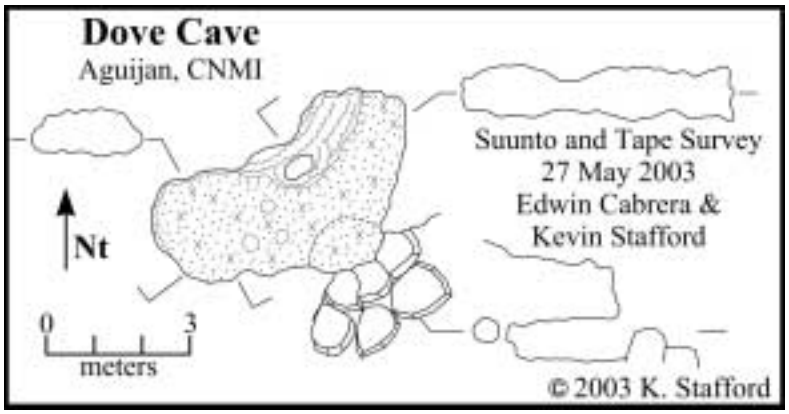

Figure 71: Map of Dove Cave.

Dripping Tree Fracture Cave (Median Valley, Tinian – Figure 72)
Dripping Tree Fracture Cave, developed in the Mariana Limestone (QTmca), is located approximately 200 meters south of Unai Dangkolo and consists of a long fracture oriented approximately 335°. The feature was mapped for almost 300 meters with several small fractures intersecting it at high angles. The majority of the feature is unroofed, but two sections, each approximately 20 meters long, have roofs composed of large breakdown blocks. The feature has been formed by solutional modifications of a bank-margin failure crack. It is up to 5 meters wide and greater than 16 meters deep, with depth varying greatly depending on the amount of breakdown and alluvium present. Throughout the feature, speleothems are present, with larger accumulations present in the roofed portions. At the deepest part of the feature, the southern end, there is a segment containing 1.5-meter deep brackish water. Although no direct connection was discovered to the ocean in this part of the feature, the presence of marine fauna indicates there must be some connection. In the northern portion of the feature, where it connects directly to the ocean, a Japanese pillbox was constructed approximately 6 meters above sea level.

Immediately inland from Dripping Tree, there are several smaller fractures that are not humanly accessible. They are formed parallel to the main fracture, resulting from the inland migration of cliff margin retreat. These features show less dissolutional enhancement than that seen in Dripping Tree Fracture Cave.

Dump Coke Cave (Central Plateau, Tinian – Figure 73)

Dump Coke Cave is located 700 meters south/southeast of Puntan Lamanibot Sanhilo in Lamanibot Cove, which is locally referred to as Dump Coke because of the numerous soda bottles that were disposed of there during World War II. This breached flank margin cave, which extends inland 21 meters with and entrance width of 6 meters, is developed in the Mariana Limestone (QTmu). The cave has a maximum ceiling height of 11 meters and a floor covered in heavily weathered breakdown blocks. From the inland portion of the main chamber, a small, tube-like passage extends inland 4 meters and turns abruptly north for and additional 3 meters before terminating. This tube is 3 meters above the floor of the main chamber and has a bedrock floor for the majority of its length.

Dynasty Cave (Median Valley, Tinian – Figure 74)

Dynasty Cave is a breached flank margin cave located 100 meters north of Taga Beach in the Mariana Limestone (QTmu). The cave is 12 meters wide at the entrance and extends inland 15 meters with an entrance ceiling height of 3 meters. The majority of the cave floor is slightly below sea level, while the inland portions consist of a bedrock ledge 2 meters above the main floor. Several large breakdown blocks are located in the entrance area and appear to be pieces of the original roof. These breakdown blocks originally extended further seaward but have now been transported slightly inland by intense wave action.

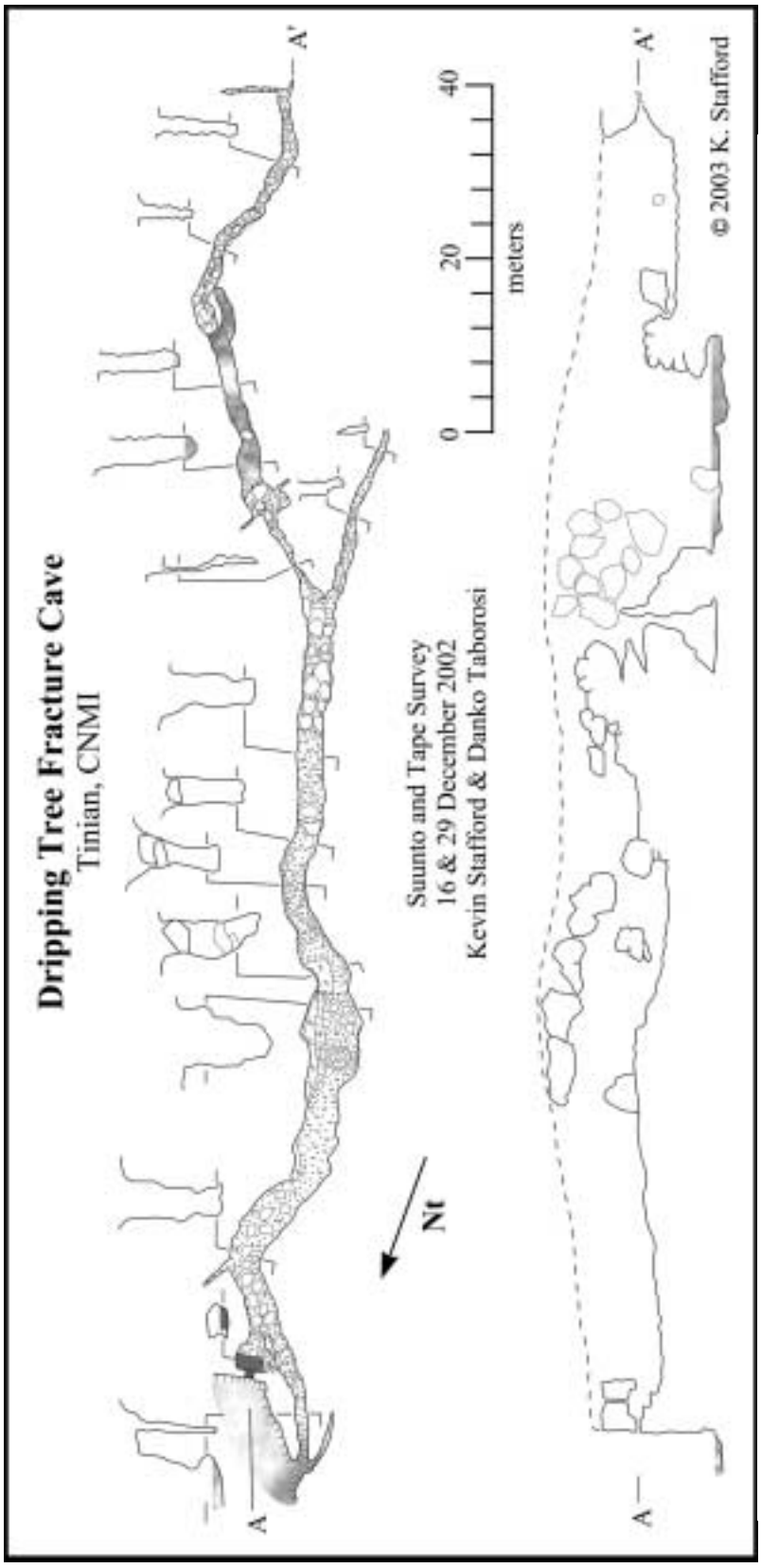

Figure 72: Map of Dripping Tree Fracture Cave.

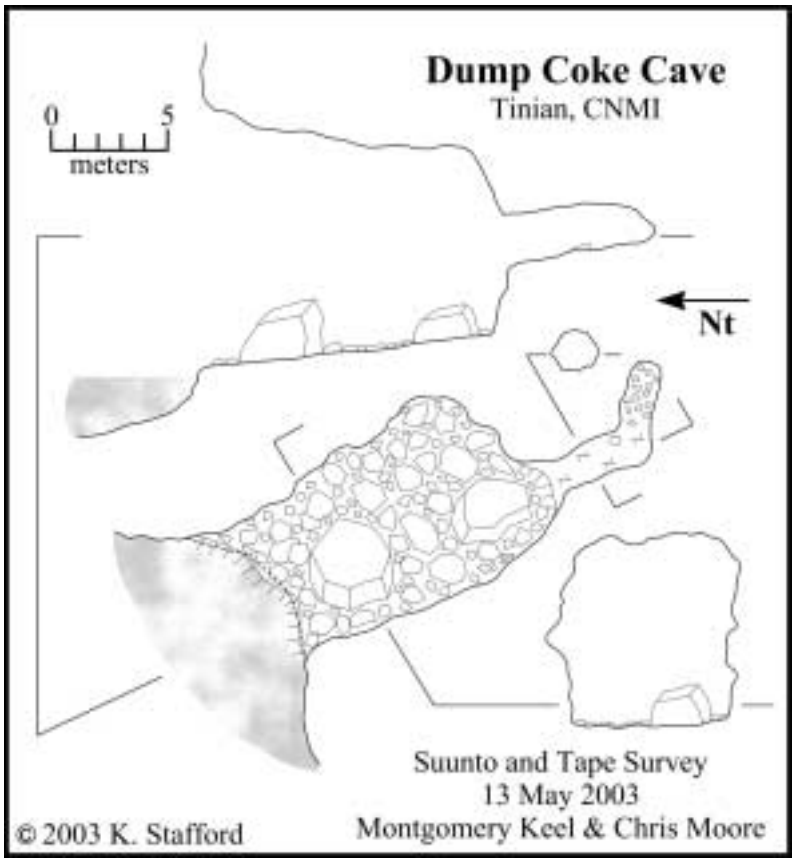

Figure 73: Map of Dump Coke Cave.

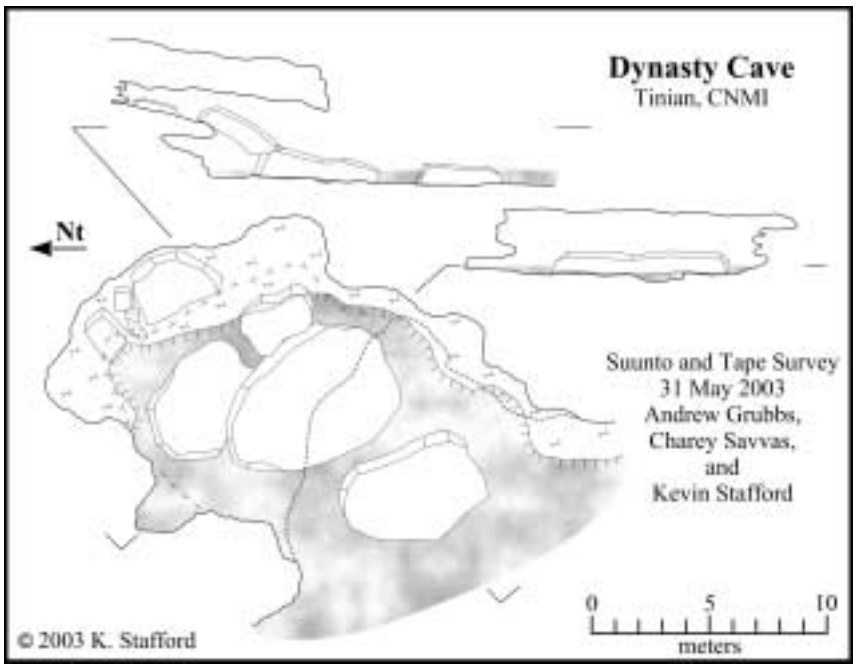

Figure 74: Map of Dynasty Cave.

East Suicide Cliff Cave (Southeastern Ridge, Tinian – Figure 75)

East Suicide Cliff Cave, a breach flank margin cave at the far eastern portion of Suicide Cliffs, was originally named Suicide Cliff Cave #1 (Stafford et al., 2002). This feature, developed in the Mariana Limestone (QTmu), contains several entrances, including a ceiling entrance. The feature is 20 meters wide and extends inland for 6 meters with a maximum ceiling height of 7 meters. The feature has some speleothems and has been modified by humans, including the construction of a partial rock wall across the two largest entrances in the eastern portions of the cave. The main chamber descends approximately 2 meters through a small passage to the north, where it connects to a second smaller chamber breached along the cliff.

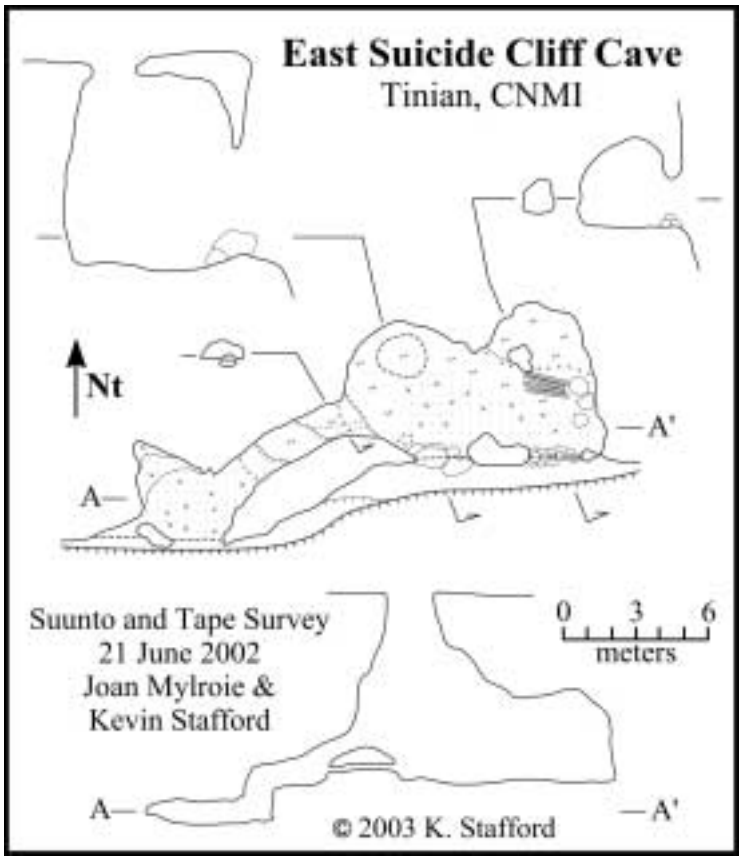

Figure 75: Map of East Suicide Cliff Cave.

Edwin's Ranch Cave (Central Plateau, Tinian – Figure 76)

Edwin's Ranch Cave is located approximately 1200 meters south of Unai Lamanibot and approximately 800 meters east of the coastline. This flank margin cave is developed in the Mariana Limestone (QTmcc) and has been breached by cliff retreat. The cave appears to be nearly complete, with 3 small entrances that are less than 1 meter high on the northern margin of the cave. The cave is 3 meters tall, 9 meters wide and 12 meters long. In the southeast portion of the cave, there are two small side chambers, while the entrances appear to be similar features that were breached. Speleothems in the cave are limited and the floor is composed primarily of alluvium of indeterminate depth. The two northwest entrances show evidence of human excavation, which makes access into the feature possible, but the northeast entrance has not been modified and is less than 10 centimeters tall.

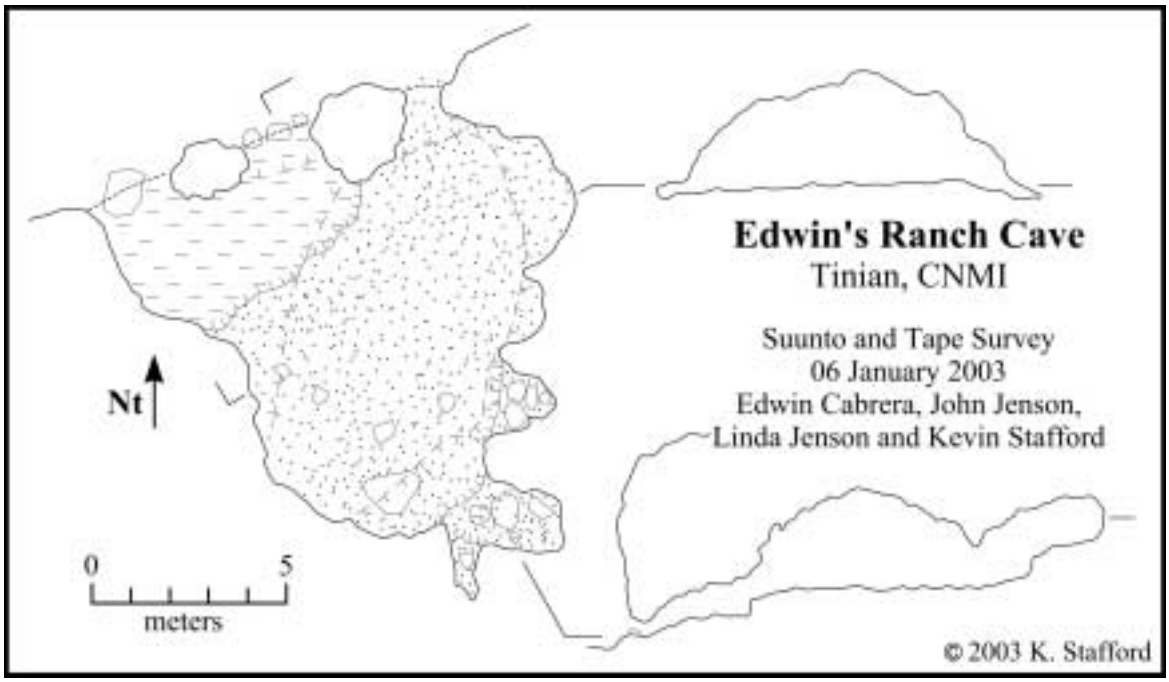

Figure 76: Map of Edwin's Ranch Cave.

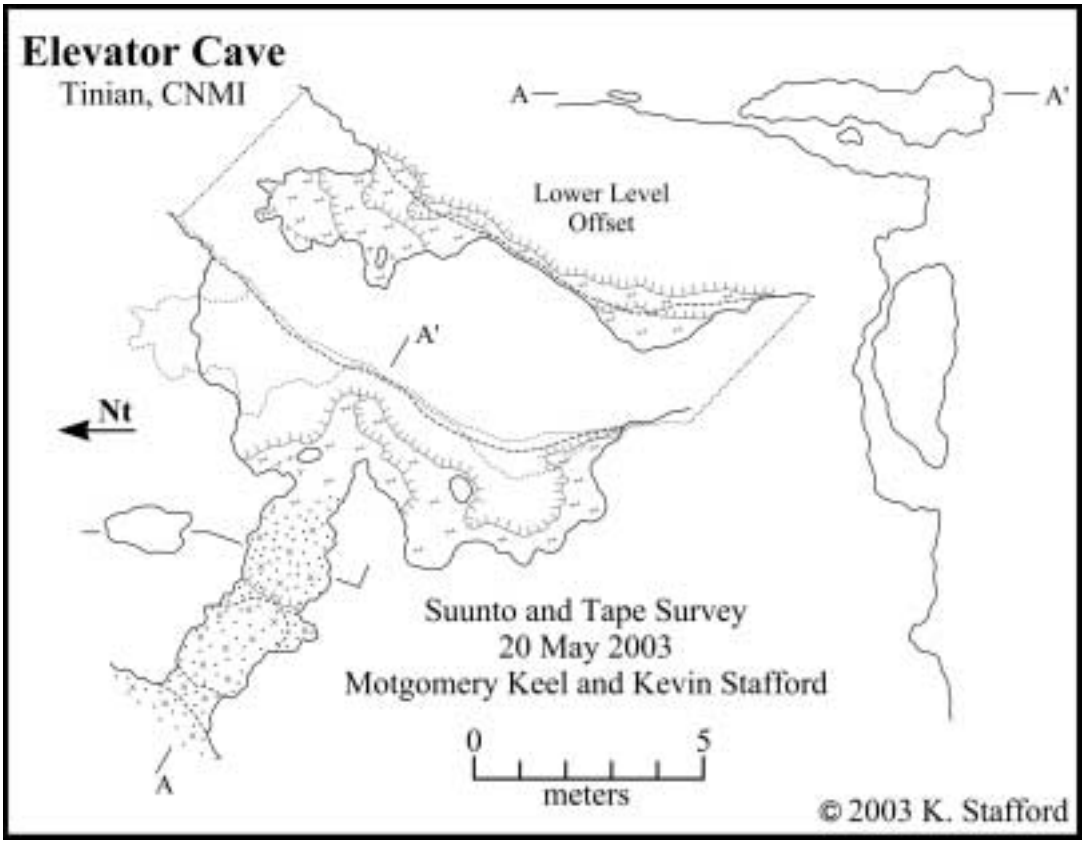

Figure 77: Map of Elevator Cave.

Elevator Cave (Southeastern Ridge, Tinian – Figure 77)

Elevator Cave is located in the central region of Suicide Cliffs in the Mariana Limestone (QTmu). This flank margin cave, composed of two distinct levels, has been breached by cliff retreat on the southeastern side and by roof collapse on the northwestern side. The upper level contains the two mentioned entrances with a cliffside width of 9 meters which narrows to 2 meters wide 3 meters inland where it continues for an additional 7 meters through a passage 1.5 meters tall. The lower level is 7 meters below the upper level and exhibits a similar entrance width, but extends inland only 3 meters. The two levels are connected by a series of small ledges, while the floor throughout is primarily bedrock with alluvium in the area near the collapsed roof entrance. The cave was named for its vertical extent, which is greater than most caves observed at Suicide Cliffs.

False Floor Cave (Southeastern Ridge, Tinian – Figure 78)

False Floor Cave is located in the southeastern region of the Piña ridge in the Mariana Limestone (QTmu). The cave is widest at the entrance (17 meters) and extends inland as two chambers. The south chamber extends inland 4 meters with a chamber 6 meters wide and a partial rock wall in the entrance area. The northern, larger chamber extends inland 9 meters and has been significantly modified by humans, including a large rock walled terrace that is 3 meters inland and 2 meters wide and a 1-meter deep excavated area covered by a deteriorating wooden floor. The majority of the cave is floored with soil and detritus with bedrock floors in the most interior regions of the northern chamber.

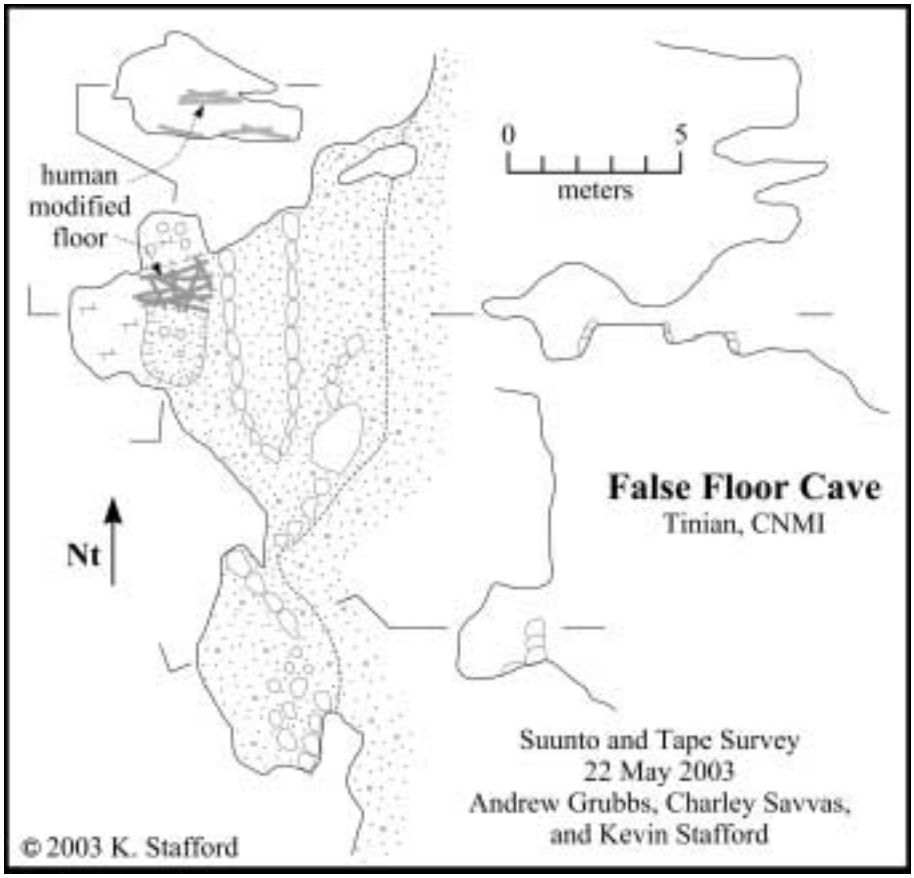

Figure 78: Map of False Floor Cave.

Five Bee Cave Complex (Southeastern Ridge, Tinian – Figure 79)

Five Bee Cave Complex is located 1900 meters southwest of Puntan Barangka on the north side of the Carolinas ridge in the Mariana Limestone (QTmc). This cave complex is consists of two flank margin remnants and a prominent notch in the scarp that is 12 meters wide and 10 meters deep. The notch contains two dissolutionally widened fractures in the northeast and southeast corners that define the notch boundaries. The cave remnant north of the notch extends inland 6 meters as two small partial chambers, while the southern remnant extends inland only 2 meters but has flowstone deposits on the inner wall. The entire complex is 40 meters long and has a soil floor throughout.

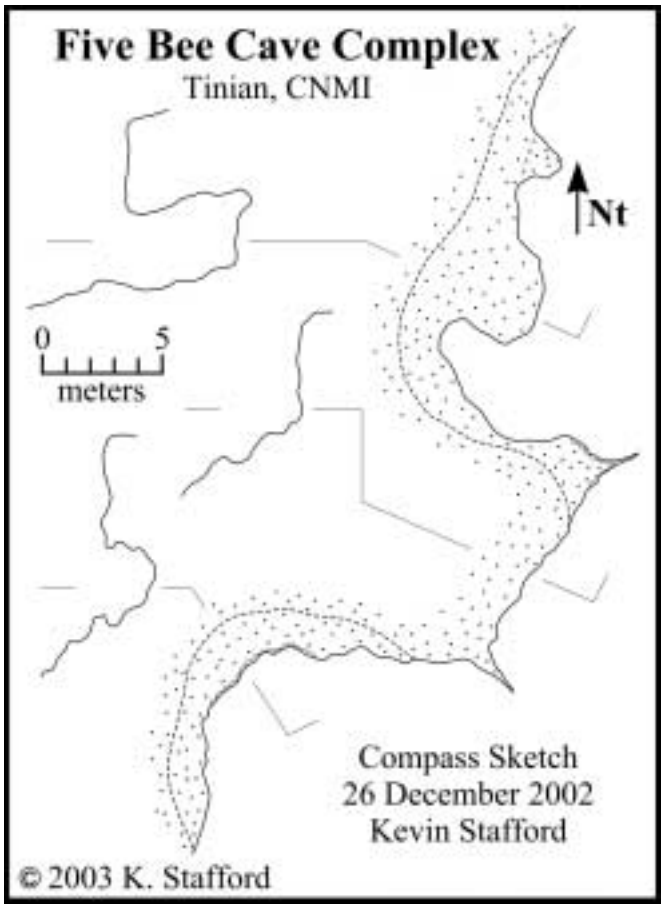

Figure 79: Map of Five Bee Cave Complex.

Flamingo Tail Caves (Central Plateau, Tinian – Figure 80)

Flamingo Tail Caves are located 900 meters west/southwest of Puntan Diapblo along a small intermittent scarp in the Mariana Limestone (QTmu). This section of scarp contains two caves and a series of well-defined notches that may represent other flank margin cave remnants where the ceiling has completely collapsed. The eastern portion of the scarp segment contains a cave with three distinct passages, averaging 2 meters in height that radiate from a central entrance area; one extends east 8 meters, one extends northeast 7 meters and one extends north 4 meters. On the western edge of the scarp segment, a small remnant cave extends inland 2 meters with a width of 4 meters and height of 0.5 meters. The ground surface along the scarp and inside the caves is composed of soil and detritus with some minor breakdown blocks in the eastern cave.

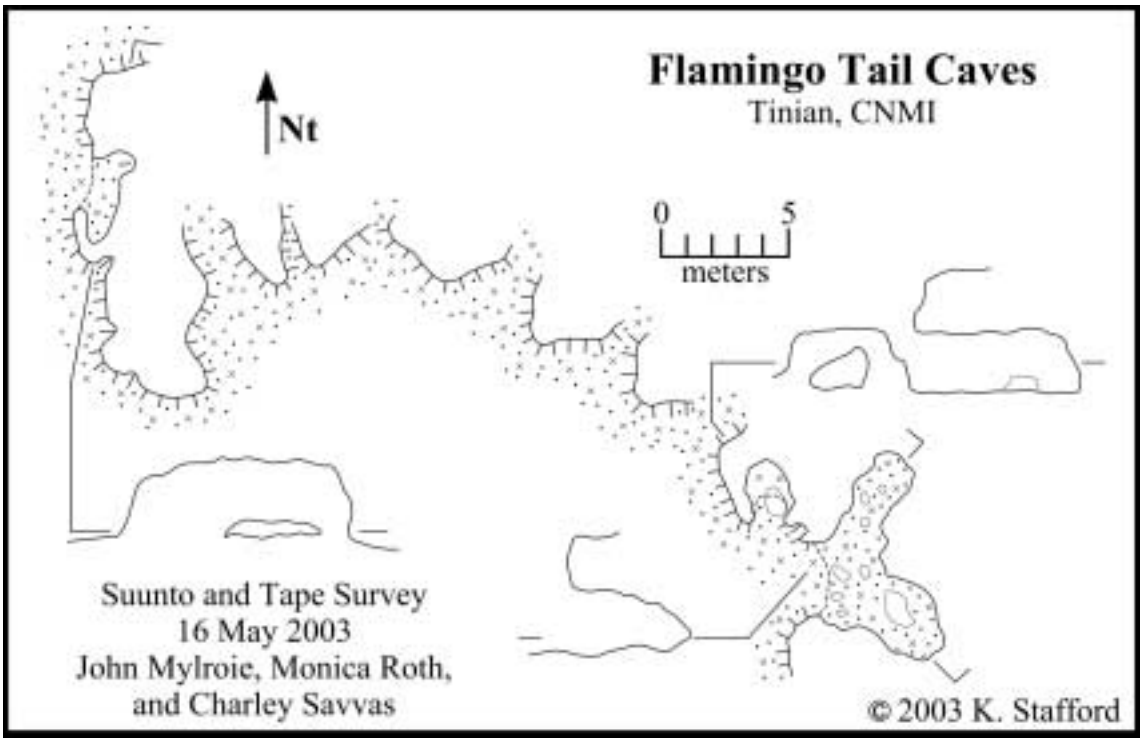

Figure 80: Map of Flamingo Tail Caves.

Fleming Point Cave (Central Plateau, Tinian – Figure 81)

Fleming Point Cave is located 700 meters north/northeast of Puntan Atgidon in a small cove developed in the Mariana Limestone (QTmu). The cave is developed along a prominent fracture or joint that is well defined in the ceiling and floor of the cave throughout the 41 meters that the cave extends inland. The cave has an entrance height of 11 meters and decreases to 6 meters, 13 meters inland from the entrance. The cave has two prominent dissolutional pockets that deviate from its linear passage; one located on the east side at 9 meters inland and one on the west side at 22 meters inland. The cave is primarily bedrock floored, but contains some large breakdown blocks in the inland portions. Based on the general morphology of the cave, its development along a prominent zone of brittle failure and observable scheiren mixing of the water near the entrance, this feature is interpreted as a structurally controlled discharge feature.

Full Bottle Cave (Southeastern Ridge, Tinian – Figure 82)

Full Bottle Cave is located approximately 500 meters west/northwest of Puntan Masalok in the Mariana Limestone (QTmu). It is developed along a fracture, oriented northwest (~310^{o}) and dipping to the northeast at approximately 60^{o}. The feature is 6 meters deep and up to 6 meters wide. The main chamber extends for 14 meters, but fractures less than 20 centimeters wide extend beyond the main chamber in northwest and southeast directions. The floor is primarily composed of breakdown with indications that the fracture extends to greater depths. Speleothems are primarily concentrated on the southwest wall of the chamber, on the footwall of the fracture. The entrance is located in the southwest portion of the feature amongst numerous breakdown blocks in the northern region of the "600 Meter" Fracture System.

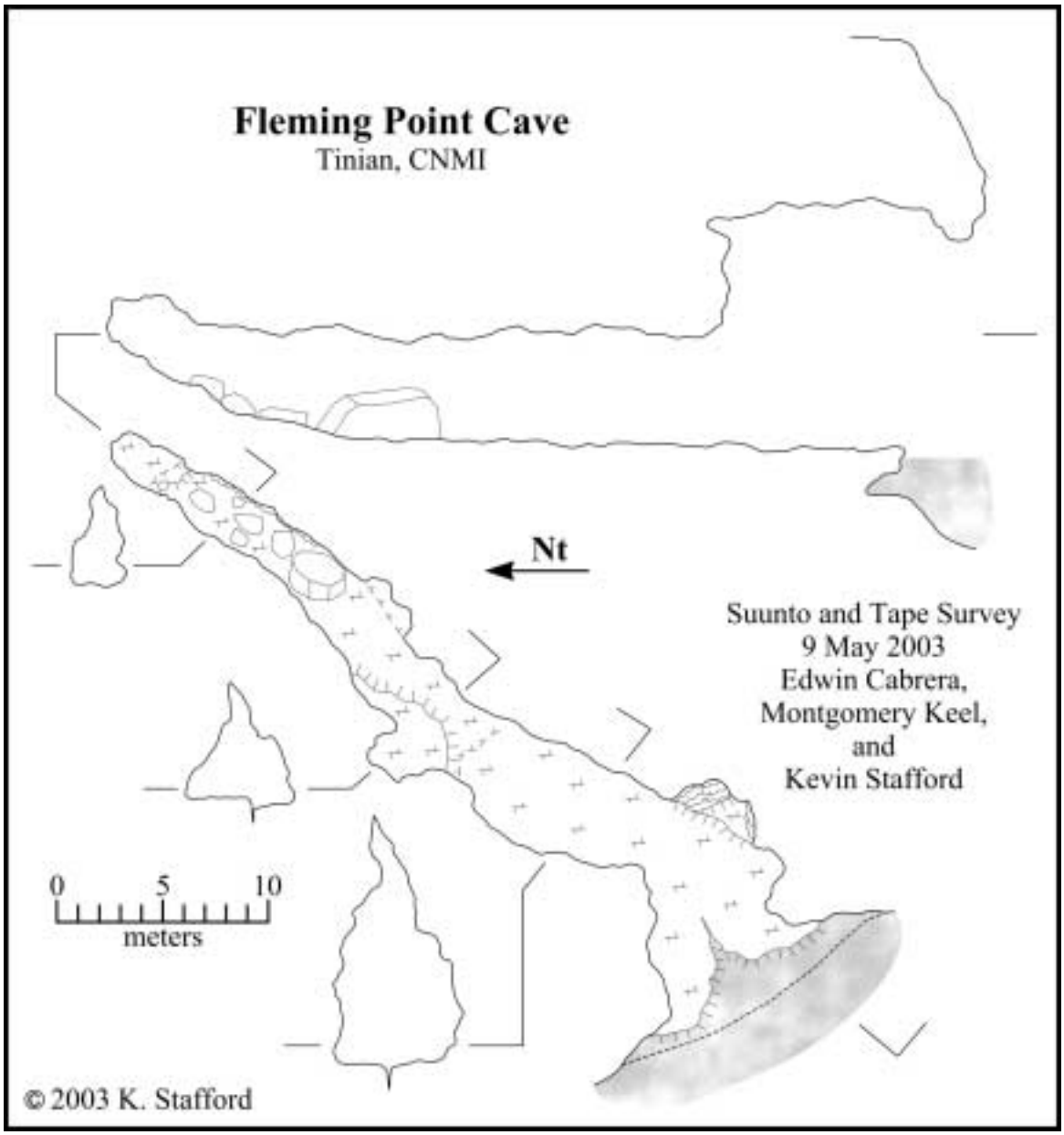

Figure 81: Map of Fleming Point Cave.

Gecko Cave (Median Valley, Tinian – Figure 83)

Gecko Cave is located approximately 200 meters southeast of Unai Masalok on the coastline at sea level. It is developed in the Mariana Limestone (QTmu) and discharges freshwater through a tubular passage. It is developed along a dissolutionally enhanced joint oriented at approximately 60°, which extends inland for more than 20 meters from a small coastal bay. Directly south of Gecko Cave is another feature that extends inland a similar distance, but is mostly water-filled, such that during exploration it could not be surveyed because of strong surf conditions. A freshwater discharge rate could not be calculated within in the cave for similar reasons, but significant fresh water could be observed mixing with saltwater inside the cave.

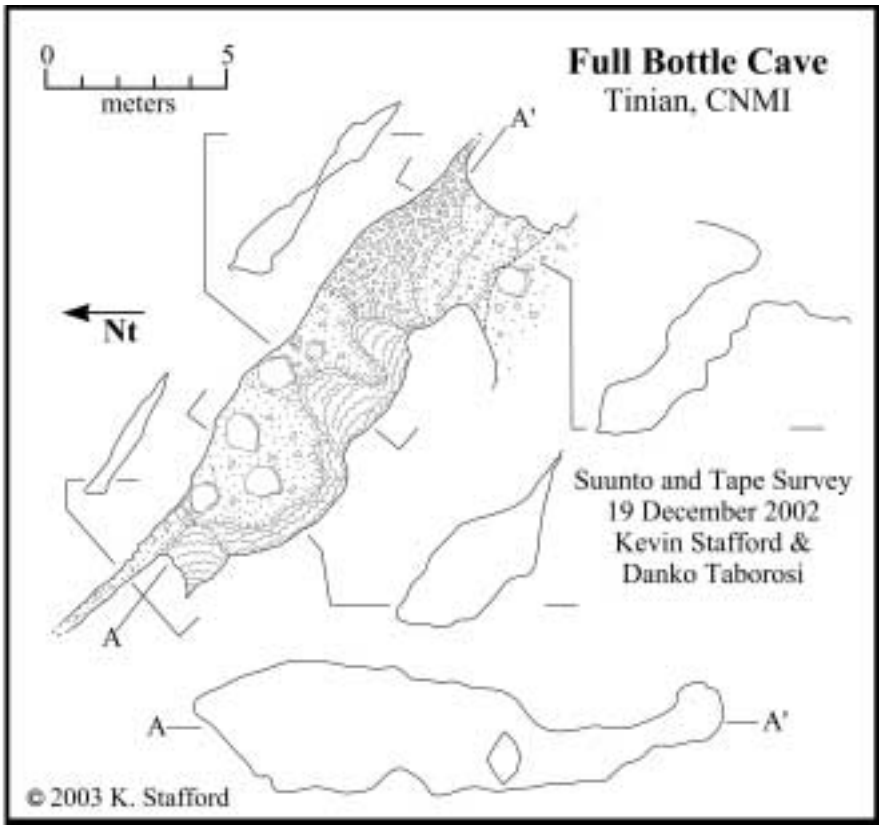

Figure 82: Map of Full Bottle Cave.

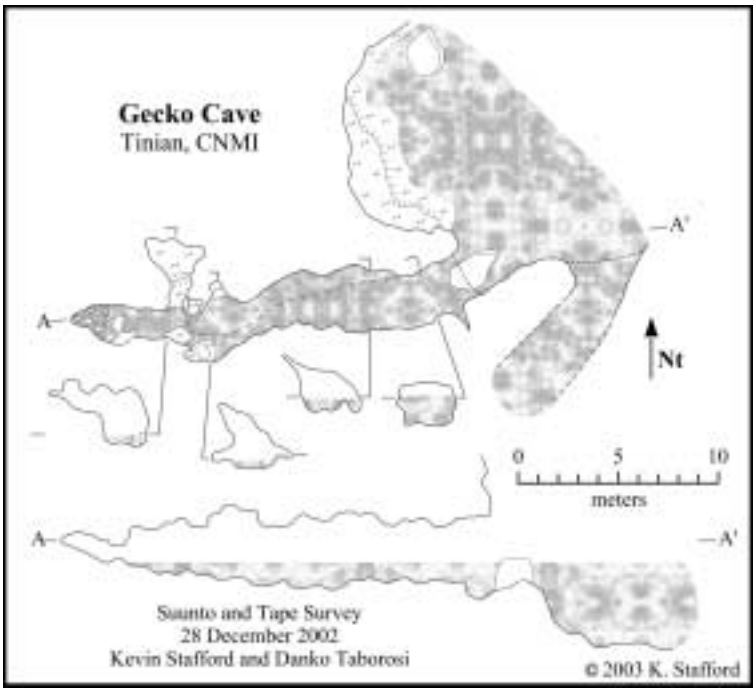

Figure 83: Map of Gecko Cave.

Goat Cave (Lower Terrace, Aguijan – Figure 84)

Goat Cave is developed in the Tagpochau Limestone (Tt) and represents a remnant of a large flank margin cave that has been intersected by cliff retreat along the southern cliff that separates the Lower Terrace and Middle Terrace of Aguijan. The feature is semicircular, with a width of 33 meters at the entrance and extending inland (north) for 16 meters with a ceiling height of approximately 14 meters. Just east of the center of the cave is an elevated bedrock area mantled by speleothems including several large stalagmites 3 meters tall. Minor roof collapse has occurred throughout the cave, but it primarily retains its dissolutional morphology. Throughout the cave extensive evidence of occupation by feral goats is found on the thin alluvium layer that covers the majority of the floor.

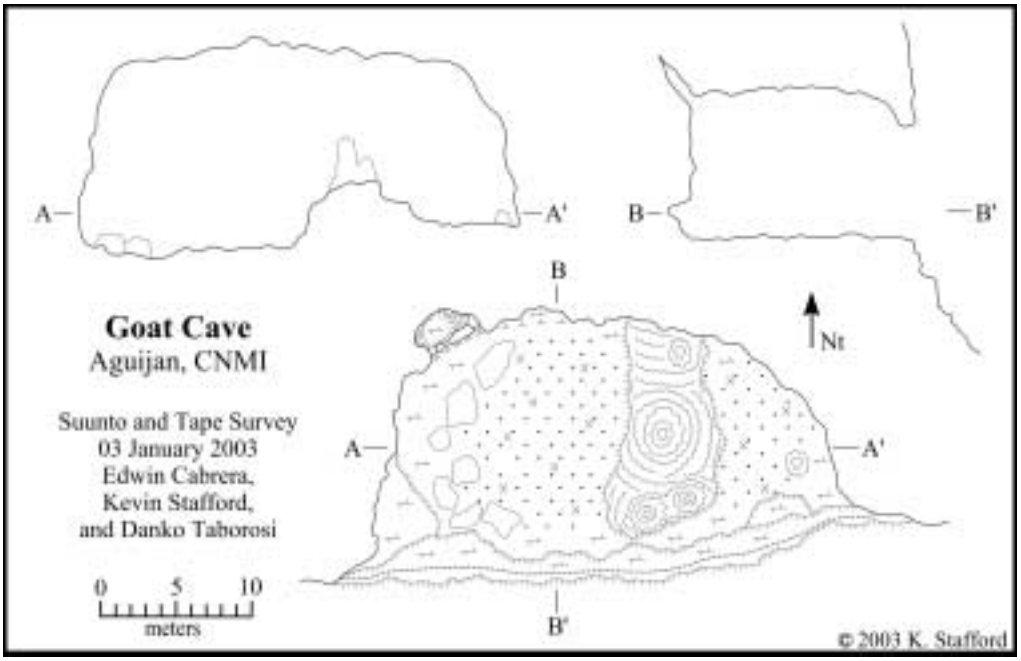

Figure 84: Map of Goat Cave.

Goat Fracture Cave (Lower Terrace, Aguijan – Figure 85)

Goat Fracture Cave is a large fracture oriented at 15°, which has two small, roofed portions. The feature is located in the northwest region of the Lower Terrace in the Mariana Limestone (QTmu). It averages 3 meters wide and generally extends 3 to 5 meters below the land surface with a floor composed primarily of breakdown blocks. Minor speleothem deposits are seen along the walls of the feature indicating that it was partially covered in the past. The feature continues for approximately 100 meters to the coast and for a shorter distance inland, but only the roofed portions were surveyed due to time constraints at the time of exploration. The feature appears to be associated with bank-margin failure, but has been modified by dissolution and collapse.

Half-Dozen Cave (Central Plateau, Tinian – Figure 86)

Half-Dozen Cave is a breached flank margin cave located approximately 2 kilometers east of Puntan Diapblo and approximately 300 meters north of the coast. It is developed in the Mariana Limestone (QTmu) and appears to have been infilled with limestone aggregate. The cave is entered at the top of a scree slope along the cliff edge, which forms an angle of

approximately 35° to the cliff and descends at a 35° slope into the cave near the cave's roof. The cave is 8 meters long and 7 meters wide with some minor speleothems in interior portions and exterior cliff wall. The feature is thought to be more extensive based on the occurrence of additional speleothems on the cliff wall, but much of the entrance appears to be currently blocked by the loose aggregate.

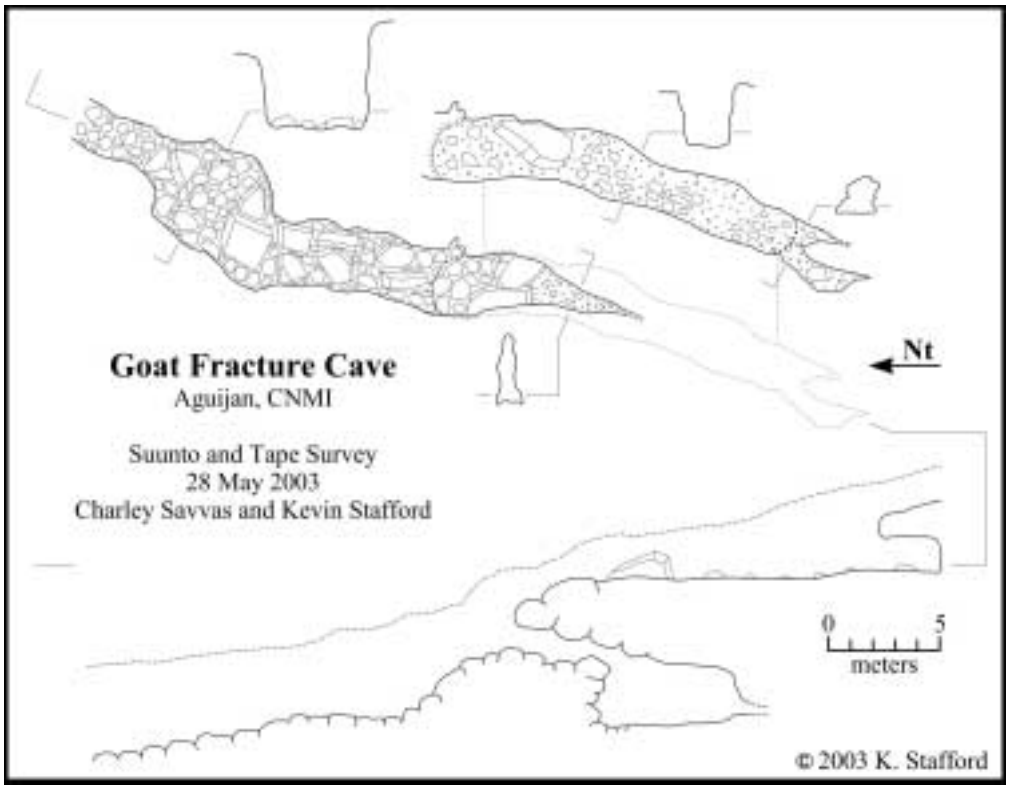

Figure 85: Map of Goat Fracture Cave.

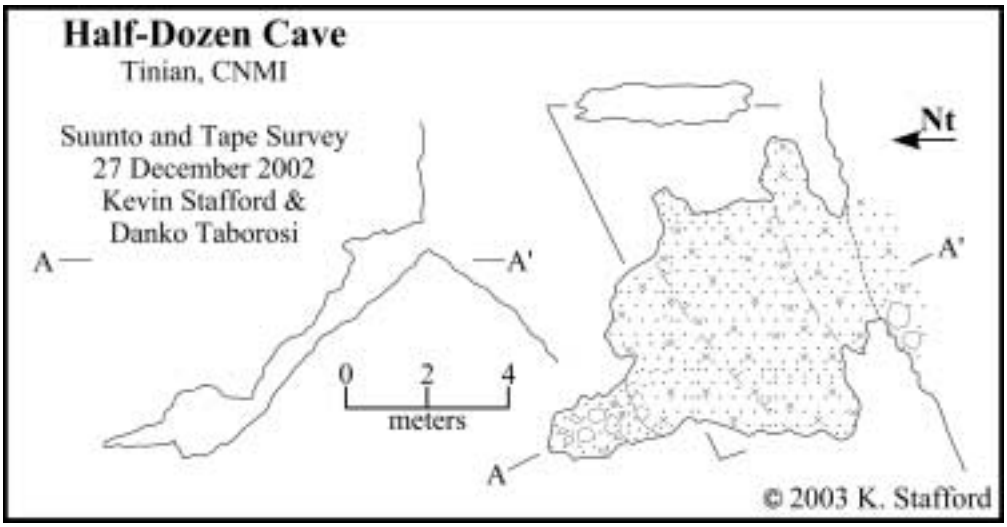

Figure 86: Map of Half-Dozen Cave.

Headless Tourist Pit (Southeastern Ridge, Tinian – Figure 87)

Headless Tourist Pit, developed in the Mariana Limestone (QTmu), is located approximately 500 meters east of Puntan Carolinas, 6 meters from the coastal cliff. The feature is on the coastal terrace, which has extensive phytokarst development. It is approximately 3 by 5 meters in diameter at the entrance and narrows to 0.5 by 3 meters at a depth of 10 meters, before widening into a joint controlled collapse chamber, which forms a littoral cave that connects to the ocean approximately 5 meters above the coastal bioerosion notch. The upper portions of the pit exhibit phytokarst development and collapse, while the restricted middle region contains minor secondary deposits. The lower chamber, which connects to the ocean, is approximately 8 meters wide and 15 meters long, with joints extending to the northeast and northwest. This feature is evidence of pit formation acting as vadose fast flow routes on the island of Tinian. Although it does not provide fast flow recharge to the aquifer, because of its direct connection to the ocean, it does demonstrate the presence of pits on Tinian.

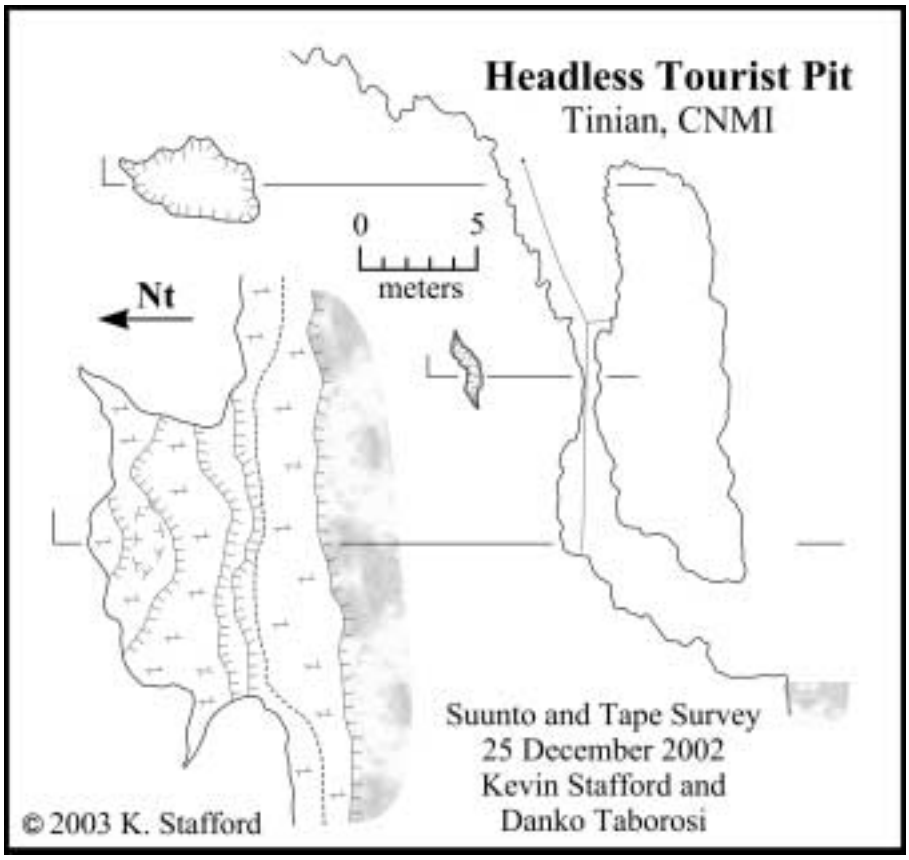

Figure 87: Map of Headless Tourist Pit.

Hermit Crab Cave (Southeastern Ridge, Tinian – Figure 88)

Hermit Crab Cave is located in the southeast region of the Piña ridge in the Mariana Limestone (QTmu). It is a small, flank margin cave remnant developed 6 meters above the base of the scarp extending inland 6 meters with an average height of 3 meters. The floor is composed of detritus and soil with a prominent mound located in the middle of the 2.5 meter wide passage. The cave, which contained several hermit crabs at the time of survey, is easily reached by a short climb.

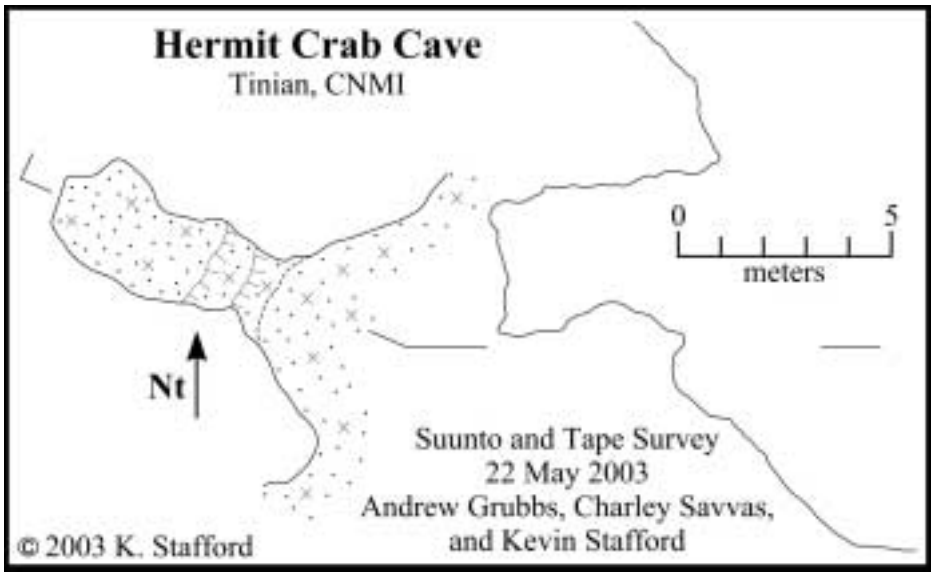

Figure 88: Map of Hermit Crab Cave.

Hidden Beach Cave (Median Valley, Tinian – Figure 89)

Hidden Beach is located at Unai Asiga, 1000 meters north of Unai Dangkolo, on the east coast. It is developed in the Mariana Limestone (QTmca) and extends inland 80 meters with an average width of 11 meters, but the majority of the ceiling is absent. The entrance is located at sea level and has a carbonate sand floor sloping gently inland. The cave has several small passages that extend from the north and south sides of this east/west trending feature, but they all terminate within 5 meters. The ceiling is present 27 meters inland, where it forms a 5-meter wide arch across the cave, before the ceiling is breached by a large collapse measuring 20 meters by 7 meters that connects to the surface, leaving less than 5 meters of ceiling width around the periphery of the large skylight entrance. Farther inland the ceiling remains intact for the remainder of the cave except for the most inland portions, which is breached and connects to the land surface. Minor speleothems are seen throughout the cave and one significant side passage is present in the southeast corner of the feature near the seaward entrance. This passage is located 3 meters above the floor on the cave wall and forms a looped passage over 10 meters long, averaging 2 meters in height and width. This significant feature not only represents one of the larger caves on Tinian, but it well represents an intermediate stage in the transition from flank margin caves to coves that are seen on Tinian. The coves located farther south at Unai Masalok and Unai Dangkolo have experienced greater erosion from coastal process, while more intact caves like Liyang Dangkolo show limited breaching primarily by ceiling collapse. Therefore, Hidden Beach Cave shows the transition stages in coastal erosion from complete flank margin caves to coves on carbonate islands.

Hollow Column Cave (Lower Terrace, Aguijan – Figure 90)

Hollow Column Cave is a remnant flank margin cave that has been intersected by cliff retreat on the southern side of Aguijan. It is developed in the Mariana Limestone (QTmu) and extends inland for 20 meters with an average width of 8 meters. In the inland portions of the cave some speleothems are present, including one column that is approximately 3 meters tall. The cave appears to be the side chamber of a larger flank margin cave that has been removed by cliff retreat. A narrow, dissolutionally widened joint trending approximately north is present in the ceiling and may represent structural control on the original dissolution of this chamber.

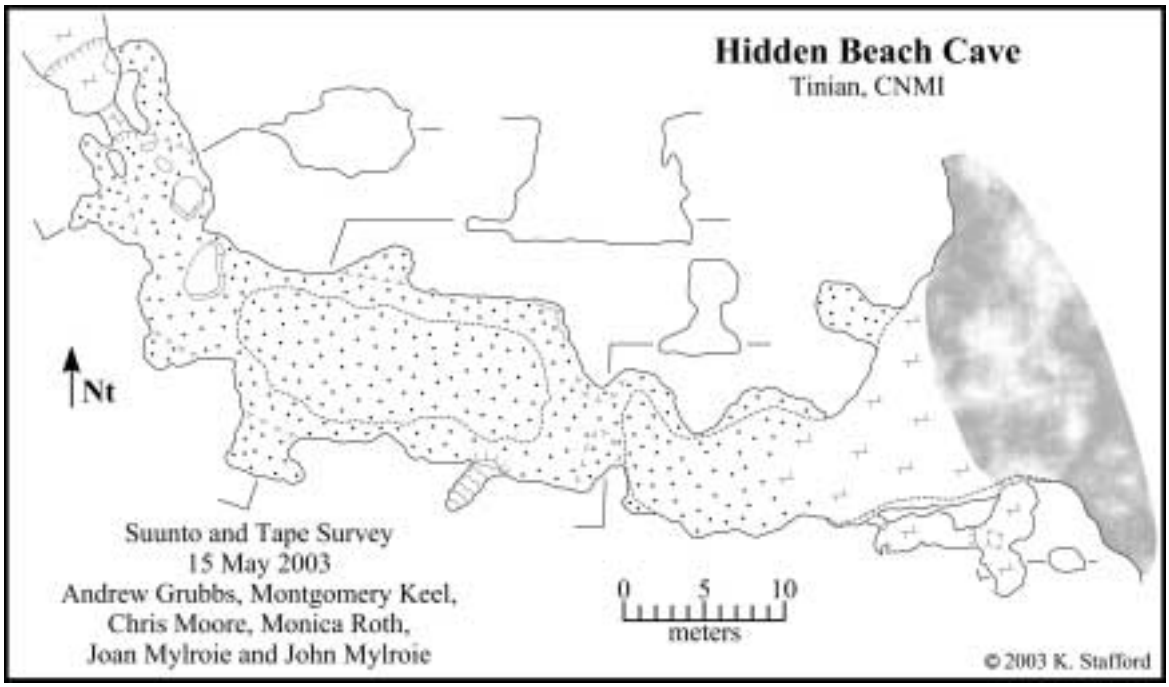

Figure 89: Map of Hidden Beach Cave.

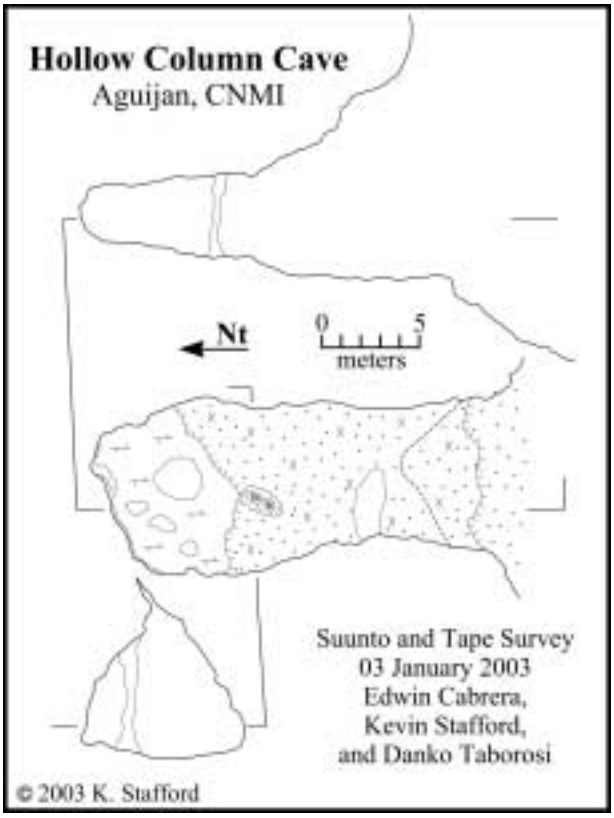

Figure 90: Map of Hollow Column Cave.

Insect Bat Cave (Middle Terrace, Aguijan – Figure 91)

Insect Bat Cave is located on the southwest side of the Middle Terrace in the Mariana Limestone (QTmu). It is developed along a fracture trending 120° and extends inland 30 meters with two distinct levels. The upper level is approximately 15 meters above the land surface and averages 3 meters in width, with a narrow slot in the floor that connects to the lower level, which has an average width of 2 meters. A small passage extends to the northeast for 5 meters from the lower level with an average width of 1.5 meters. The feature appears similar to sea-level fracture caves that discharge freshwater and is interpreted as representing a paleo-discharge feature that developed along a fracture.

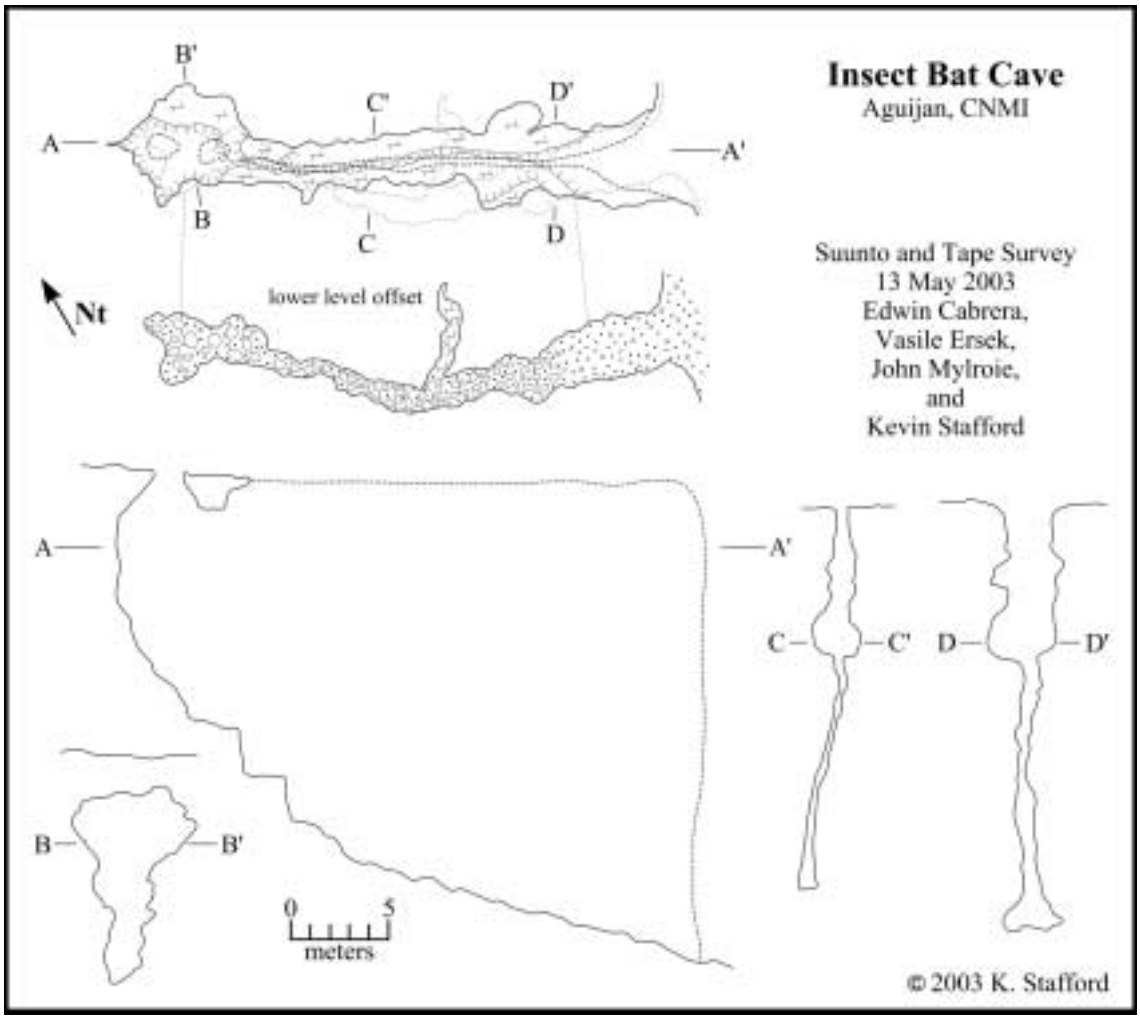

Figure 91: Map of Insect Bat Cave.

Isotope Cave (Upper Terrace, Aguijan – Figure 92)

Isotope Cave is a flank margin cave located in the northwest region of the Upper Terrace in the Mariana Limestone (QTmu). It covers an area of 15 by 23 meters, with two entrances and a large chamber. The two entrances located in the southern portion of the cave connect through 1-meter a tall passage that averages 3 meters wide with alluvium floors. At the junction of the two entrance passages, the cave is 5 meters wide and 2.5 meters tall and dips to the north, where

the cave continues and turns north through a 2 meter wide, 1.5 meter tall passage that connects to the main chamber. The main chamber is 10 by 15 meters with and average ceiling height of 3 meters and numerous large breakdown blocks covering the floor. In the southern portion of the main chamber, extensive deposits of flowstone cover the floor and walls, while stalactites cover the ceiling and several stalagmites line the southeast wall. The northern portion of the main chamber is approximately 2 meters tall, but appears much shallower because of the numerous large breakdown blocks that fill the area. In the far northeast part of the cave a small, 5-meter long, 1-meter tall passage in the breakdown can be reached by a short downclimb. The cave is named for several large (1.5 meter tall), "broomstick" stalagmites, which were located and appear ideal for U/Th isotope analysis for age dating.

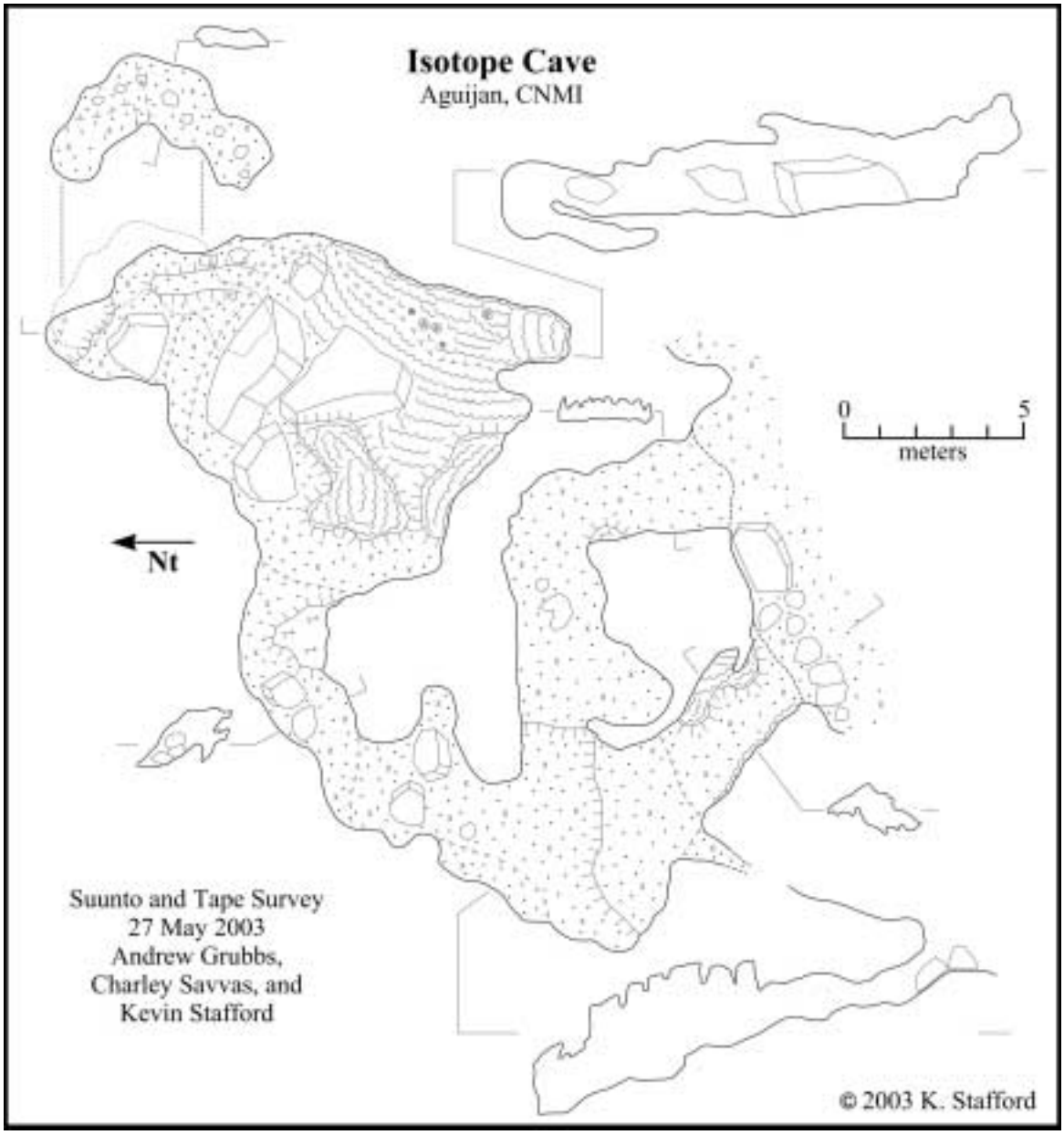

Figure 92: Map of Isotope Cave.

John's Small Cave (Median Valley, Tinian – Figure 93)

The entrance to John's Small Cave is located approximately 200 meters west of the Unai Dangkolo and is developed in the Mariana Limestone (QTmca). This FM cave is oriented roughly north by northeast with a length of 35 meters, width of 15 meters and depth of 12 meters. The entrance area is a complex collapse composed of numerous blocks and sediment. The southern portion of the cave exhibits less collapse, but has extensive speleothems and alluvium derived from sources to the south, in the direction of the small, unsurveyed passage at the far southern end of the cave. Throughout the cave, the original dissolutional morphology can be seen, but in most locations it is obscured by collapse or overprinted by speleothems. This cave and Liyang Dangkolo are approximately 20 meters apart in the subsurface, based on a surface survey that connects them.

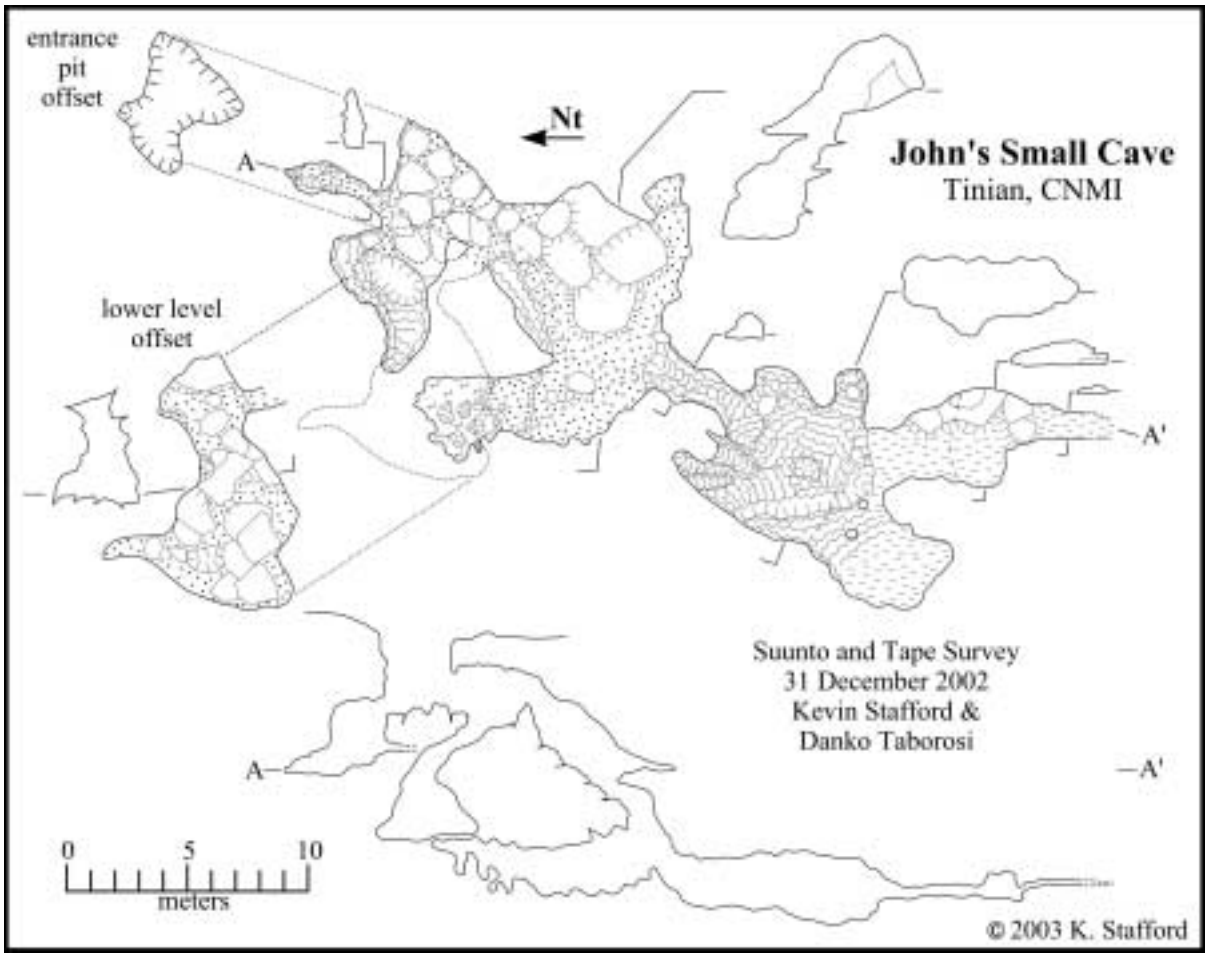

Figure 93: Map of John's Small Cave.

Lasu Recharge Cave (North-Central Highland – Figure 94)

Lasu Recharge Cave is located 1100 meters south of Mount Lasu on the eastern edge of a large closed depression, where allogenic waters from the igneous outcrops are sinking in the Tagpochau Limestone (Tt). This feature, located in a large bamboo grove, has much plant debris at its entrance indicating significant recharge during rain events. The central portion of the

feature is a collapsed entrance approximately 2.5 meters deep and oriented along a fracture trending southeast (~135°). The second entrance is located at the western edge of the feature where it meets the large closed depression and is where allogenic water primarily enters the feature. On the western side of the feature, there is another fracture trending southeast (~155°), which forms the far interior wall. Water follows this 20-centimeter, dissolutionally widened fracture to the northwest. Although this feature only measures 6 meters by 9 meters with a total depth of 3 meters, it is significant as a point source recharge feature for groundwater.

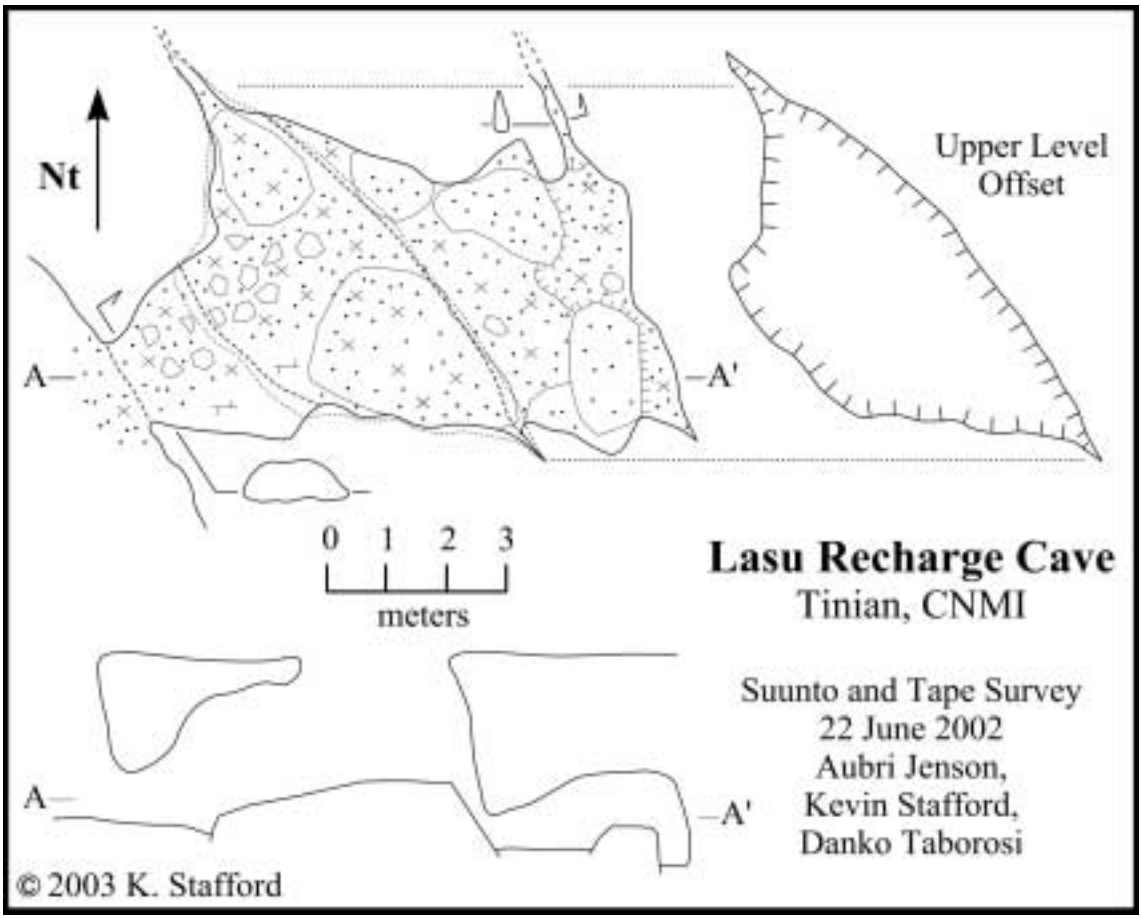

Figure 94: Map of Lasu Recharge Cave.

Leprosy Caves (Median Valley, Tinian – Figure 95)

The Leprosy Caves are breached, flank margin caves developed in dipping foreshore deposits in the Mariana Limestone (QTmu) on the coastline, approximately 200 meters south of the historic Leprosarium site. The site consists of series of three small caves and two large caves along a section of coast 120 meters long. The two large caves measure roughly 16 meters by 20 meters each with maximum ceiling heights of 8 meters. A ceiling breach on the inland side has created a second entrance to the southern large cave. The caves contain bedrock floors with some breakdown and carbonate sand near the entrances, but are devoid of speleothems. These caves all show evidence of being impacted by intense surf, which may explain the complete absence of speleothems.

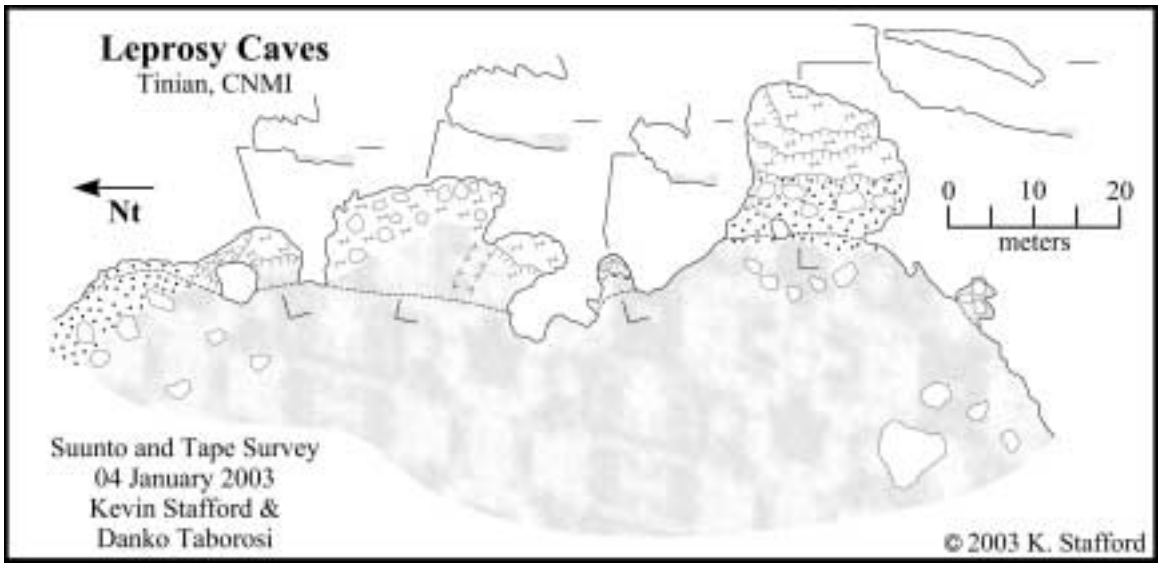

Figure 95: Map of Leprosy Caves.

Leprosy Discharge Feature (Median Valley, Tinian – Figure 96)

The Leprosy Discharge Feature is located near the "Historic Leprosarium Site" in the Mariana Limestone (QTmu). The feature is approximately 25 meters long, 7 meters wide and 2 meters deep. The feature has two small natural bridges located in the eastern portion where weathering of dipping foreshore deposits has eroded out beds preferentially. Along the walls of the feature that are in contact with ocean water, there are small-scale dissolutional features that appear to represent mixing dissolution from discharging freshwater. Minor mixing of fresh water was observed, but due to strong surf conditions, no significant salinity variations could be detected.

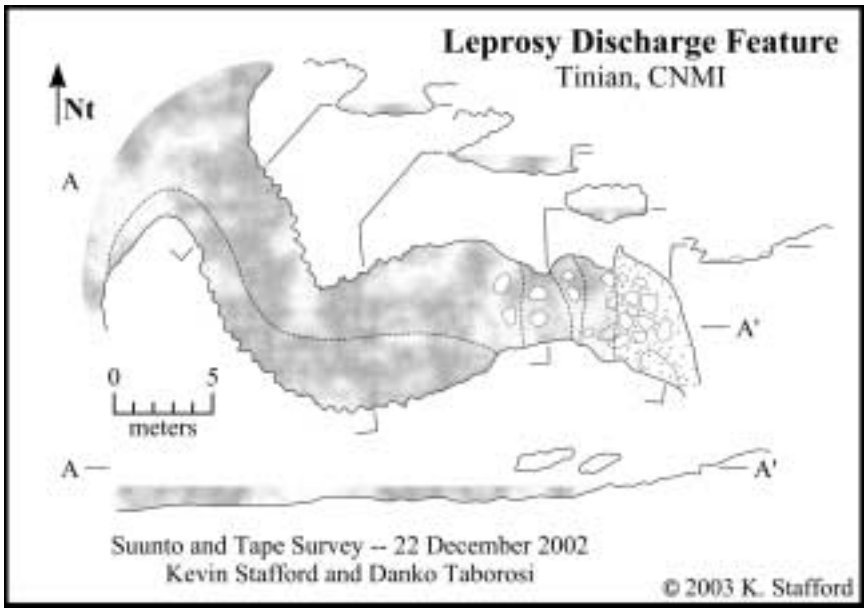

Figure 96: Map of Leprosy Discharge Feature.

Liyang Atkiya (Lower Terrace, Aguijan – Figure 97)

Liyang Atkiya is the largest cave yet discovered on Tinian or Aguijan, has a length of 200 meters and a width ranging from 25 meters in the 15-meter tall entrance chamber to 8 meters wide and 5 meters tall in the inland portions. The feature is developed in the Mariana Limestone (QTmu) along the southern side of the Lower Terrace on Aguijan. The entrance is developed along the base of a small cliff and measures approximately 7 meters wide and 1.5 meters tall. From the entrance the cave extends to the north into a large chamber with numerous large breakdown blocks, which form a steep slope over a distance of approximately 80 meters. At the base of the breakdown slope, in the main chamber, are several pools of freshwater and numerous speleothems. This region is also coated with a thin layer of black sediment, possible manganese, which not only coats the walls, but forms thick, black mud and causes a black coloration to the pools of water.

Continuing north, past a man-made rock wall, there is a small 1-meter diameter tube that extends for less than 2 meters into a small chamber containing more black sediment and speleothems. From this small chamber a long, linear passage extends for 75 meters, while continuing to slowly descend deeper. This passage trends northwest and appears to be developed along a fracture. However, large amounts of breakdown from the ceiling completely cover the floor adding complexity to the passage. In the northern portions of the cave, the main passage turns abruptly west and continues in the same fashion, while the original passage trend continues for 30 meters at a slightly higher level and smaller size. The west trending passage was surveyed for 50 meters at a near-level elevation, but two passages continue from this west passage that were not surveyed because of field logistics. However, the main trend continues for approximately 30 meters past the end of the survey as a 2-meter wide, 1-meter tall passage, while a second passage branched off to the south into a series of small, maze-like passages.

This cave represents a complex morphology that does not fit traditional models for carbonate island karst. The large entrance chamber is similar to a flank margin cave that has undergone extensive collapse, but has no side chambers as normally observed in flank margin caves. The long, linear passages appear to follow fractures and in several places retain scallops on the walls that indicate phreatic flow. These scallops are oriented towards the entrance, indicating that water would have flowed upwards through the cave towards the entrance, having originated in the most inland portions of the cave. Much of the interior area of the cave contains extensive breakdown, but low mazy areas may indicate the areas where water entering the explored portion of the cave merged into a single conduit.

Liyang Barangka (Southeastern Ridge, Tinian – Figure 98)

Liyang Barangka is a large, collapsed, flank margin cave located on the east coast, 600 meters north/northwest of Puntan Barangka in the Mariana Limestone (QTmu). The feature is 65 meters long, up to 50 meters wide and 15 meters deep. The majority of the feature does not retain a roof, but large breakdown blocks covering the bedrock floor throughout the feature appear to have once formed the roof. Ceiling remnants occur along the edges of the feature, extending less than 5 meters from the walls, while a single, small, covered chamber extends from the southwest corner of the feature for 6 meters. The eastern region of the feature extends below sea level and the entire feature shows evidence of impacts from intense storm events. The walls have flowstone deposits, while numerous large breakdown blocks in the central area have eroded speleothems on them. This feature is similar to the coves near Unai Dangkolo, but appears to be more severely impacted by coastal processes.

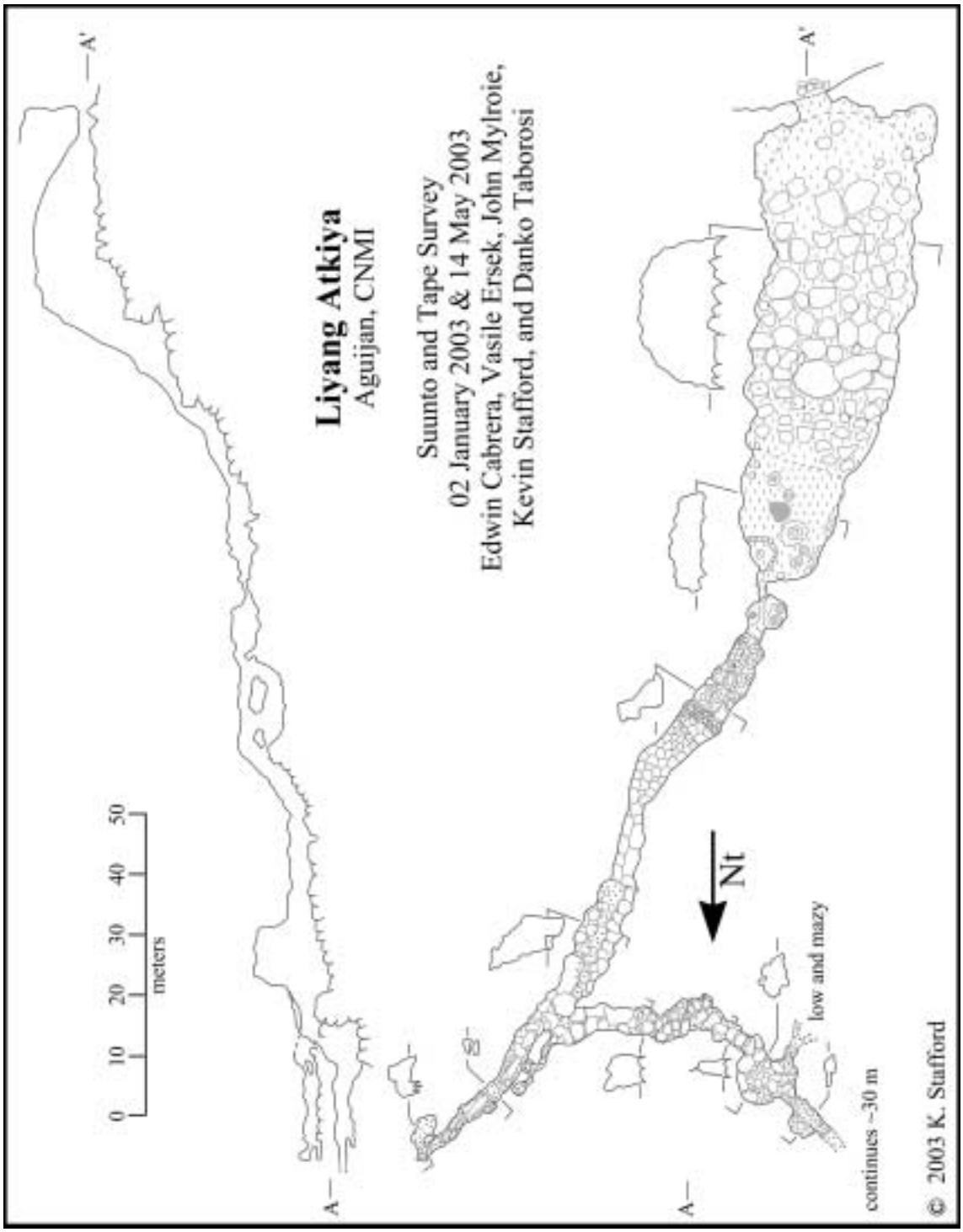

Figure 97: Map of Liyang Atkiya.

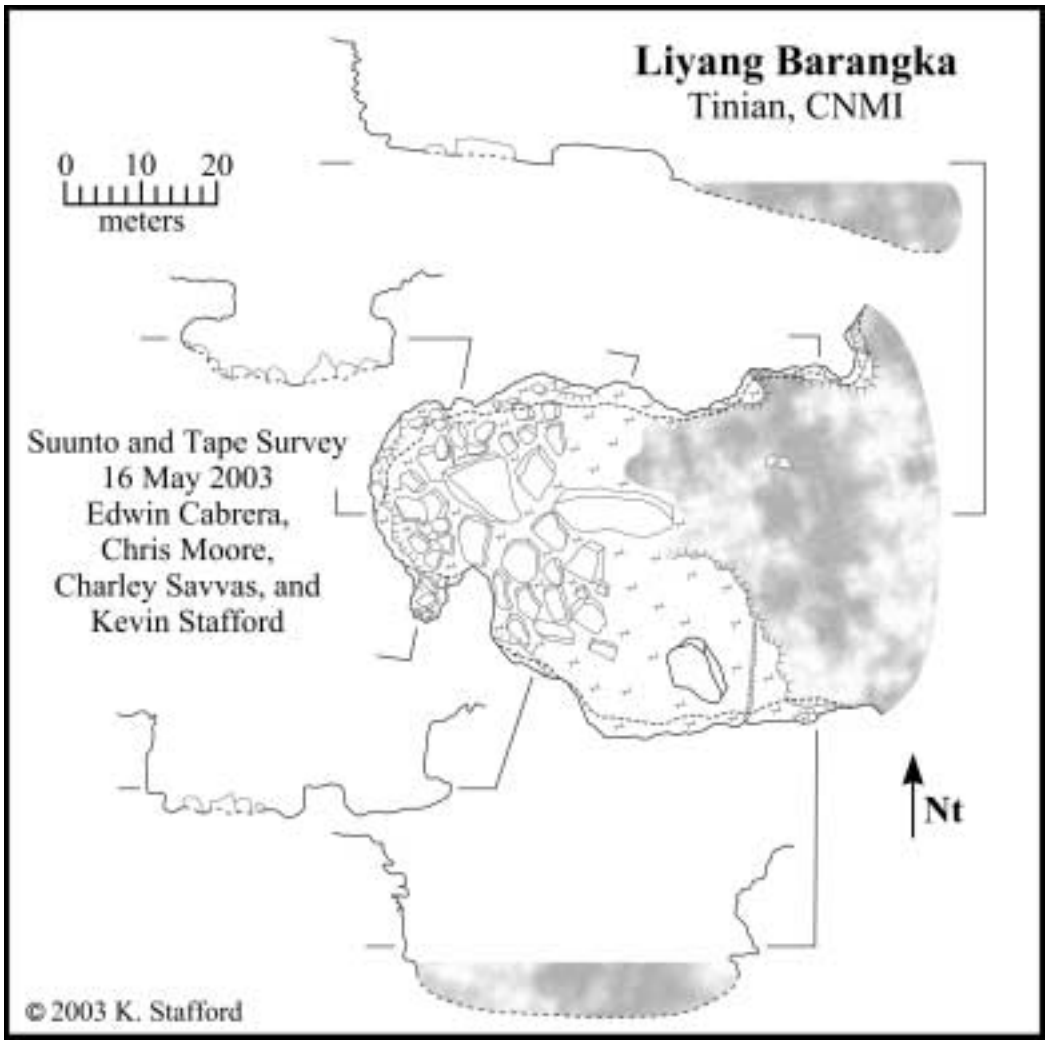

Figure 98: Map of Liyang Barangka.

Liyang Dangkolo (Median Valley, Tinian – Figure 99)

Liyang Dangkolo, also known as Long Beach Cave, the largest cave on Tinian, is approximately 100 meters inland from Long Beach (Unai Dangkolo). It is developed in the Mariana Limestone (QTmca) and measures approximately 35 meters by 70 meters with a central main chamber that extends to 16 meters depth. The cave contains several large bedrock pillars that separate areas and numerous smaller passages extending off of the main chamber in all directions. The cave appears to be predominantly intact with four entrances located in the ceiling of the main chamber, requiring a vertical descent to enter to the cave. In various areas of the cave, speleothems are extensive, while the main chamber floor is composed of breakdown talus created by the collapse of the ceiling. In the far eastern part of the cave, there is a large amount of carbonate sand, which may indicate a second breached entrance, possibly Andyland Cave. Through the center of the cave, a dissolutionally enhanced, north/south trending fracture is present that is associated with the largest collapse entrance. This large cave represents archetypical flank margin cave development for the Island of Tinian. Throughout the cave, minor human modifications have been made including the construction of a stacked rock wall in the east central area.

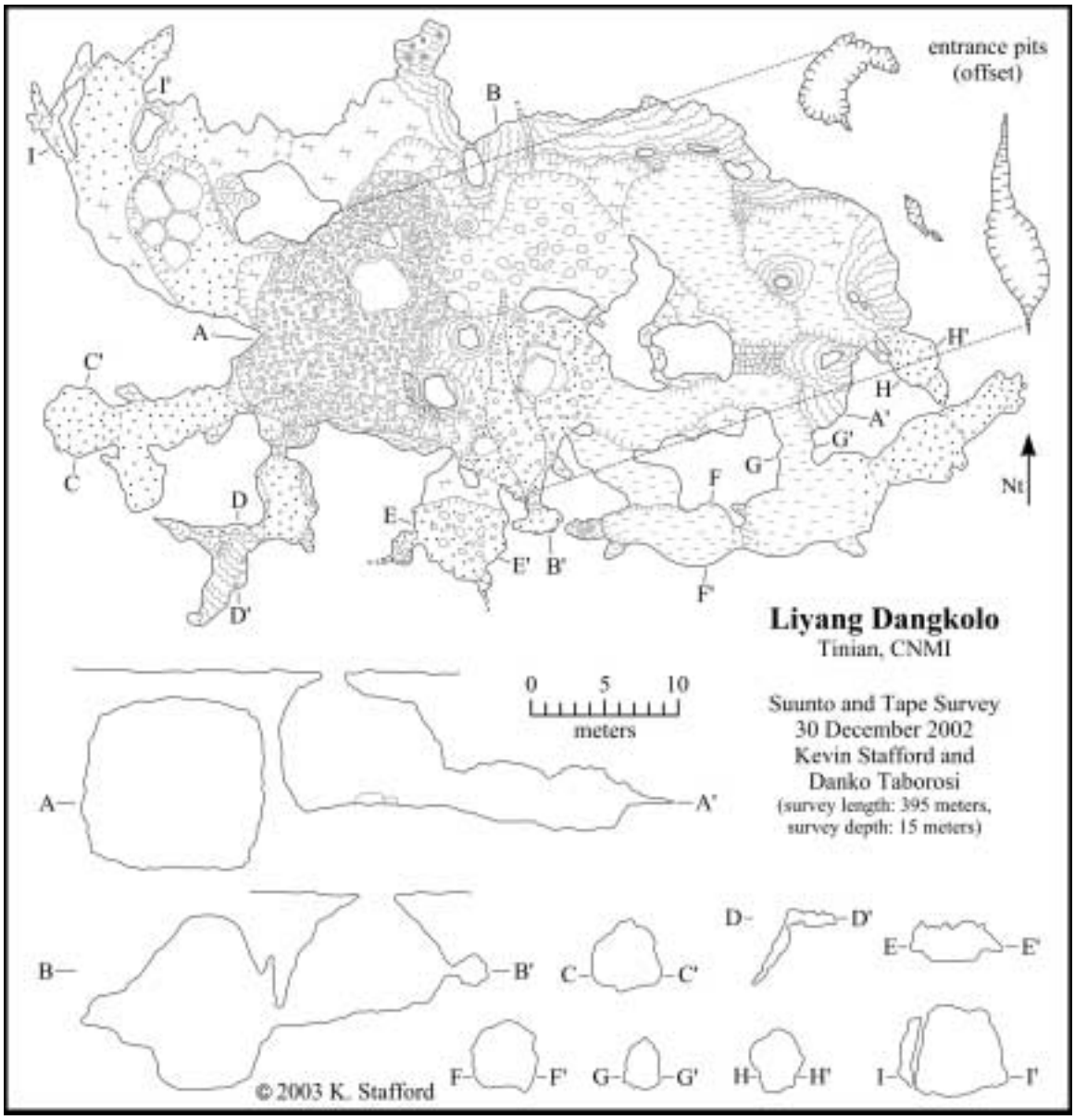

Figure 99: Map of Liyang Dangkolo.

Liyang Diapblo (Central Plateau, Tinian – Figure 100)

Liyang Diapblo is a large, breached, flank margin cave on the western coast, 300 meters southeast of Puntan Diapblo in the Mariana Limestone (QTmu). The entrance to the feature a small cove, 40 meters wide that extends inland 70 meters with a large bedrock mass (12 meters wide by 35 meters long) in the middle. The cave is divided into several areas. South of the large bedrock mass, the feature contains no roof and extends up to 4 meters below sea level. East of the bedrock mass is a small chamber that extends inland 8 meters with a height of 4 meters. Northeast of the bedrock mass is a large passage with a breakdown covered floor that extends 30 meters with and average width of 8 meters and average ceiling height of 6 meters. Northwest of the bedrock mass is a large chamber 15 meters wide, 20 meters deep and 8 meters tall that contains a large flowstone mound 4 meters tall in the center of the chamber and several smaller

flowstone deposits around the periphery of the chamber. Directly north of the bedrock mass is a series of smaller interconnected passages leading to the eastern and western parts of the cave. This cove appears to have formed by roof collapse of the flank margin cave that consisted of a large chamber with several smaller side chambers separated from main chamber by a large bedrock pillar.

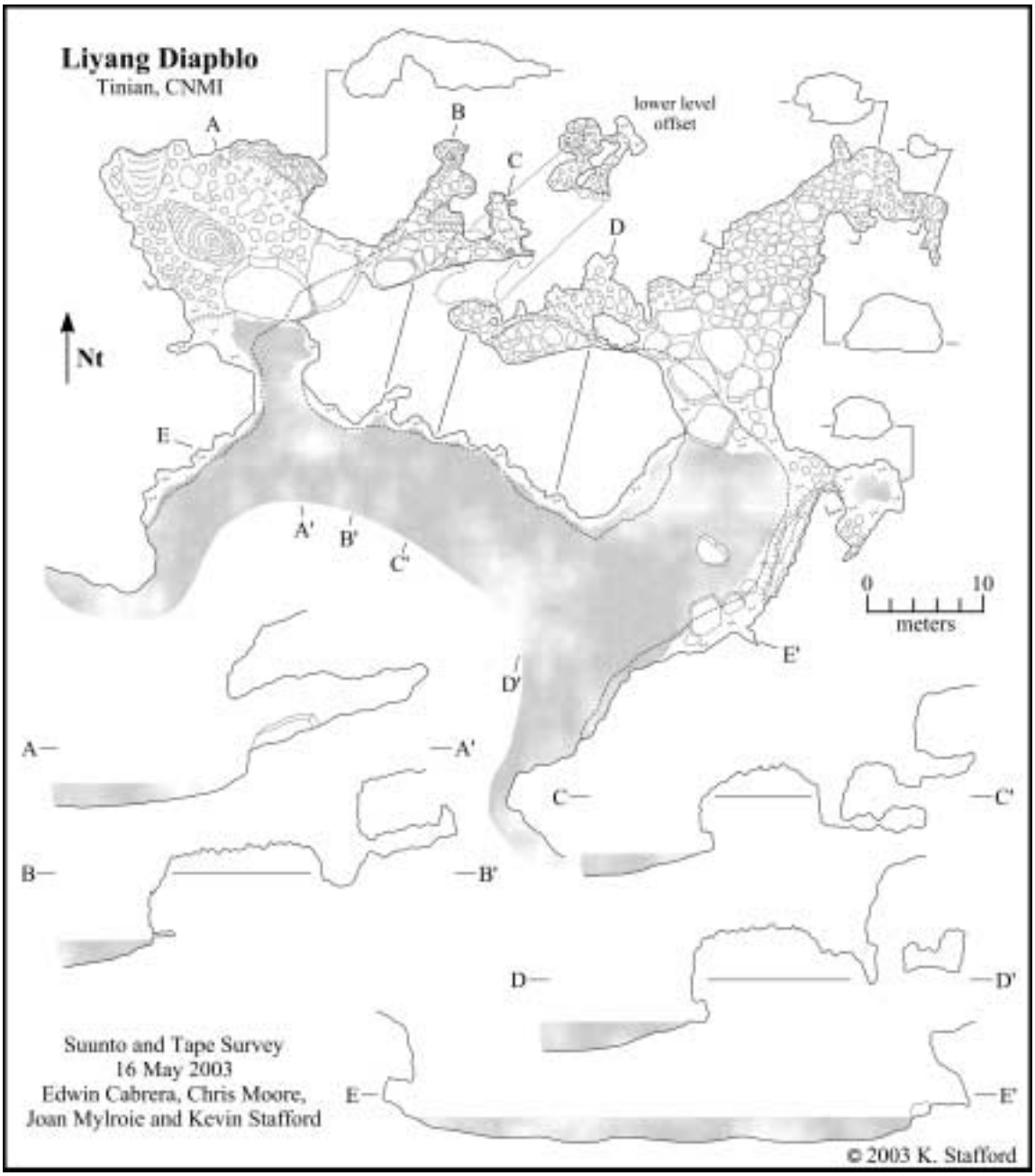

Figure 100: Map of Liyang Diapblo.

Liyang Gntot (North-Central Highland, Tinian – Figure 101)

Liyang Gntot is located on the northern scarp of Mount Lasu, approximately 3600 meters west of Unai Chiget in the Tagpochau Limestone (Tt). The cave consists of three distinct chambers that extend inland from a common entrance 16 meters wide. The individual chambers average 3 meters tall and 4 meters deep with floors composed of soil, detritus and scattered breakdown blocks. The feature shows evidence of minor human modification, primarily through leveling of soil floors and was not surveyed at the time of discovery because of time constraints while visiting the region.

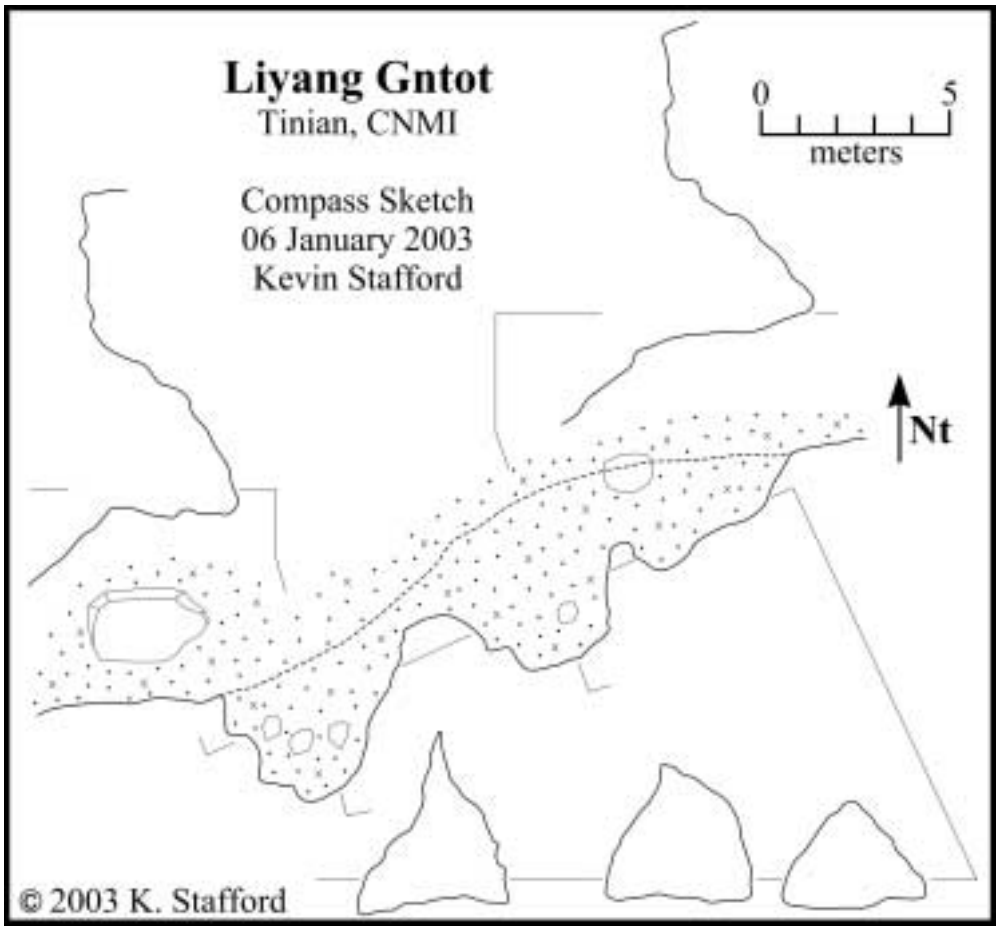

Figure 101: Map of Liyang Gntot.

Liyang Lomuk (Middle Terrace, Aguijan – Figure 102)

Liyang Lomuk is a breached, flank margin cave located in the north-central region of the Middle Terrace in the Mariana Limestone (QTmu). It consists of two flank margin cave remnants that extend west of the local scarp. The northern remnant is composed of a main chamber 5 meters wide, 6 meters deep and 3 meters tall, with two small, elevated passages extending from the southwest side of the main chamber. The main floor is composed of alluvium with the elevated areas composed of bedrock. The southern cave remnant is smaller and extends inland 5 meters. It is split vertically by a 0.5 to 1 meter thick bedrock shelf with the lower floor composed of alluvium and a small 0.5-meter deep depression in the east-central part. The cave is named after nearby trees referred to as “Lomuk” in the Chamorro language.

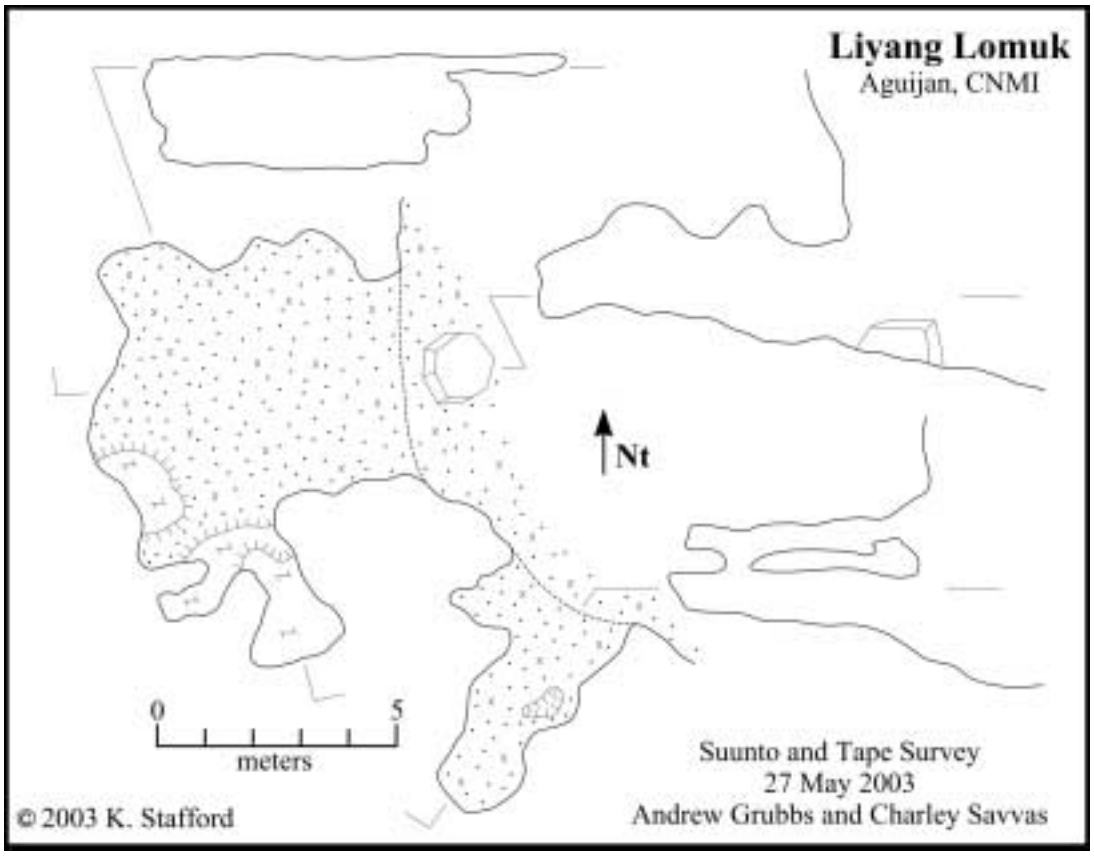

Figure 102: Map of Liyang Lomuk.

Liyang Mohlang (Southeastern Ridge, Tinian – Figure 103)

Liyang Mohlang is located in the north central part of Carolina's Ridge, in the Tagpochau Limestone (Tt). Two entrances are present in the northwestern portions of the cave, with the larger one containing a concrete staircase. The feature is 20 meters deep, 25 meters wide and 34 meters long, consisting of a chamber with by a large bedrock pillar. Speleothems are extensive in the eastern part of the cave, while the part is dominated by breakdown. The overall morphology of the cave appears to be that of flank margin cave; however, the large accumulation of breakdown, with a ceiling that shows little evidence of collapse, complicates this interpretation.

Liyang Popporput (Southeastern Ridge, Tinian – Figure 104)

Liyang Popporput is a fracture cave located approximately 1000 meters southwest of Puntan Barangka, along the northeastern cliffs of Carolina's Ridge. It is developed in the Mariana Limestone (QTmca) as a steeply dipping, dissolutionally enhanced fracture that is oriented northwest at a bearing of 80^{o}. This fracture cave is 40 meters long, 23 meters deep and has a maximum width of 2 meters. The feature is located in a region with numerous smaller fractures that cannot be explored as extensively. In the western part of the feature, where there is a partial roof of collapse material, some minor speleothems coat the walls.

Cliff retreat in this region has created a complicated assemblage of fracture caves that are acting as fast flow routes transferring water to the subsurface. It is expected that some of the features in this area extend to greater depths, but are either too small to explore, are blocked by breakdown as in this feature, or have not yet been discovered.

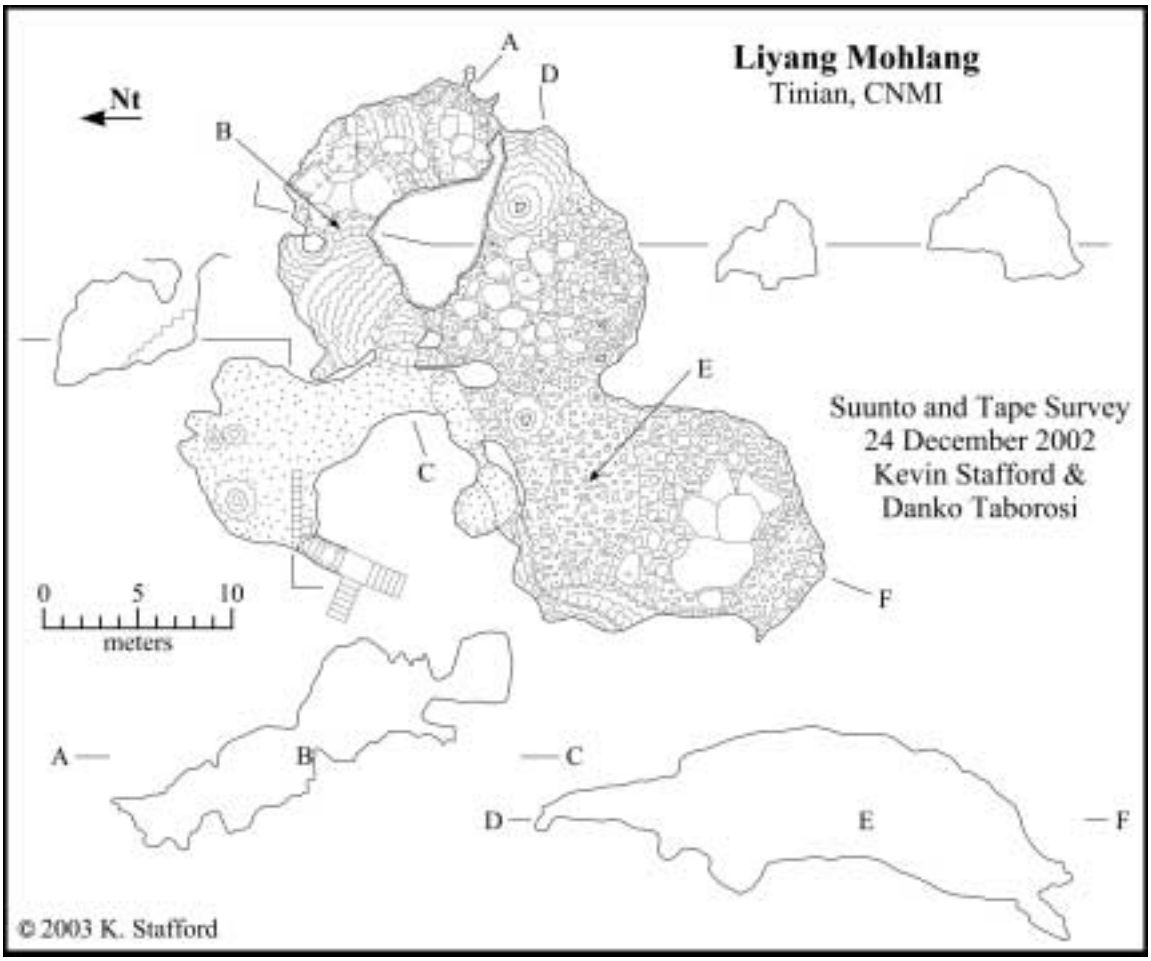

Figure 103: Map of Liyang Mohlang.

Liyang Sampapa (Central Plateau, Tinian – Figure 105)

Liyang Sampapa is located 250 meters south of Puntan Lamanibot Sampapa on the west coast. It is developed in the Mariana Limestone (QTmca) and extends inland 20 meters with a width of 8 meters and a bedrock floor. The entrance area of the cave is below sea level. The feature appears to be developed along an east/west trending joint trending that is well defined on the land surface, but less defined inside the cave. The feature appears to discharge minor amounts of fresh-water, but a definitive observation of discharge could not made at the time of survey because of strong surf conditions.

Liyang Umumu (Central Plateau, Tinian – Figure 106)

Liyang Umumu is located 900 meters north/northeast of Puntan Diapblo in the Mariana Limestone (QTmu), less than 3 meters below the land surface. It is a banana hole type cave with an average height of 1 meter, depth of 3.5 meters and entrance width of 11 meters. This small feature contains extensive speleothems including flowstone covering all walls and the floor in the northeast portion of the cave, several columns, and numerous stalactites covering the majority of the ceiling. The floor is primarily composed of soil and detritus with some scattered breakdown blocks.

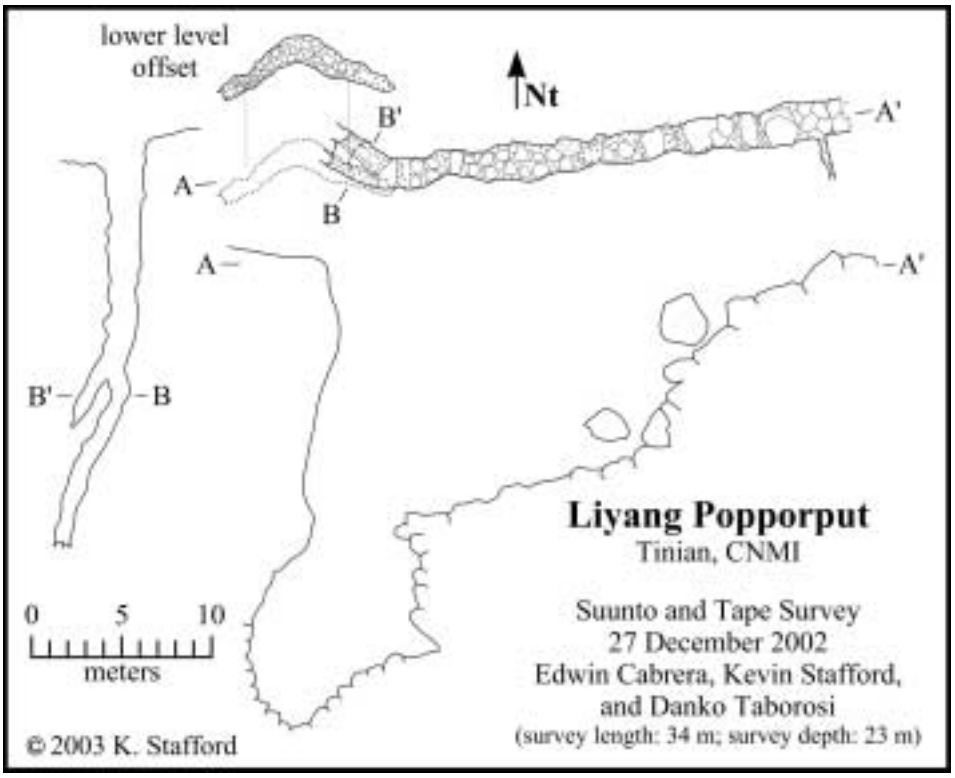

Figure 104: Map of Liyang Popporput.

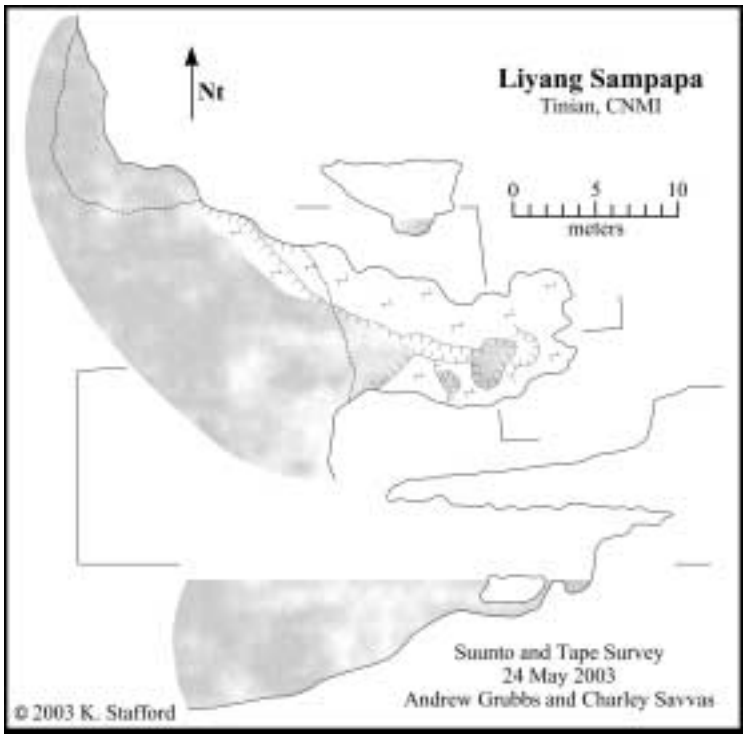

Figure 105: Map of Liyang Sampapa.

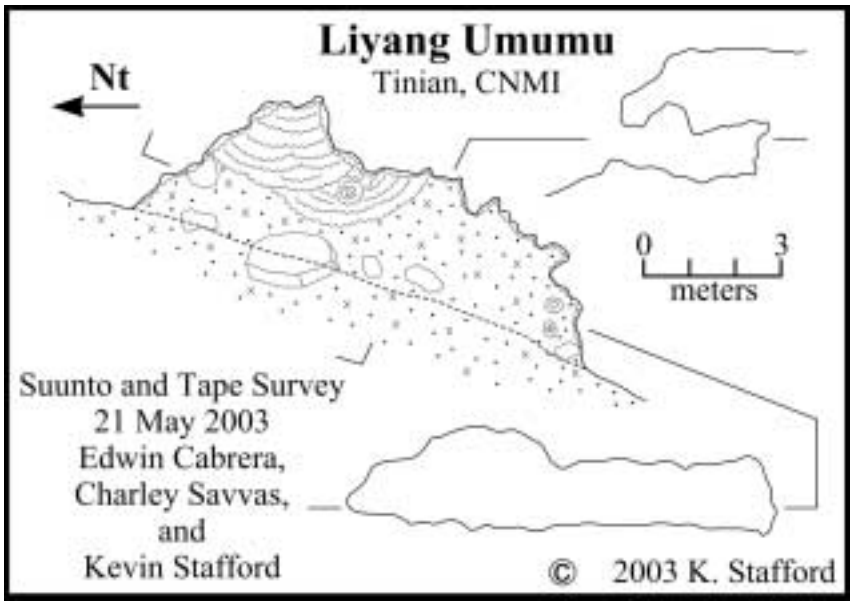

Figure 106: Map of Liyang Umumu.

Lizard Cave (Middle Terrace, Aguijan – Figure 107)

Lizard Cave is a small flank margin cave located on the north-central side of the Middle Terrace in the Mariana Limestone (QTmu). The cave extends inland 7 meters as two passages that average 3 meters wide and less the 2 meters tall. The floor is composed of alluvium and breakdown. One small passage continues from the inland portion of the southwest passage. The entrance area and northwest passage show evidence of extensive use by local fauna, primarily feral goats.

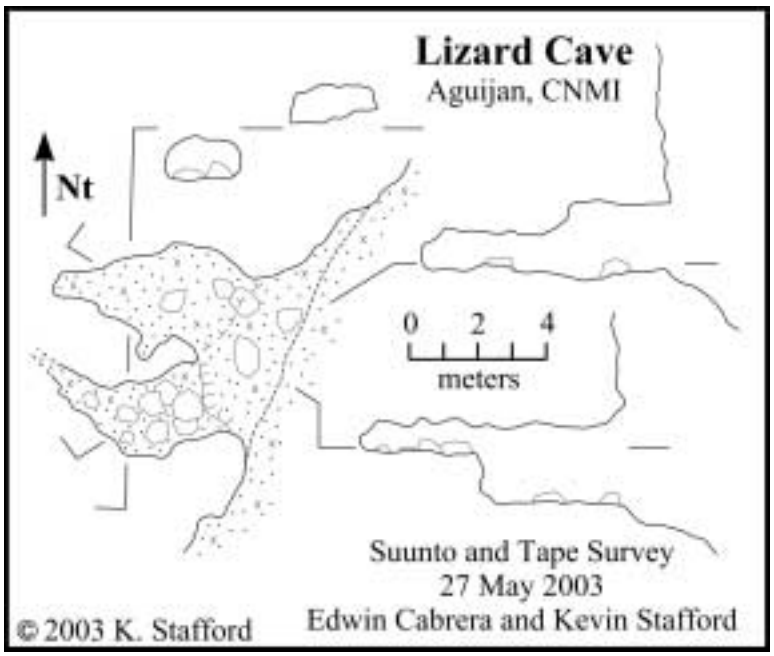

Figure 107: Map of Lizard Cave.

Lower Suicide Cliff Cave Complex (Southeastern Ridge, Tinian – Figure 108)

Lower Suicide Cliff Cave Complex is located near sea level, 2100 meters southwest of Puntan Kastiyu in the Mariana Formation (QTmu). It consists of a series of breached flank margin caves along a 190-meter. The cave complex is separated from the ocean by a series of algal-rimmed pools and extends inland up to 50 meters from the coast. The northern cave extends inland 25 meters with an average width of 10 meters. South of the northern cave is a long natural arch that retains an outer wall that is less than 3 meters, forming a 7-meter wide, 10-meter tall, and 50-meter long passage. South of the natural arch passage, three remnant cave chambers extend inland with development that trends inland and up the seaward dipping beds. The southern end of this cave complex is bounded by several large breakdown blocks produced from regional cliff retreat. This complex of caves provides and excellent example of lithologic control on the development of flank margin caves.

Masalok Fracture Cave Complex (Southeastern Ridge, Tinian – Figure 109)

The Masalok Fracture Cave Complex is located approximately 300 meters west/northwest of Puntan Masalok in the Mariana Limestone (QTmu), along the same fracture as the "600 Meter" Fracture System. This fracture strikes northwest and dips approximately 80^{o} to the northeast. At 42 meters, this feature is the deepest karst feature currently known on the island of Tinian. The main portion of the cave can be reached by a series of climb-downs, but the lower levels require the use of ropes and vertical equipment for safe exploration. Speleothems are common throughout the entire feature, especially in the form of flowstone coating the passage walls. The ceiling is composed primarily of large breakdown blocks, while the floor consists of breakdown and alluvium. Exploration in the main cave, which extends farthest to the northwest, was halted in both the northwest and southeast portions by breakdown. However, exploration in the eastern part of the feature led to the deepest parts of the cave, which includes a 40 meter near-vertical descent from the eastern most entrance. Based on survey data, the main, western part, of the cave and the eastern part of the cave are separated by less than 2 meters of breakdown blocks, confirming that they are effectively one cave. There is ponded fresh-water and a thick layer of mud at the maximum depth, in the eastern part of the cave, indicating that this area of the cave floods during recharge events. This feature demonstrates the importance of fractures as fast flow routes in eogenetic karst.

Mendiola Arch Cave Complex (Central Plateau, Tinian – Figure 110)

Mendiola Arch Cave Complex is located 1200 meters southeast of Puntan Atgidon on the southern edge of a large cove referred to locally as Mendiola Cove after the name of the landowner. It is a series of breached, flank margin caves developed in the Mariana Limestone (QTmu). The complex is split into two areas by a cave remnant that forms a natural arch that is 6 meters wide and 10 meters tall. Northeast of the arch is a series of four cave chambers which range from 5 to 15 meters wide and extend inland up to 20 meters with and average ceiling height of 5 meters. South of the natural arch, two larger caves have entrance widths of 18 and 24 meters and extend inland up to 25 meters. The caves in this complex primarily contain bedrock floors with breakdown blocks and cobbles. Based on the proximity of the features, it appears that some, if not all of the features were connected in the past and have been isolated as individual cave remnants by erosional, coastal processes.

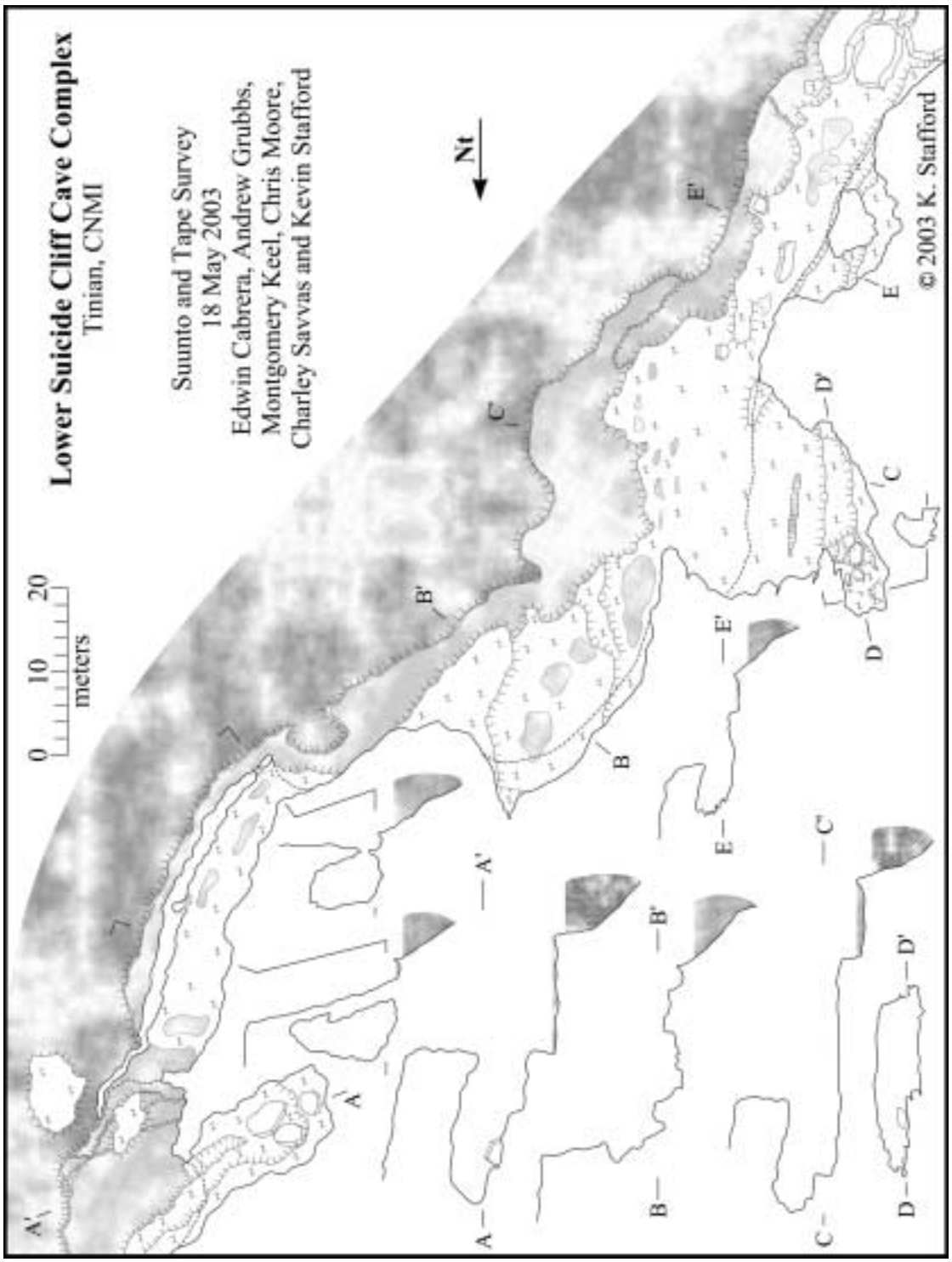

Figure 108: Map of Lower Suicide Cliff Cave Complex.

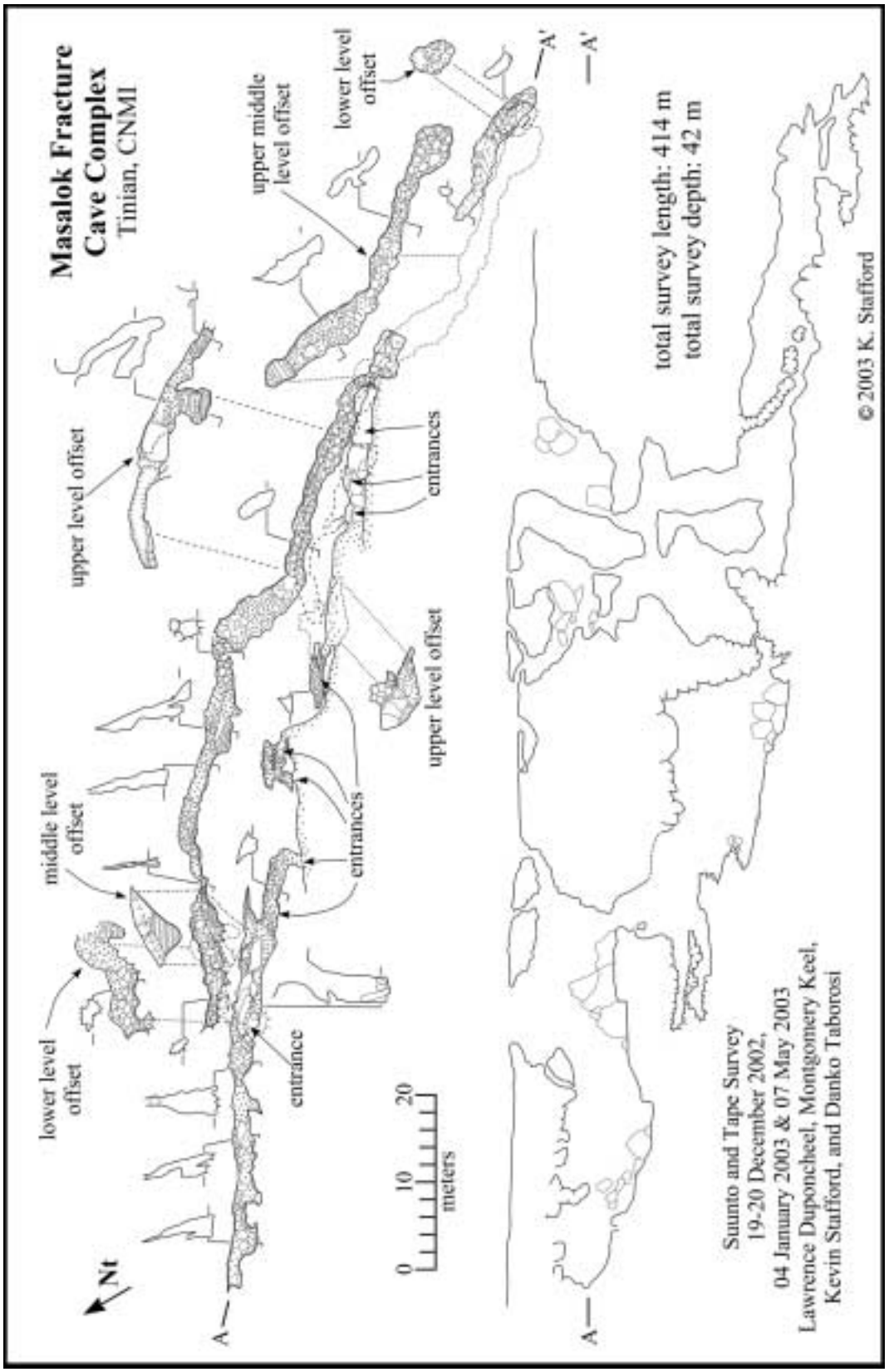

Figure 109: Map of Masalok Fracture Cave Complex.

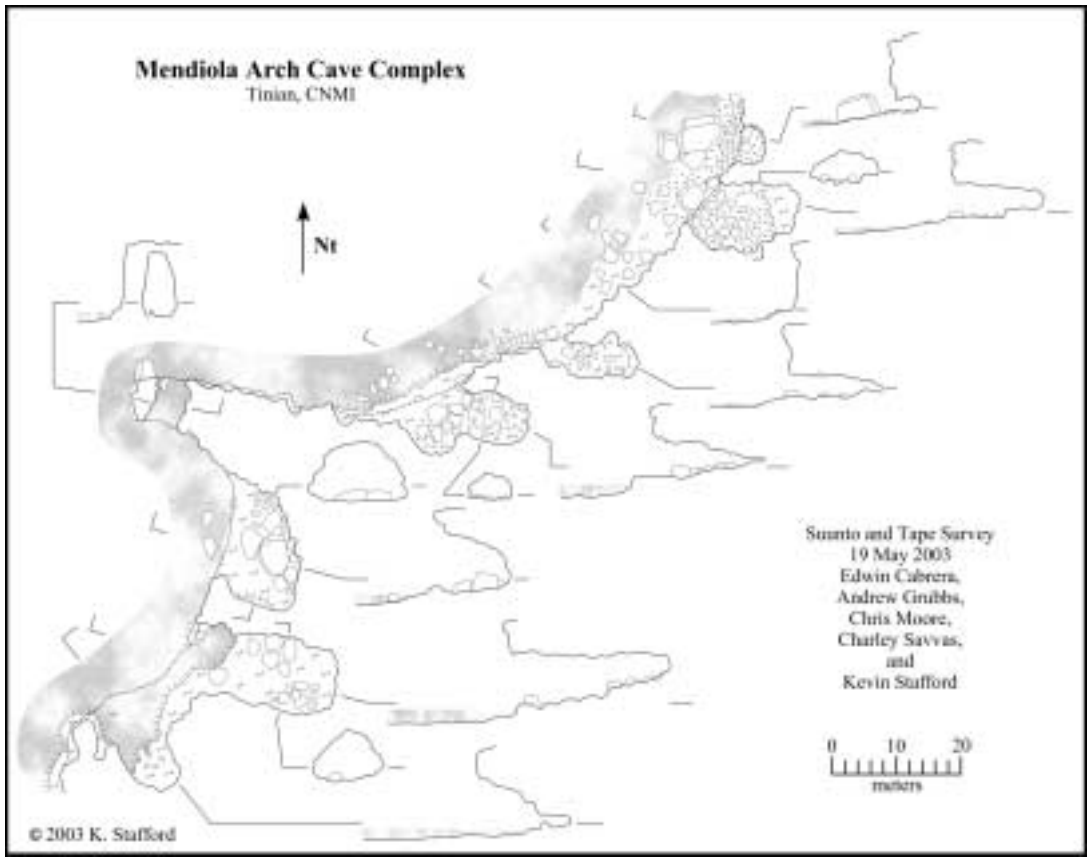

Figure 110: Map of Mendiola Arch Cave Complex.

Metal Door Cave (North-Central Highland, Tinian – Figure 111)

Metal Door Cave is a remnant, flank margin cave located 600 meters east of 8th Avenue on the northern scarp of Mount Lasu in the Tagpochau Limestone (Tt). It has an entrance area 10 meters wide that is divided by a 2-meter long bedrock column on the south side. The cave extends inland 15 meters with an average ceiling height of 3 meters and several small terrace levels in the inland part. The floor is primarily composed of soil and small rock fragments and has been extensively modified by humans. A 5-meter long, 2-meter tall rock wall conceals the majority of main entrance, while the main portion of the chamber has a leveled floor. The name of the cave is derived from a large metal door that was found 30 meters from the entrance.

Metal Spike Cave Complex (Median Valley, Tinian – Figure 112)

The Metal Spike Cave Complex is located approximately 500 meters inland from Unai Dangkolo, oriented northeast, approximately 10 meters west of the road to the same region. This feature consists of a series of collapsed flank margin caves in the Mariana Limestone (QTmca) with a few remaining chambers. It appears that the entire feature was connected in the past, but due to cliff retreat and collapse it is now disjointed. When connected, this feature would have been more than 130 meters long.

The southwestern part contains the largest collapsed chamber, which is approximately 12 meters in diameter and 2 meters deep, indicating that a large void collapsed at depth to create this surface expression. To the south of this collapse feature is a small roofed chamber approximately 5 meters by 6 meters with a 2-meter tall ceiling. To the west of the large collapse feature is a

large section of remnant flank margin cave that is developed along and partially under the western edge of the collapse. This chamber extends to a depth of 8 meters and contains speleothems throughout, including large columns in the entrance area.

Northeast of the large collapse feature is a 30 meter section of 5 meter high cliff wall, that has several small solutional chambers with speleothems located in and around them. This appears to be the remnants of the inland wall of flank margin cave development that has been almost completely removed by cliff retreat.

Continuing northeast across a 15-meter section of large angular limestone blocks, a second collapsed feature is present. This feature is approximately 5 meters by 10 meters with parts of the original roof remaining. Extending off the northeast corner of this second collapse feature is a small passage extends for an additional 8 meters, which contains speleothems and additional breakdown.

In the northeastern part of the cave complex is a series of partially breached chambers that extend are connected for approximately 40 meters with widths ranging from 4 to 8 meters and a maximum ceiling height of 5 meters. The southwestern portion of this region is a ceiling collapse entrance approximately 5 meters by 10 meters, with roofed chambers extending to the east and south. The far northeastern part consists of a 25-meter long passage that terminates in a 4 meter by 6-meter chamber with speleothems. This chamber is under the road to Unai Dangkolo. In the middle part of this passage, a pit entrance, which is approximately 1.5 meters in diameter, breaches the surface.

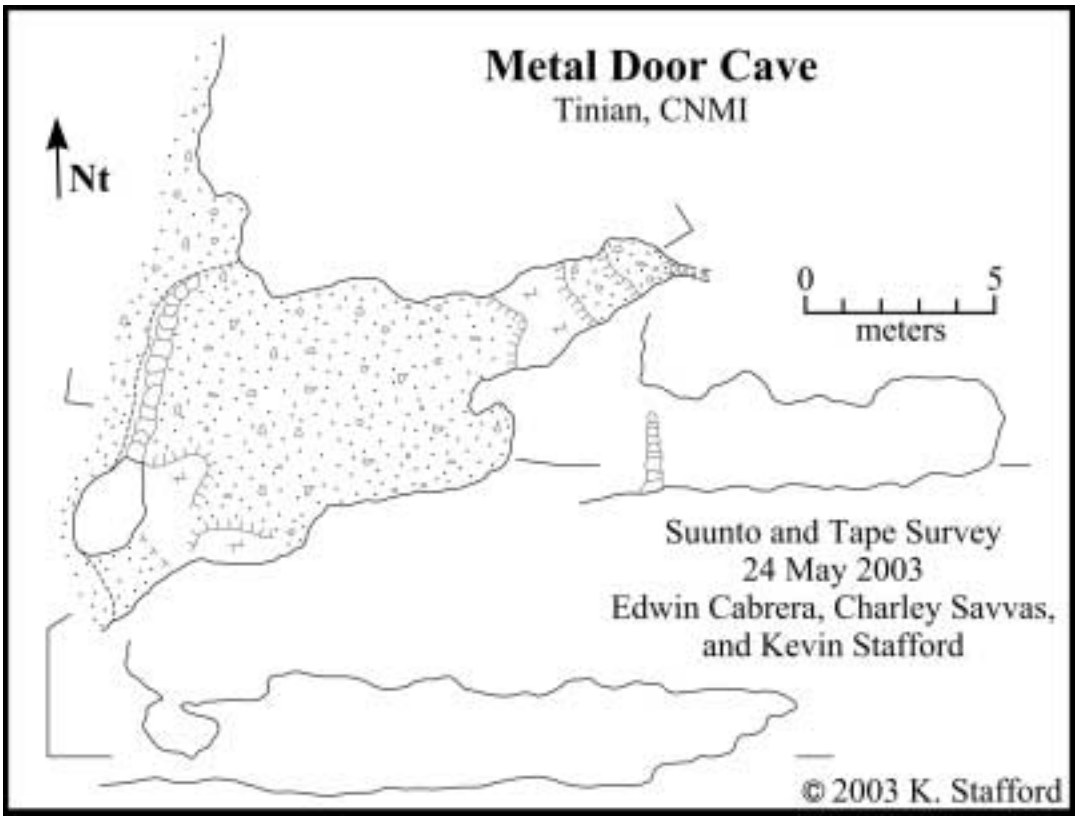

Figure 111: Map of Metal Door Cave.

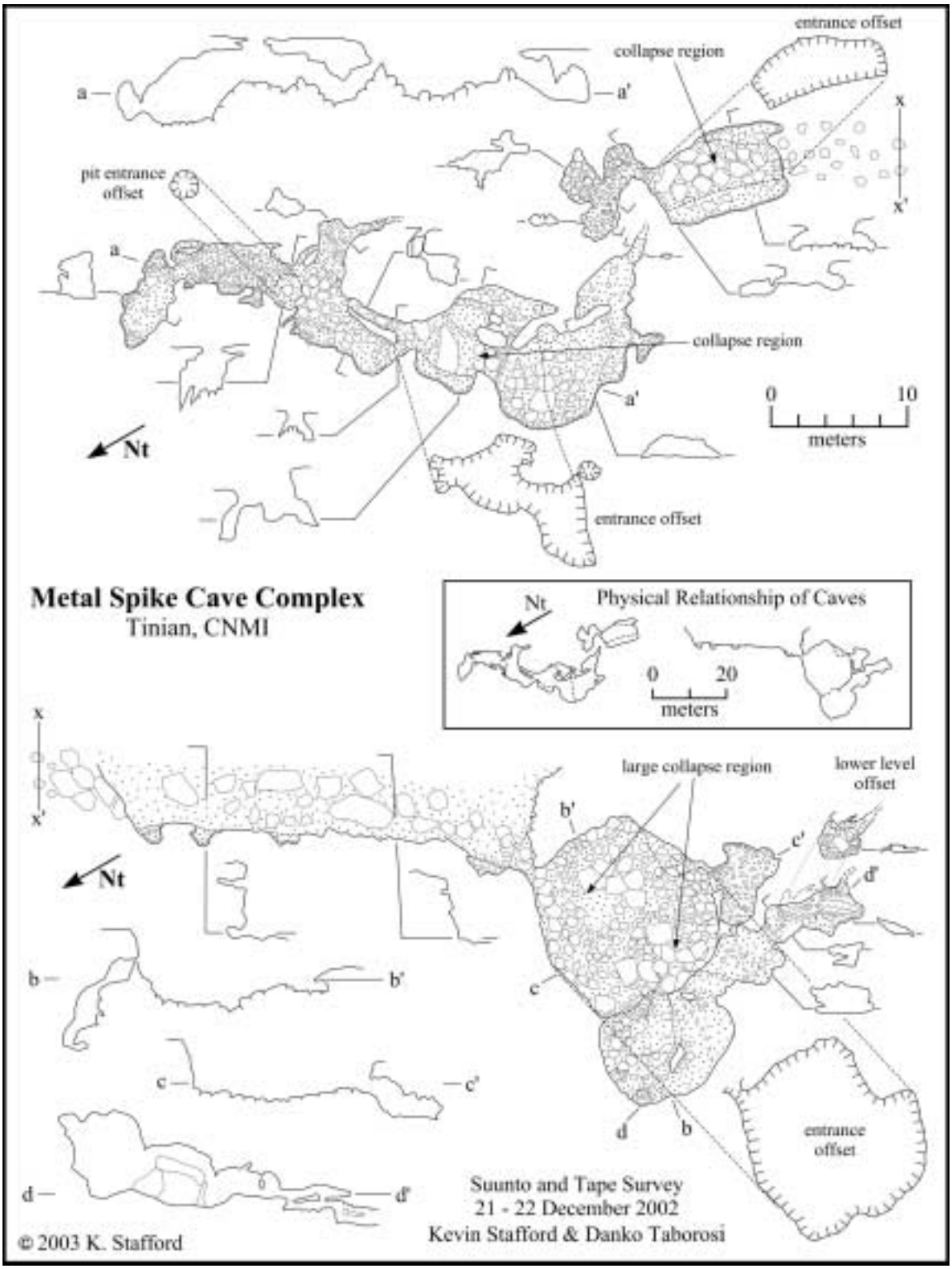

Figure 112: Map of Metal Spike Cave Complex.

Metal Stretcher Cave (Southeastern Ridge, Tinian – Figure 113)

Metal Stretcher Cave is located in the central portion of Suicide Cliffs, 25 meters above the base of the cliff. This feature is developed in the Tagpochau Limestone (Tt) and represents a remnant flank margin cave exposed by cliff retreat. It measures 12 meters wide at the entrance and extends inland 8 meters with a ceiling height of 6 meters. The feature contains speleothems, including two large columns in the entrance area. The cave appears to have had minor human modification in the entrance floor area, but is primarily in its original condition with only minor alluvium covering the floor.

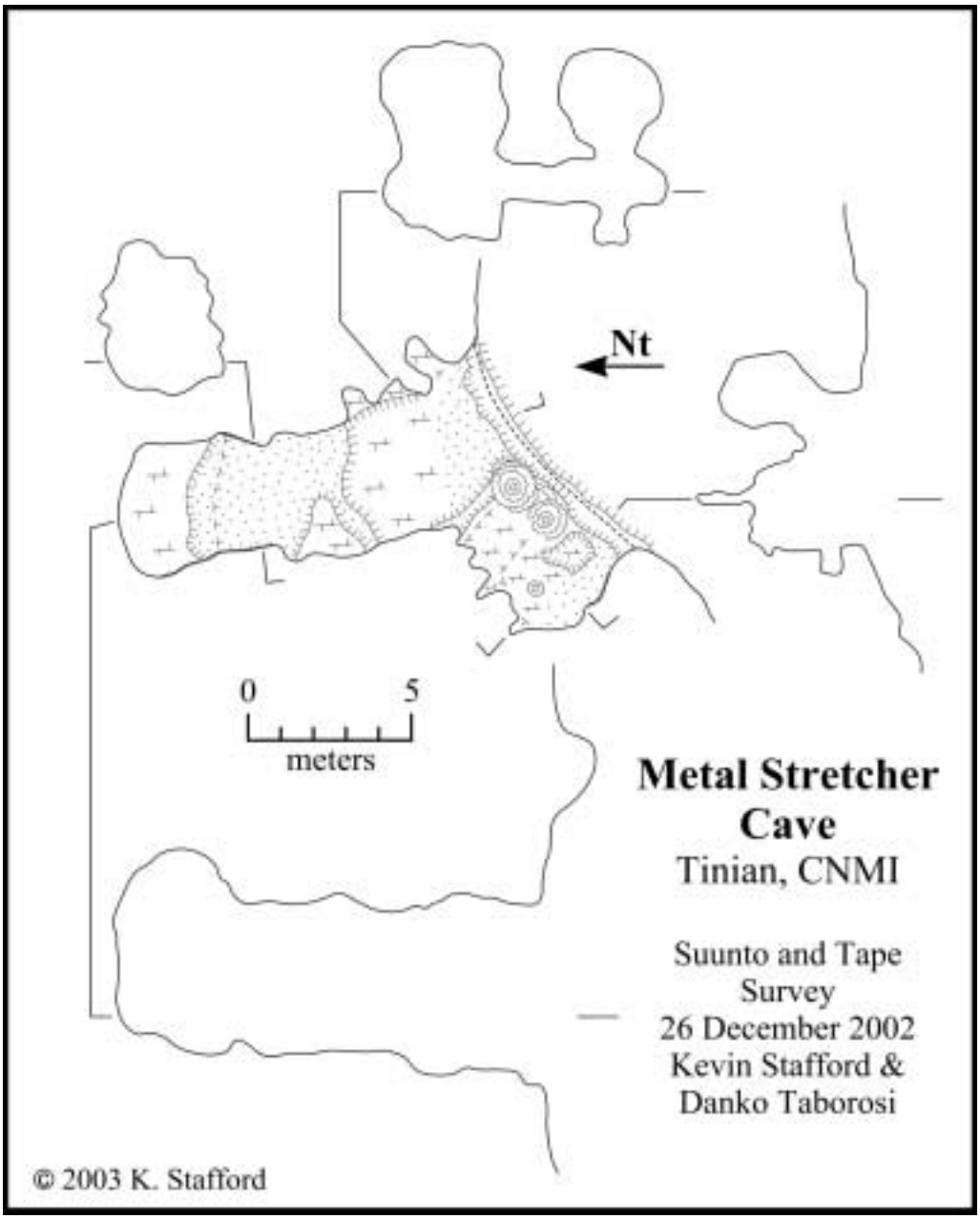

Figure 113: Map of Metal Stretcher Cave.

Modified Cave (Southeastern Ridge, Tinian – Figure 114)

Modified Cave is located in the central portion of Suicide Cliffs, at the base of the cliff, in the Tagpochau Limestone (Tt). The feature is a flank margin cave, which has extensive human modification to the entrance chamber, but little modification other than floor morphology in the larger, northern chamber. The feature is 9 meters by 4 meters with a maximum ceiling height of 3 meters. The larger chamber is a typical small, flank margin chamber with some ceiling collapse. This feature, although modified in the entrance area, represents a second horizon of dissolutional development along Suicide Cliffs, with the other prominent horizon located approximately 20 meters higher.

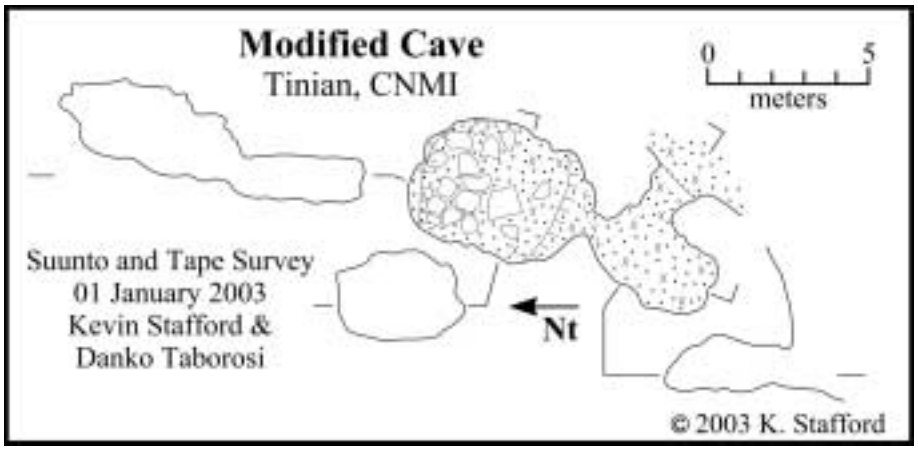

Figure 114: Map of Modified Cave.

Monica Wants to be Like Kevin Cave (Southeastern Ridge, Tinian – Figure 115)

Monica Wants to be Like Kevin Cave is located 800 meters east of Puntan Diapblo in the Mariana Limestone (QTmu). This flank margin cave remnant has an entrance 11 meters wide and extends inland 12 meters where it widens to 14 meters. The ceiling height averages 5.5 meters but decreases inland. The floor is composed of soil and detritus with a moderate amount of breakdown blocks in the middle of the cave.

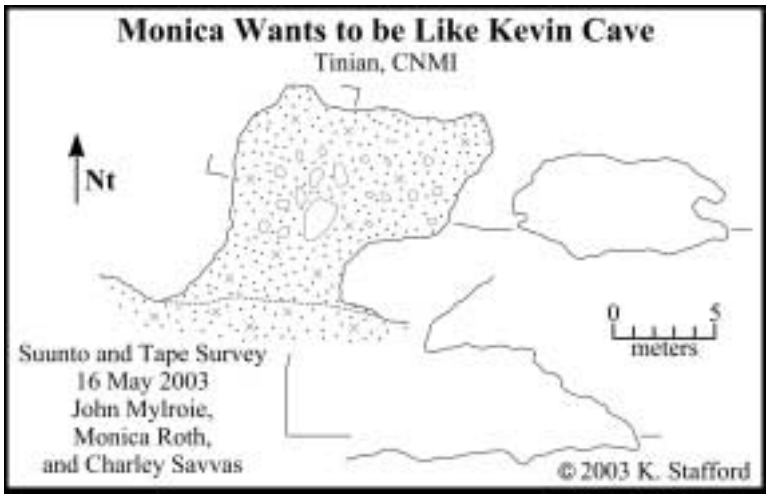

Figure 115: Map of Monica Wants to be Like Kevin Cave.

Natural Arch Cave (Middle Terrace, Aguijan – Figure 116)

Natural Arch Cave is a flank margin cave, developed in Mariana Limestone (QTmu), approximately 5 meters high on the scarp face in the southwest region of the Middle Terrace. It consists of a large entrance that is 18 meters wide and 8 meters tall with two passages extending to the north. The northeast passage extends inland for 4 meters, while the northwest passage extends inland 8 meters before intersecting a fracture-controlled passage 12 meters long that is oriented at 35°. The floor is composed primarily of alluvium in the entrance area with elevated levels containing bedrock floors. The fracture-controlled passage and the entrance passage leading to it, contain some minor guano deposits mixed with alluvium. The name of the cave is derived from a bedrock arch, 20 to 50 centimeters in diameter, that extends from the west wall of the inland passage.

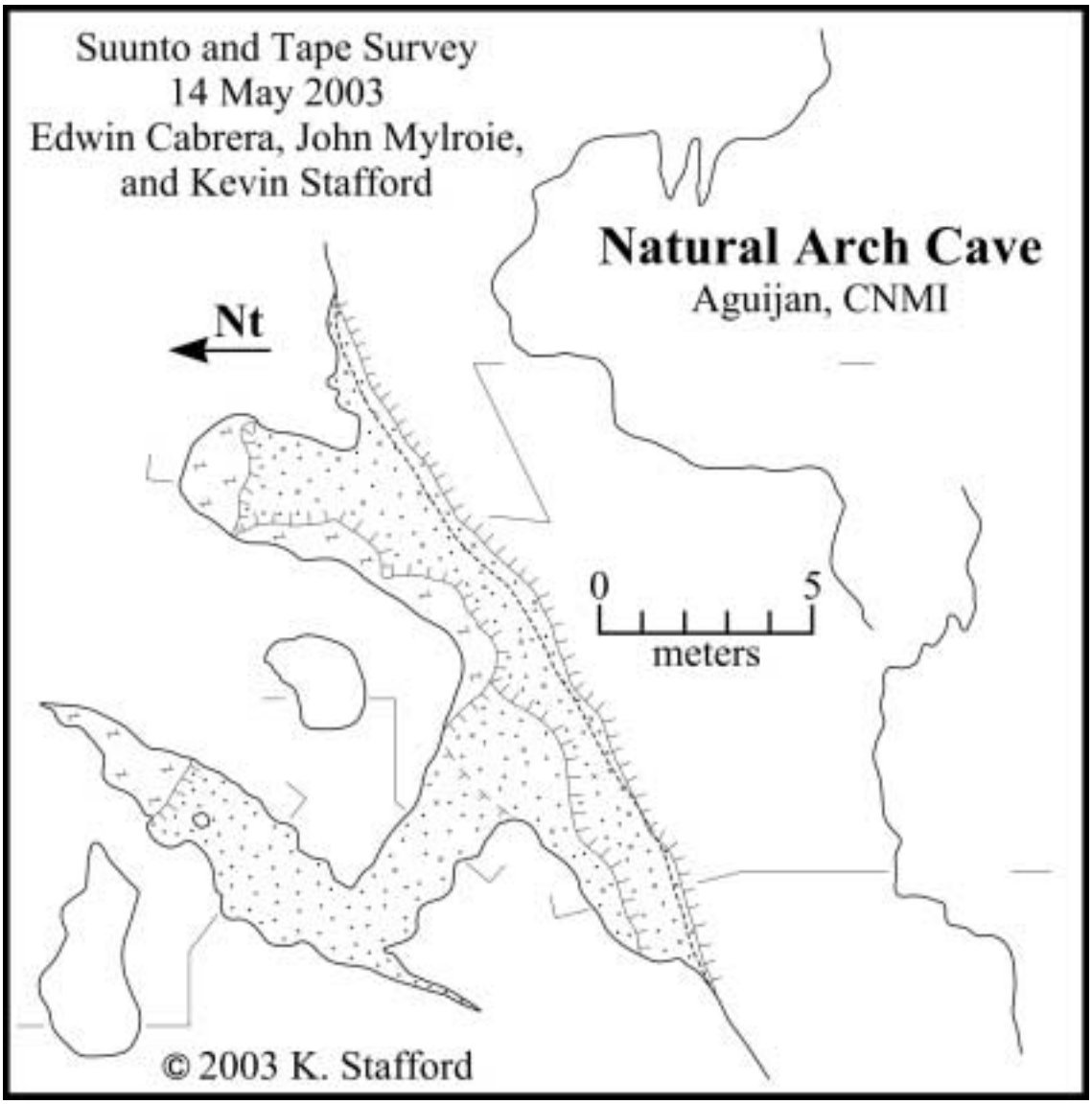

Figure 116: Map of Natural Arch Cave.

North Unai Dangkolo (Median Valley, Tinian – Figure 117)

North Unai Dangkolo is the northern scarp of Unai Dangkolo and the two coves north of it. It is developed in the Mariana Limestone (QTmca) and covers 300 meters of coastline. The northern most cove has a width of 50 meters and extends inland 20 meters with ceiling remnants extending from the wall less than 5 meters for the majority of the cove, which is floored with carbonate sand. The main cove at North Unai Dangkolo has a seaward width of 85 meters and extends inland 95 meters with the width decreasing to 25 meters at a distance of 35 meters inland. Small regions are roofed near the cove walls and minor amounts of well-weathered flowstone can be seen in places. The entire cove is floored with carbonate sand with several large collapse blocks located on the north and south side of cove near the shoreline. Several prominent fractures are dissolutionally widened throughout the cove and a 15-meter long, 3-meter wide, 1-meter tall pillbox is constructed in the northeast corner of the cove. The northern scarp of Unai Dangkolo is 90 meters south of this large cove and extends inland 60 meters before it turns south into dense vegetation, which prevented a continuation of the survey along the perimeter of Unai Dangkolo. However, Andyland cave was located at this southward bend in the cove. The majority of North Unai Dangkolo is floored with carbonate sand, but dense vegetation grows in the regions that are farther inland and more protected from normal coastal processes.

Northern Playground Cave (Southeastern Ridge, Tinian – Figure 118)

Northern Playground Cave is located in the southeast region of the Piña ridge and consists of two caves developed in the Mariana Limestone (QTmu). The larger cave has an entrance 5 meters wide that is 6 meters tall and extends inland 6 meters with a 2-meter wide and 2.5 meters tall passage extending from the southwest corner of the main chamber for 4 meters. The smaller cave is located 4 meters northeast of the larger cave and extends inland 4.5 meters with an average width of 3 meters and ceiling height of 2 meters. The majority of the cave is floored with soil and detritus, but a small ledge in northern portion of the larger cave is bedrock as is the passage extending from the southwest corner of the larger cave.

Nuestra Señora de Santa Lourdes Cave Complex
(Central Plateau, Tinian – Figure 119)

This cave complex, including the Nuestra Señora de Santa Lourdes shrine located at feature "C", consists of a series of flank margin caves that developed on a consistent horizon and were modified for use during World War II. This series of caves is developed in the Mariana Limestone (QTmu) and have been breached by cliff retreat at the boundary between the Median Valley and Central Plateau. The caves vary in size and degree of human modification. Features A, C and D are typical flank margin caves with minor excavation to their floors, while the ceilings and walls appear to have been modified little, except for feature C, which has two small side passages that where excavated. Feature B has been highly modified leaving little evidence of the original floor, ceiling or walls, making its origin unclear. Feature E is extensively modified, including cement floor and supporting walls, as well as widened regions that are reinforced with concrete. It is doubtful that much of this feature is of original dissolutional origin, because of the constant height of the chamber at 1.6 meters and the extensive talus debris located outside its eastern entrance. In addition to the modifications during the World War II Japanese occupation, feature C has a modified floor of limestone aggregate and a cement shrine it the center.

Figure 117: Map of North Unai Dangkolo.

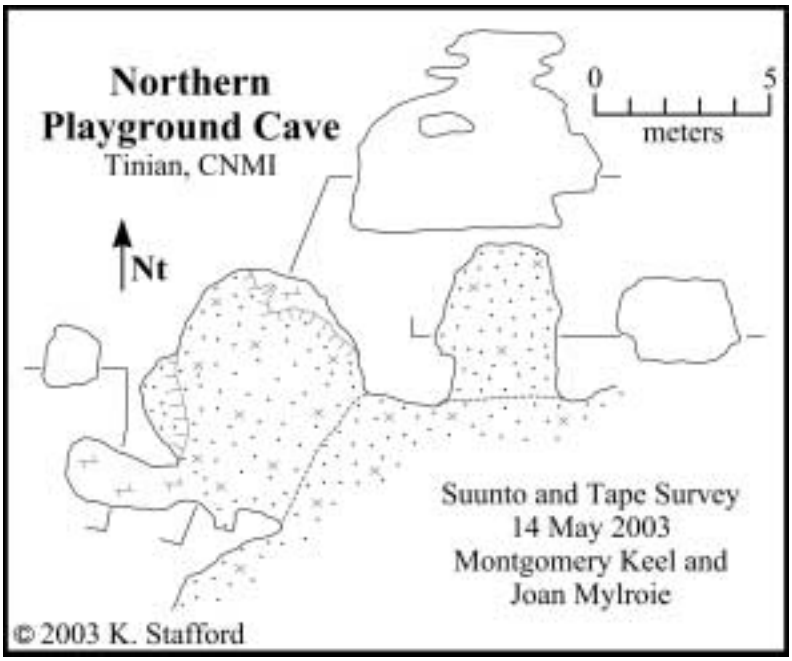

Figure 118: Map of Northern Playground Cave.

Orange Cave (Central Plateau, Tinian – Figure 120)

Orange Cave is located 700 meters west/southwest of Puntan Diapblo in the Mariana Limestone (QTmu). This breached, flank margin cave has an entrance 14 meters wide and extends inland 16 meters with an average ceiling height of 3 meters. The cove is a single chamber that has been severely impacted by intense storm events, creating a floor covered in well-worn breakdown blocks and cobbles.

Orphan Kids Cave Complex (Lower Terrace, Aguijan – Figure 121)

Orphan Kids Cave Complex is developed in the Mariana Limestone (QTmu) and located on the Lower Terrace on the southern side of Aguijan. This feature consists of three caves spread approximately 75 meters along a low cliff face. The caves are developed along a northwest trending fault with a dips approximately 35^{o} to the northeast. The three caves contain extensive speleothems and breakdown, with the northern feature extending to a depth of 4 meters and the middle and southern feature extend to 17 meters depth. All three features show evidence of extending to greater depths, but collapse and breakdown prevented further exploration. In association with these features, there are numerous dissolutionally enhanced surface fractures, which follow the same general trend. However, no additional features were located that could be entered by humans, nor any that showed signs of speleothems.

Pebble Cave (Central Plateau, Tinian – Figure 122)

Pebble Cave is located 700 meters southeast of Puntan Atgidon in the Mariana Limestone (QTmu). It is a flank margin cave remnant located less than 1 meter above sea level in the northeastern portion of a large cove referred to locally as Mendiola Cove after the landowner. The entrance of the cave is 22 meters wide and 7 meters tall, with the cave extending inland 9 meters. The cave is floored with carbonate sand and pebble size carbonate clasts, in addition to several large breakdown blocks, which appear to be remnants of the collapsed ceiling located in the southern part of the cave.

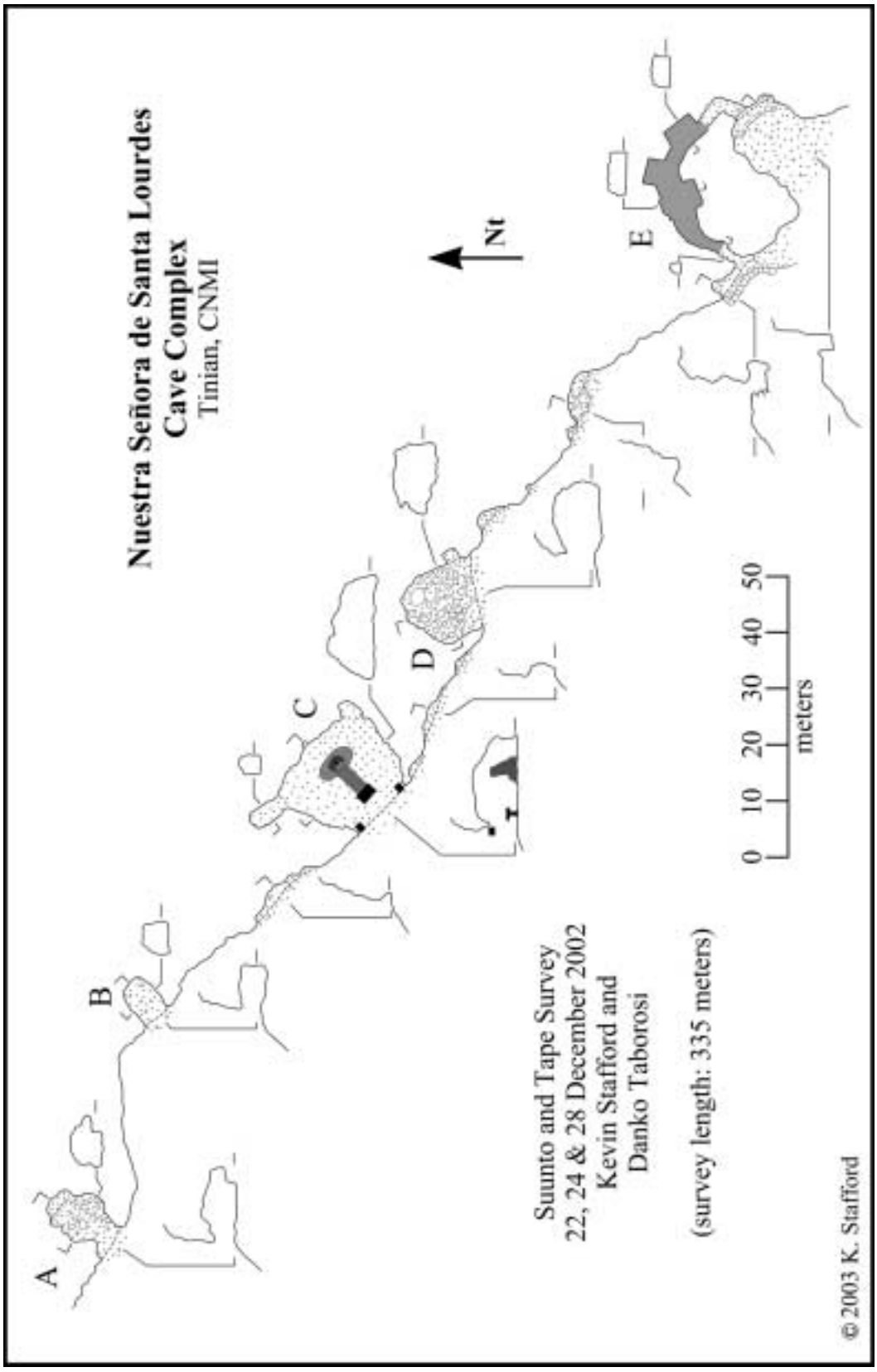

Figure 119: Map of Nuestra Señora de Santo Lourdes Cave Complex.

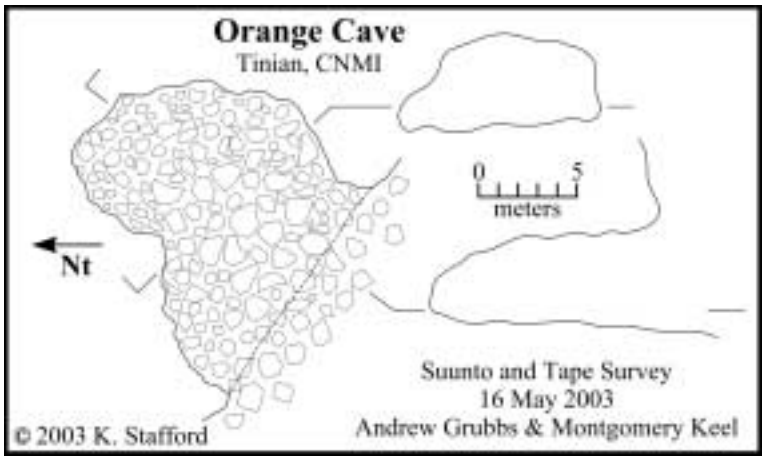

Figure 120: Map of Orange Cave.

Pepper Cave (Upper Terrace, Aguijan – Figure 123)

Pepper Cave is a small flank margin cave located in the northwest portion of the Upper Terrace in the Mariana Limestone (QTmu). It consists of a single chamber 5 meters wide, 3 meters deep and less than 2 meters tall. The floor is composed of alluvium and minor human modification consisting of a 6-meter long rock wall, which extends from the northern side of the entrance to the southeast.

Piña Cave Complex (Southeastern Ridge, Tinian – Figure 124)

Piña Cave Complex is located in the southeastern region of the Piña ridge and consists of three caves developed in the Mariana Limestone (QTmu). The larger cave is located at the southern end of this scarp segment and consists of three primary parts. The entrance area is 6 meters wide and extends inland, to the north for 5 meters forming the soil and detritus floored, entrance chamber. From the entrance chamber, a bedrock-floored passage extends 8 meters to the west as an upper level passage. To the south, a passage extends 4 meters and terminates in an elevated ledge. The two other caves are small and located 38 meters northeast of the larger cave. These two small caves are 3 meters apart with the western cave developed 2 meters high on the scarp and the eastern cave developed at the base of the scarp. Both caves extend inland 2 meters with ceiling heights less than 2 meters. The western cave exhibits a bedrock floor and the eastern cave has a soil, detritus and breakdown floor.

Playground Cave (Southeastern Ridge, Tinian – Figure 125)

Playground Cave is located in the southeast region of the Piña ridge and is composed of two caves along a scarp segment that is developed in the Mariana Limestone (QTmu). The larger cave extends inland to the west with an entrance 13 meters wide and a 1-meter by 2-meter bedrock column located in southern part of the entrance. It reaches its largest dimension in the northern part of this cave, where it extends inland 7 meters with a ceiling height of 9 meters. A smaller passage, 2 meters wide, extends west from the larger cave for 4 meters. In this larger portion, a collapsed rock wall is present which indicates human modification of the feature, but the remainder of the cave has a soil and detritus floor. The smaller cave is 8 meters northeast of the larger cave and has two entrances separated by a 2-meter diameter bedrock column. The west entrance leads to a small passage that is 1 meter tall, while the east passage has a ceiling height of 7 meters and extends to the north, roughly parallel to the scarp face, for 4.5 meters, forming the majority of this smaller cave.

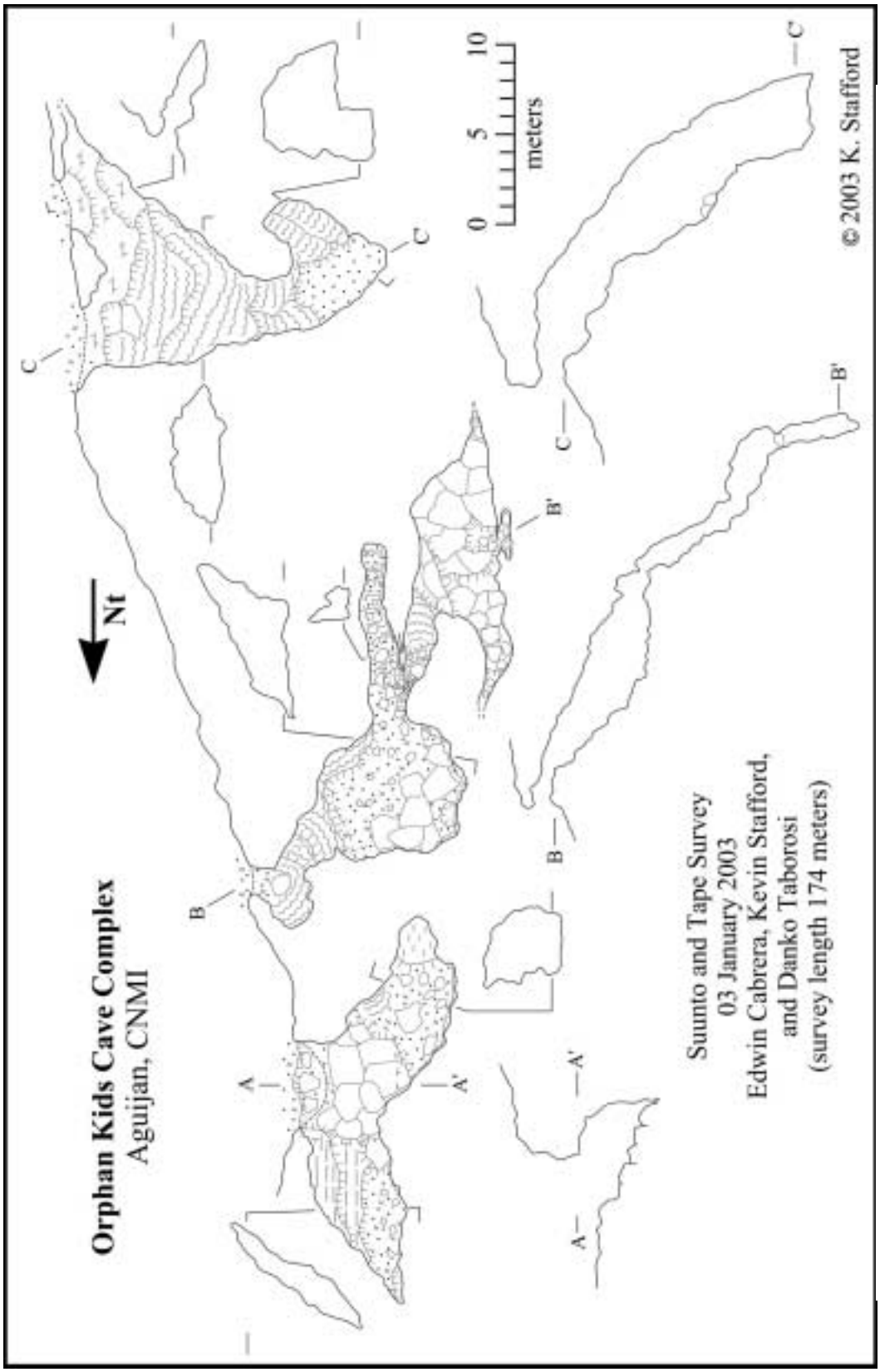

Figure 121: Map of Orphan Kids Cave Complex.

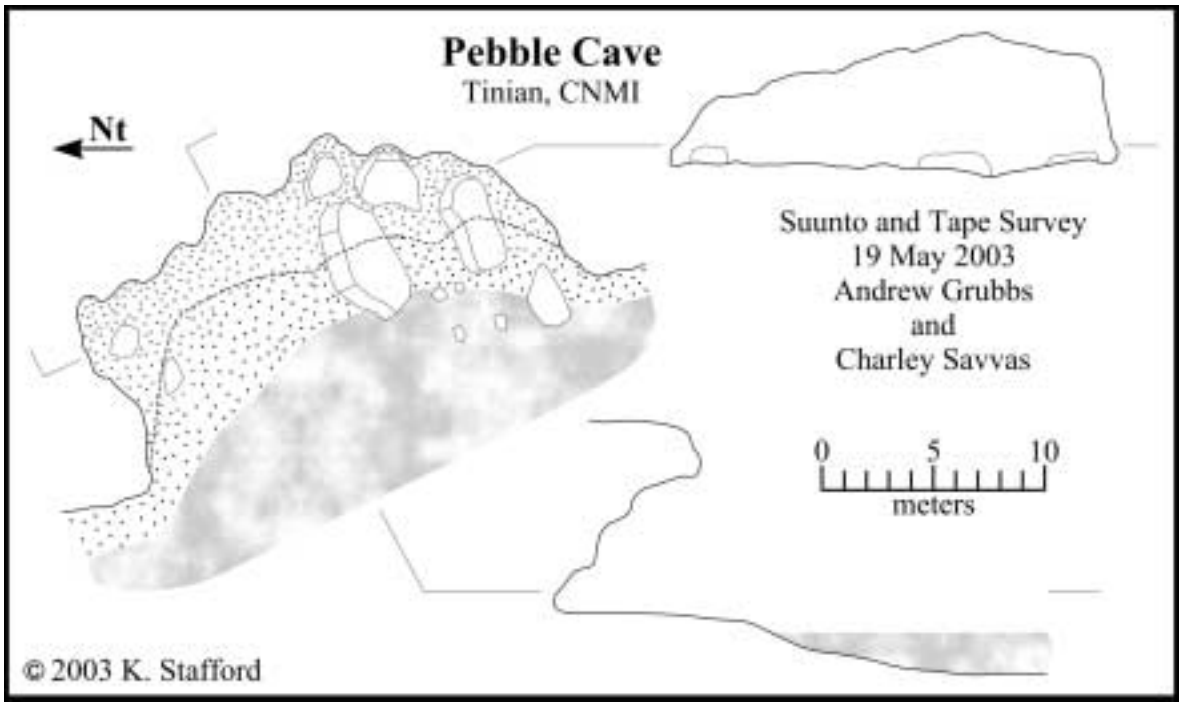

Figure 122: Map of Pebble Cave.

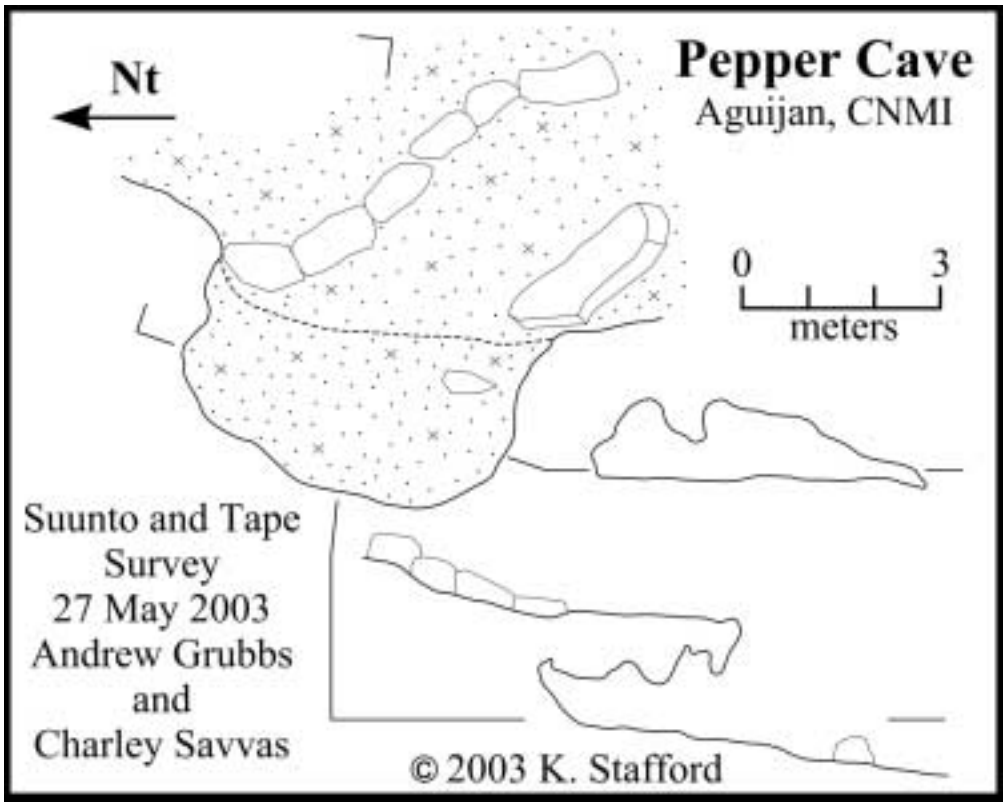

Figure 123: Map of Pepper Cave.

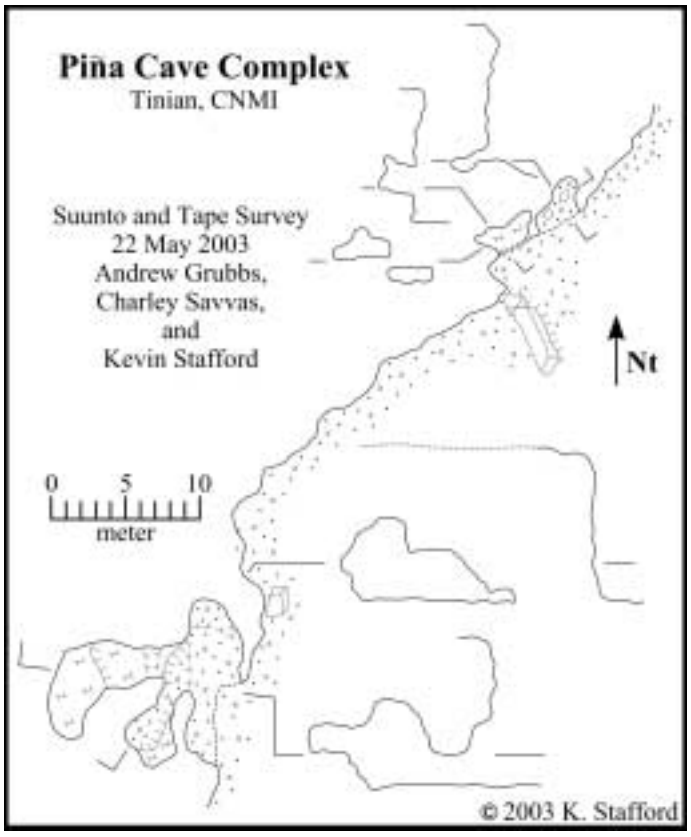

Figure 124: Map of Piña Cave Complex.

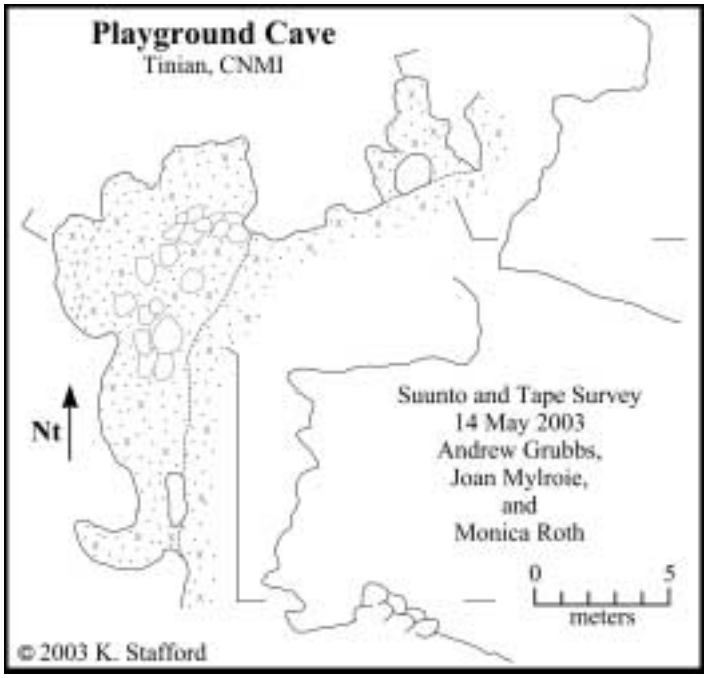

Figure 125: Map of Playground Cave.

Plunder Cave (Median Valley, Tinian – Figure 126)

Plunder Cave is located near the Water Cave, approximately 2 kilometers south of Taga Beach and 300 meters inland from the west coast. It is developed at the boundary between the Median Valley and the Southeastern Ridge provinces along a northeast/southwest trending fault that dips at approximately 35° to the southeast. This dissolutionally enlarged fracture cave is formed in the Mariana Limestone (QTmu) and is approximately 43 meters by 12 meters, extending to a depth of 13 meters. The cave consists primarily of one large chamber that contains extensive speleothems and much breakdown. In the central parts of the cave, a small, lower chamber is present in the breakdown blocks, where stacking of collapse material has created a larger void that is humanly passable. In the northern parts of the cave, large breakdown blocks have been covered by massive speleothem accumulations, but void space beneath these blocks has left a smaller passage. On the map, locations marked 1, 2, and 3 represent locations where geologic specimens were taken for future isotope analysis.

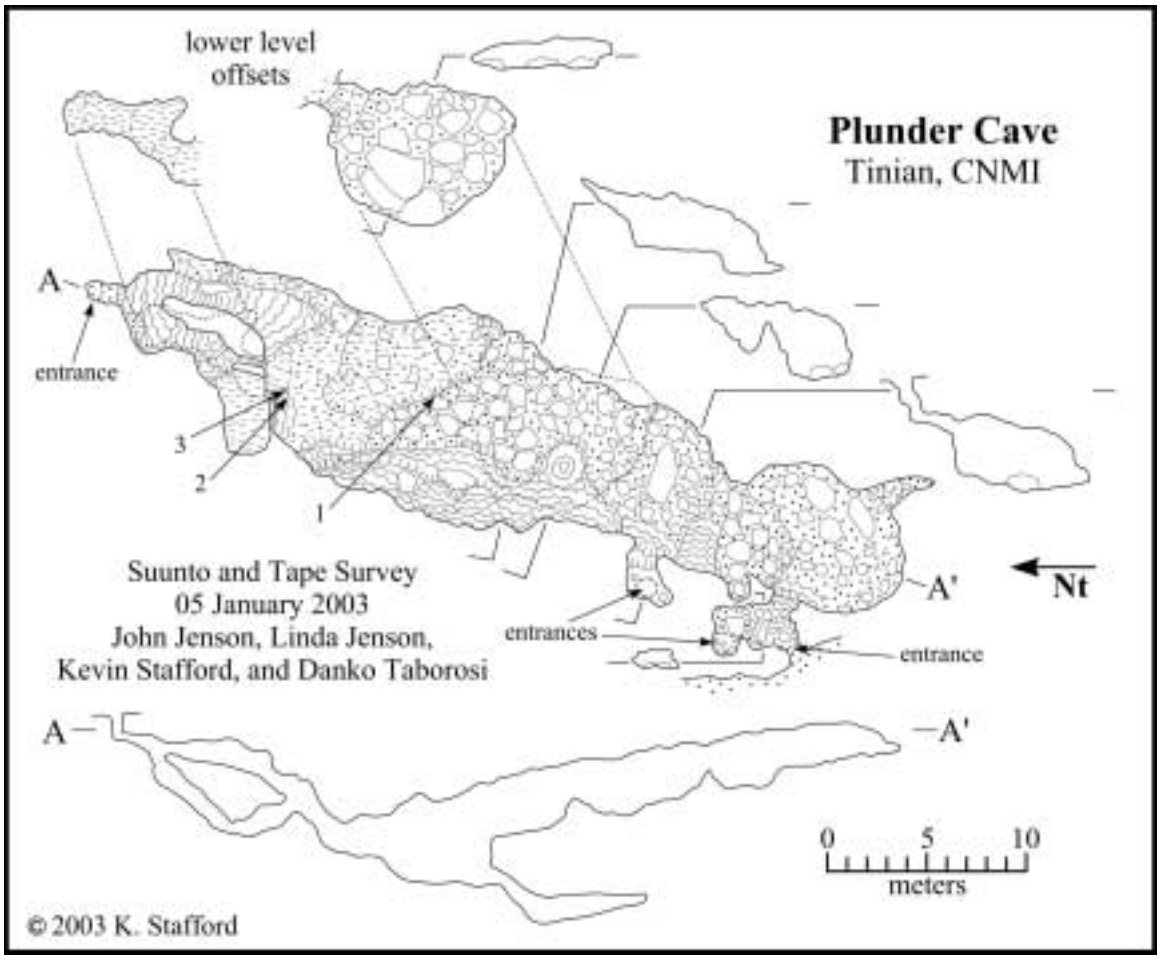

Figure 126: Map of Plunder Cave.

Radio Inactive Cave (Southeastern Ridge, Tinian – Figure 127)

Radio Inactive Cave is located in the central region of Suicide Cliffs in the Mariana Limestone (QTmu). It is a flank margin cave remnant that has been breached by scarp retreat with a 13-meter wide cliff entrance and a 2-meter diameter pit entrance in the inland part of the

cave. The cave extends 21 meters inland with an average ceiling height of 3 meters, forming a chamber with an average width of 7 meters that is partially divided by three bedrock columns. The scarp entrance area has a bedrock floor with some speleothems, primarily has stalagmites and columns. In the inland areas, near the pit entrance, the cave has fewer speleothems and the floor is covered with alluvium. The cave has been slightly modified by humans with some leveling of alluvial floors and deteriorating wooden floors. The cave is named for a Japanese military radio that was found in the there.

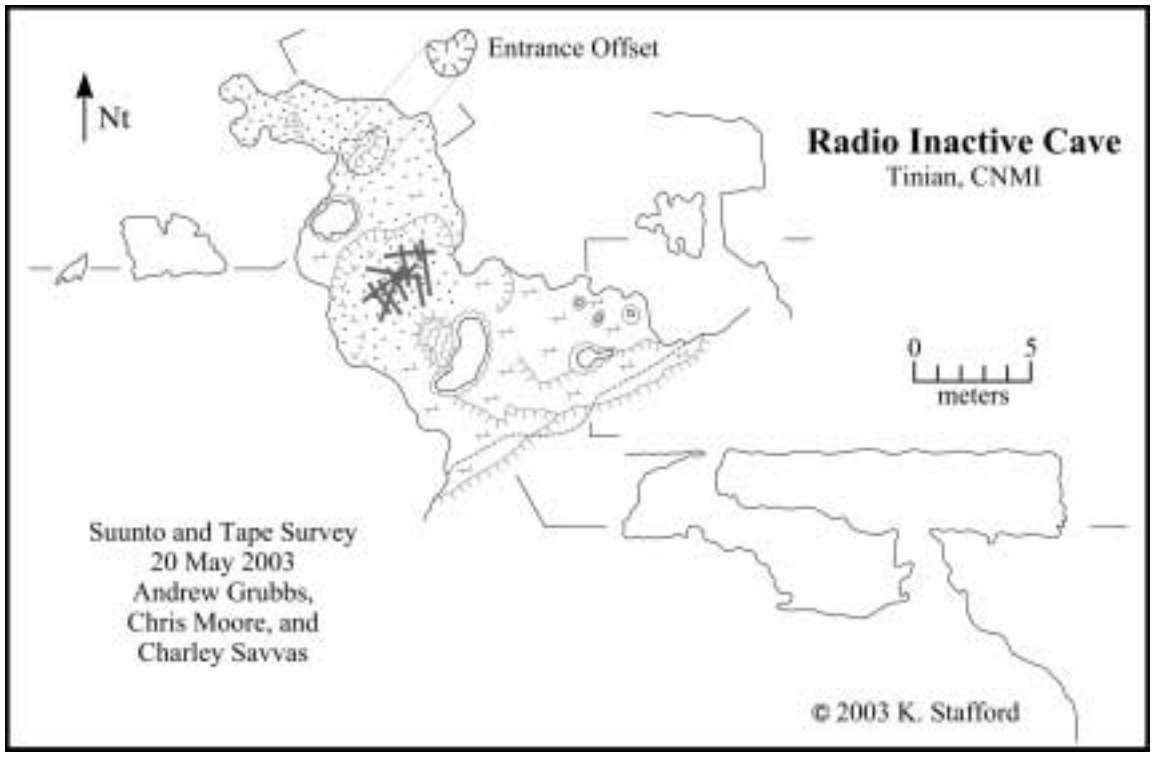

Figure 127: Map of Radio Inactive Cave.

Red Snapper Cave (Central Plateau, Tinian – Figure 128)

Red Snapper Cave is located 900 meters south of Puntan Lamanibot Sampapa at the top of the coastal scarp in the Mariana Limestone (QTmu). It is a collapsed, flank margin cave remnant similar to the coves seen near Unai Dangkolo, except that it is 10 meters above sea level without a carbonate sand floor. The feature is divided by a large bedrock remnant on the coastal scarp side, which forms two collapsed entrances 11 and 16 meters wide. The feature extends inland 43 meters, decreasing in depth inland but averaging 4 meters. The most inland 5 meters remains roofed, as do several smaller regions on the periphery of the feature where bedrock pillars provided additional support for the roof. Several small terraces subdivide the feature, while the floor is primarily composed of bedrock with scattered breakdown blocks that appear to be remnants of the original roof. Speleothem deposits, including flowstone, stalactites and stalagmites are seen throughout, but are more abundant in the areas that still retain protective ceiling remnants. The feature, although located well above mean sea level, appears to have been heavily impacted by numerous intense storm events and is primarily devoid of vegetation.

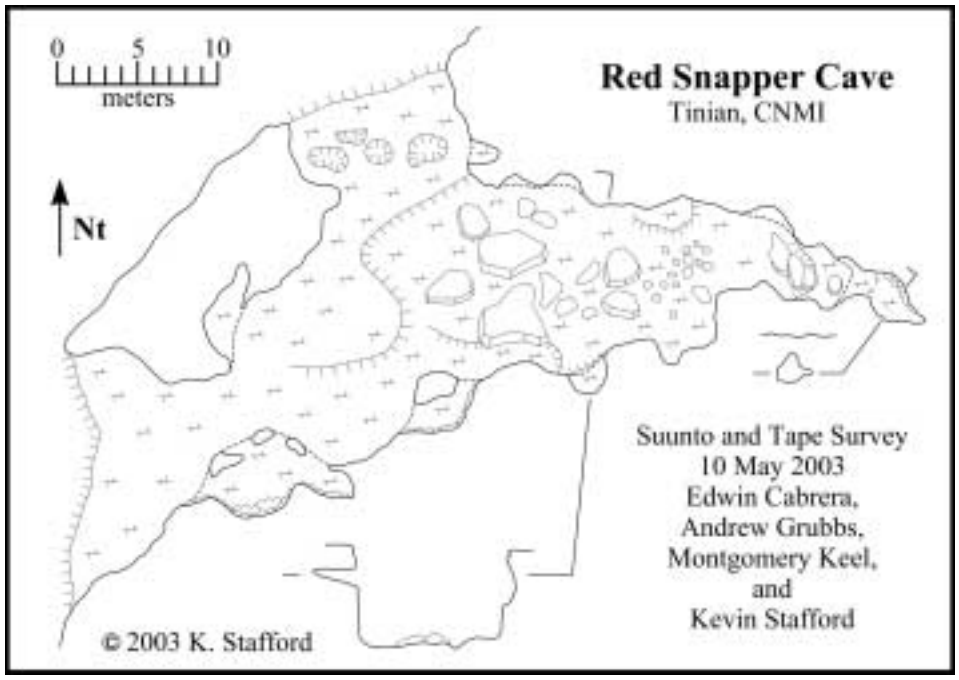

Figure 128: Map of Red Snapper Cave.

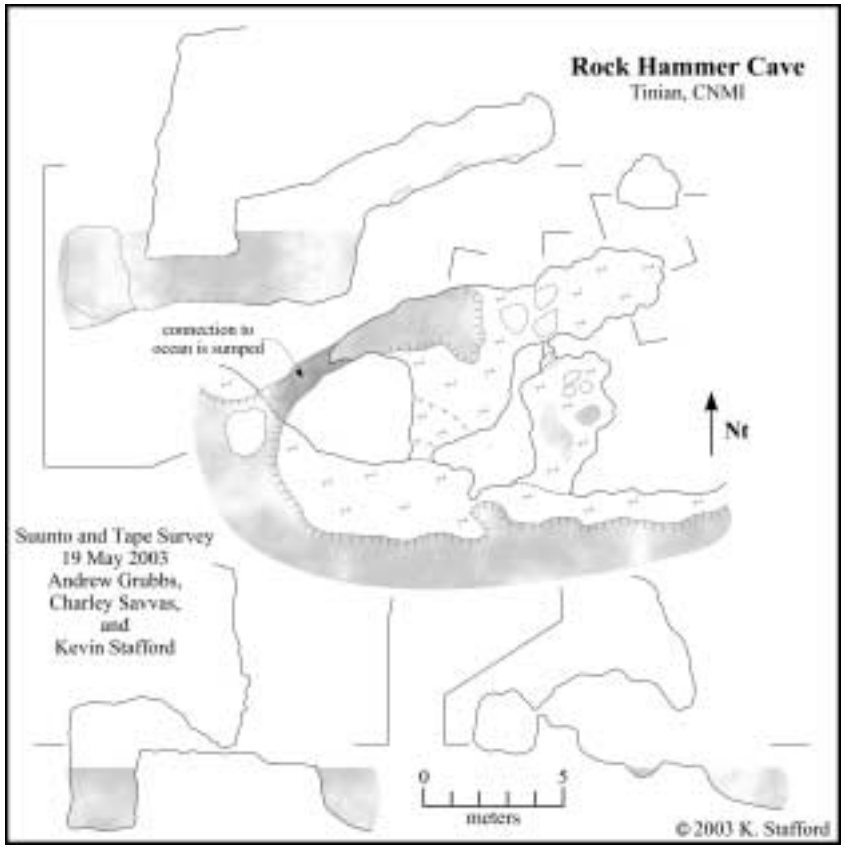

Figure 129: Map of Rock Hammer Cave.

Rock Hammer Cave (Central Plateau, Tinian – Figure 129)

Rock Hammer Cave is a flank margin cave located 900 meters southeast of Puntan Atgidon in the Mariana Formation (QTmu). It is positioned 1 meter above mean sea level at a prominent headland in the cove locally referred to as Mendiola Cove after the landowner. The cave is breached at three locations, with one entrance submerged below sea level. The most prominent entrance is 2 meters wide and trends inland as a single chamber for 5 meters, where it is connected to the main cave chamber by a small, 20-centimeter wide passage. The main chamber has two entrances; the western entrance is located 1 meter below sea level and was not entered because of strong surf conditions, while the second entrance is located between the sumped entrance and the prominent entrance. This second entrance was partially blocked at the time of discovery, but with minor removal of bedrock, it was enlarged to allow entry through a 40-centimeter tall crawlway. The crawlway opens less than 1 meter inland into a 2-meter tall passage, which extends east for 10 meters connecting to the prominent entrance chamber. The west side of the main chamber drops below sea-level near-vertically into a pool of water 5 meters long and 2 meters wide. The entire feature is primarily retains a bedrock floor, excluding some breakdown blocks. Few speleothem deposits were seen in the cave, but the cave is a good example of how flank margin cave chambers that barely connected to each other and the surface.

Rogue Cave (Northern Lowland, Tinian – Figure 130)

Rogue Cave is located 150 meters northeast of Unai Lamlam on the northwest coast. It is a discharge type feature developed in the Mariana Limestone (QTmu), extending inland 9 meters from a cove 31 meters wide and 19 meters deep. The majority of the cave is below sea level, but a bench up to 7 meters wide extends from the cave with partially roofed sections. The cave consists of a chamber 3 meters in diameter that extends below sea level 1.5 meters and a smaller tube that extends inland from the chamber 6 meters at 2 meters above sea level. The smaller tube has a distinct fracture or joint, which runs through the ceiling and floor, while a larger, dissolutionally widened fracture extends from the entrance below sea level. The feature showed some indication of freshwater discharge below sea level, but due to strong surf conditions a positive identification of discharge was not possible. However, based on the morphology of the cave and the distinct joint in the floor and ceiling, this feature is classified as a discharge feature.

Rootcicle Cave (North-Central Highland, Tinian – Figure 131)

Rootcicle cave is a collapsed banana hole feature that is developed in the Mariana Limestone (QTmca). This feature is located approximately 300 meters northeast of the Lasso Shrine at Mt. Lasu on a small terrace level above the Laderan Mangpang scarp. This feature has a central entrance formed by collapse and is elongated in a northwest/southeast direction, with dimensions of 10 meters by 33 meters. Through the long axis of the cave, there is a fault trending 120^{o}-130^{o} and dipping approximately 75^{o} to the southeast. The fault has dropped the southern portion of the cave by approximately 2 meters relative to the northern portions. This fault trend extends to the east as a low passage that is not humanly passable. The cave contains numerous speleothems as well as large amounts of breakdown and talus associated with the entrance collapse.

Scorpion Cave (Middle Terrace, Aguijan – Figure 132)

Scorpion Cave is a small flank margin cave located in the north-central region of the Middle Terrace in the Mariana Limestone (QTmu). It extends inland 11 meters with a maximum width of 9 meters and average ceiling height of 2 meters. The northern and western parts of the cave are slightly elevated with bedrock floors, while the main chamber contains an alluvial floor with three large breakdown blocks. Narrow dissolutional features extend up to two meters into

the ceiling in the western part, while a narrow passage extends from the southern edge of the main chamber. The cave was named after a 5 mm long scorpion found during the survey.

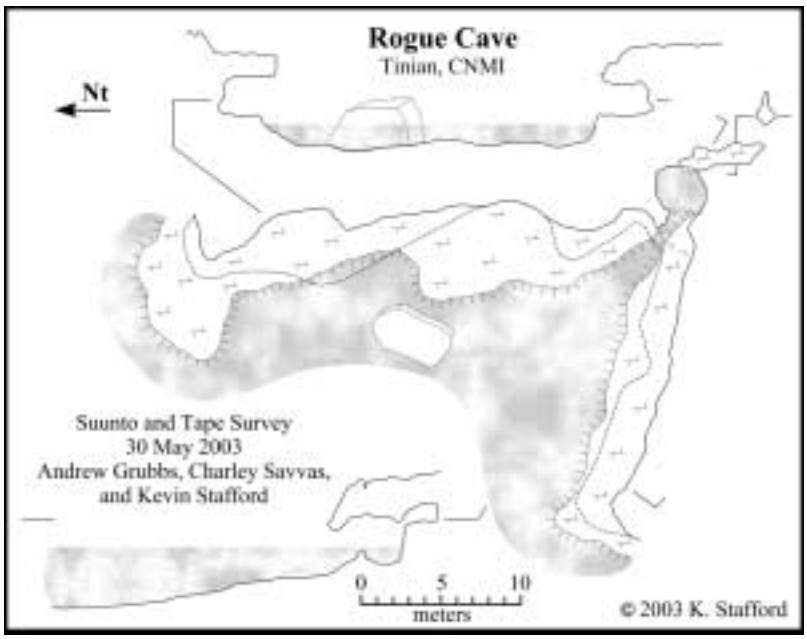

Figure 130: Map of Rogue Cave.

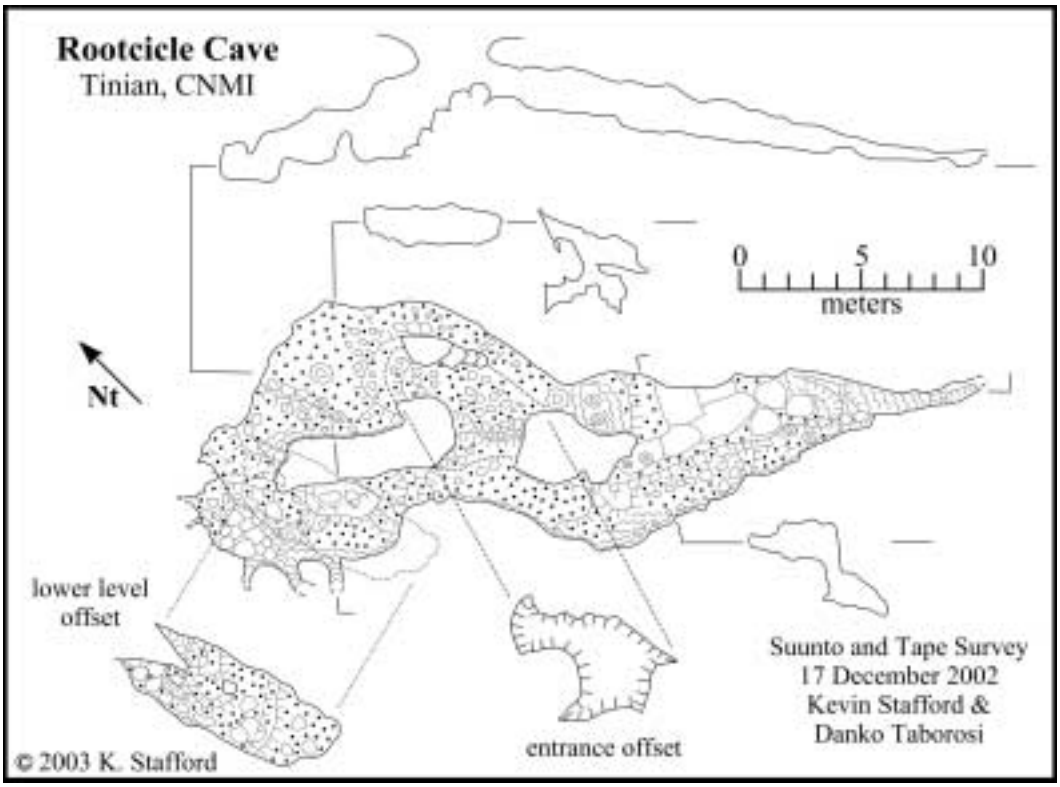

Figure 131: Map of Rootcicle Cave.

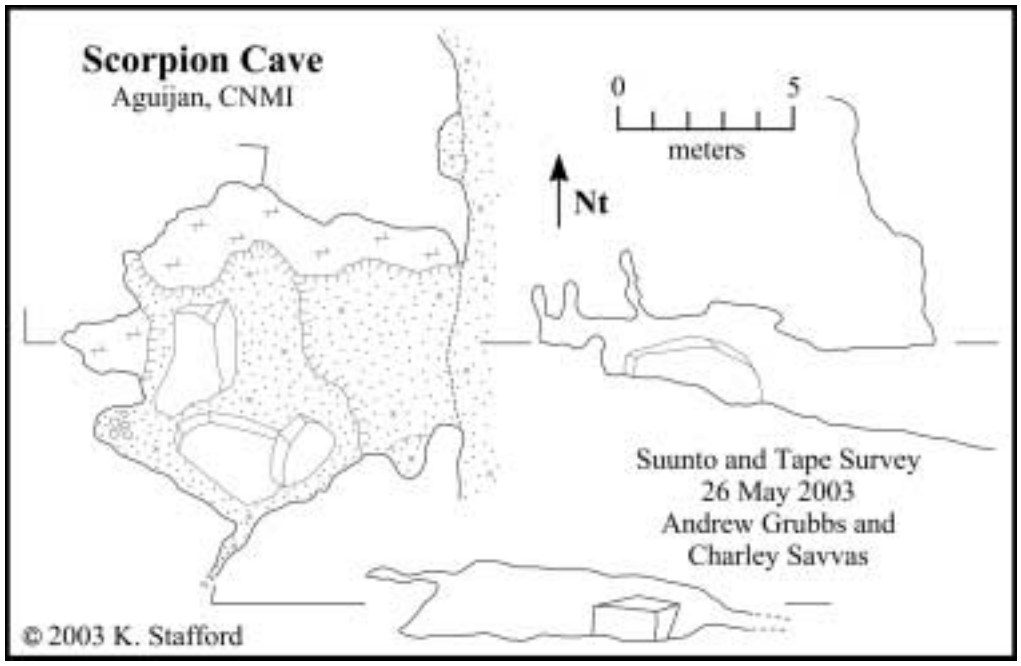

Figure 132: Map of Scorpion Cave.

Screaming Bat Cave (Upper Terrace, Aguijan – Figure 133)

Screaming Bat Cave consists of two flank margin cave remnants in the northwest region of the Upper Terrace in the Mariana Limestone (QTmu). Both cave remnants extend to the west approximately 5 meters, with an average width of 2 meters. The floor in the northern cave remnant is primarily alluvium, while the floor in the southern cave remnant is primarily bedrock. The name of the cave is derived from fruit bats that were feeding on breadfruit trees in the region at the time of survey.

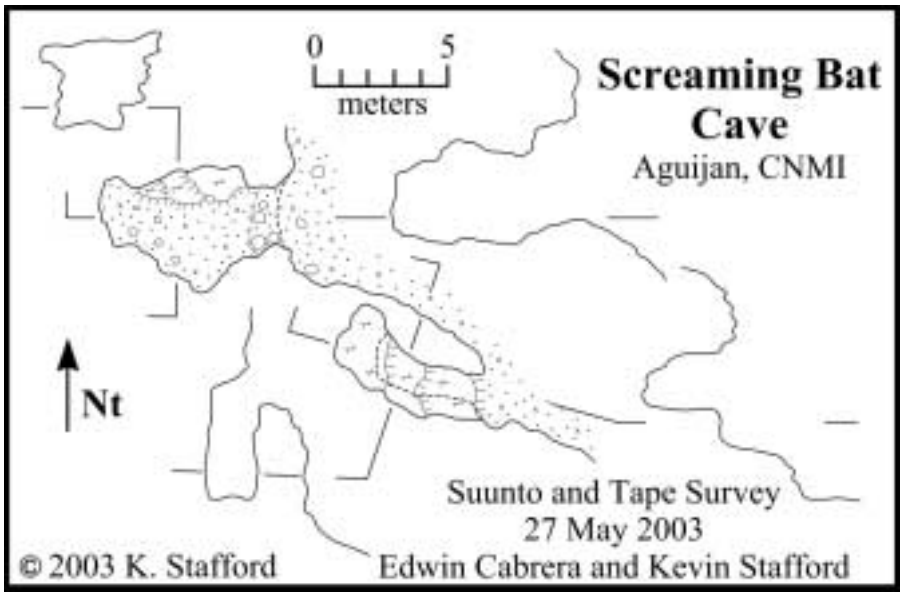

Figure 133: Map of Screaming Bat Cave.

Skip Jack Cave (Southeastern Ridge, Tinian – Figure 134)

Skip Jack Cave is located 1500 meters northwest of Puntan Carolinas on the west coast at sea level. It is a breached, flank margin cave consisting of two primary chambers developed in the Mariana Limestone (QTmu). The entrance chamber is 18 meters wide and extends inland 14 meters, with a height above sea level of 8 meters and depth below sea level of 5 meters. Several small passages extend from this entrance chamber along fractures oriented north/south, while the second chamber extends inland 25 meters from the northeast corner of the entrance chamber. The second chamber ascends above sea level with an average width of 13 meters and height of 5 meters. The second chamber contains several large breakdown blocks covering a bedrock floor with a large mound of flowstone along the western edge of the chamber. This cave is not easily accessed from the surface, but requires a coastal swim from a small inlet located 400 meters north of the feature.

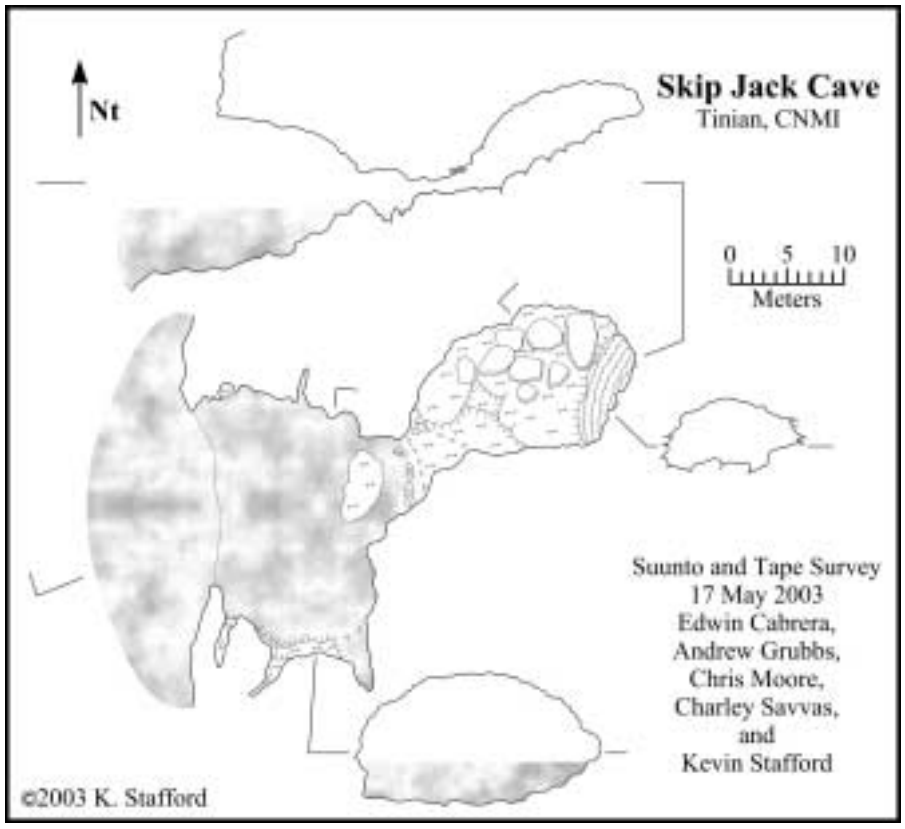

Figure 134: Map of Skip Jack Cave.

Skull Cave Complex (Southeastern Ridge, Tinian – Figure 135)

Skull Cave Complex is located in the southeastern region of the Piña ridge in the Mariana Limestone (QTmu). It consists of three flank margin cave remnants that extend inland to the west. The southern cave in the complex is located 2.5 meters high on the scarp and extends inland 3 meters with a bedrock floor with a ceiling height of 1.5 meters and an entrance width of 8 meters. The middle cave in the complex is 1.5 meters wide at the entrance, then widens to 8 meters and extends inland 5 meters. This middle cave has a large breakdown block, partially concealing the 1-meter tall entrance, which then increasing to 2.5 meters tall with a soil and detritus floor and a small bedrock ledge in the southwest corner. The largest cave is located at the

northern edge of the complex and consists of soil and detritus floored chamber that extends inland 10 meters with an average width of 8 meters. The entrance area consists of three breached entrances; two at ground level and one 2 meters above the ground surface. This cave is named for the skull-like appearance of the three entrances. The entire complex shows minor human modification primarily in the form of leveled floors.

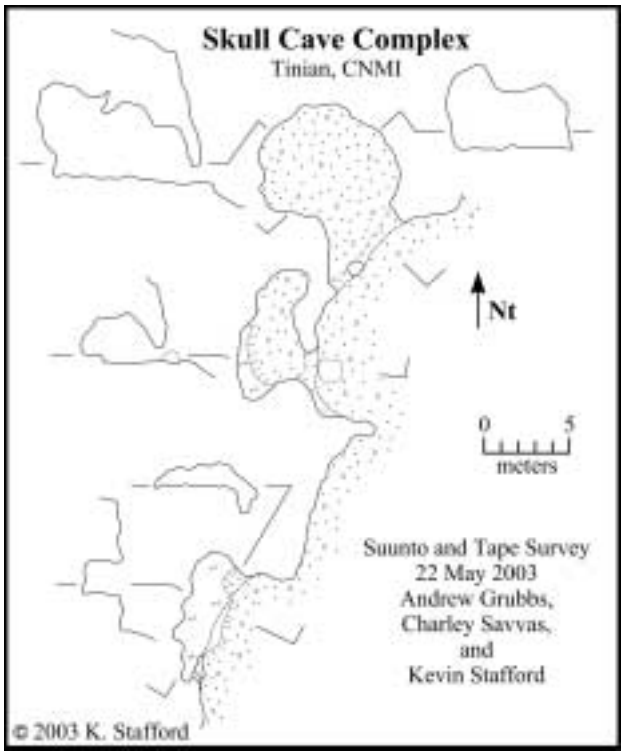

Figure 135: Map of Skull Cave Complex.

Skylight Cave (Southeastern Ridge, Tinian – Figure 136)

Skylight Cave is located in the central region of Suicide Cliffs in the Mariana Limestone (QTmu). The cave is located 5 meters below the top of the cliff with a cliffside entrance that is 9 meters wide and 2 meters tall. The cave extends inland 12 meters with and average width of 4 meters before it is breached on the inland side by ceiling collapse. The cave contains several speleothem columns as well as a large flowstone mound along the eastern side. The inland part contains several large breakdown blocks and a soil and detritus floor, while the regions near the cliff edge contain a bedrock floor. The feature is primarily a linear passage extending inland to the north, with several small solutional pockets that extend east and west of the main cave.

Solitary Cave (Southeastern Ridge, Tinian – Figure 137)

Solitary Cave is located 1500 meters south of Unai Masalok, is the only cave that has been identified on the western scarp of Piña ridge. This small, flank margin cave remnant is developed in the Mariana Limestone (QTmu). The cave has and entrance 2 meters wide, extends inland 2 meters and widens to 3 meters with a ceiling height of 1.5 meters. The cave appears to have been extensively modified, including some enlargement of the cave and the construction of a rock wall 2.5 meters long and 1 meter tall, which conceals the majority of the entrance. This feature was not surveyed at the time of discovery, because it was the only feature located during

the exploration of this region and a survey crew did not return to the region in order to survey this small, solitary feature.

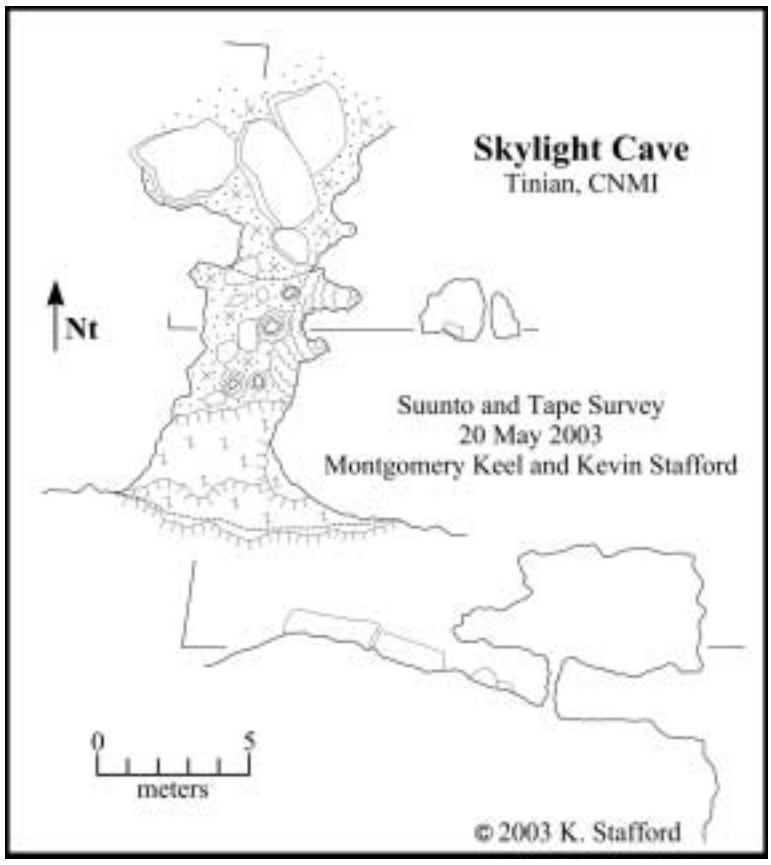

Figure 136: Map of Skylight Cave.

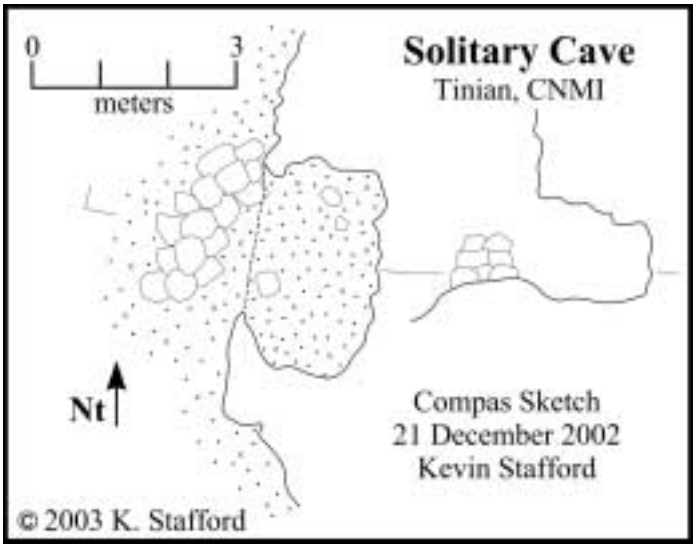

Figure 137: Map of Solitary Cave.

South Mendiola Cave (Central Plateau, Tinian – Figure 138)

South Mendiola Cave is located 1200 meters north of Puntan Diapblo at the southern end of a large cove referred to as Mendiola Cove after the landowner. The cave is a large, flank margin cave developed in the Mariana Limestone (QTmcc) at sea level. The cave has an entrance 40 meters wide and extends inland 48 meters with an average ceiling height of 8 meters. In the central part of the cave, there is a 10-meter diameter skylight entrance exists, while along the northern edge of the chamber a second entrance connects to the ocean below sea level. The cave is bedrock floored with numerous large and medium size breakdown blocks covering large areas of the floor.

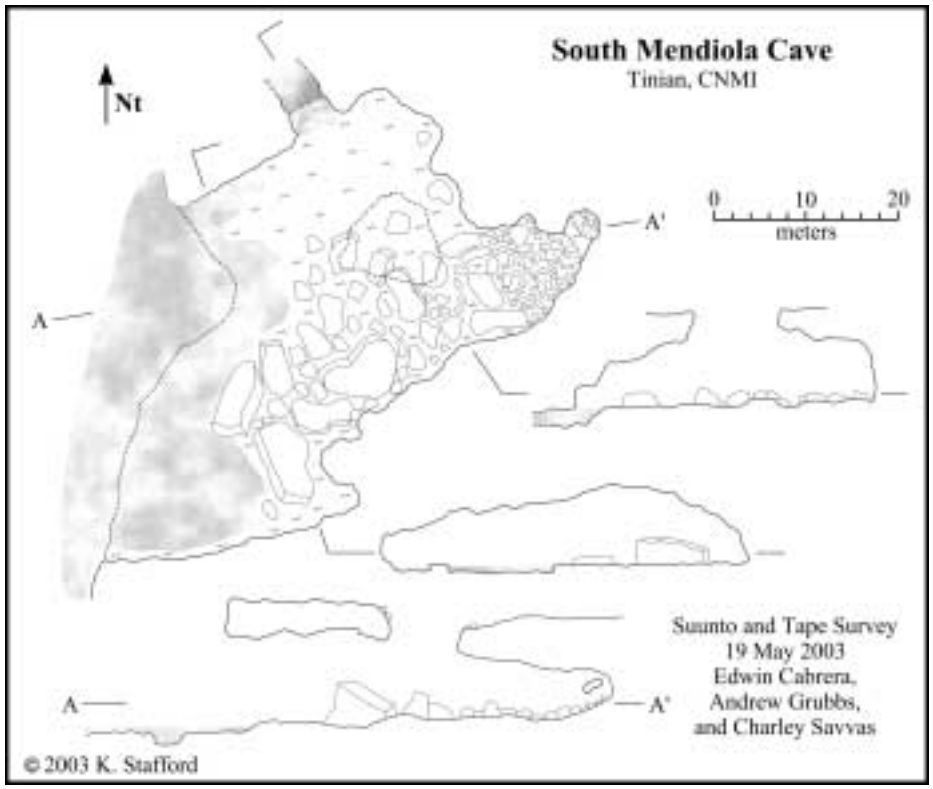

Figure 138: Map of South Mendiola Cave.

South Unai Dangkolo (Median Valley, Tinian – Figure 139)

South Unai Dangkolo is a large pocket beach developed in the Mariana Limestone (QTmca) just south of Unai Dangkolo and developed in the Mariana Limestone (QTmca). The feature is 20 meters by 40 meters and contains some small remnant cave chambers and speleothems, which indicate that this was originally a large flank margin chamber that has been breached by coastal processes including the removal of the majority of the roof. A small dissolutionally enhanced fracture connects this feature to Unai Dangkolo to the north, while a less developed extension of this same fracture extends to the south from the feature in the direction of Dripping Tree Fracture Cave. Although not surveyed during fieldwork, Unai Dangkolo, to the north, appears to have a similar flank margin cave origin, but is much larger and has been more extensively eroded by coastal processes.

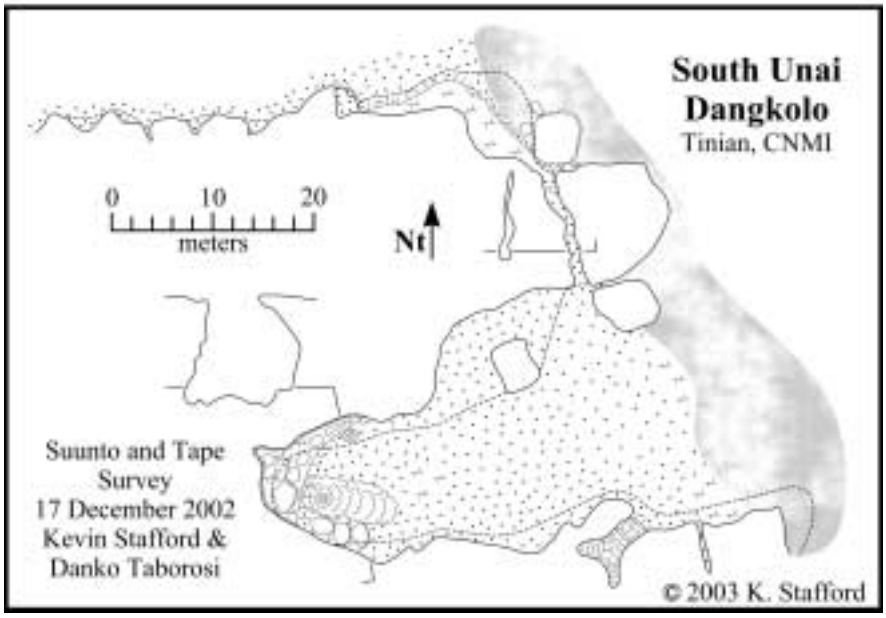

Figure 139: Map of South Unai Dangkolo.

Spider Cave (Middle Terrace, Aguijan – Figure 140)

Spider Cave is a small, breached flank margin cave located in north-central region of the Middle Terrace in the Mariana Limestone (QTmu). The cave has a maximum width of 8 meters exposed along the scarp entrance and extends inland up to 5 meters with a height ranging from 1 to 2 meters. The floor is composed of alluvium and is elevated in the central part of the opening and in the western part of the cave. The name is derived from several large spiders (~8 centimeters in diameter) that were present in the cave at the time of survey.

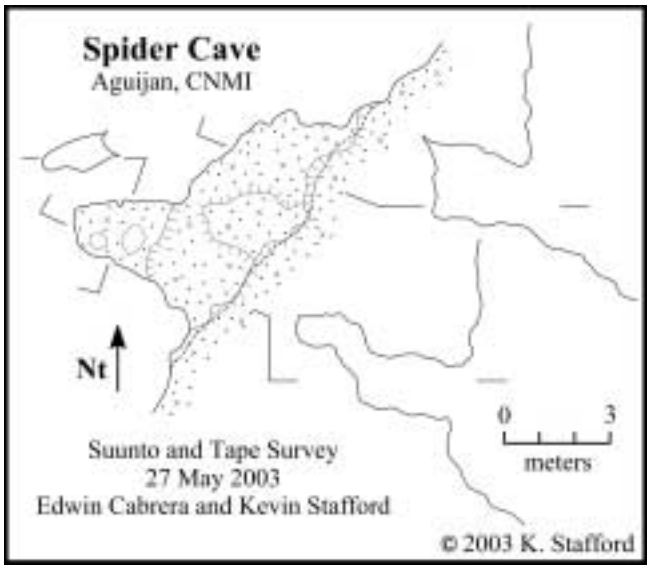

Figure 140: Map of Spider Cave.

Swarming Termites Cave (Middle Terrace, Aguijan – Figure 141)

Swarming Termites Cave is a breached, flank margin cave in the eastern region of the Middle Terrace in the Mariana Limestone (QTmu). The cave consists of three main parts, which extend from a 9-meter wide entrance. The northeast portion is a small chamber extending 3 meters inland, the north-central portion is a small passage extending 8 meters inland, and the southern portion is a small passage extending 13 meters inland. All three parts about 3 meters high at the entrance, reducing down to about 1-meter inland. The floor is composed of alluvium with scattered breakdown blocks. The cave appears to be the remnants of a larger flank margin cave, representing the "fingers" that would have extended off of the main chamber of the original cave. The cave is named after the large quantities of termites that were swarming in the region in the early evening.

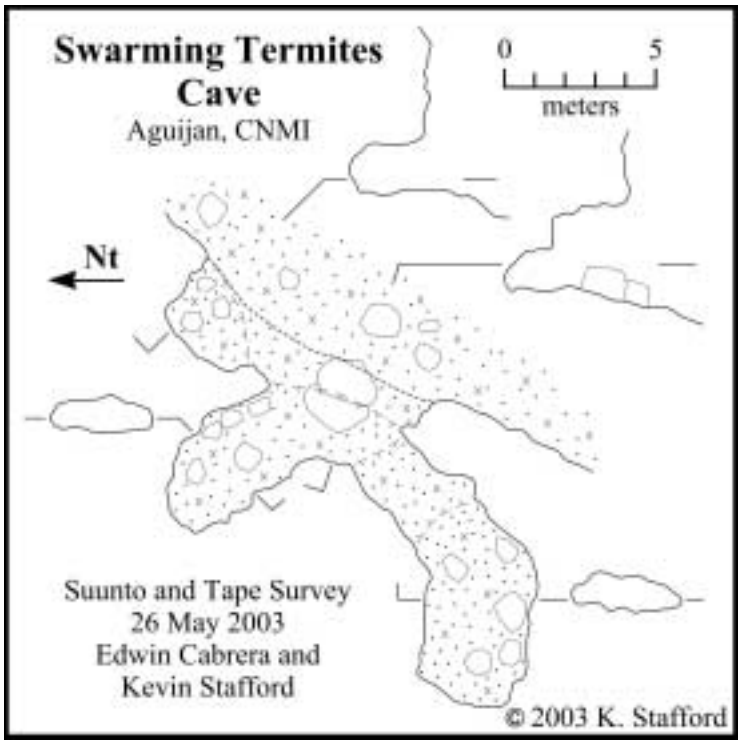

Figure 141: Map of Swarming Termites Cave.

Swiftlet Cave (Lower Terrace, Aguijan – Figure 142)

Swiftlet Cave is a large, breached flank margin cave on the northwest side of the Lower Terrace approximately 15 meters above sea level. It is developed in the Mariana Limestone (QTmu) and consists of a large chamber 70 meters wide and 30 meters deep that is approximately 18 meters tall in the roofed inland half of the main chamber. The ceiling of the main chamber contains extensive spelean and phototropic speleothems, while the floor is composed of alluvium and large breakdown blocks with elevated bedrock levels on the seaward (northern) side. In the western part of the cave, a passage 8 meters wide and 6 meters tall extends for 20 meters and contains extensive speleothem deposits in the inland portions. In the eastern portion of the cave a steeply dipping, fissure-like passage extends for approximately 50 meters with extensive speleothem deposits throughout and a large colony of Mariana Swiftlets occupying the elevated areas. This eastern extension connects to the main chamber through three small passages, which are reached by short climbs.

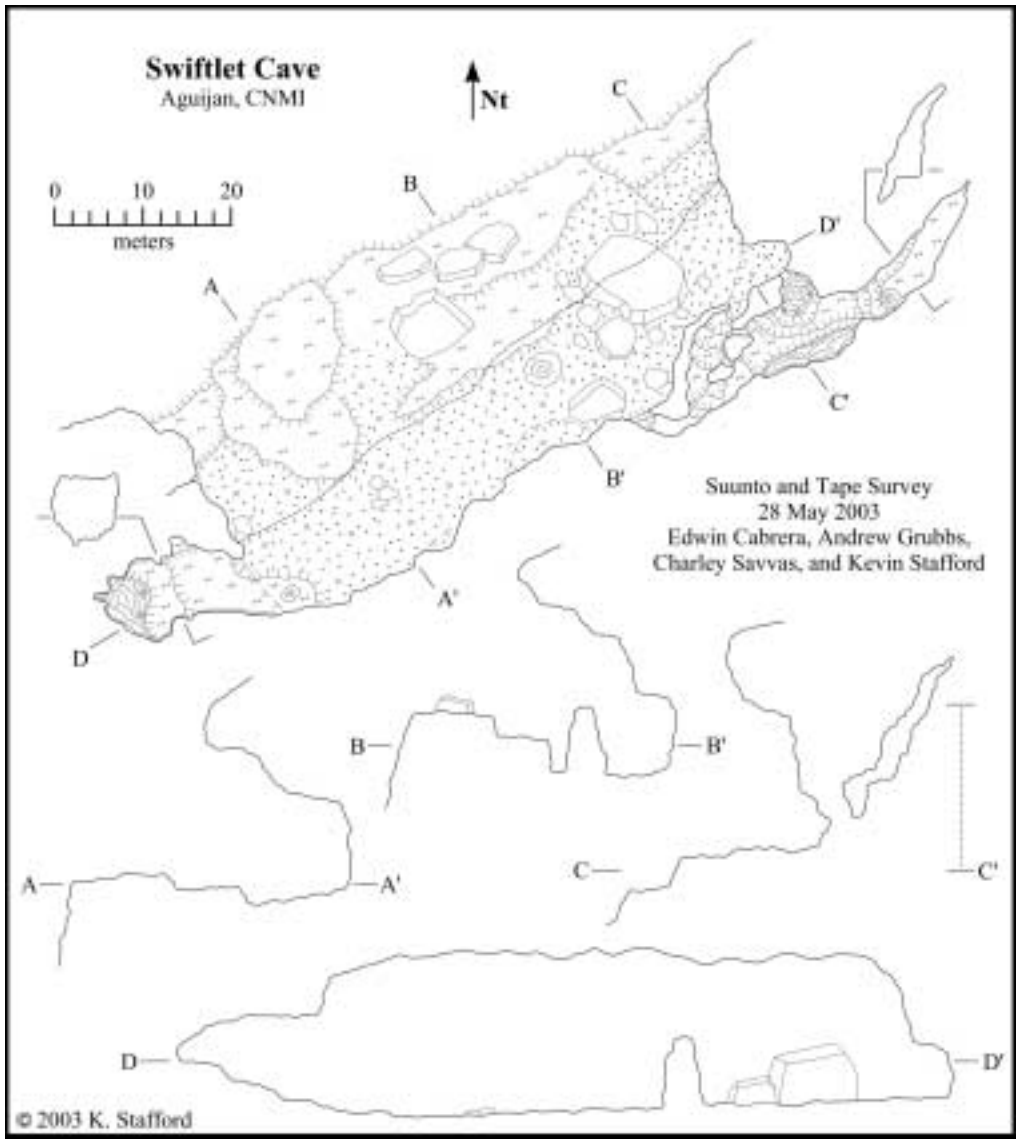

Figure 142: Map of Swiftlet Cave.

Swimming Hole Cave Complex (Median Valley, Tinian – Figure 143)

Swimming Hole Cave Complex is located 700 meters south of the historic Leprosarium site on the west coast. It consists of three flank margin cave remnants developed in the Mariana Limestone (QTmu). The northern cave in the complex forms a looped passage with two entrances; the larger, northern entrance is 10 meters wide and the smaller, southern entrance is 1.5 meters wide. The loop passage extends inland 8 meters with an average width of 2.5 meters and height of 1.5 meters. The middle cave in the complex also contains two entrances forming a looped passage, with the two entrances averaging 2 meters wide and extending inland 9 meters with and average width of 3 meters and height of 1.5 meters. The southwestern cave has a single 2-meter wide entrance and extends inland 12 meters, where it widens to 7 meters with a ceiling height of 1.5 meters. The caves in this complex have soil and detritus floors with some breakdown blocks located near the entrances. All three caves show evidence of human modification, primarily the leveling of floors.

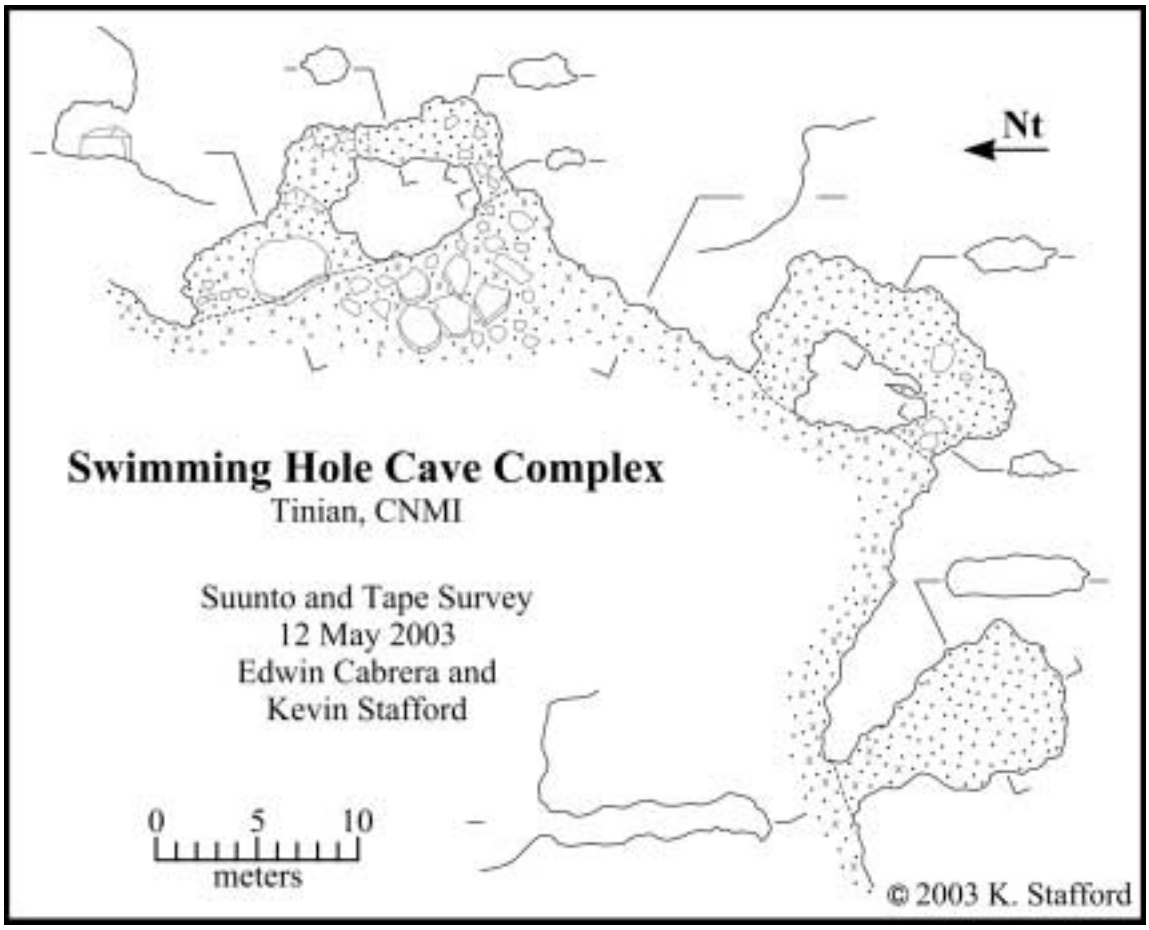

Figure 143: Map of Swimming Hole Cave Complex.

Toppled Column Cave (Middle Terrace, Aguijan – Figure 144)

Toppled Column Cave is formed along a fracture oriented at 5° in the southwest region of the Middle Terrace. It is developed in the Mariana Limestone (QTmu) and extends inland 23 meters with an average width of 2.5 meters. The feature is 8 meters tall in the entrance and decreases to 5 meters inland. The floor is composed of alluvium and large breakdown blocks in the entrance area and composed of bedrock in the inland part where the floor is elevated. The feature is similar to fracture-controlled, fresh-water discharge features seen at sea level on Tinian and is interpreted as a paleo-discharge feature. The cave is named for the large, broken stalagmite that is wedged in the passage near the entrance.

Tridactid Cave Complex (Middle Terrace, Aguijan – Figure 145)

Tridactid Cave Complex is located in the eastern region of the Middle Terrace in the Mariana Limestone (QTmu). It is composed of a series of flank margin caves that have been breached by scarp retreat. The features located in the southern part of the complex are shallow and extend inland less than 5 meters with and average height of 3 to 4 meters. In the northern part there is a larger flank margin remnant, which extends inland 35 meters and has bedrock columns dividing the entrance area. This larger remnant averages 1 to 2 meters tall and contains large amounts of breakdown in the middle of the chamber. The larger chamber is connected by a 2-meter deep ledge to a second passage that extends inland 20 meters with a ceiling height of 10

meters created by a floor drop of 8 meters. In the central region there is a split-level flank margin remnant, with a lower level that extends inland 8 meters and an upper level that extends inland 20 meters. The upper level contains two pits, which connected to small chambers that appear to have been partially excavated. In these excavated areas there are several well-worn, tridactid clam shells that appear to have been used for digging the poorly lithified bedrock walls and floor, thus giving the cave complex its name. Based on the proximity of the caves and their corresponding driplines, it is likely that most of these remnant flank margin caves where connected as one single cave in the past and have been separated by scarp retreat.

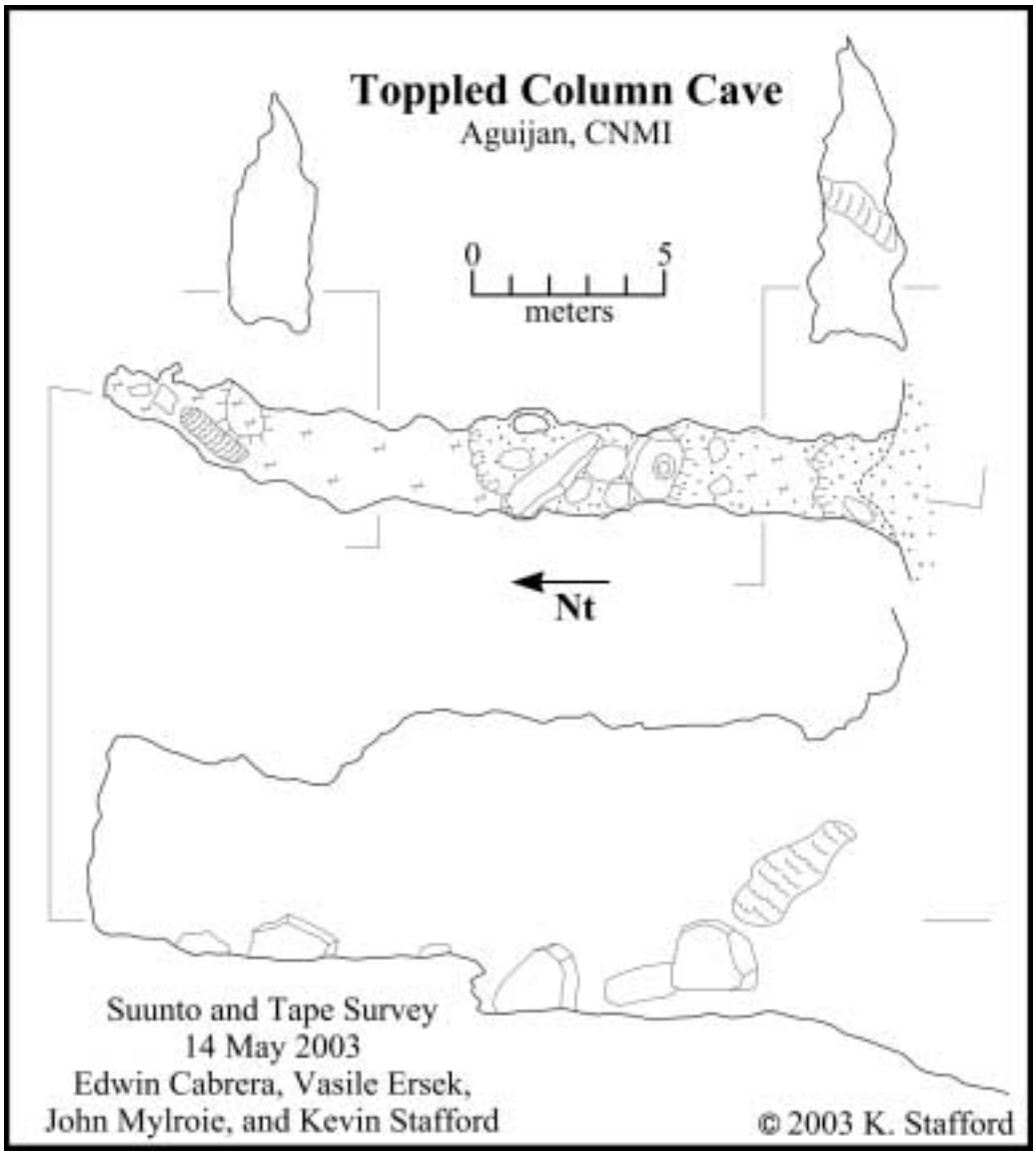

Figure 144: Map of Toppled Column Cave.

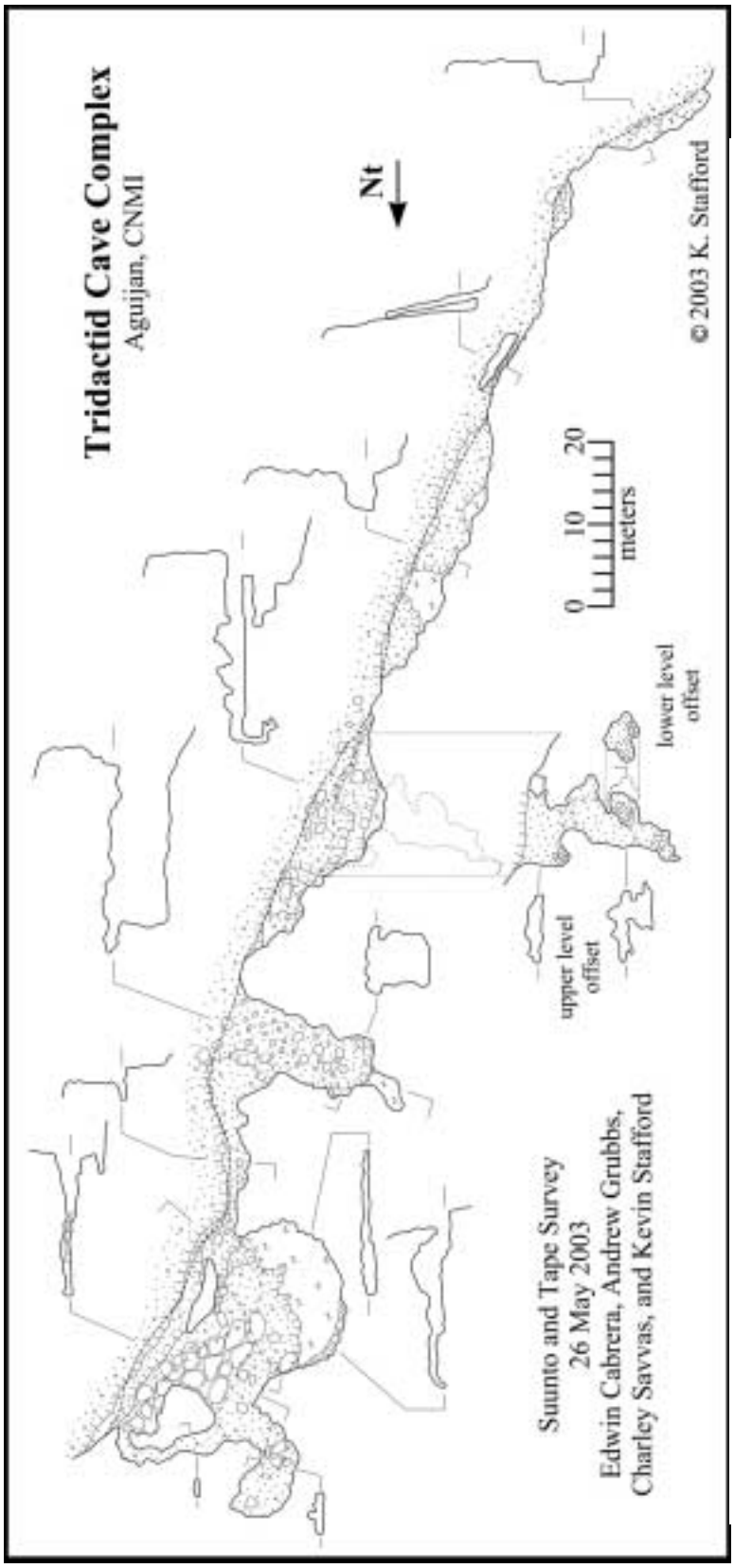

Figure 145: Map of Tridactid Cave Complex.

Twin Ascent Caves (Southeastern Ridge, Tinian – Figure 146)

These two caves are located in the central part of Suicide Cliffs, approximately 25 meters above the base of the cliff. They are the remnants of a breached flank margin cave developed in the Tagpochau Limestone (Tt) and are connected by a small, roofed ledge approximately 0.5 meters tall, indicating that the two features were joined as one cave prior to cliff retreat. The larger of the features is 11 meters by 15 meters with a maximum ceiling height of 9 meters, while the smaller feature is 8 meters by 10 meters with a similar ceiling height. In both caves, speleothems are present and in the larger feature minor excavation of the floor indicates that the feature was modified for use during WWII.

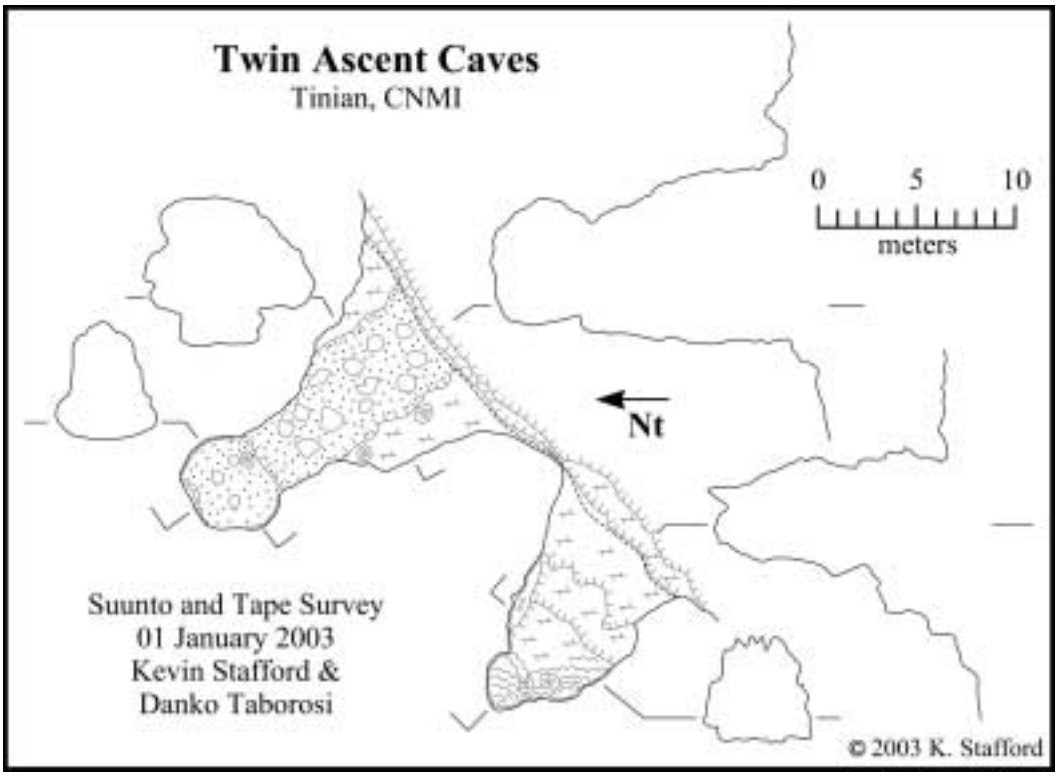

Figure 146: Map of Twin Ascent Caves.

Unai Chiget (Northern Lowland, Tinian – Figure 147)

Unai Chiget is located at the boundary between the Central Plateau and the Northern Lowland on the east coast of Tinian where the Northern Lowland has been down-dropped relative to the rest of the island along the Chiget fault, which trends 250^{o} in the Mariana Limestone (QTmca). The feature is a small embayment that has an average water depth between 0.5 and 1.5 meters and extends inland for 160 meters along the fault scarp, while cliff retreat and dissolution have widened the region to approximately 30 meters. At the seaward end of the feature, a series of large algal mounds are formed at the coastline, protecting the inland parts of the feature from more extensive wave erosion. The southern wall of the feature extends further inland and has a maximum height of 35 meters near the coastline, while the northern wall averages 4 meters and diminishes in height inland. Along the cliff walls, at sea level and up to 2 meters above sea level, is a well-developed, 1 to 2 meter deep, bioerosional notch. This feature shows extensive dissolution along the fault line and subaqueous grooves indicate that this feature may discharge fresh water, although no definitive evidence was seen.

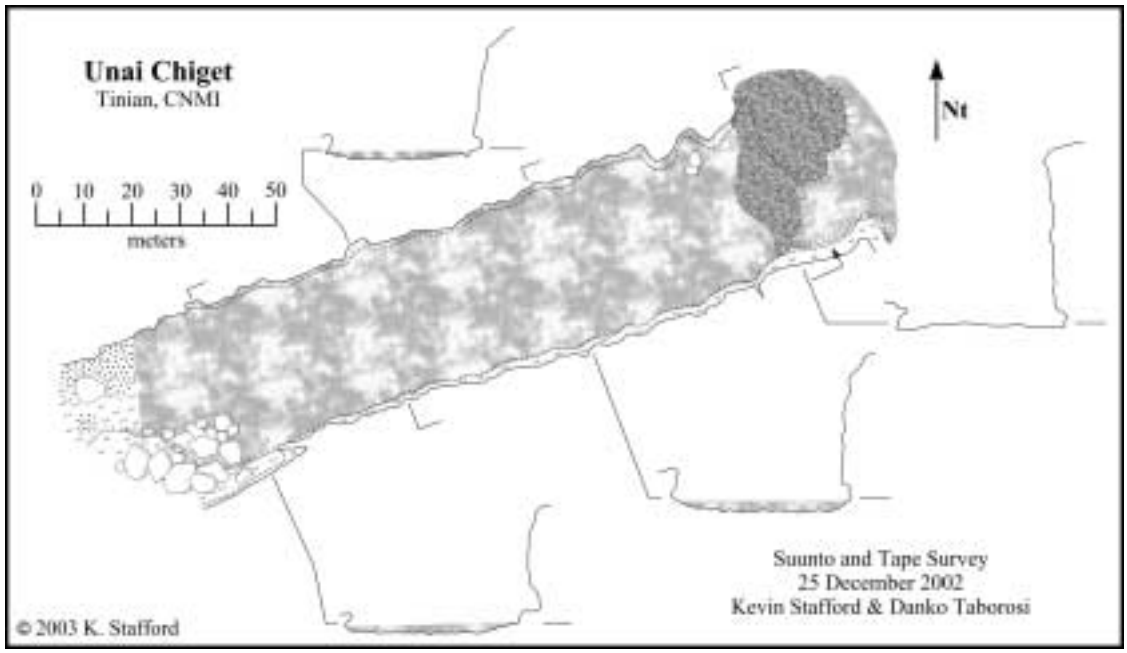

Figure 147: Map of Unai Chiget.

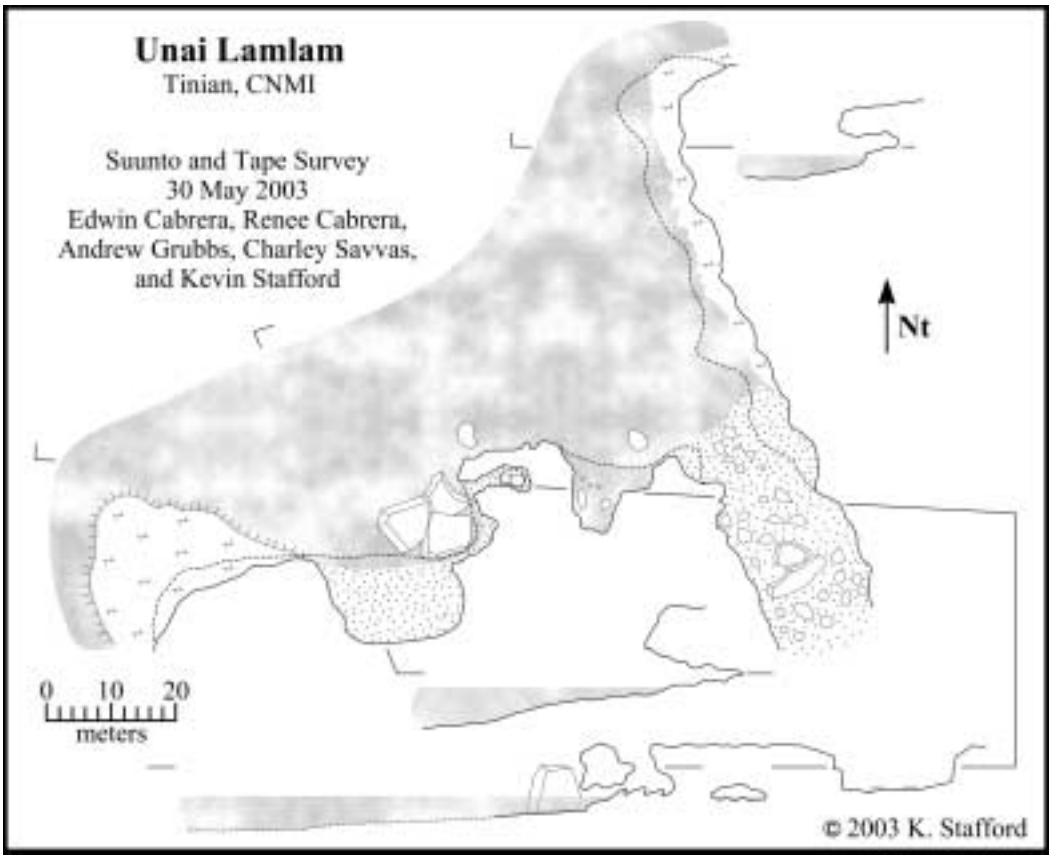

Figure 148: Map of Unai Lamlam.

Unai Lamlam (Northern Lowland, Tinian – Figure 148)

Unai Lamlam is a cove 110-meter wide, extending inland 90 meters in the Mariana Limestone (QTmcc) on the northwest coast. The main part of the cove is along the eastern edge of the feature and extends inland the greatest distance, where it narrows to 18 meters. The western portion of the cove contains two flank margin cave remnants that extend inland 15 meters from their ceiling drip lines, with average heights of 1.5 meters. The more protected interior regions of the cove contain carbonate sand beaches, while the more seaward regions have bedrock floors. In several areas, large breakdown blocks are presents, which appear to be remnants of collapsed ceilings.

Unai Masalok (Median Valley, Tinian – Figure 149)

Unai Masalok is a series of pocket beaches located on the east coast of the island and developed in the Mariana Limestone (QTmca). This series of four beaches is approximately 150 meters wide and extends inland for up to 50 meters. The individual beaches have several small remnant cave passages that extend inland from the cliff walls, remnant bedrock pillars, and speleothems. The overall morphology of the beaches and the presence of speleothems indicate that Unai Masalok was a series of flank margin caves that were breached by coastal processes and cliff retreat. Based on the available evidence, these features would have consisted of large flank margin cave chambers that were possibly connected where each of the individual pocket beaches are separated along the coastline. Throughout the feature there are numerous joints, which appear to be associated with cliff retreat. No evidence of offset could be discerned along these joints, but they appeared to trend roughly parallel to the coastline with variations in actual orientations throughout.

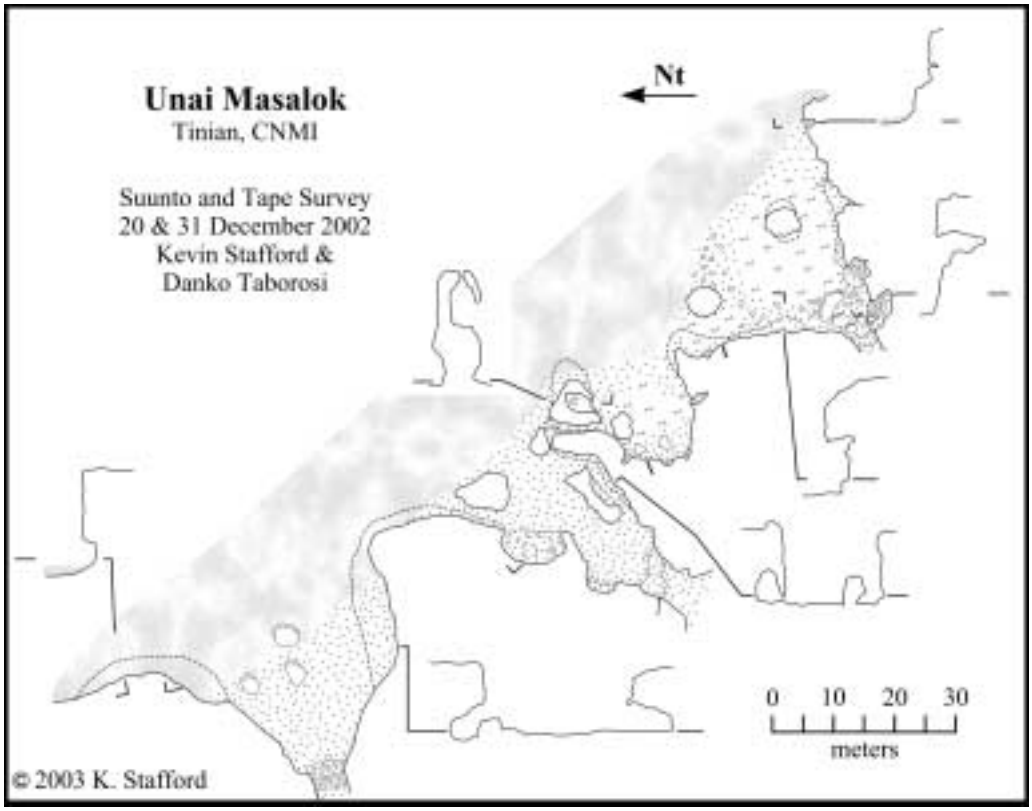

Figure 149: Map of Unai Masalok.

Water Cave (Median Valley, Tinian – Figure 150)

The Water Cave is located near Plunder Cave, approximately 2000 meters south of Taga Beach and 300 meters inland from the west coast. It is developed at the boundary between the Median Valley and the Southeastern Ridge provinces along a northeast/southwest trending fault that dips at approximately 35° to the southeast. This dissolutionally enlarged fracture cave is formed in the Mariana Limestone (QTmu) and is approximately 35 meters by 14 meters, descending to a depth of 13 meters where there is a 1-meter deep, linear pool of fresh water is encountered along the southern wall of the cave. The cave has extensive secondary deposits along in the central and northeastern parts, while the western parts are composed of much collapse material.

This feature shows evidence of extensive use by the Japanese military during World War II, probably because of the available water source in the bottom of the cave. There are anecdotal reports that the cave was sealed during the war on Tinian, which may explain the extensive breakdown and rubble in the western parts of the cave. However, the two entrances to the cave are small passages located in solid bedrock indicating that there was another entrance to this cave that is still blocked, if the reports are true.

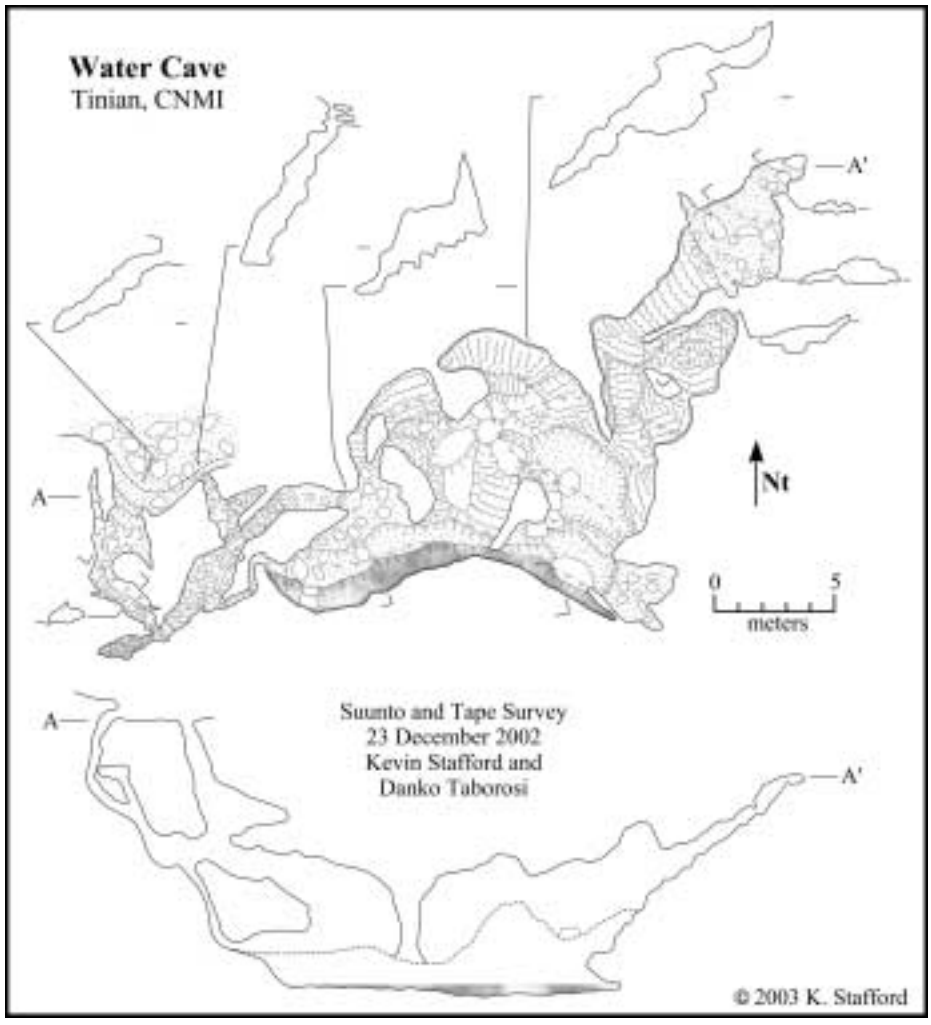

Figure 150: Map of Water Cave.

Waypoint Cave (Middle Terrace, Aguijan – Figure 151)

Waypoint Cave is a small, flank margin cave located in the eastern region of the Middle Terrace in the Mariana Limestone (QTmu). It consists of a small chamber, 5 meters wide and 1.5 meters tall, that has two scarp entrances on the east side and two small passages extending from the west side, with the entrances and passages roughly aligned. The floor consists of alluvium with minor breakdown blocks in the main chamber and a bedrock floor in the northern entrance passage.

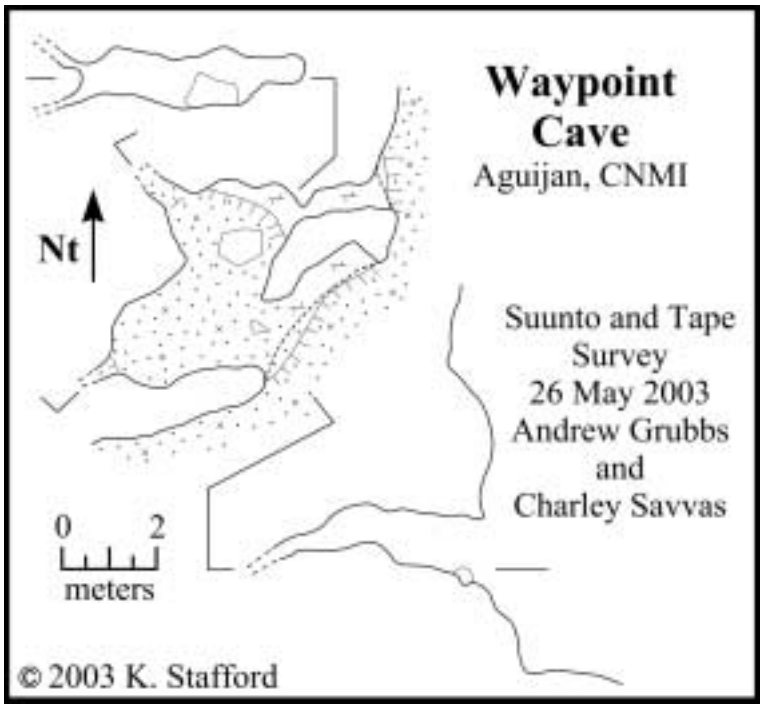

Figure 151: Map of Waypoint Cave.

West Lasu Depression Cave (Central Plateau, Tinian – Figure 152)

West Lasu Depression Cave is a closed depression recharge, located 1500 meters northwest of the peak of Mount Lasu in the Mariana Limestone (QTmu). The feature is approximately 25 meters in diameter and 4 meters deep, with the northern 5 meters of the feature covered by a 3-meter tall ceiling. The feature appears to be a significant recharge point with water being concentrated into the depression from the southwest edge. Lack of sediment coating the walls indicate that water does not pond here and enters the subsurface as diffuse flow, but that it acts as a fast flow route. This feature represents the most significant recharge feature that has be located northwest of Mount Lasu.

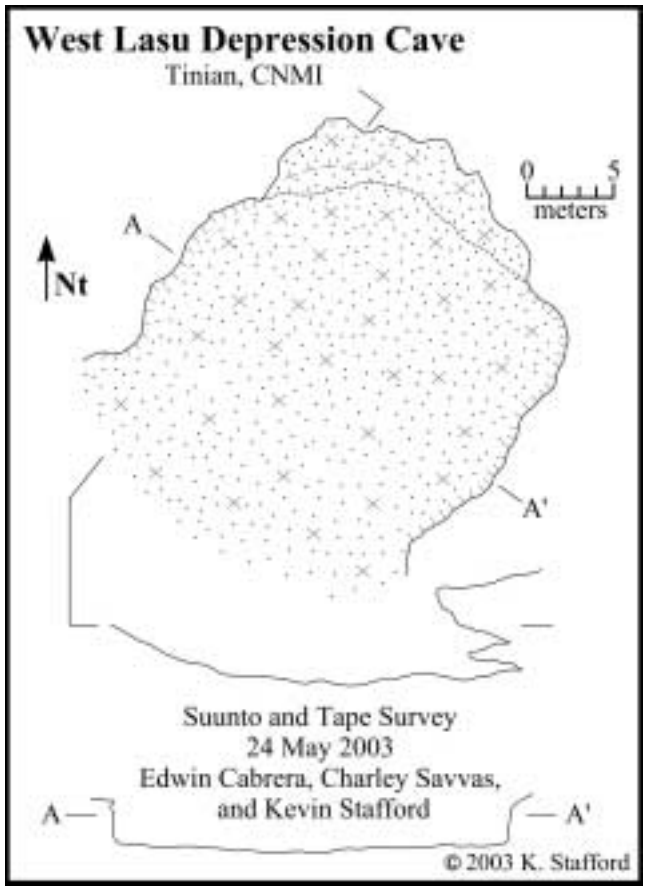

Figure 152: Map of West Lasu Depression.

West Suicide Cliff Caves (Southeastern Ridge, Tinian – Figure 153)

West Suicide Cliff Caves, developed in the Mariana Limestone (QTmu), are located at the west end of Suicide Cliffs near Carolina's Limestone Forest. This series of caves is located near the base of the cliff and represent a series of features breached by cliff retreat. The two caves on the southeastern portion of the series are approximately 18 meters by 6 meters each with ceiling heights ranging from 3 to 6 meters. They exhibit few speleothems and have extensive alluvium deposits on their floors. The largest, center cave, in this series is approximately 10 meters by 14 meters with a ceiling height of 6 meters. Associated with the center cave are two small cave remnants above the main chamber and a third small cave beneath it. West of the central cave are three small caves that do not extend inland a significant distance and a fourth larger remnant cave that is approximately 70 meters to the northwest of the central cave. The remnant cave that is the farthest to the west is approximately 8 meters by 10 meters with little ceiling remaining because of cliff retreat.

It is not possible to tell if these features were originally connected prior to cliff retreat, but it is thought that at least some of the features were joined in the past, because they are developed along a consistent horizon and are closely spaced, especially in the central and southeastern portions of this series.

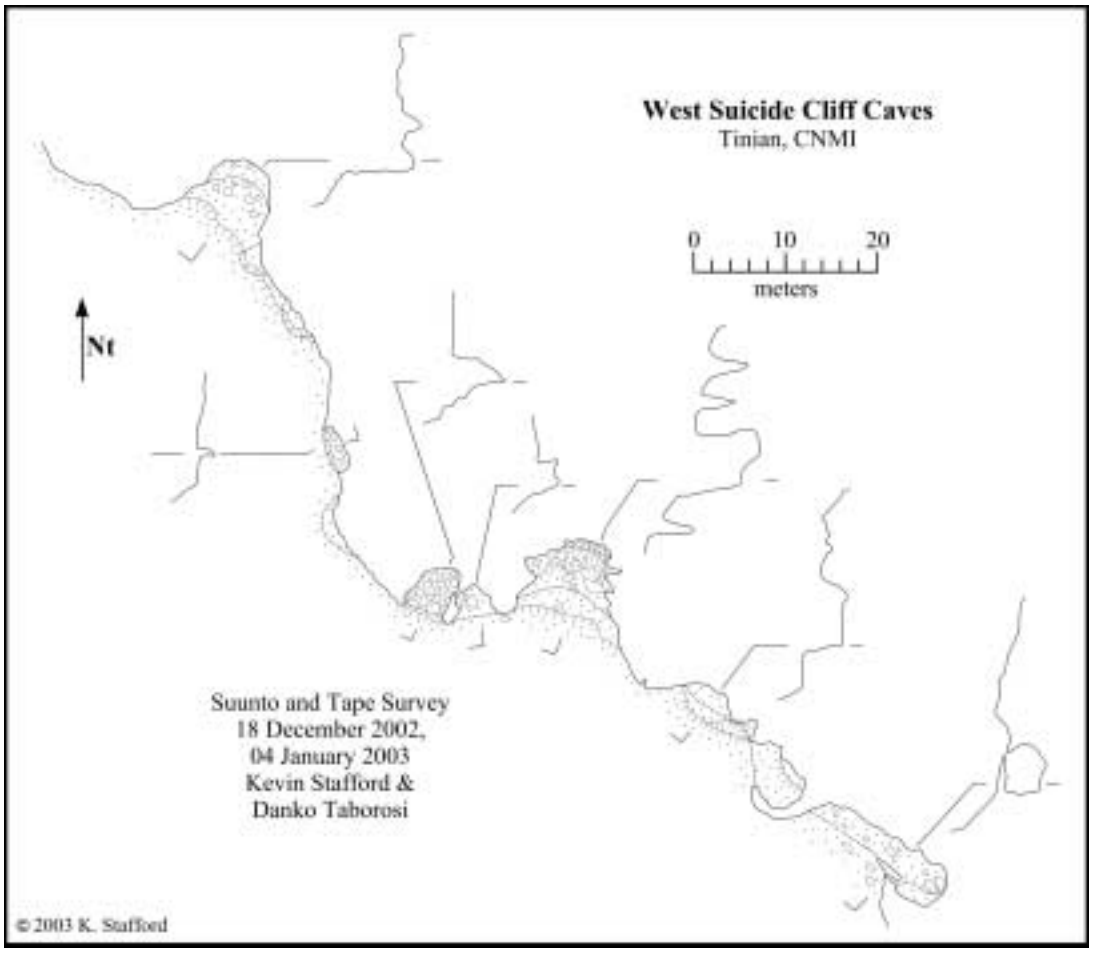

Figure 153: Map of West Suicide Cliff Cave Complex.

APPENDIX C

ORIENATATION DATA

Table 3: Fissure cave primary orientations grouped by physiographic province.

Central Plateau	Median Vally	North-Central Highland	Northern Lowland	Southeastern Ridge
Orientation	Orientation	Orientation	Orientation	Orientation
314	19		323	247
258	261			239
60	293			286
74	200			309
219	234			130
				277
				74

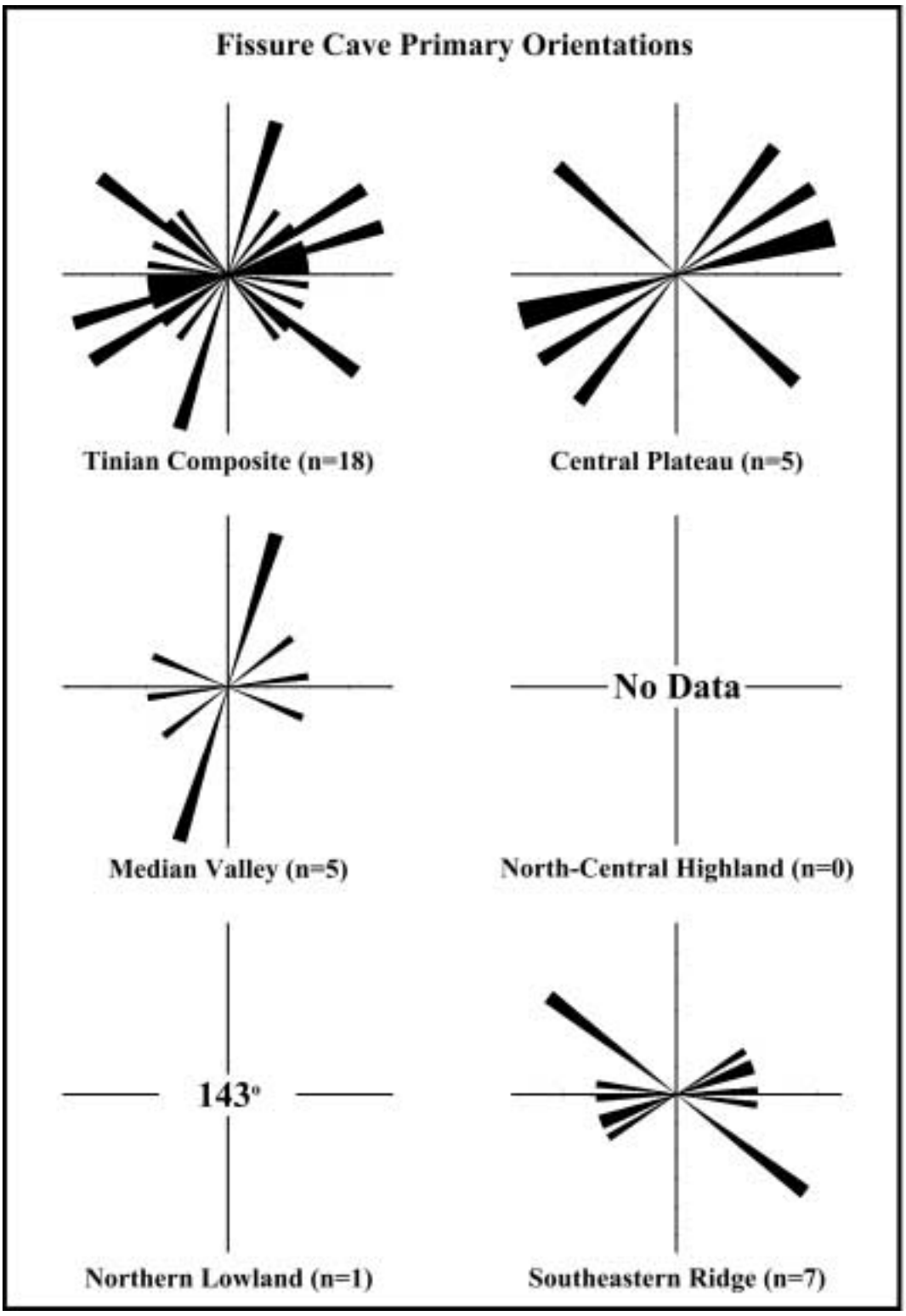

Figure 154: Rose diagrams of fissure cave primary orientations grouped by physiographic province.

Table 4: Fissure cave segment orientations with segment length grouped by physiographic province.

Central Plateau		Median Valley		North-Central Highland		Northern Lowland		Southeastern Ridge	
Length Orientation	Segment Length (m)	Length Orientation	Segment Length (m)	Length Orientation	Segment Length (m)	Length Orientation	Segment Length (m)	Length Orientation	Segment Length (m)
298	5.1	19	9.6			344	6.9	61	29.0
192	6.6	212	8.1			111	6.9	76	20.2
359	1.5	61	5.9					66	90.5
320	9.0	61	9.6					57	17.3
298	2.6	34	11.9					82	15.5
265	2.4	24	12.6					61	57.4
343	3.8	358	8.5					89	41.9
232	6.7	40	4.4					55	29.6
260	19.6	24	25.9					80	12.0
241	4.8	352	8.9					271	9.2
243	16.6	244	7.8					239	13.2
292	18.0	4	20.7					311	2.9
63	3.4	355	5.6					270	3.4
97	14.3	39	7.4					228	2.9
223	6.2	71	5.9					274	3.9
		49	7.4					231	12.6
		112	8.1					222	11.8
		14	7.4					23	3.7
		177	4.4					14	3.7
		230	2.6					236	3.2
		217	4.4					213	13.9
		228	4.8					77	4.1
		211	8.9					107	8.8
		235	3.7					68	10.5
		359	6.7					304	17.8
		359	10.4					308	23.0
		217	4.4					241	4.0
		247	3.0					321	19.2
		2	4.6					57	4.9
		340	2.2					113	5.8
		238	3.8					119	3.8
		147	2.7					83	25.3
		272	5.7					165	4.5
		251	5.2					62	45.8
		274	6.8					74	20.9
		140	13.5					38	12.8
		200	43.5					40	9.4
		72	2.5					48	16.2
		83	5.6					77	14.3
		82	6.0					53	7.1
		312	3.1					50	7.4

Table 4 (continued): Fissure cave segment orientations with segment length grouped by physiographic province.

Central Plateau		Median Valley		North-Central Highland		Northern Lowland		Southeastern Ridge	
Length Orientation	Segment Length (m)	Length Orientation	Segment Length (m)	Length Orientation	Segment Length (m)	Length Orientation	Segment Length (m)	Length Orientation	Segment Length (m)
		282	3.0					64	6.8
		354	5.0					88	16.2
		24	3.3					123	4.1
		339	5.2					159	5.7
		334	3.4					112	15.1
		56	2.0					82	21.9
		270	3.6					68	7.6
		14	2.7					154	3.5
		213	2.3					160	3.3
		318	5.8					57	5.5
		257	2.0					59	7.4
		44	11.6					79	10.1
		332	5.0					105	11.0
		66	5.7					77	20.9
		32	13.4					77	3.8
		350	9.2					112	5.8
		328	13.5					67	17.5
		119	5.5					97	4.1
		96	8.4					66	5.4
		70	6.7					102	9.0
		246	18.9						
		309	3.3						
		179	1.1						
		246	0.3						
		249	2.0						
		222	7.5						
		348	0.8						
		253	2.7						

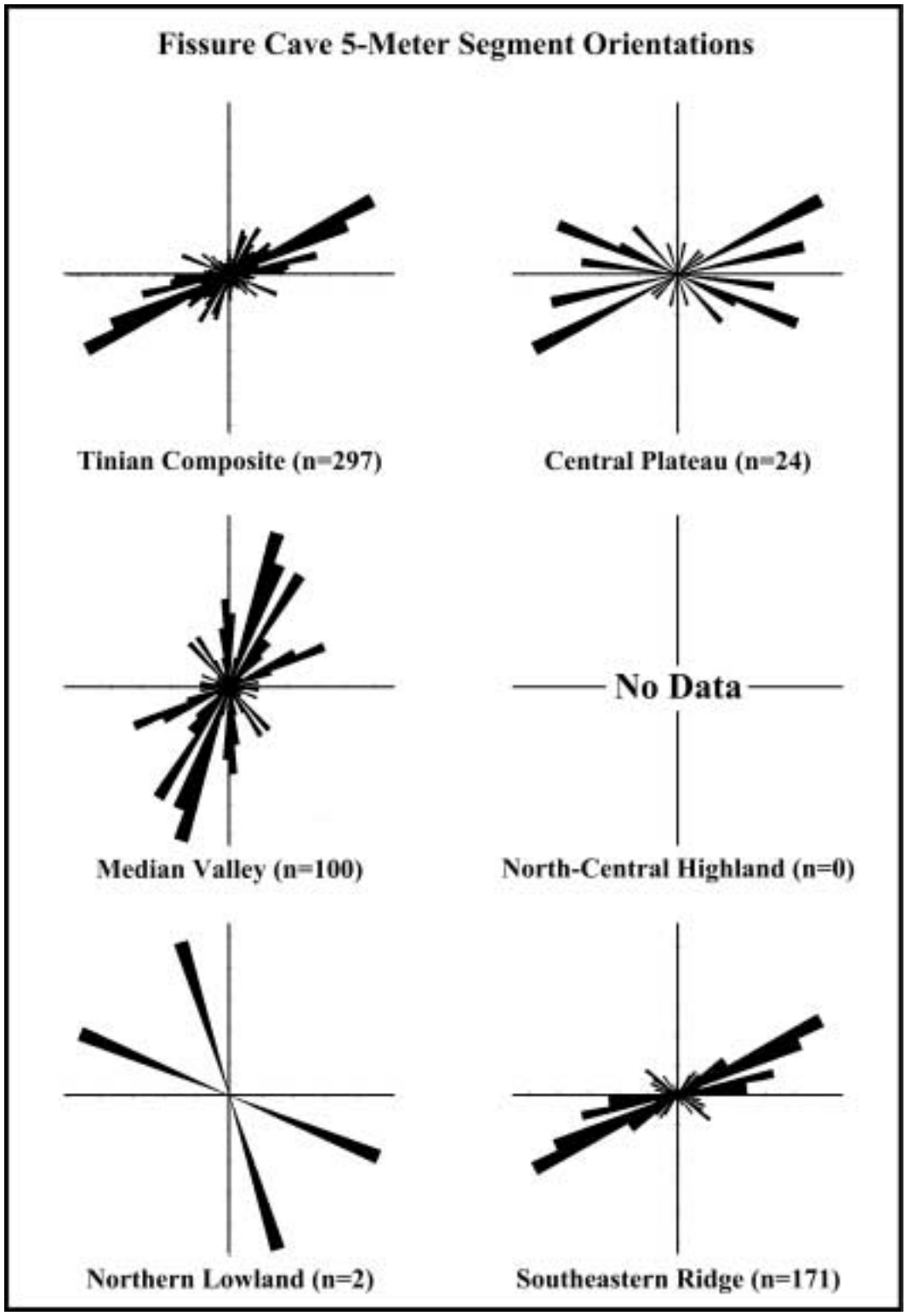

Figure 155: Rose diagrams of fissure cave, five-meter segment orientations grouped by physiographic province.

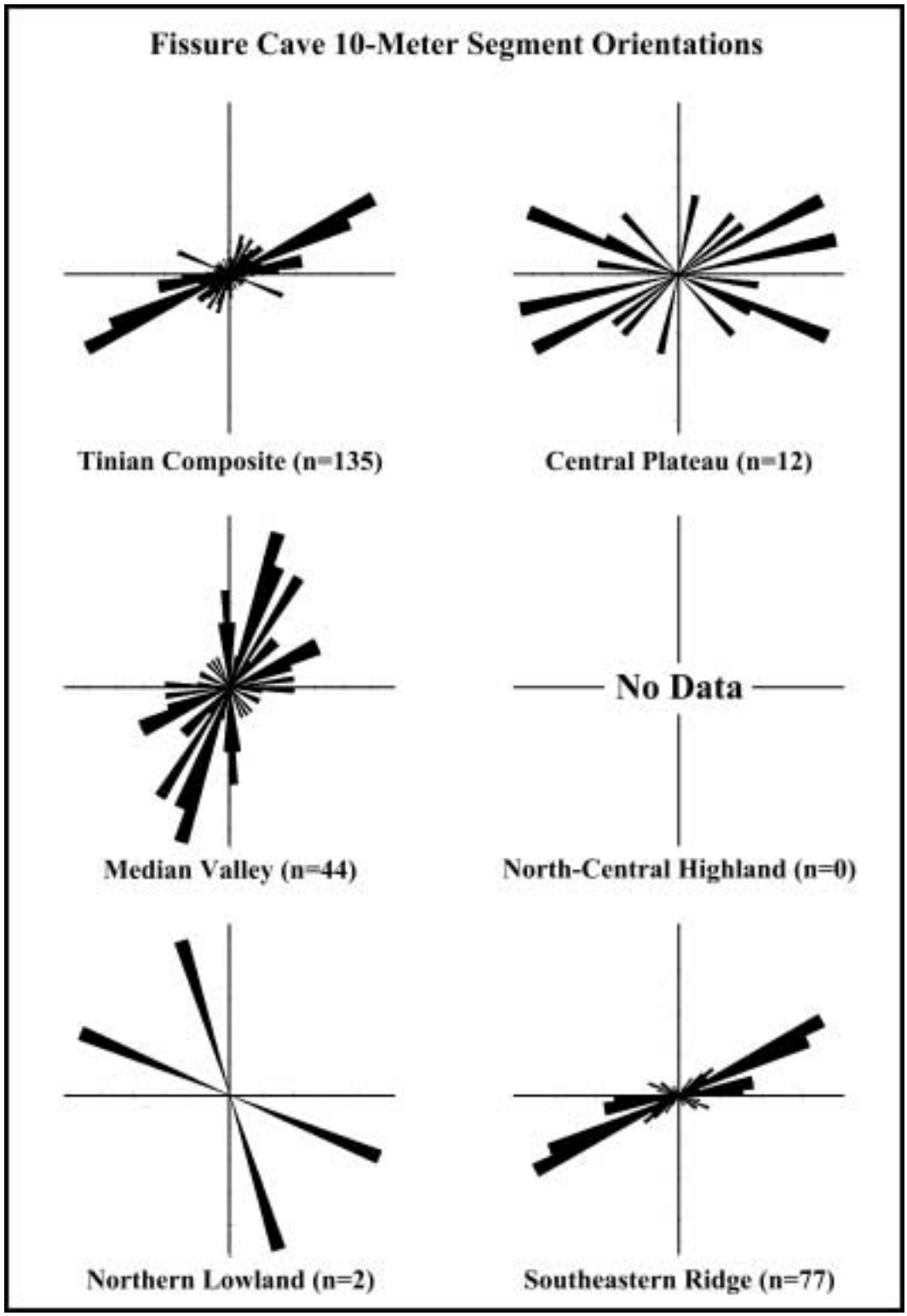

Figure 156: Rose diagrams of fissure cave, ten-meter segment orientations grouped by physiographic province.

Table 5: Mixing zone cave primary orientations grouped by physiographic province.

Central Plateau	Median Vally	North-Central Highland	Northern Lowland	Southeastern Ridge
Orientation	Orientation	Orientation	Orientation	Orientation
301	270	102	147	318
182	40	123		176
147	194	142		126
258	350	178		80
229	174	179		130
253	211	161		313
234	95	77		279
263	30	36		245
75	257			122
88	131			279
51	249			72
194	108			118
60	311			297
336	287			279
12	268			226
213	329			22
221	95			231
203	102			176
181	90			130
158	257			115
333	250			194
332	310			206
115	332			2
260	73			135
150	36			327
34	49			281
89	41			333
293				313
93				321
107				250
105				320
289				278
85				304
294				188
136				102
210				149
220				309
250				54
98				54
64				341
75				330
39				302
50				279
41				329
340				1
34				308

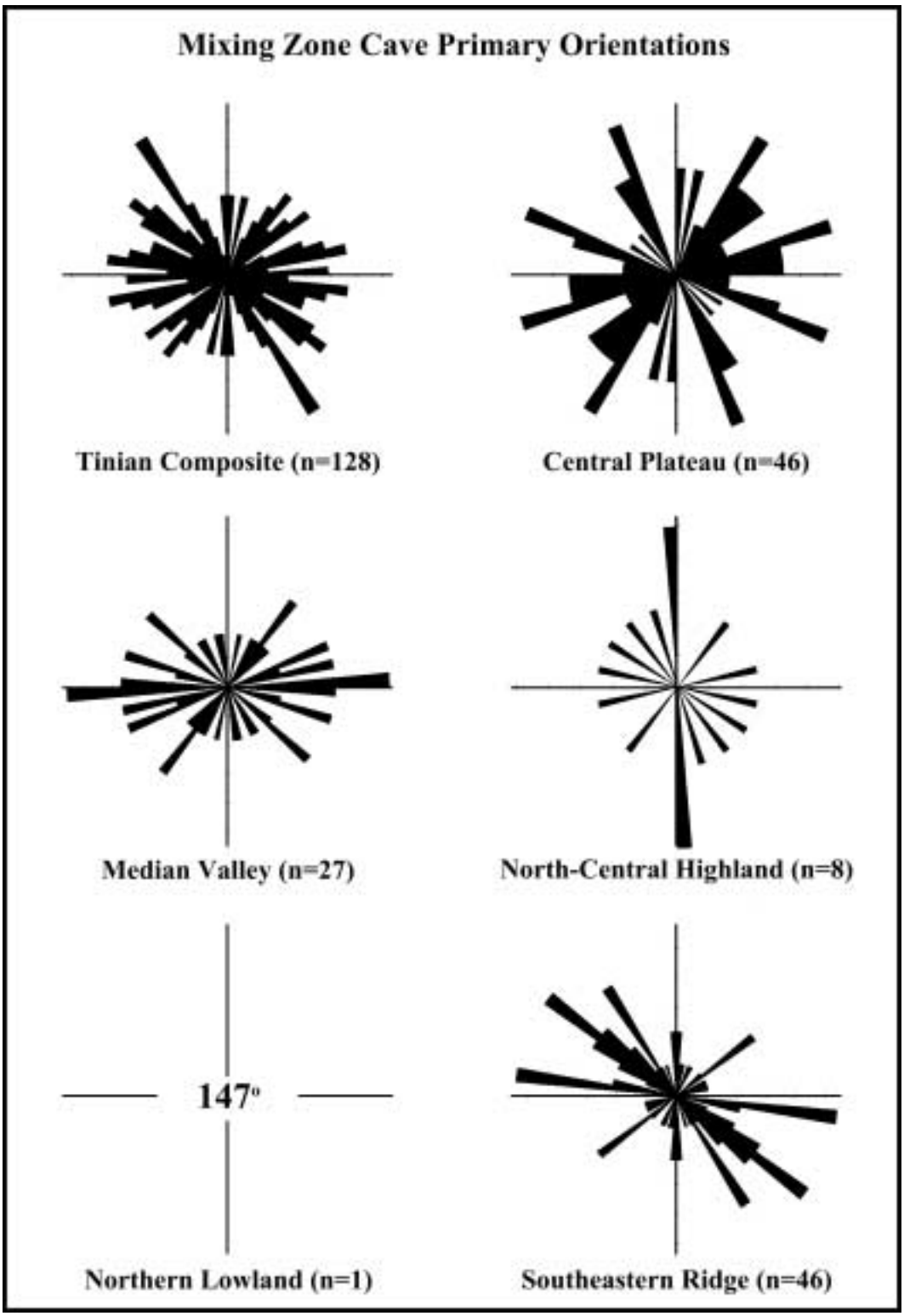

Figure 157: Rose diagrams of mixing zone cave, primary orientations grouped by physiographic province.

Table 6: Mixing zone cave segment orientations with segment length grouped by physiographic province.

Central Plateau		Median Valley		North-Central Highland		Northern Lowland		Southeastern Ridge	
Length	Segment	Length	Segment	Length	Segment	Length	Segment	Length	Segment
Orientation	Length (m)	Orientation	Length (m)	Orientation	Length (m)	Orientation	Length (m)	Orientation	Length (m)
301	16.8	37	1.7	102	12.8	155	42	316	7.5
204	42.0	77	1.3	142	8.7	189	6.125	47	11.8
132	3.2	89	2.9	178	1.3	79	5.26	140	4.0
179	8.4	116	6.9	179	1.3	170	6.875	176	7.4
55	6.1	66	6.6	250	3.0			18	6.7
108	3.6	86	2.2	10	5.5			91	2.1
188	6.9	195	3.7	68	4.8			147	3.9
258	12.2	40	4.1	21	5.3			80	4.9
234	14.2	80	4.3	166	3.5			135	1.1
201	13.6	42	5.9	153	4.4			107	1.2
262	3.5	69	6.6	181	2.9			130	3.0
238	1.9	214	18.1	96	2.1			313	10.1
268	1.2	101	20.2	77	13.4			355	3.0
256	1.6	194	16.2	68	11.6			169	2.1
234	9.9	76	17.5	171	7.9			153	2.9
231	15.4	350	13.8	229	22.6			75	4.0
276	15.8	335	4.5	34	4.9			83	10.2
257	3.0	146	10.1	22	11.5			352	6.5
246	2.7	57	8.8	62	6.3			344	6.0
42	9.9	147	13.6	35	10.9			63	11.1
75	10.8	149	16.9					328	4.8
285	9.9	211	17.2					166	3.6
311	5.5	148	20.6					298	2.0
246	4.4	106	30.1					90	1.4
311	4.6	74	20.2					24	9.9
45	5.3	116	13.0					97	3.1
36	10.7	181	12.8					89	2.5
269	6.9	88	9.7					122	8.4
194	14.7	134	14.2					64	3.0
271	6.2	28	14.0					182	18.2
50	12.6	247	17.6					279	9.3
68	15.2	287	5.0					351	6.9
92	6.9	18	7.7					252	3.8
129	15.2	291	11.7					351	6.4
158	26.6	33	21.2					111	3.25
31	9.5	361	10.8					126	5.08
101	55.1	212	13.2					144	11.92
101	12.4	280	8.0					68	17.58
90	18.2	171	15.7					143	2.25
8	29.7	274	14.3					297	5.5
213	1.5	146	11.5					190	29.5
215	0.9	131	16.8					279	84.9

Table 6 (continued): Mixing zone cave segment orientations with segment length grouped by physiographic province.

Central Plateau		Median Valley		North-Central Highland		Northern Lowland		Southeastern Ridge	
Length Orientation	Segment Length (m)	Length Orientation	Segment Length (m)	Length Orientation	Segment Length (m)	Length Orientation	Segment Length (m)	Length Orientation	Segment Length (m)
221	6.4	98	18.3					56	28.2
182	0.7	106	18.3					316	10.8
197	5.1	49	4.2					142	12.6
214	5.0	249	4.6					153	18.4
181	4.2	345	19.8					186	30.0
158	1.3	242	13.0					40	24.6
330	12.0	257	6.9					266	26.2
338	5.2	29	7.0					177	13.4
284	3.7	26	14.7					36	10.8
254	11.6	101	51.3					21	24.8
355	13.8	313	43.6					30	19.3
308	14.5	343	34.7					231	19.0
115	1.3	18	44.2					178	6.1
153	2.6	5	32.8					102	15.4
168	2.5	155	34.3					166	23.1
196	1.9	146	29.4					112	5.8
214	2.1	52	15.5					46	13.9
220	2.2	89	18.9					152	8.9
235	2.1	323	21.5					166	12.4
176	4.5	203	7.2					234	9.8
214	6.4	278	10.9					129	2.7
293	7.2	268	54.7					210	4.0
31	9.6	332	10.9					201	5.9
48	11.9	121	38.9					276	6.6
26	10.7	155	24.5					135	5.3
64	9.7	257	7.6					2	4.4
232	7.7	288	5.7					23	7.1
247	5.7	309	6.7					68	12.3
150	8.9	335	6.0					198	11.6
91	19.3	290	7.6					169	7.9
168	23.8	173	3.8					336	1.6
268	13.8	354	5.2					10	3.1
212	14.4	312	9.5					95	3.8
160	5.7	260	6.2					128	6.6
81	6.3	249	9.0					176	14.5
34	5.9	281	2.6					223	9.3
165	8.5	350	2.9					157	2.2
230	9.7	268	6.7					54	3.6
271	14.8	298	11.9					333	4.0
356	6.0	346	26.7					301	2.0
192	20.7	333	8.1					43	1.8
111	10.7	335	0.3					106	17.1

Table 6 (continued): Mixing zone cave segment orientations with segment length grouped by physiographic province.

Central Plateau		Median Valley		North-Central Highland		Northern Lowland		Southeastern Ridge	
Length Orientation	Segment Length (m)	Length Orientation	Segment Length (m)	Length Orientation	Segment Length (m)	Length Orientation	Segment Length (m)	Length Orientation	Segment Length (m)
204	9.1	330	18.6					284	4.4
298	49.1	58	6.0					347	11.6
47	37.6	253	4.3					316	4.2
34	27.8	328	6.4					254	15.1
118	49.1	284	8.3					229	13.3
66	19.2	262	7.4					268	12.3
293	3.6	27	22.1					176	24.5
198	9.5	92	1.2					187	27.5
93	4.5	72	1.0					186	24.5
107	15.4	73	1.2					320	9.0
105	14.3	27	1.4					202	8.1
289	16.4	95	20.6					286	4.8
345	8.9	360	68.4					308	2.7
85	43.0	93	83.1					15	7.6
294	12.0	298	15.6					278	5.6
278	25.0	156	27.2					188	10.9
327	16.8	76	22.2					191	3.1
13	10.2	90	59.4					102	1.8
185	10.8	268	53.1					236	5.5
238	16.2	252	20.9					149	14.9
39	11.0	258	47.2					309	10.7
50	11.0	337	53.7					308	2.2
41	16.1	223	15.9					1	2.2
340	11.0	109	9.3					329	5.7
34	11.9	164	10.4					279	3.8
192	14.3	237	5.8					54	16.2
258	13.5	118	7.8					47	6.5
250	9.5	36	13.5					341	1.6
152	15.4	320	5.7					330	2.2
248	40.2	332	12					27	10.5
292	15.9	73	38.4					306	5.9
236	4.7	202	21.1						
194	5.4	68	22.1						
176	7.1	49	22.6						
158	10.3	83	25.6						
60	28.4	41	38.4						
263	27.0	13	19.7						
144	36.6	294	10.8						
221	18.5	320	18.2						
		84	11.3						
		36	39.3						
		22	21.6						

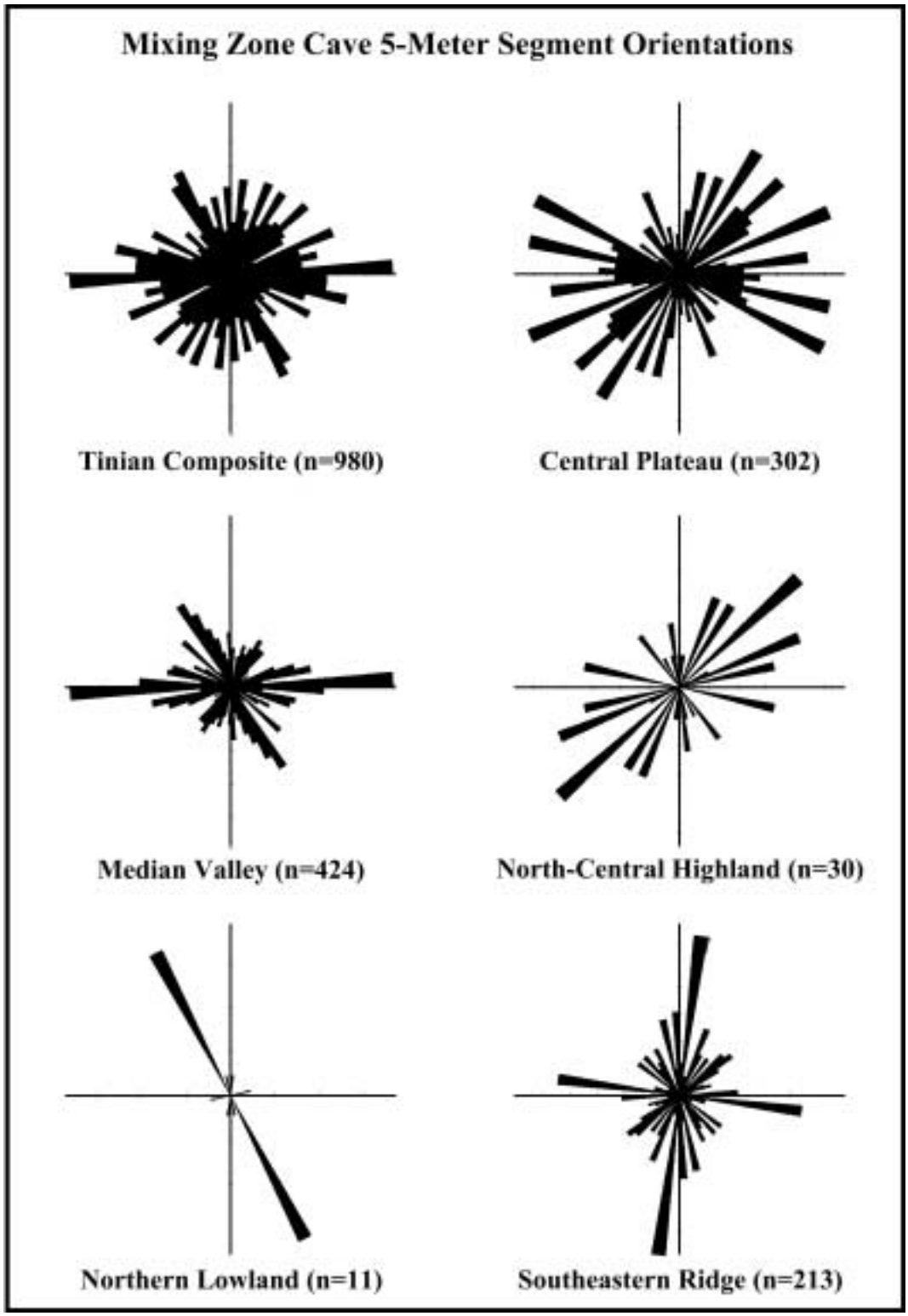

Figure 158: Rose diagrams of mixing zone cave, five-meter segment orientations grouped by physiographic province.

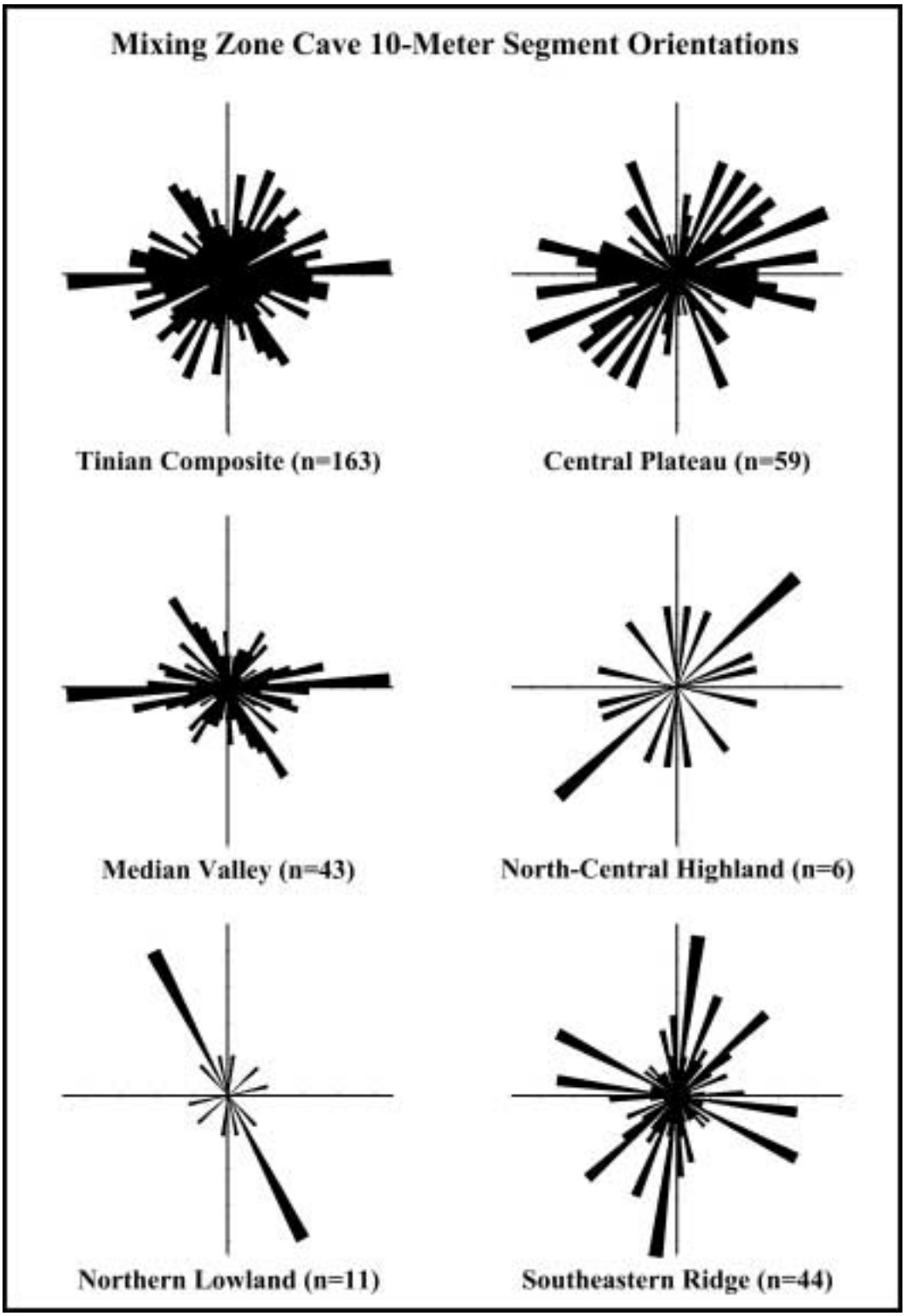

Figure 159: Rose diagrams of mixing zone cave, ten-meter segment orientations grouped by physiographic province.

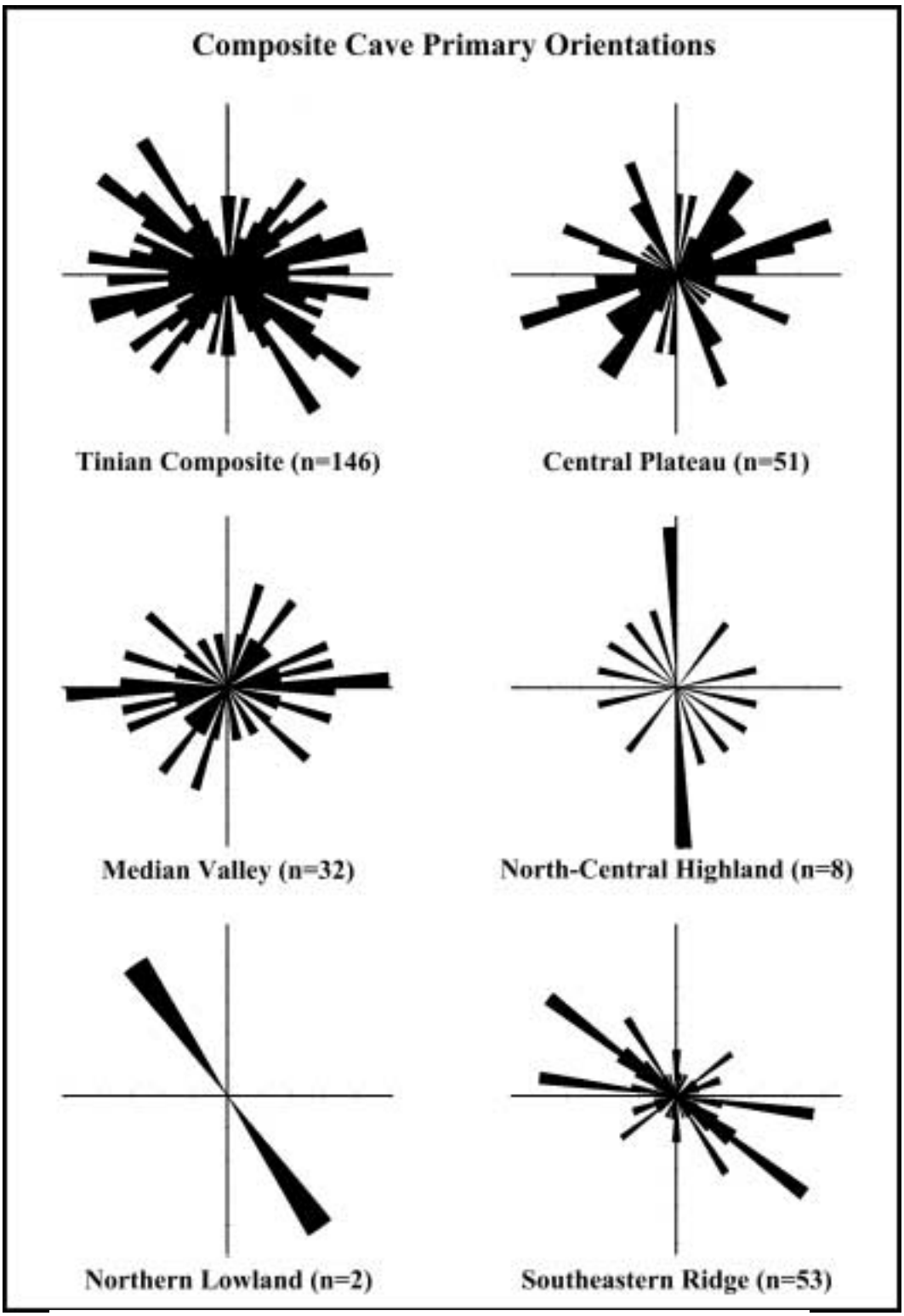

Figure 160: Rose diagrams of composite cave, primary orientations grouped by physiographic province.

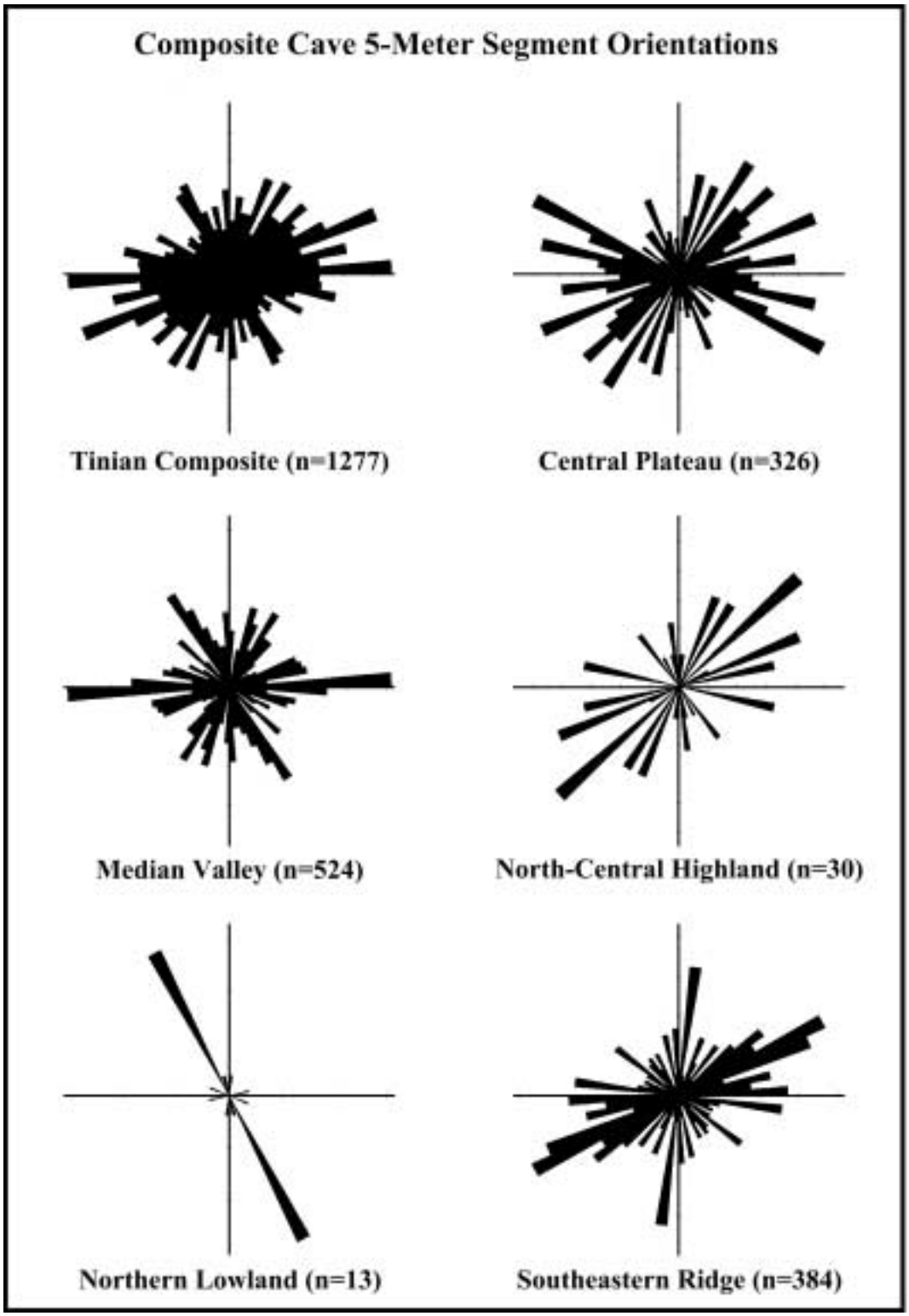

Figure 161: Rose diagrams of composite cave, five-meter segment orientations grouped by physiographic province.

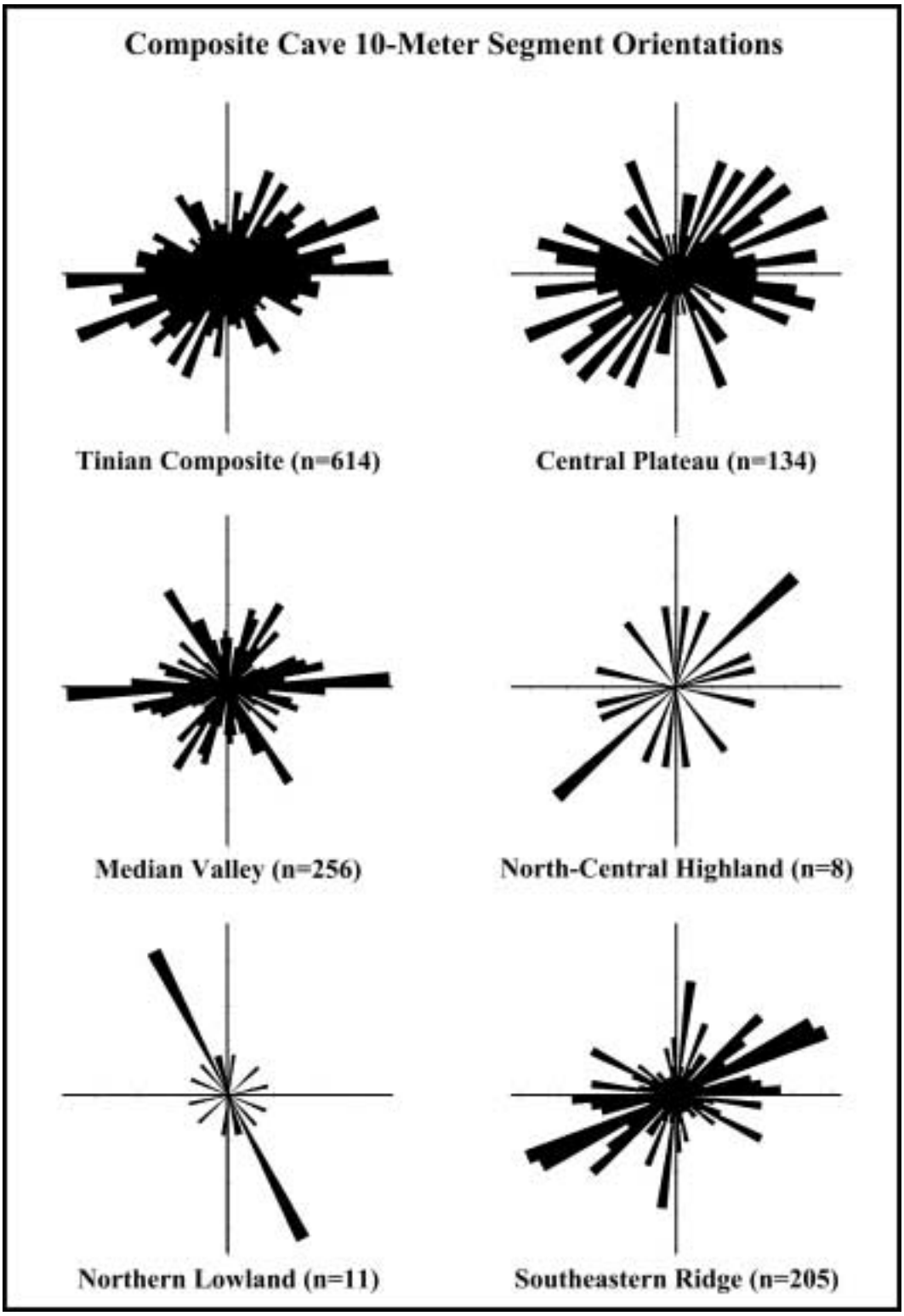

Figure 162: Rose diagrams of composite cave, ten-meter segment orientations grouped by physiographic province.

Table 7: Mixing zone cave, entrance width segment orientations with segment length grouped by physiographic province.

Central Plateau		Median Valley		North-Central Highland		Northern Lowland		Southeastern Ridge	
Length Orientation	Segment Length (m)	Length Orientation	Segment Length (m)	Length Orientation	Segment Length (m)	Length Orientation	Segment Length (m)	Length Orientation	Segment Length (m)
205	38.0	354	1.9	225	20.9	45	109.3	45	10.4
258	9.0	86	32.7	267	11.8			264	21.7
213	5.5	123	10.3	271	1.6			196	6.0
194	4.6	258	22.2	67	16.5			197	3.9
187	7.4	151	33.9	193	11.5			216	19.4
343	49.6	156	16.8					240	17.5
336	9.7	176	25.2					216	4.8
301	24.4	189	21.9					261	21.5
289	20.7	325	5.8					203	6.6
294	8.0	181	16.5					8	18.1
96	37.2	230	4.4					24	34.9
300	1.5	178	75.0					29	18.7
100	1.9	157	29.0					2	51.8
278	5.4	157	17.4					209	21.7
291	6.9	26	10.1					189	18.8
254	5.6	66	3.0					325	5.0
247	5.3	118	44.0					181	14.2
226	7.2	344	17.8					230	3.8
249	10.5	325	19.8					233	8.1
13	2.1	149	41.5					219	1.6
341	4.8							214	4.5
254	3.2							214	4.5
300	37.1							194	6.4
200	10.4							297	2.2
195	6.4							242	3.2
40	8.6							192	12.4
74	10.2							251	3.7
79	22.1							239	13.5
12	39.4							174	15.3
187	16.6							224	5.6
229	23.4							160	4.3
274	10.9							204	7.3
301	6.9							276	9.1
318	5.9							9	2.2
135	12.1							229	24.4
262	13.6							227	13.0
110	17.7							92	5.1
305	12.7							222	4.9
154	21.9							190	5.3
35	40.7							211	10.5
								76	13.4
								241	10.9

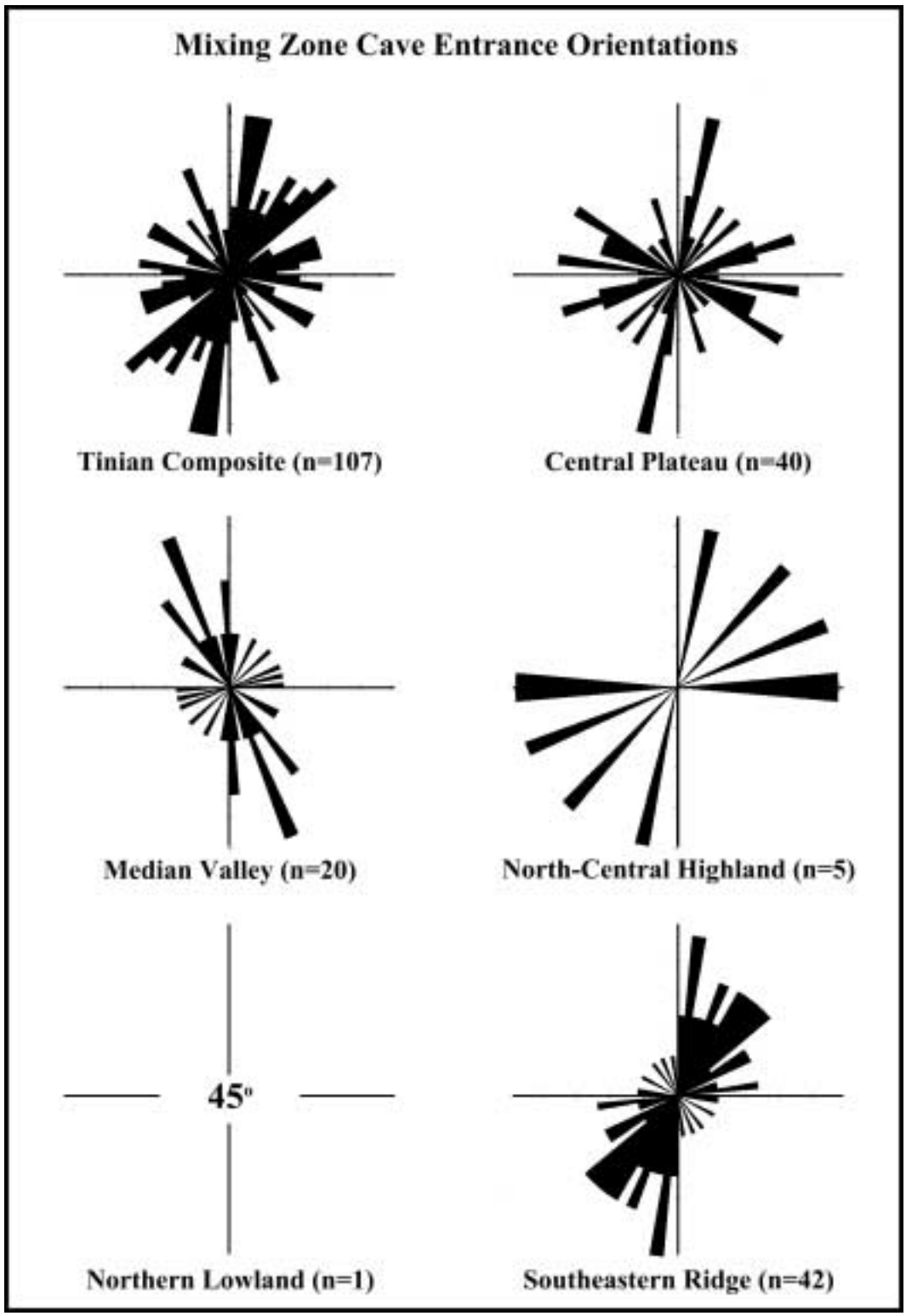

Figure 163: Rose diagrams of mixing zone cave entrance width orientations grouped by physiographic province.

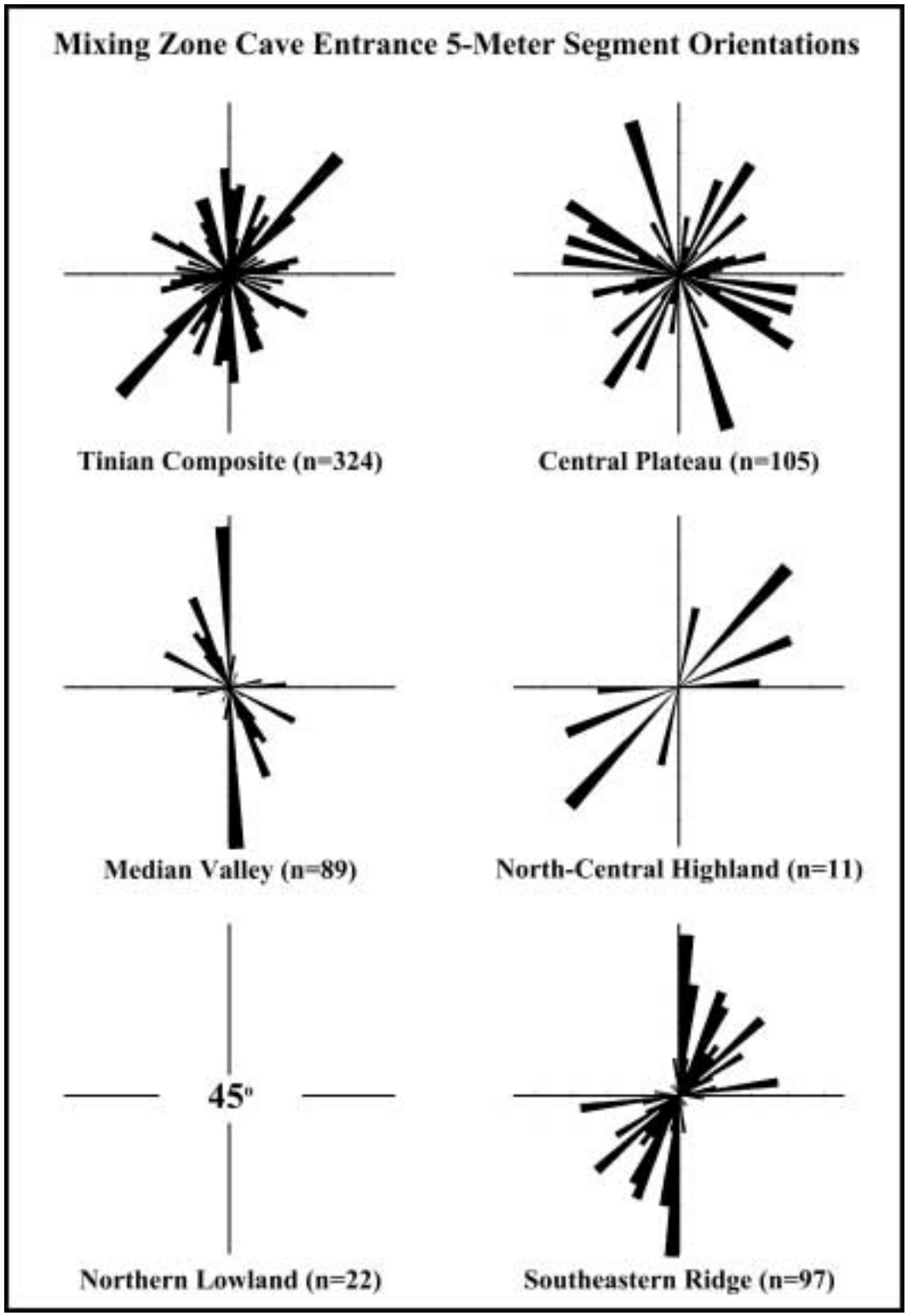

Figure 164: Rose diagrams of mixing zone cave entrance width, five-meter segment orientations grouped by physiographic province.

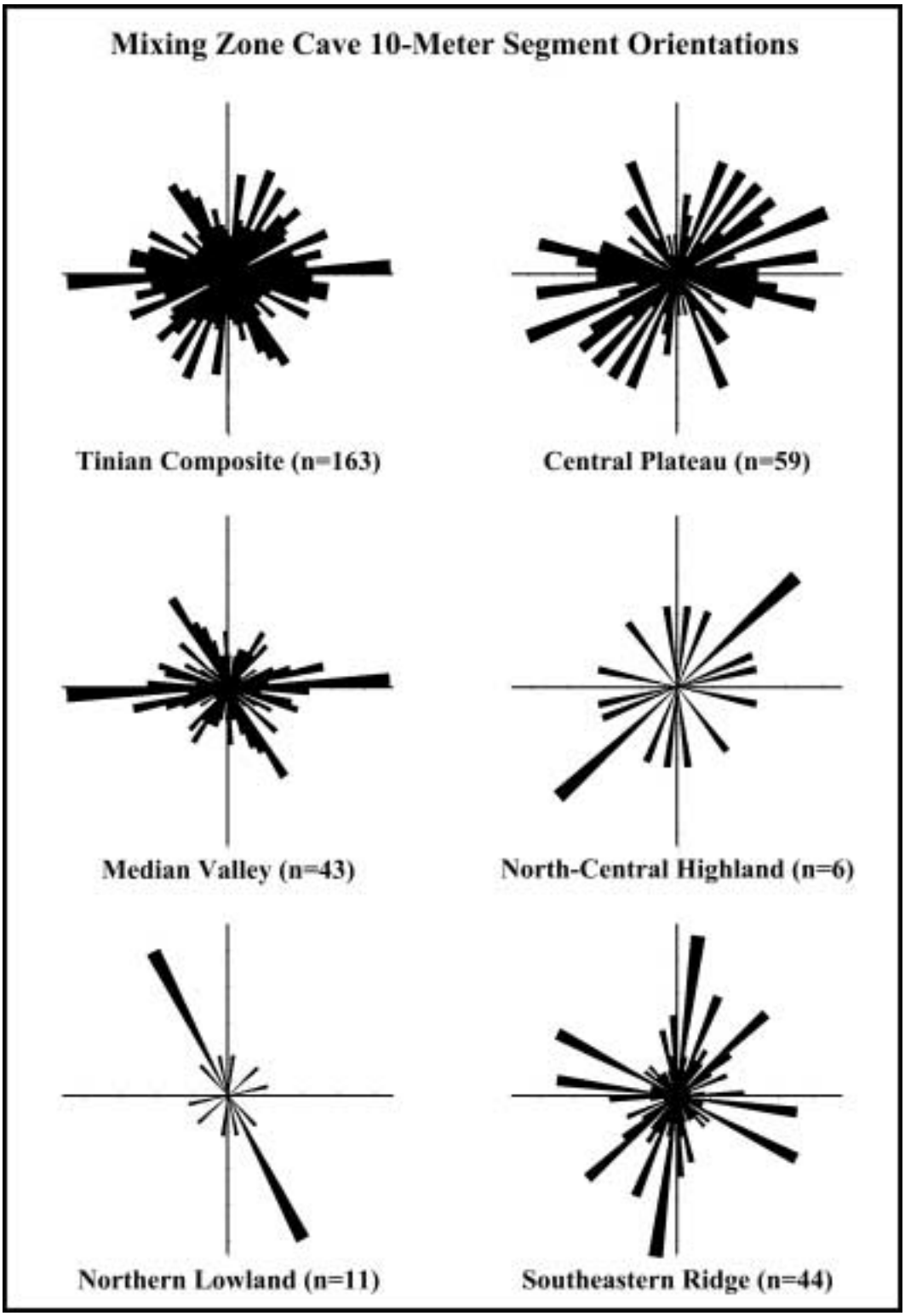

Figure 165: Rose diagrams of mixing zone cave entrance width, ten-meter segment orientations grouped by physiographic province.

Table 8: Mixing zone cave, penetration segment orientations with segment length grouped by physiographic province.

Central Plateau		Median Valley		North-Central Highland		Northern Lowland		Southeastern Ridge	
Length Orientation	Segment Length (m)	Length Orientation	Segment Length (m)	Length Orientation	Segment Length (m)	Length Orientation	Segment Length (m)	Length Orientation	Segment Length (m)
310	22.2	90	17.9	120	10.8	330	79.3	150	9.5
3	12.2	11	17.0	342	7.6			354	7.5
138	3.6	33	3.9	1	1.3			271	6.2
294	7.6	183	15.7	171	4.7			257	1.6
277	21.4	20	10.5	269	13.8			306	5.5
238	17.3	46	38.8	37	32.7			135	11.4
246	3.5	81	51.1					111	5.3
46	17.2	211	32.1					171	6.8
34	10.7	101	9.0					293	6.6
9	14.8	114	16.2					82	9.6
171	35.1	70	5.8					279	9.5
210	1.6	76	19.4					122	45.3
204	1.1	126	4.4					278	63.3
202	5.7	107	49.5					226	35.8
186	5.2	334	39.9					284	8.6
181	4.1	135	16.9					133	26.6
172	1.7	336	24.9					337	8.8
149	20.0	269	66.8					24	44.3
354	13.3	81	48.3					260	17.4
272	1.8	82	7.5					338	12.8
304	7.0	131	8.8					294	3.8
329	9.2	141	12.5					109	6.4
35	65.1	223	29.5					179	4.5
109	3.6	239	18.3					96	12.5
300	4.8	220	38.3					136	2.1
295	13.8	74	34.0					167	2.6
329	7.7							117	7.6
334	11.8							153	4.3
13	7.0							135	21.0
292	13.4							249	40.4
304	23.8							149	9.5
199	11.5							85	5.1
196	13.6							129	3.4
243	8.2							187	10.9
210	19.2							279	2.0
247	14.9							154	16.1
215	16.4							152	9.9
21	13.8							197	2.2
64	11.0							147	5.9
106	41.0							115	3.8
251	15.0							136	7.8
267	46.9							181	5.1
								166	5.1

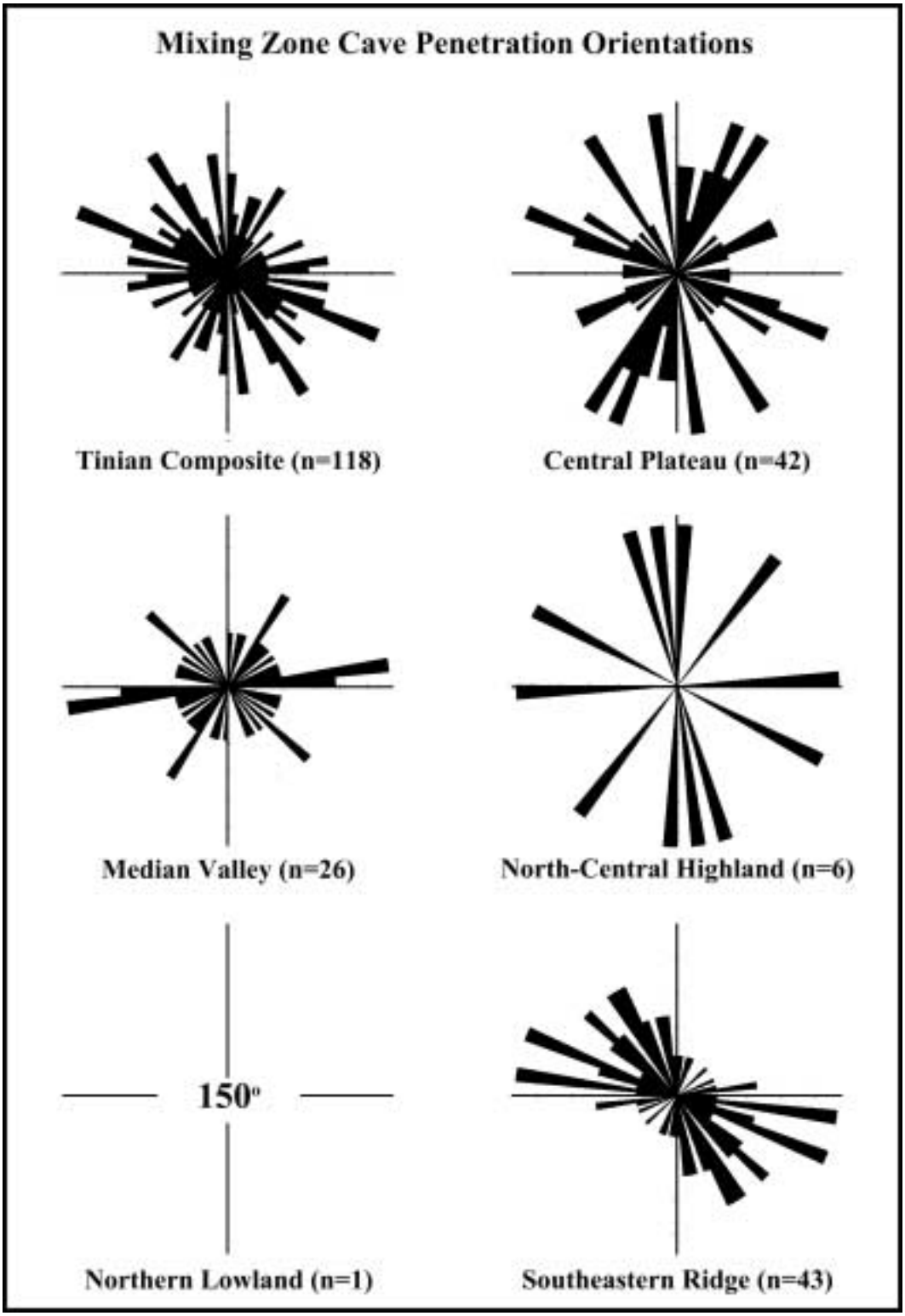

Figure 166: Rose diagrams of mixing zone cave penetration orientations grouped by physiographic province.

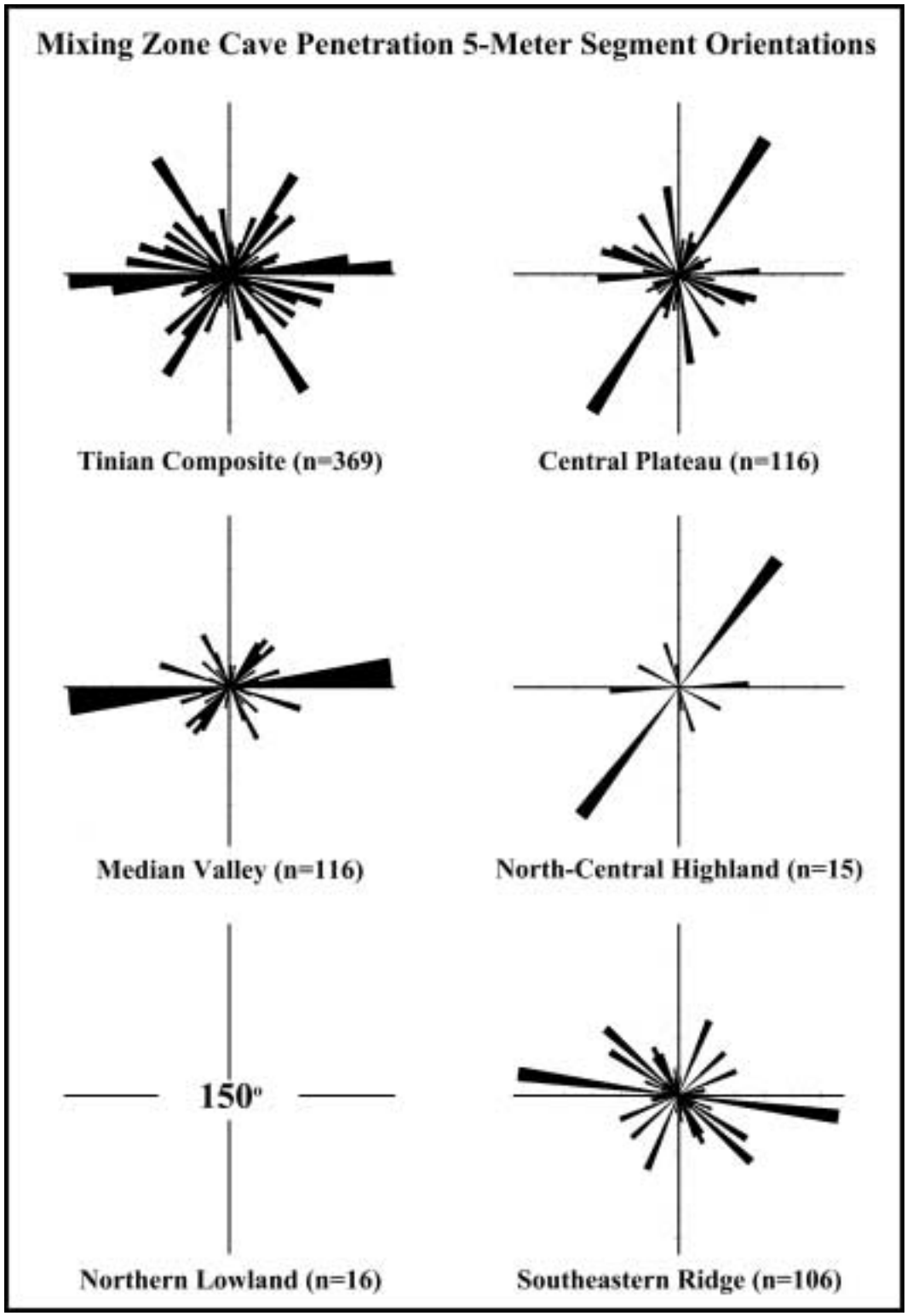

Figure 167: Rose diagrams of mixing zone cave penetration, five-meter segment orientations grouped by physiographic province.

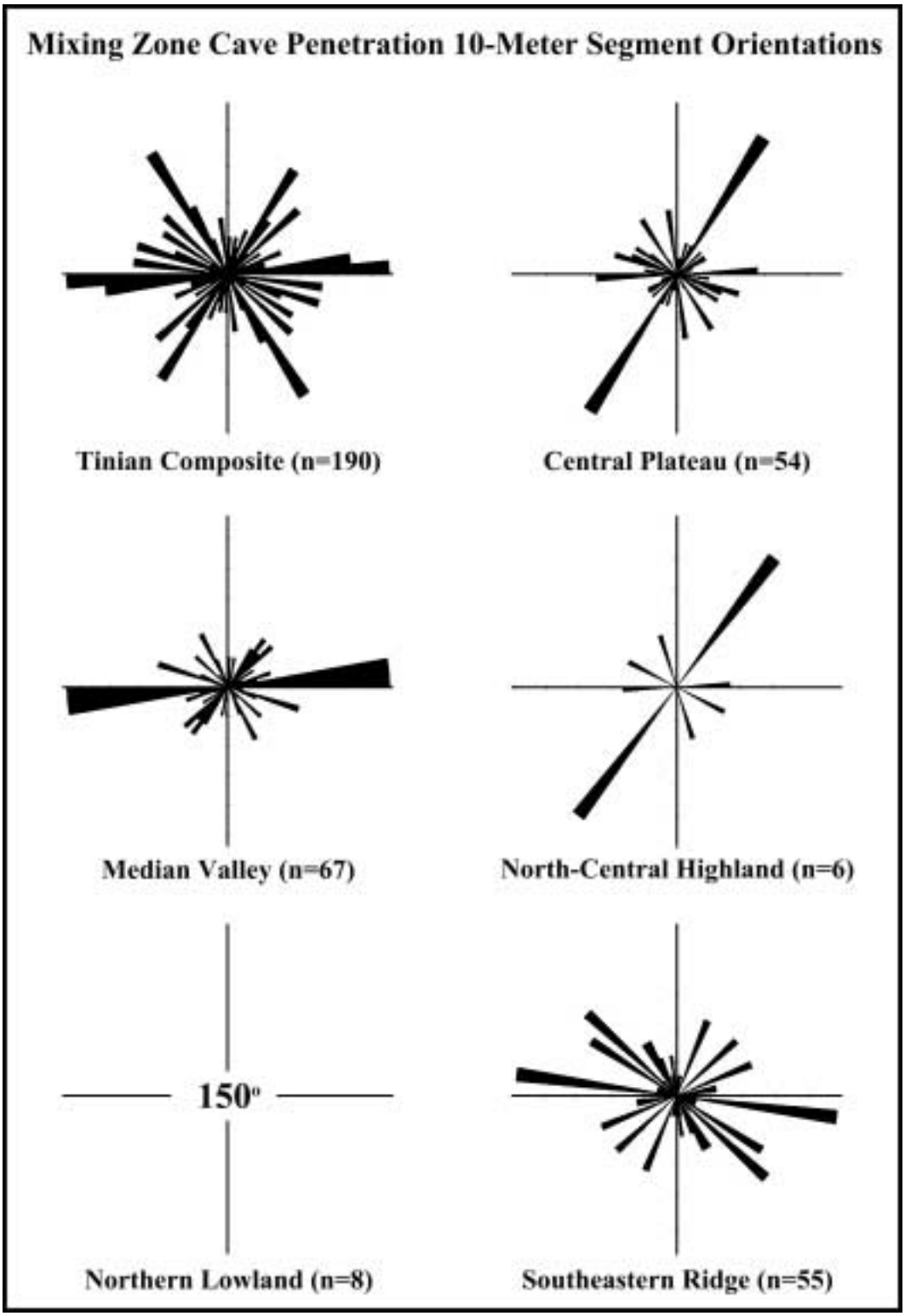

Figure 168: Rose diagrams of mixing zone cave penetration, ten-meter segment orientations grouped by physiographic province.

Table 9: Mixing zone cave, maximum width segment orientations with segment length grouped by physiographic province.

Central Plateau		Median Valley		North-Central Highland		Northern Lowland		Southeastern Ridge	
Length Orientation	Segment Length (m)	Length Orientation	Segment Length (m)	Length Orientation	Segment Length (m)	Length Orientation	Segment Length (m)	Length Orientation	Segment Length (m)
205	42.0	345	7.5	225	20.9	45	109.3	45	11.7
258	9.0	86	32.7	267	11.8			264	21.7
213	5.5	123	10.3	271	1.6			196	7.4
222	7.3	258	22.2	67	16.5			197	3.9
202	11.5	290	8.6	193	11.5			216	19.4
343	49.6	150	42.4	307	10.9			240	17.5
336	9.7	156	19.7					36	6.4
301	24.4	308	15.2					261	21.5
289	20.7	176	25.2					203	6.6
293	13.1	13	27.7					7	18.4
278	53.3	325	5.8					24	34.9
308	1.5	154	21.7					197	20.7
100	1.9	215	5.0					2	51.8
278	5.4	21	30.7					128	27.4
291	6.9	259	14.3					209	21.7
254	5.6	210	6.9					35	24.8
247	5.3	57	21.3					325	5.0
74	8.5	178	75.0					309	8.3
264	11.7	157	29.0					185	12.2
17	3.8	157	17.4					241	10.1
326	7.6	221	13.3					23	9.9
128	7.7	246	7.4					214	7.9
113	74.7	118	44.0					257	3.7
200	10.4	344	18.8					20	12.0
195	6.4	310	21.8					241	4.1
222	13.4	149	41.5					242	3.2
254	13.0							196	16.6
79	22.1							251	3.7
291	5.7							239	13.5
187	17.9							339	28.1
49	30.0							74	8.1
94	12.4							190	7.5
299	9.2							204	7.5
318	5.9							276	8.1
130	21.0							11	3.2
157	14.4							229	24.4
110	17.7							227	13.0
115	13.2							92	5.1
154	21.9							222	4.9
35	40.7							190	5.3
176	8.1							211	10.5
192	49.6							256	16.1
								241	15.8

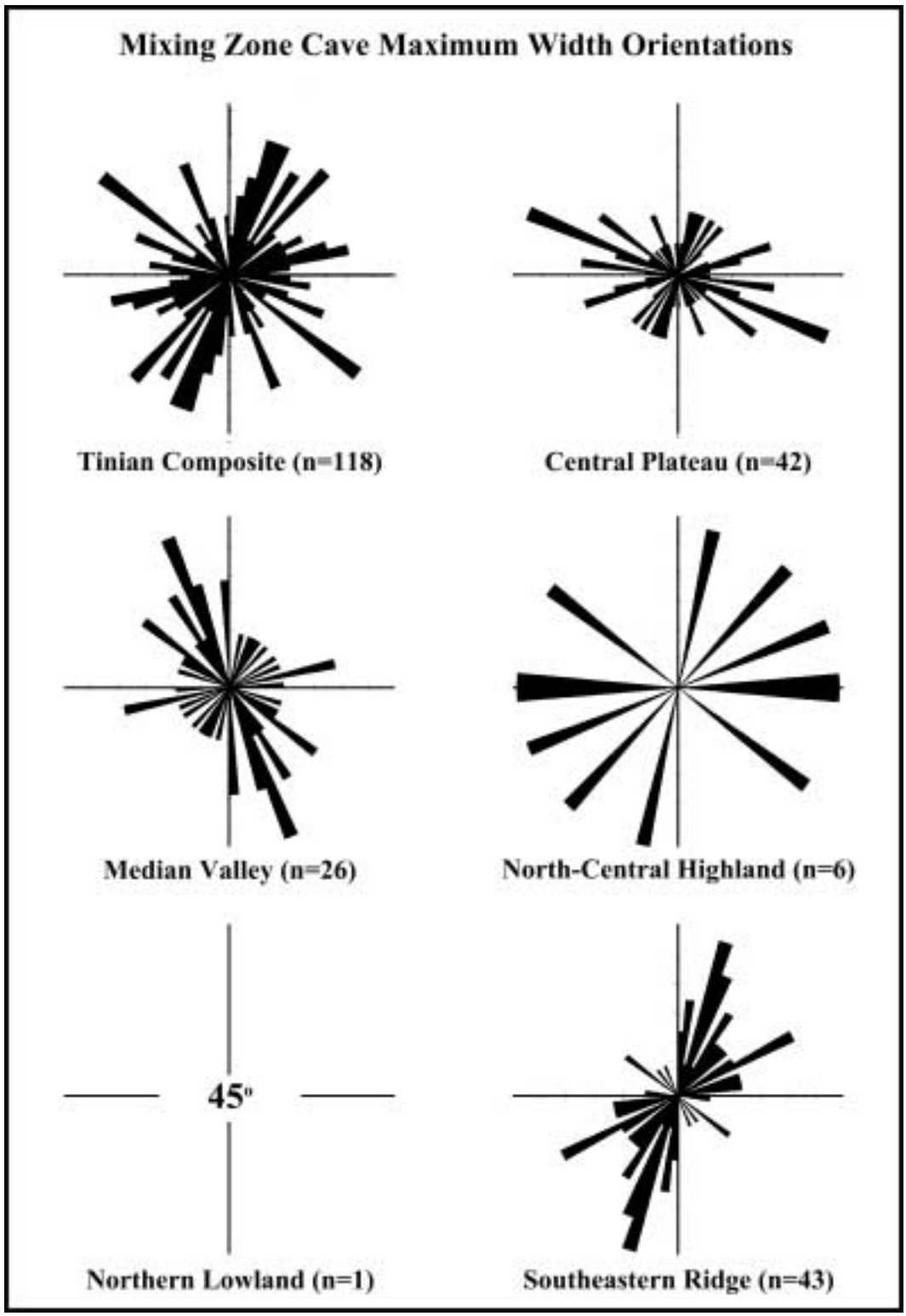

Figure 169: Rose diagrams of mixing zone cave maximum width orientations grouped by physiographic province.

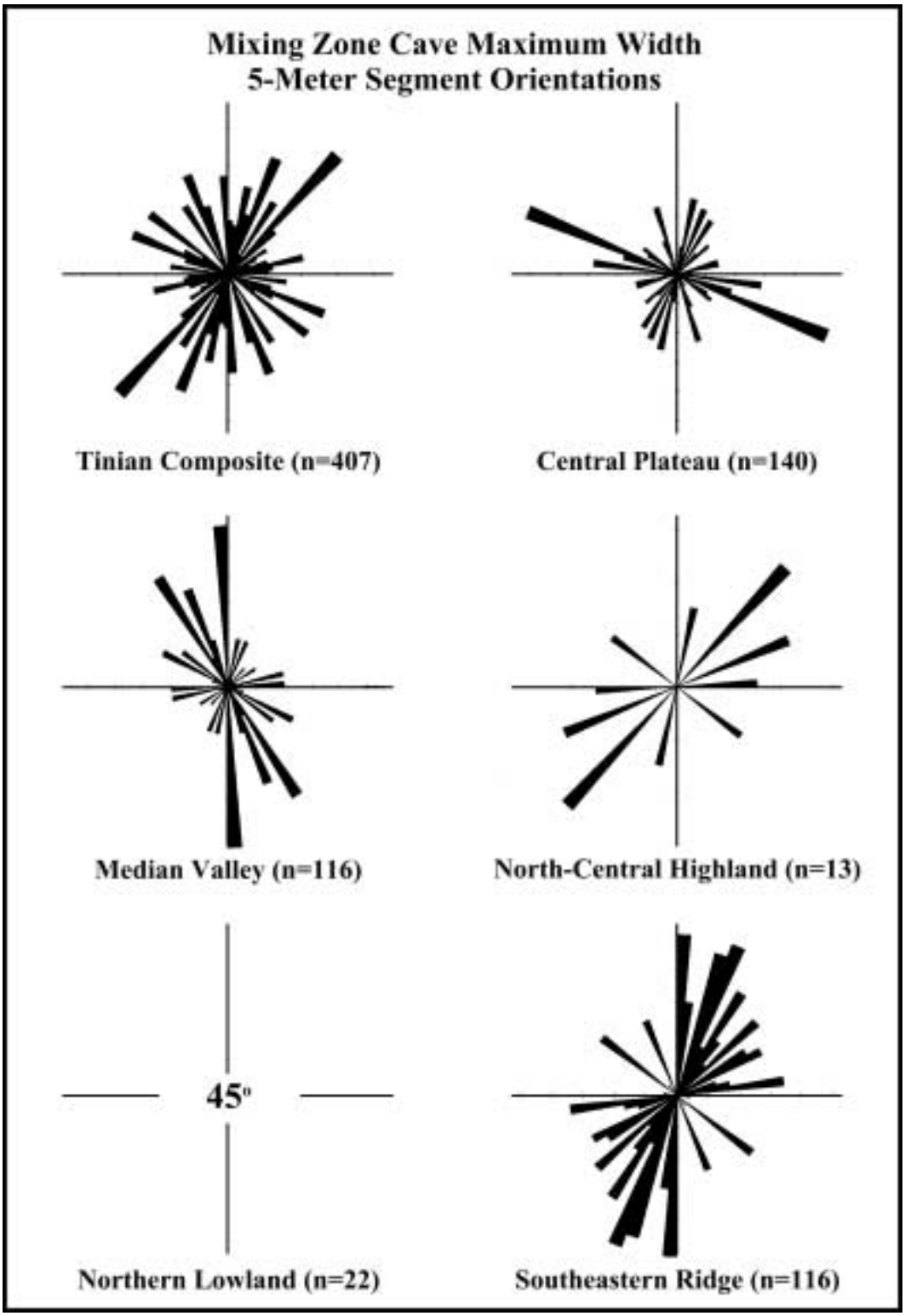

Figure 170: Rose diagrams of mixing zone cave maximum width, five-meter segment orientations grouped by physiographic province.

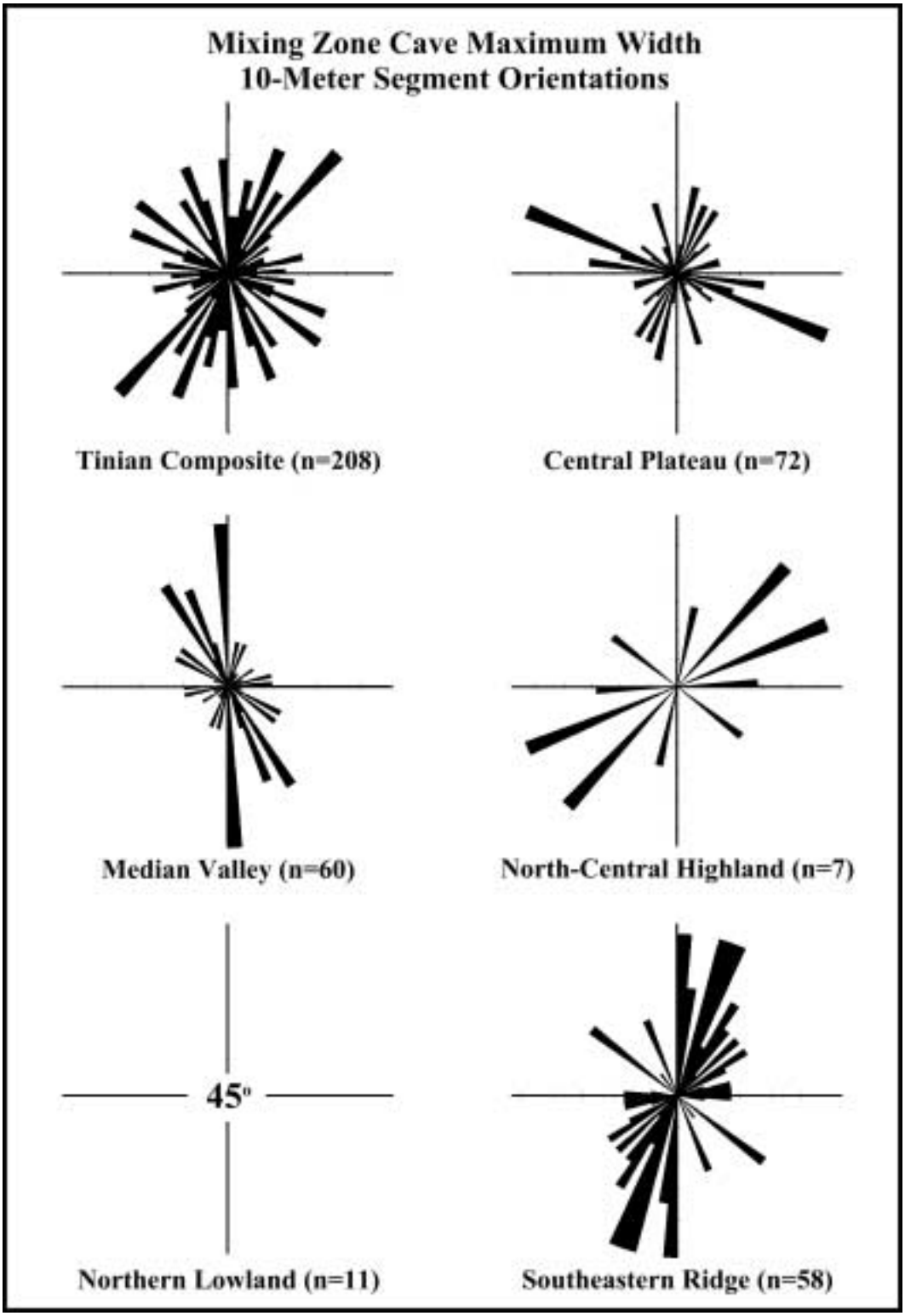

Figure 171: Rose diagrams of mixing zone cave maximum width, ten-meter segment orientations grouped by physiographic province.

Table 10: Faults orientations reported by Doan and coworkers (1960) segment length grouped by physiographic province.

Central Plateau		Median Valley		North-Central Highland		Northern Lowland		Southeastern Ridge		Boundary Areas	
Fault Orientation	Segment Length (m)	Fault Orientation	Segment Length (m)	Fault Orientation	Segment Length (m)	Fault Orientation	Segment Length (m)	Fault Orientation	Segment Length (m)	Fault Orientation	Segment Length (m)
356	790	42.5	3876		159	44.5	1693	87	778	68	796
176	783	38	1378	39	189	320	1784	157	304	94	193
14.5	1287	59	983	7	306	39	920	142	421	74	607
9	413	82	496	14	229	27	883	136	397	100	284
15	521	39	603	59	179	40	1387	156	923	72	493
23	498	37	1379	314	309	287	716	32	88	59	379
20	478	29	384	3	513	186	698	106	192	59	381
7	508	42	194	40	804	338	378	24	384	102	314
198	822	37	2176	40	221	23	207	308	176	322	323
193	579	41	304	9	377	16	293	181	191	312	369
295	518	32	623	23	205	42	884	338	495	304	379
303	283	38	1793	349	399	223	679	315	526	298	694
13	194	55	207	36	506	41	93	307	225	26	746
20	998	105	376	36	208	289	794	6	878	47	699
38	877	48	701	316	798	96	224	13	701	39	583
38	813	366	324	253	476	323	308	13	1198	395	594
24.5	523	175	785	42	1093	319	192	45	694	341	803
38	476	308	293	370	207	329	1007	3.5	694	360	369
41	395	330	908	321	420	330	208	180	683	19.5	283
70	699	343	275	17	413	40	281	136	177	17	279
20	812	343	493	11	419	38	814	80	493	12.5	516
7.5	597	352	512	356	306	12	1477	64	193	354	399
7	503	358.5	523	324	295			309	498	16	624
22	2184	6	1783	327	316			215	493	15	567
12	307	4	694	73	279			283	513	15	302
8	222	122	401	72	304			136	214	333	320
21	766	2	678	72	87			338	193	326	316
347	513	187	493	154	196			3	698	103	316
13	524	336	492	154	1108			13	416	99	1179
34	678	343	413	154	201			53	199	327	294
40	823	334	423	235	1178			349	1121	349	362
169	564	326	285	47	193			349	285	27	394
214	493	312	604	66	294			349	99	61	296
162	221	313	478	215	317			27	303	39	1076
102	394	324	523	229	302			45.5	528	66	294
222	709	194	801	342	513			241	102	15	375
222	194	156.5	516	350	1120			241	824	2	109
37.5	867	148	308	40	1196			315	823	339	217
43	493	34	209	12	419			32	491	66	304
18.5	1123	46	497	12	301			136	461		
29	308	343	513	12	584			298	313		
36	493	22	179	15	1103			300	1282		
317	281	342	505	22	362			116	307		
16	196	187	317					3	209		
16	423	352	624					352	778		
16	283	351	601					116	1092		
54	404	357	978					116	493		
54	176	39	319					16	498		
251	283	328	692					48	478		
251	1624	85	598					61	421		

Table 10 (continued): Fault orientations reported by Doan and coworkers (1960) segment length grouped by physiographic province.

Central Plateau		Median Valley		North-Central Highland		Northern Lowland		Southeastern Ridge		Boundary Areas	
Fault Orientation	Segment Length (m)	Fault Orientation	Segment Length (m)	Fault Orientation	Segment Length (m)	Fault Orientation	Segment Length (m)	Fault Orientation	Segment Length (m)	Fault Orientation	Segment Length (m)
68	688							61	309		
43	716							44.5	1281		
43	575							80	205		
43	423							80	716		
22	394							30	504		
43	88							28.5	203		
43	476							69	388		
36	522							55	390		
27.5	279							117	683		
32	301							124	493		
67	720							18	281		
74	776							190	215		
37	1483							68	406		
30	396							116	308		
16	396							39	389		
23	324										
33	297										
103	978										
91	1023										
83	182										
55	776										
40	496										
54	324										
59	393										
94	878										
60	196										
40	778										
38	620										
37	612										
47	906										
28	679										
52	289										
23	308										
302	76										
66	879										
58	194										
69	316										
33	421										
44	385										
72	397										
82	197										
43	406										
242	294										
317	307										

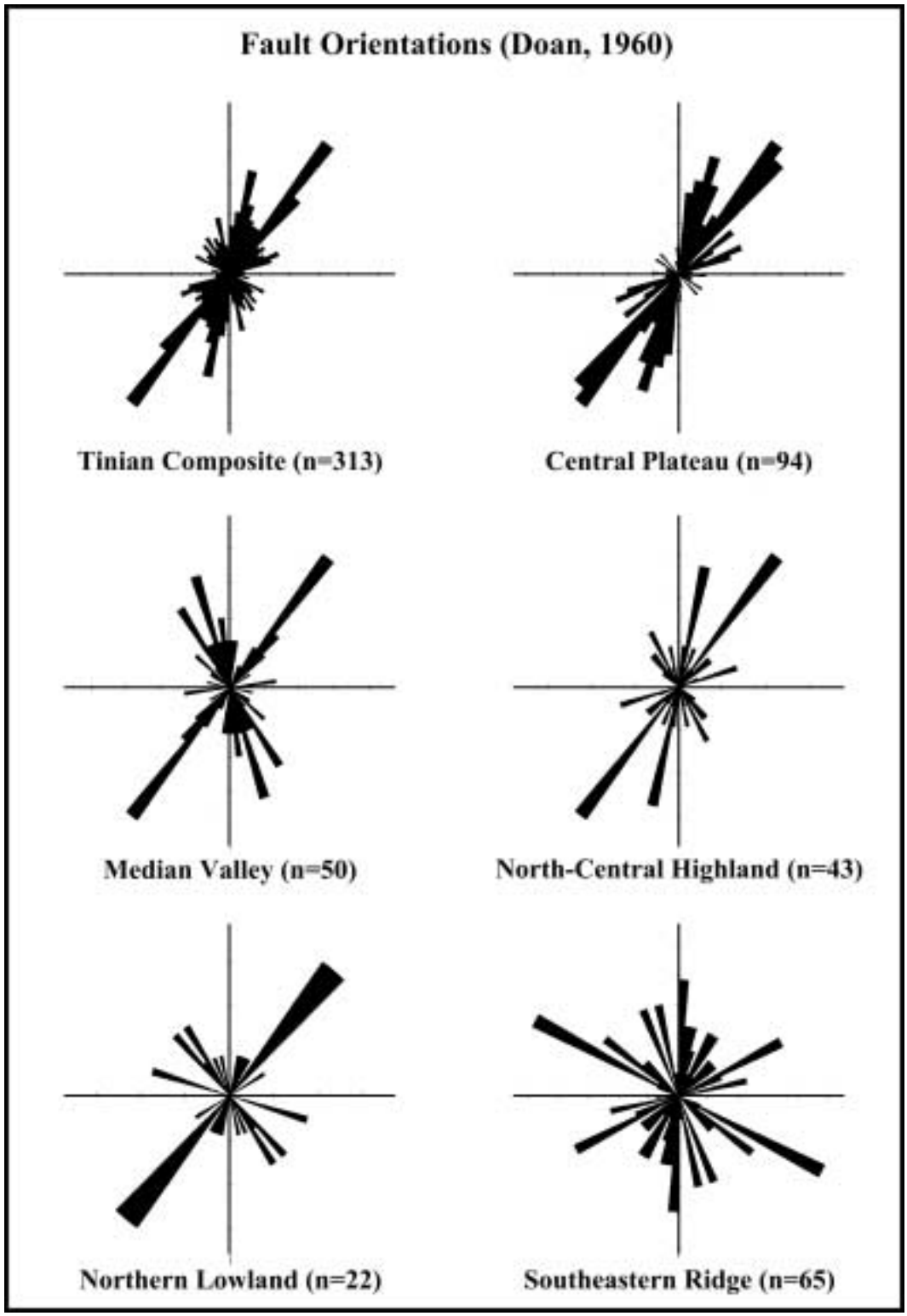

Figure 172: Rose diagrams of fault orientations (Doan et al., 1960) grouped by physiographic province.

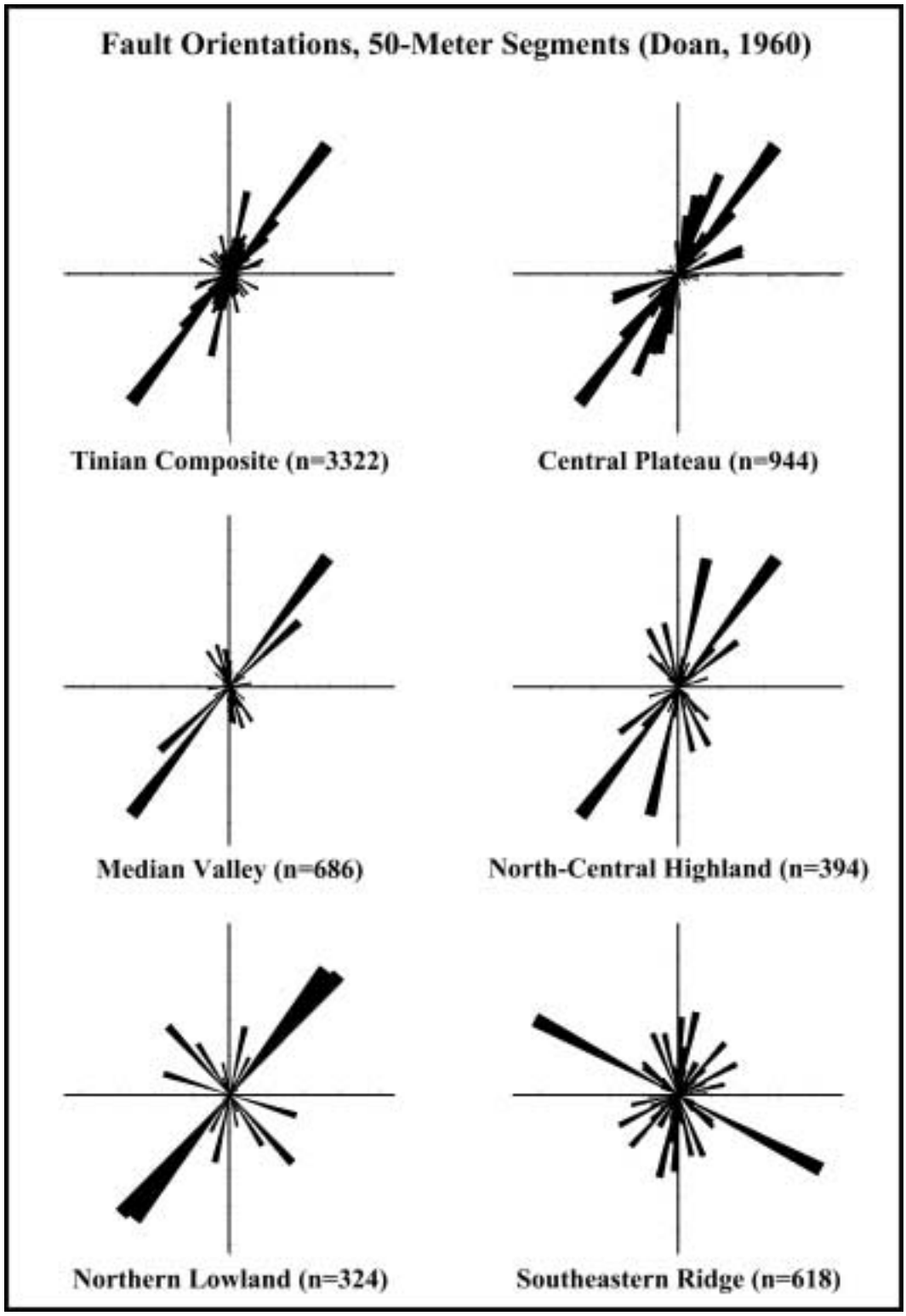

Figure 173: Rose diagrams of fifty-meter, fault segment orientations (Doan et al., 1960) grouped by physiographic province.

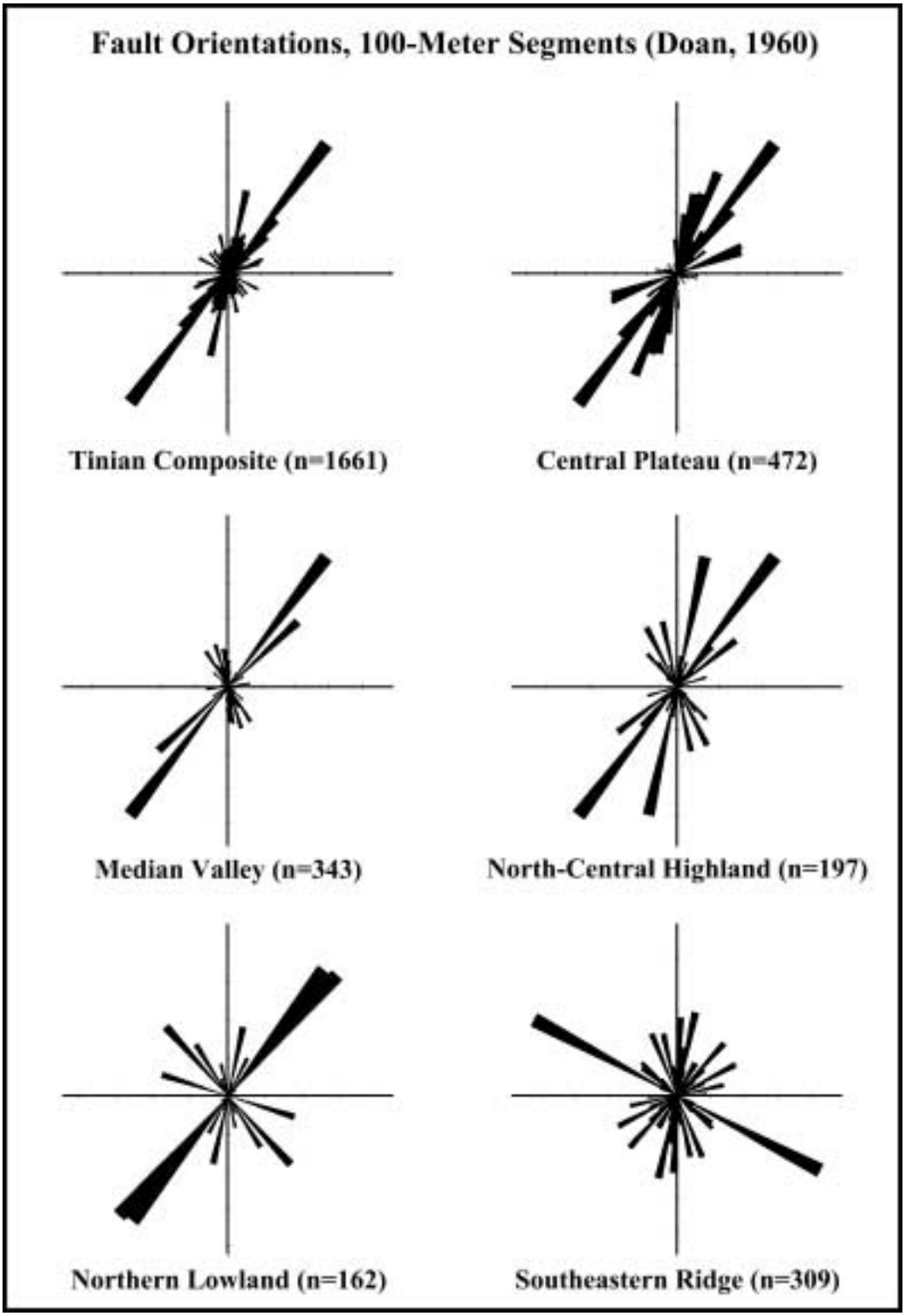

Figure 174: Rose diagrams of one hundred-meter, fault segment orientations (Doan et al., 1960) grouped by physiographic province.

Table 11: Joint (Doan et al., 1960) orientations grouped by physiographic province.

Central Plateau	Median Vally	North-Central Highland	Northern Lowland	Southeastern Ridge
Orientation	Orientation	Orientation	Orientation	Orientation
78	61		281	58
92	339		256	173
70	170		278	171
70	70		87	30
76	53		93	1
74	1		63	9
81	108		285	71
5	168		41	245
116	340		51	89
137	345		66	69
212	350		311	172
218	186		309	208
195	185		303	172
229.5	39		156	106
230	305		136	356
232	10		156	354
226.5	81			28
231	118			12
221	148			188
223	325			170
221	172.5			7
221	191			5
308	164			128
160	195			68
59	7			35
55				287
58				195
79				184
97.5				253
86				250
48				177
63				130
52.5				198
84				
84				
75				
94				
83				

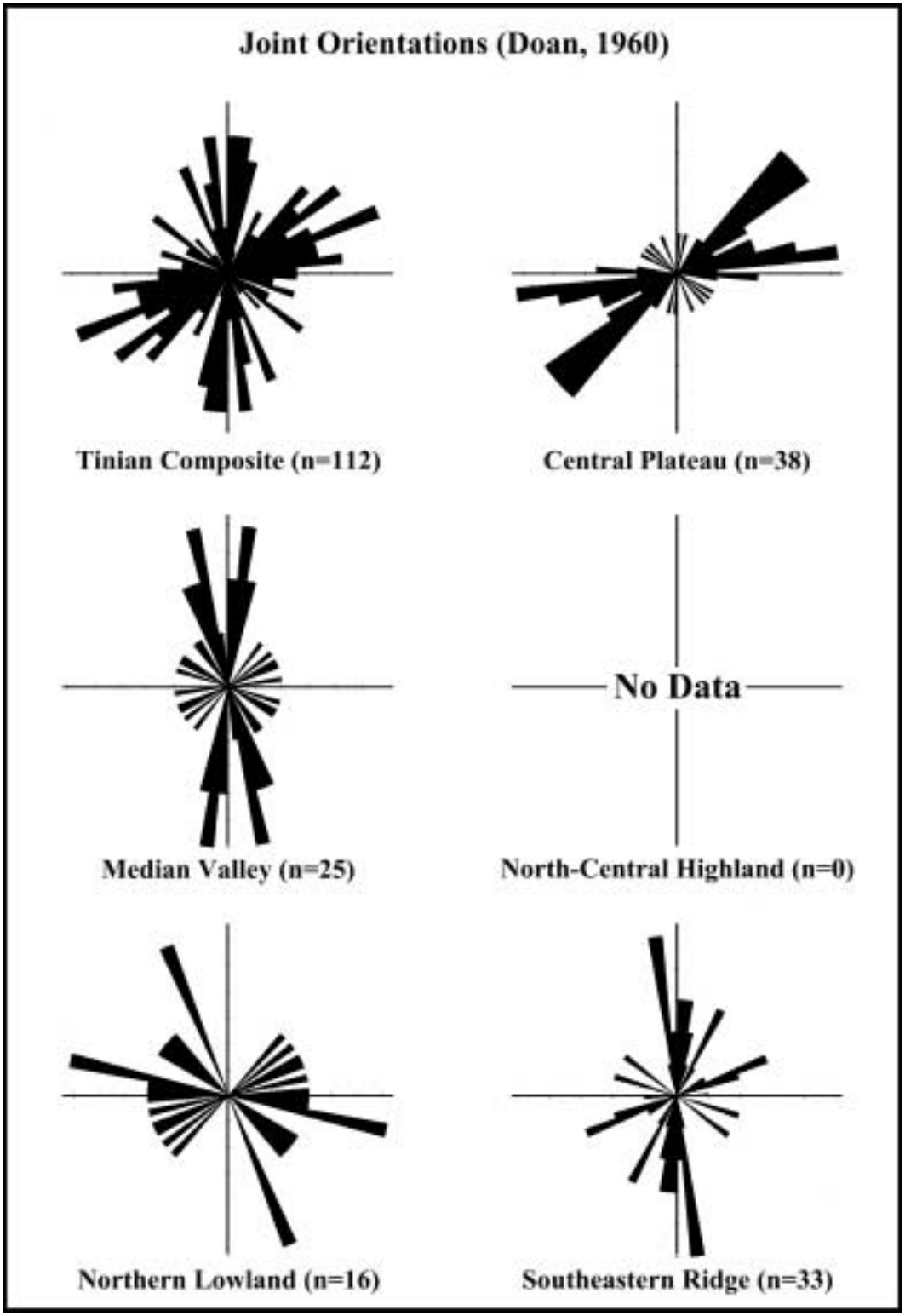

Figure 175: Rose diagrams of joint orientations (Doan et al., 1960) grouped by physiographic province.

Table 12: Fracture orientations measured during fieldwork grouped by physiographic province.

Central Plateau	Median Vally	North-Central Highland	Northern Lowland	Southeastern Ridge
Orientation	Orientation	Orientation	Orientation	Orientation
128	121.5		102	107
158.5	209.5		16	17
114.5	174		332	259
110	77.5		294	173
80	137		163	127
170.5	69		137	132
46	78		102	125
86	134		98	323
83.5	96		301	219
112	344		331	340
261	16.5		127	302
271	42		152	13
248	203		336	251
259	35		122	6
70	16.5		124	313
253	37.5		118	62
264	350.5		310	102
202	320.5		104	352
24	117		147	189
292	64.5		98	209
240	312.5		121	130
240	315		45	292
328	137		292	218
120	224		302	349
98	18.5		283	343
203.5	24		291	266
186	37		268	185
203.5	23.5		291.5	171
290.5	35		253	101
214.5	135.5		246	133
206.5	159.5		289	25
124	142		307.5	284
211	281		107	20
216	340		134	290
234	168		132	19
275.5	188.5		136.5	297
210.5	204		152.5	111
348	309.5		124.5	103
120.5	349		129	181
267	7		133	113
233	186		144	202
108	177		138	40
238.5	165		166	159
227	212		132	40
321.5	331		146.5	30
356	265		158	42
266	353		153	6
296	5.5		137	3
275	268.5		103	315
310	190		108	10
0	183.5		84	
51	219		48	
118	1.77		188	
281	182		186	
227	201		300.5	
66	224		278	

Table 12 (continued): Fracture orientations measured during fieldwork grouped by physiographic province.

Central Plateau	Median Vally	North-Central Highland	Northern Lowland	Southeastern Ridge
Orientation	Orientation	Orientation	Orientation	Orientation
124	175		183.5	
24	347		162.5	
321.5	306		203	
266	5		83	
299	352		91	
261	2		152	
5	3.5		192	
1	2		178	
43	316.5		167	
14	321		112	
0.5	266		171	
11	178		202	
43	185		51	
345	307		73	
64	331		209	
92.5	358.5		332	
149.5	2		203	
5	296		202	
243	197.5		39	
60	249		22	
247	332		211	
208	345		216	
62	75		37	
49	180		229	
238	20		97	
63	181		154	
288	186		204	
221	255		16	
284.5	336		146	
240.5	216.5		137.5	
327	9.5			
339	210			
346	305			
1	24			
60	331			
28	8			
356	65			
34	2			
336	61			
354	36			
2.5	93			
4.5	44			
265.5	28			
339.5	90			
333	21			
296	34			
327	65			
	65			
	51.5			
	6			

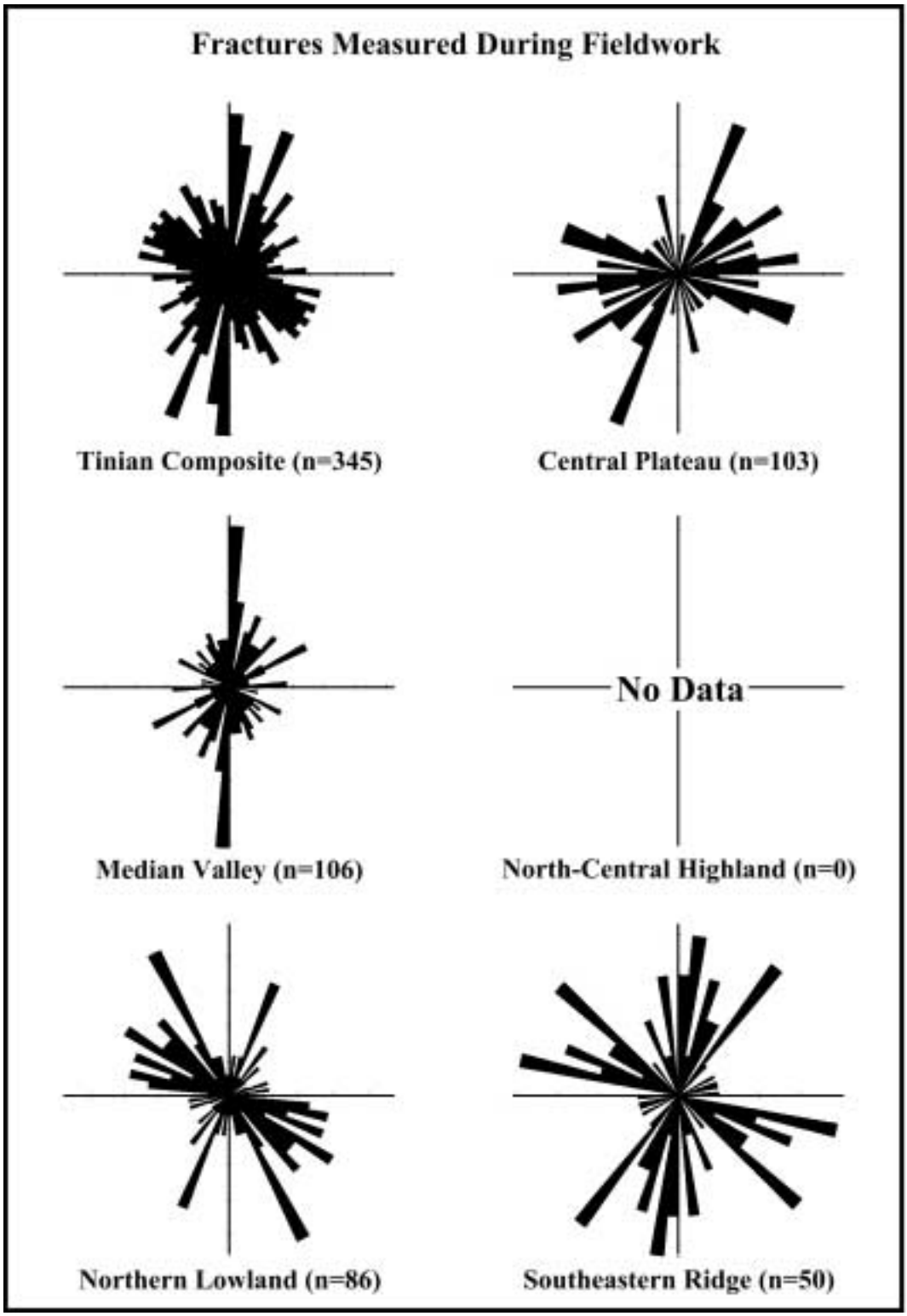

Figure 176: Rose diagrams of orientations of fractures measured during fieldwork grouped by physiographic province.

Table 13: Inland scarp segment orientations with segment length grouped by physiographic province.

Central Plateau		Median Valley		North-Central Highland		Northern Lowland		Southeastern Ridge	
Scarp Orientation	Segment Length (m)	Scarp Orientation	Segment Length (m)	Scarp Orientation	Segment Length (m)	Scarp Orientation	Segment Length (m)	Scarp Orientation	Segment Length (m)
142	174.2	22	348.4	7	406.5			179	271.0
100	116.1	338	116.1	350	309.7			147	193.5
125	154.8	0	96.8	9	271.0			113	251.6
92	154.8	343	212.9	19	348.4			70	212.9
100	251.6	9	154.8	25	406.5			8	116.1
2	290.3	29	290.3	43	154.8			43	174.2
310	116.1	61	135.5	350	174.2			92	58.1
268	135.5	48	271.0	299	522.6			21	38.7
310	58.1	324	154.8	314	309.7			39	193.5
275	116.1	1	367.7	279	135.5			7	58.1
240	77.4	68	96.8	41	154.8			34	212.9
293	135.5	42	96.8	4	174.2			49	116.1
270	58.1			26	271.0			229	232.3
242	271.0			4	193.5			223	193.5
298	503.2			47	96.8			227	135.5
15	309.7			2	58.1			223	251.6
8	96.8			314	251.6			218	193.5
35	212.9			308	425.8			224	174.2
32	232.3			356	96.8			221	135.5
123	348.4			334	193.5			227	232.3
98	290.3			289	116.1			233	251.6
104	290.3			335	348.4			267	154.8
71	735.5			6	290.3			310	193.5
88	367.7			33	329.0			6	116.1
59	96.8			4	135.5			13	174.2
100	387.1			54	174.2			352	348.4
77	212.9			22	406.5			29	77.4
72	503.2			36	251.6			4	135.5
				3	77.4			52	96.8
				69	483.9			90	116.1
								58	135.5
								18	174.2
								22	174.2
								35	387.1
								4	135.5
								50	580.6
								103	464.5
								129	251.6
								357	193.5
								330	522.6
								321	251.6
								5	329.0

Table 13 (continued): Inland scarp segment orientations with segment length grouped by physiographic province.

Central Plateau		Median Valley		North-Central Highland		Northern Lowland		Southeastern Ridge	
Scarp Orientation	Segment Length (m)	Scarp Orientation	Segment Length (m)	Scarp Orientation	Segment Length (m)	Scarp Orientation	Segment Length (m)	Scarp Orientation	Segment Length (m)
								351	483.9
								342	193.5
								330	309.7
								239	367.7
								224	445.2
								222	793.5
								307	348.4
								205	329.0
								207	329.0
								175	96.8
								229	174.2
								176	135.5
								213	212.9
								268	58.1
								243	154.8
								200	174.2
								234	135.5
								47	116.1
								352	271.0
								17	232.3
								335	212.9
								37	387.1
								331	154.8
								8	251.6
								350	271.0
								279	929.0
								2	445.2
								333	174.2
								2	116.1
								306	193.5
								324	135.5
								354	425.8
								59	193.5
								34	445.2
								14	619.4
								7	232.3
								21	329.0
								2	116.1
								337	135.5
								0	271.0
								1	174.2
								295	212.9
								88	329.7

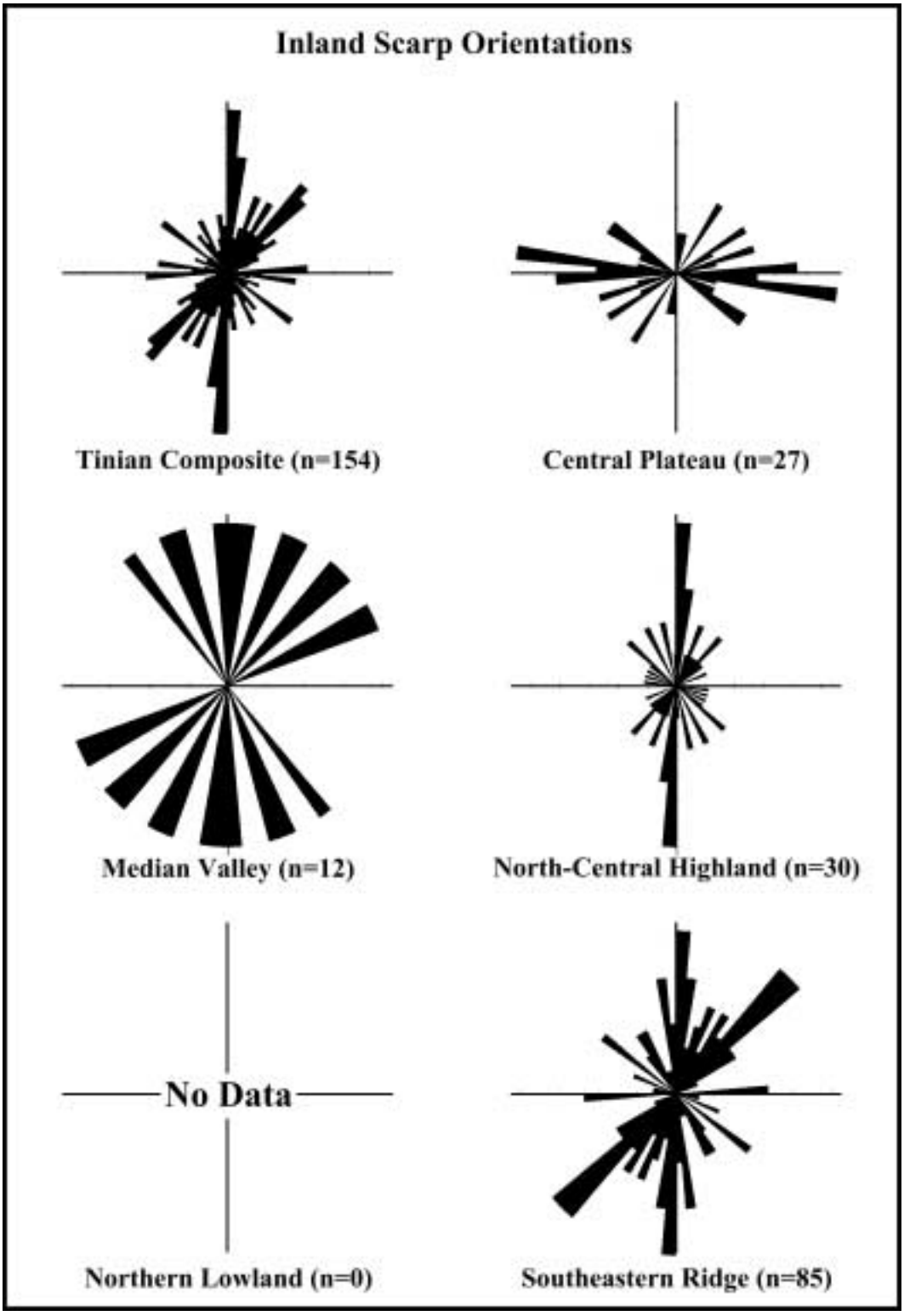

Figure 177: Rose diagrams of inland scarp orientations grouped by physiographic province.

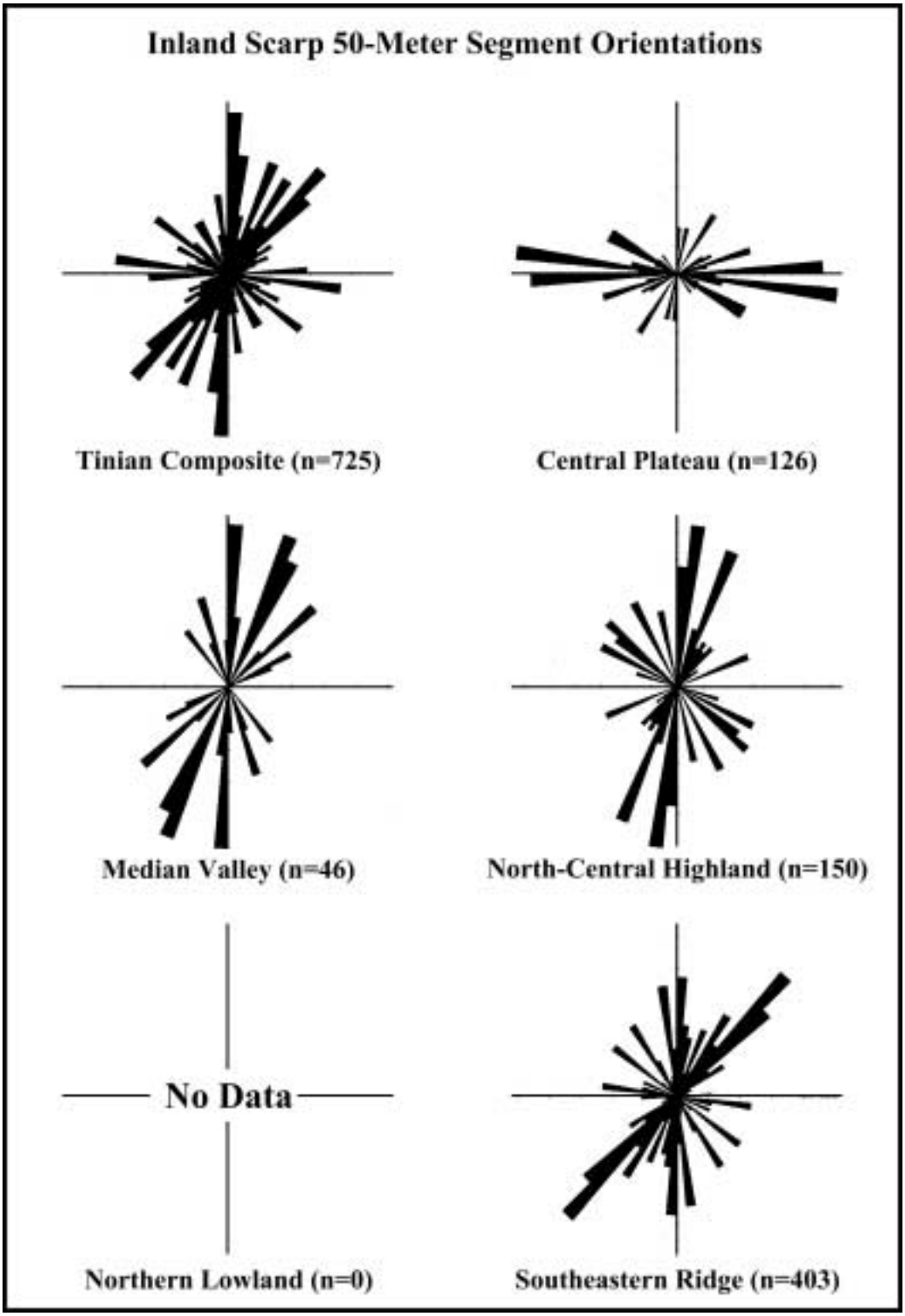

Figure 178: Rose diagrams of inland scarp, fifty-meter segment orientations grouped by physiographic province.

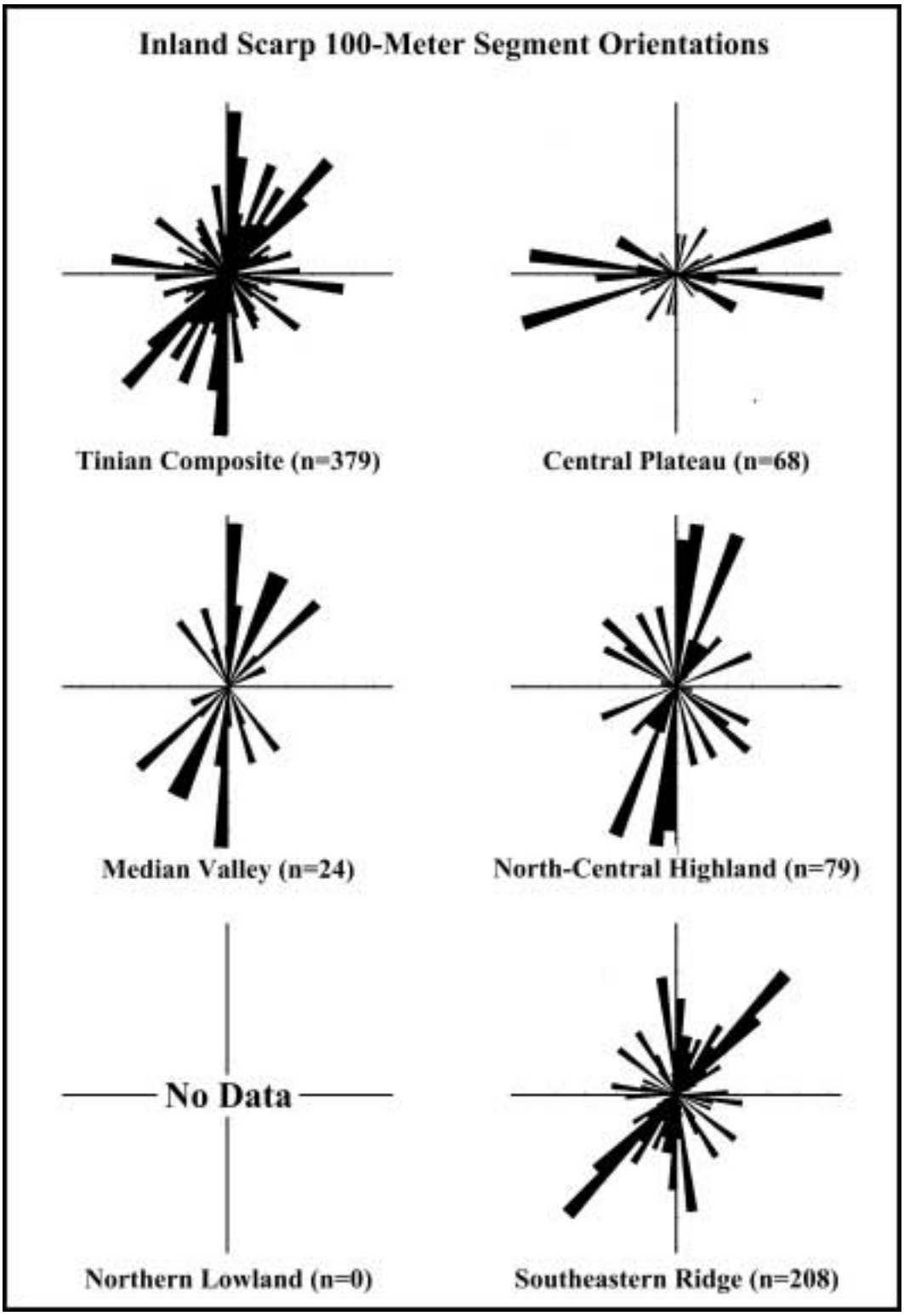

Figure 179: Rose diagrams of inland scarp, one hundred-meter segment orientations grouped by physiographic province.

Table 14: Coastal scarp segment orientations with segment length grouped by physiographic province.

Central Plateau		Median Valley		North-Central Highland		Northern Lowland		Southeastern Ridge	
Scarp Orientation	Segment Length (m)	Scarp Orientation	Segment Length (m)	Scarp Orientation	Segment Length (m)	Scarp Orientation	Segment Length (m)	Scarp Orientation	Segment Length (m)
8	77.4	158	193.5					93	193.5
63	174.2	122	116.1					77	116.1
90	212.9	118	193.5					91	367.7
65	96.8							138	232.3
90	212.9							111	116.1
112	309.7							151	561.3
135	174.2							188	135.5
168	154.8							162	116.1
193	154.8							124	251.6
94	77.4							162	135.5
147	212.9							190	174.2
101	193.5							189	483.9
203	116.1							191	251.6
216	251.6							225	96.8
216	154.8							149	58.1
193	38.7							197	77.4
226	212.9							196	212.9
261	58.1							187	271.0
228	116.1							194	387.1
223	290.3							177	96.8
218	77.4							211	135.5
242	116.1							186	212.9
220	77.4							211	367.7
268	77.4							226	271.0
180	38.7							190	58.1
192	116.1							258	96.8
141	116.1							119	96.8
115	193.5							186	96.8
176	212.9							148	290.3
227	96.8							175	116.1
204	116.1							165	77.4
185	212.9							210	116.1
187	464.5							151	58.1
223	367.7							242	96.8
254	77.4							213	212.9
242	193.5							212	309.7
285	232.3							155	77.4
313	96.8							206	174.2
216	135.5							82	77.4
175	58.1							185	232.3
202	271.0							194	212.9
206	425.8							161	483.9

Table 14 (continued): Coastal scarp segment orientations with segment length grouped by physiographic province.

Central Plateau		Median Valley		North-Central Highland		Northern Lowland		Southeastern Ridge	
Scarp Orientation	Segment Length (m)	Scarp Orientation	Segment Length (m)	Scarp Orientation	Segment Length (m)	Scarp Orientation	Segment Length (m)	Scarp Orientation	Segment Length (m)
130	77.4							155	212.9
183	96.8							168	193.5
236	193.5							103	174.2
184	77.4							167	77.4
196	329.7							234	116.1
98	193.5							150	77.4
143	174.2							201	77.4
186	96.8							286	290.3
103	38.7							232	96.8
144	135.5							286	212.9
183	96.8							234	425.8
221	232.3							263	174.2
235	77.4							212	541.9
192	96.8							162	135.5
201	271.0							146	116.1
185	96.8							187	174.2
158	116.1							224	271.0
121	135.5							218	309.7
103	174.2							204	387.1
123	96.8							216	251.6
90	58.1							165	58.1
50	77.4							225	58.1
80	58.1							270	77.4
								221	251.6
								243	271.0
								260	309.7
								283	251.6
								305	232.3
								321	96.8
								17	58.1
								296	58.1
								352	96.8
								310	77.4
								346	154.8
								16	154.8
								337	387.1
								11	271.0

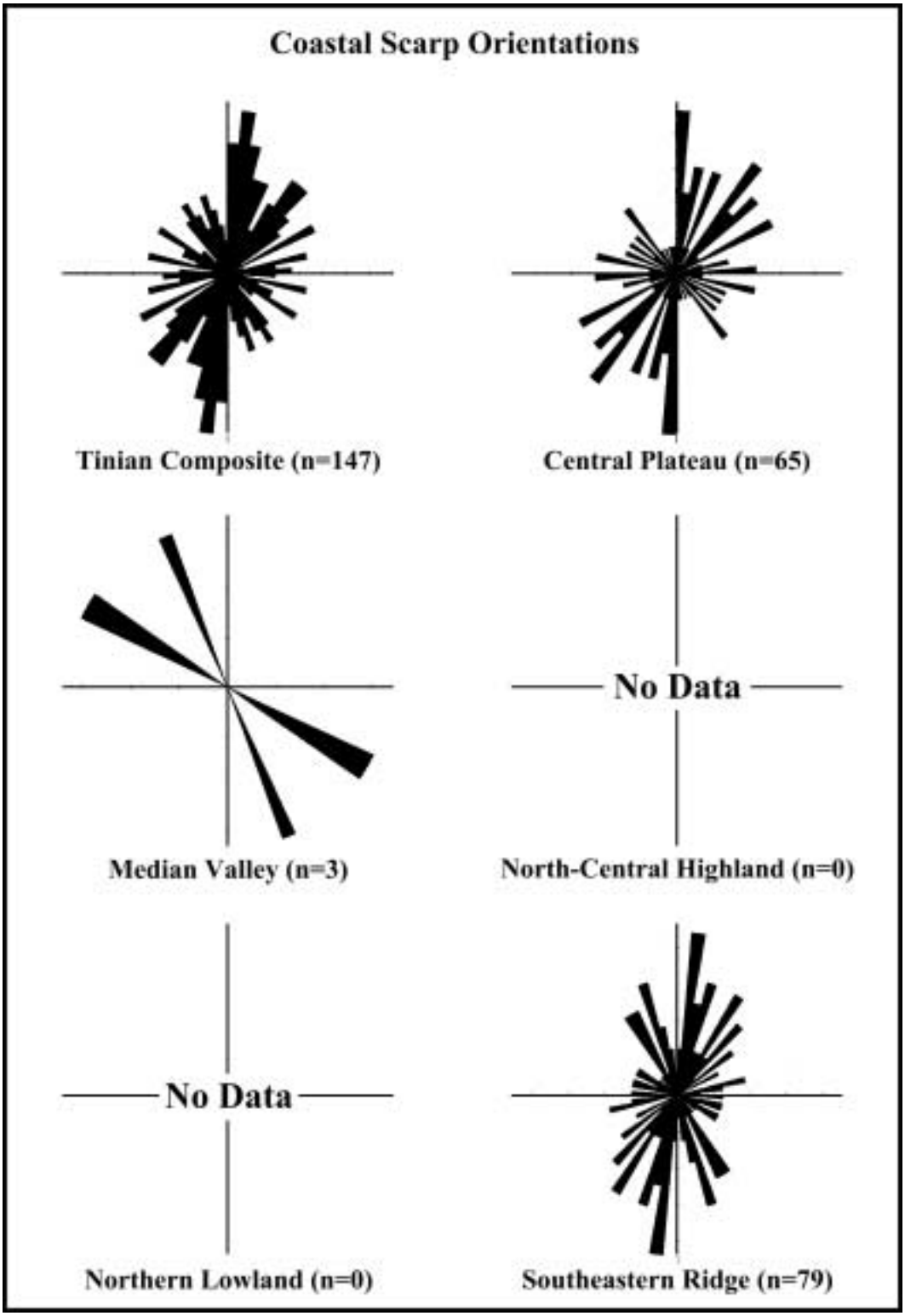

Figure 180: Rose diagrams of coastal scarp orientations grouped by physiographic province.

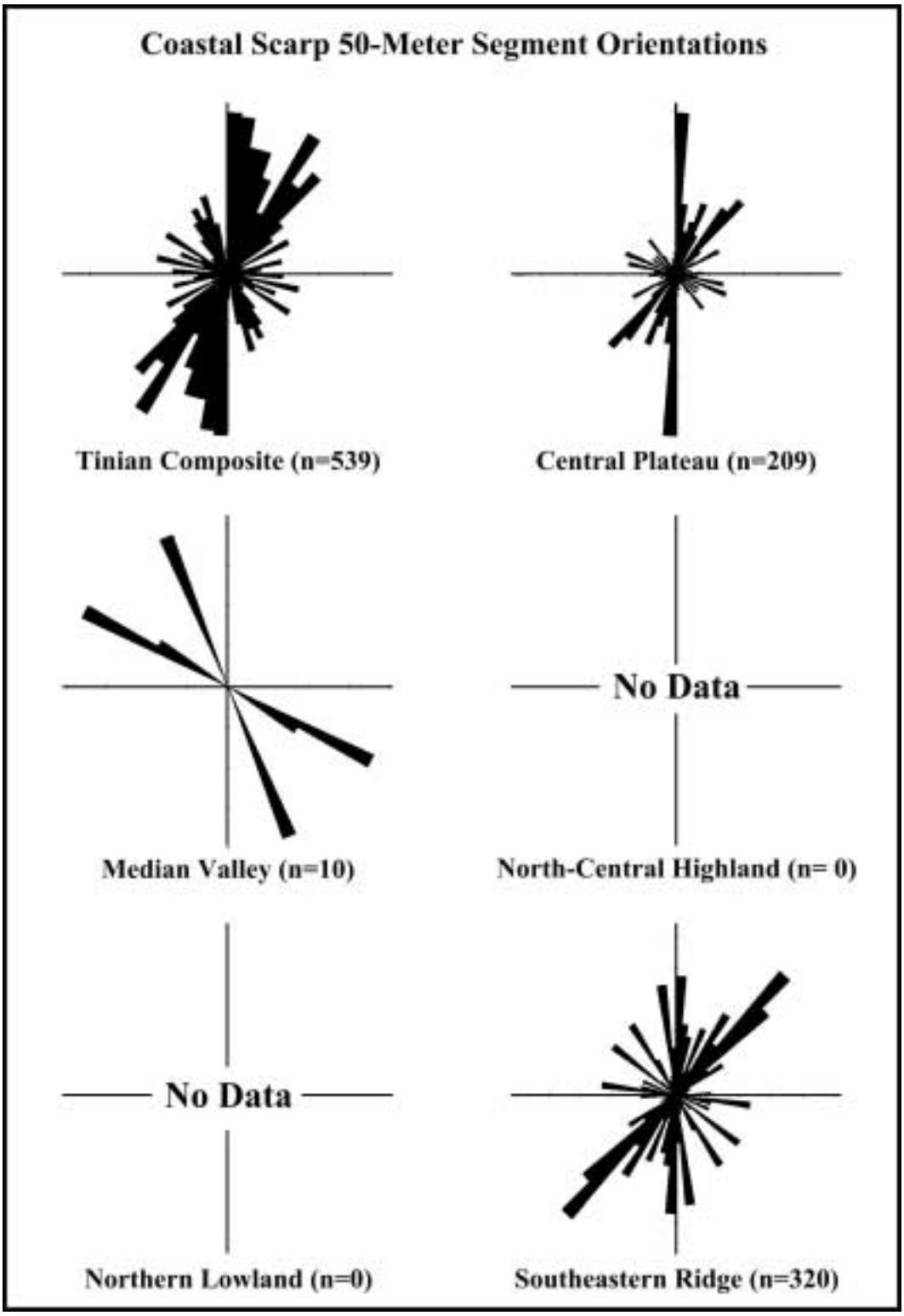

Figure 181: Rose diagrams of coastal scarp, fifty-meter segment orientations grouped by physiographic province.

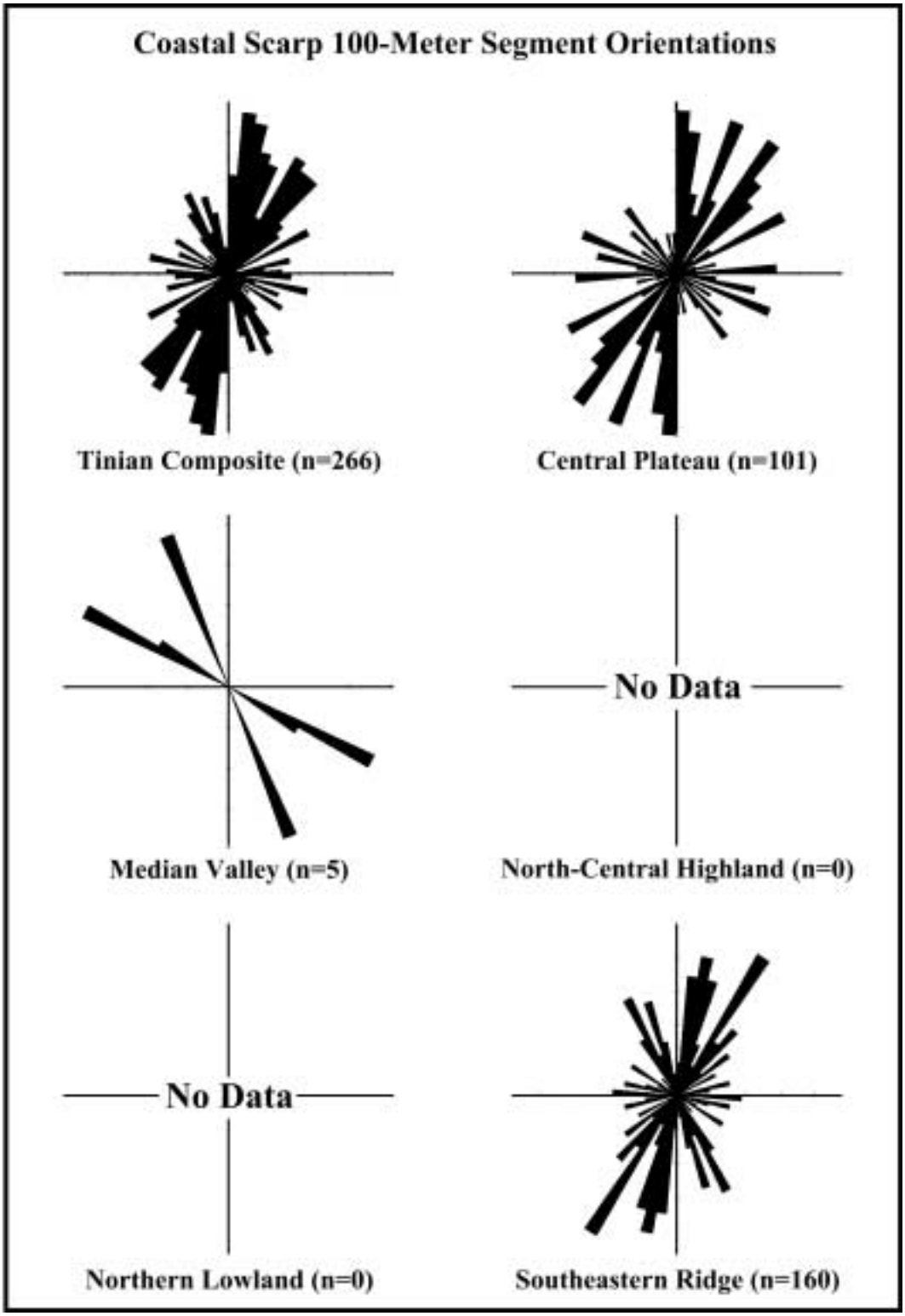

Figure 182: Rose diagrams of coastal scarp, one hundred-meter segment orientations grouped by physiographic province.

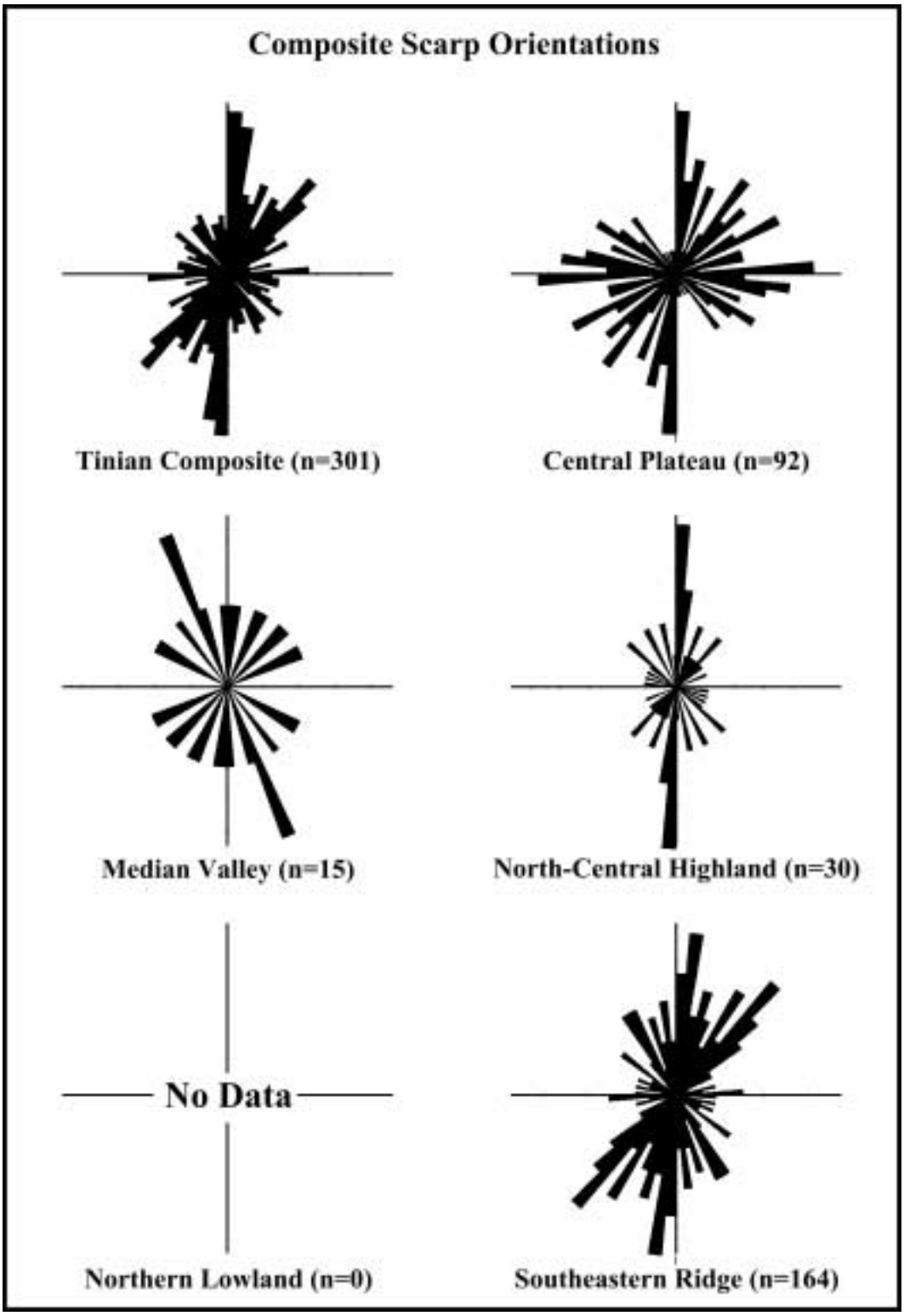

Figure 183: Rose diagrams of composite scarp orientations grouped by physiographic province.

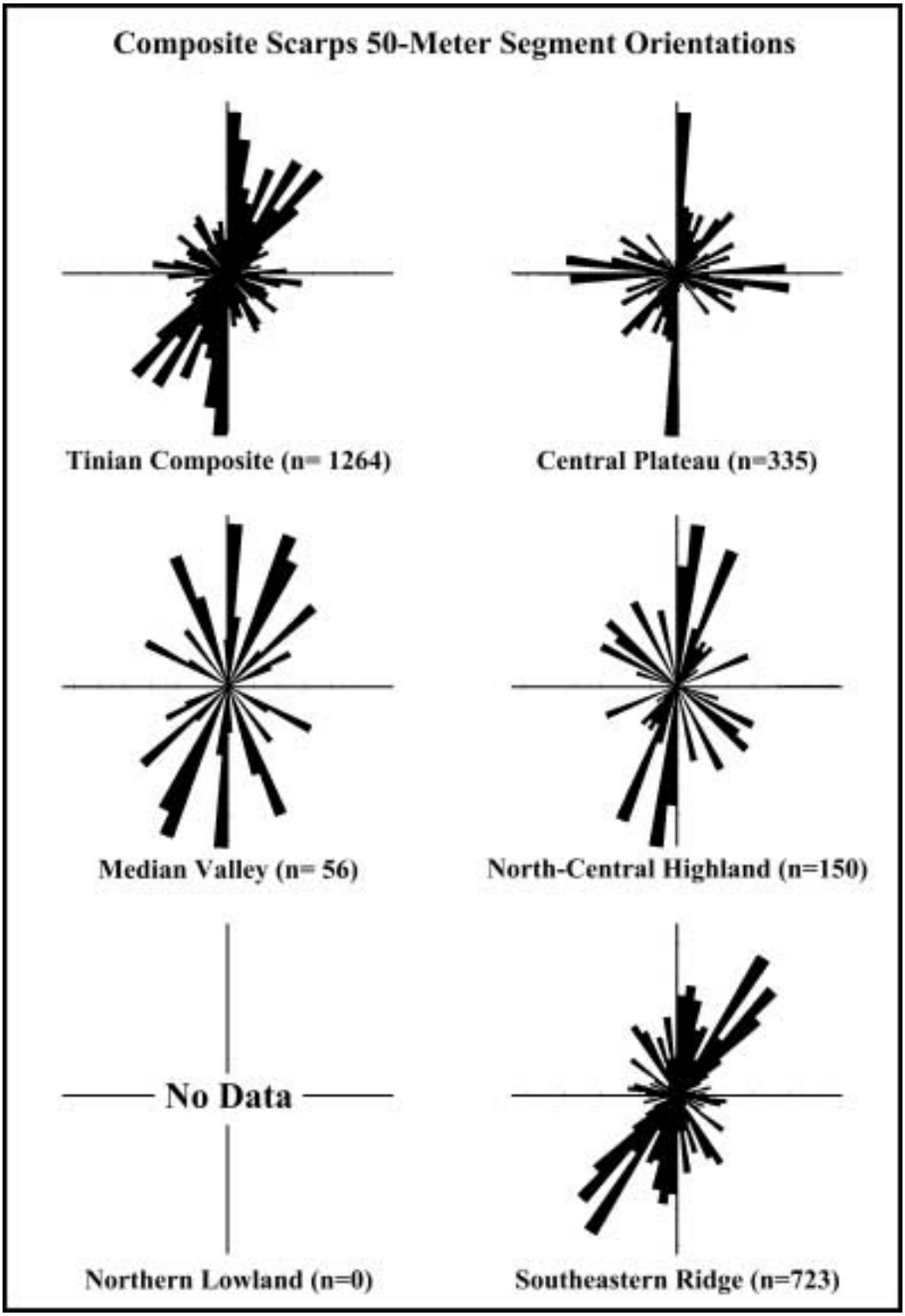

Figure 184: Rose diagrams of composite scarp, fifty-meter segment orientations grouped by physiographic province.

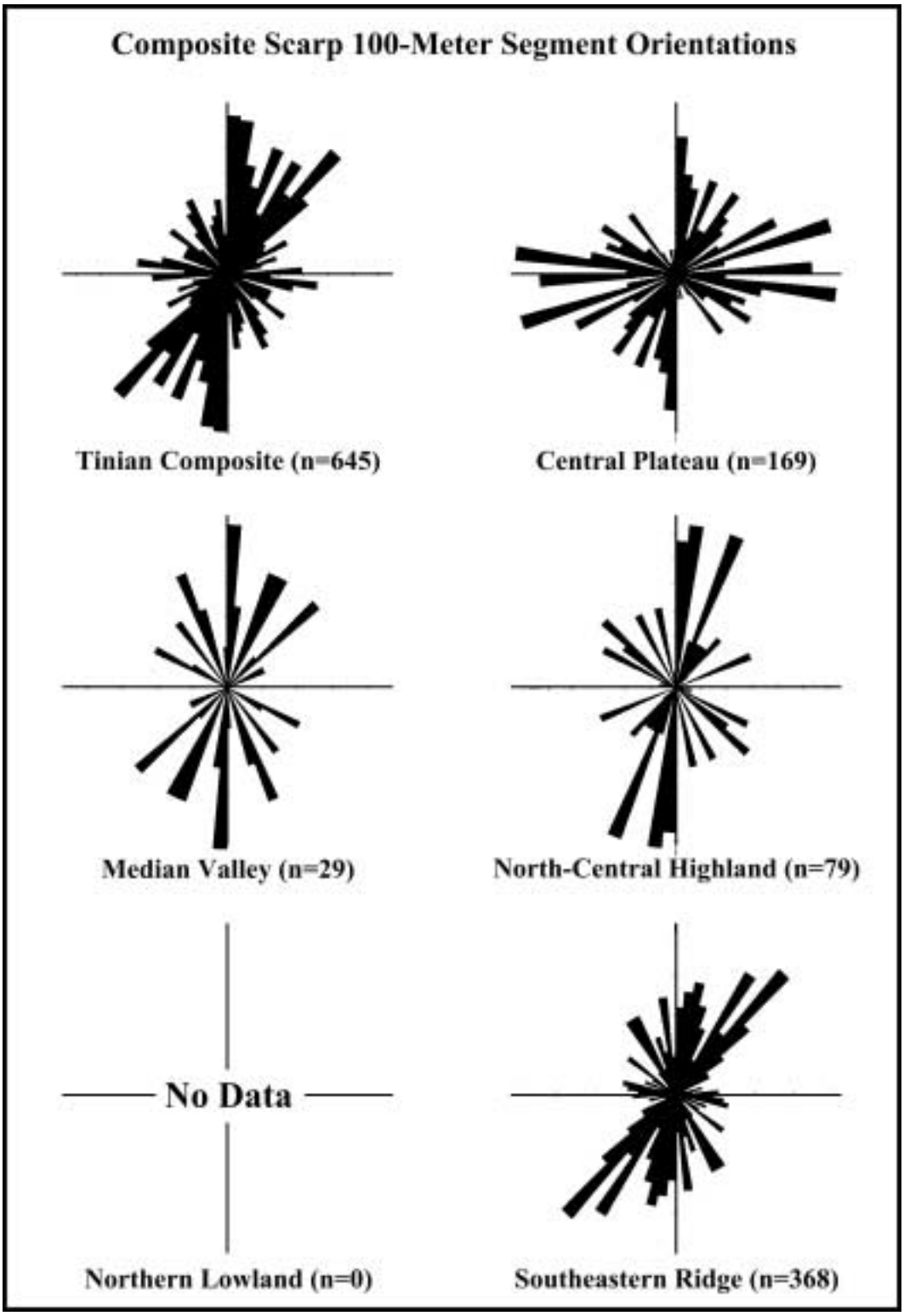

Figure 185: Rose diagrams of composite scarp, one hundred-meter segment orientations grouped by physiographic province.

Table 15: Coastline segment orientations with segment length grouped by physiographic province.

Central Plateau		Median Valley		North-Central Highland		Northern Lowland		Southeastern Ridge	
Coast Orientation	Segment Length (m)	Coast Orientation	Segment Length (m)	Coast Orientation	Segment Length (m)	Coast Orientation	Segment Length (m)	Coast Orientation	Segment Length (m)
195	367.7	105	116.1			15	58.1	93	193.5
183	309.7	138	135.5			55	426.8	77	116.1
180	96.8	168	77.4			53	212.9	91	367.7
113	77.4	103	116.1			40	426.8	138	232.3
168	135.5	138	271.0			42	987.1	111	116.1
139	193.5	198	212.9			43	445.2	151	561.3
236	58.1	189	329.0			47	193.5	188	135.5
18	69.7	171	193.5			16	232.3	162	116.1
177	154.8	179	232.3			36	212.9	124	251.6
198	154.8	142	135.5			61	135.5	162	135.5
180	193.5	119	232.3			76	96.8	190	174.2
150	174.2	97	135.5			54	329.0	196	483.9
151	96.8	122	832.3			37	483.9	191	251.6
107	251.6	124	154.8			44	232.3	225	96.8
58	116.1	141	329.0			64	309.7	149	58.1
131	96.8	155	677.4			53	251.6	197	77.4
84	135.5	176	135.5			22	193.5	190	212.9
234	135.5	127	58.1			37	329.0	167	271.0
151	58.1	150	154.8			40	522.6	194	387.1
8	77.4	176	154.8			46	483.9	177	96.8
63	174.2	201	580.6			50	212.9	211	135.5
90	212.9	201	348.4			74	116.1	196	212.9
65	96.8	180	251.6			117	116.1	211	367.7
90	212.9	122	116.1			140	271.0	226	271.0
112	309.7	174	135.5			139	271.0	190	58.1
135	174.2	233	58.1			197	58.1	256	96.8
168	154.8	159	77.4			119	96.8	119	96.8
193	154.8	117	38.7			145	406.5	160	96.8
94	77.4	163	58.1			128	154.8	148	290.3
147	212.9	163	58.1			153	425.8	175	116.1
181	193.5	211	77.4			162	445.2	168	77.4
203	116.1	181	212.9			177	193.5	210	116.1
218	251.6	146	96.8			186	348.4	151	58.1
218	154.8	171	96.8			192	445.2	242	96.8
193	38.7	249	38.7			187	135.5	213	212.9
226	212.9	170	464.5			199	174.2	212	309.7
261	58.1	166	212.9			178	290.3	155	77.4
226	116.1	117	135.5			174	271.0	206	174.2
223	290.3	167	348.4			169	193.5	82	77.4
218	77.4	136	174.2			156	174.2	185	232.3
242	116.1	176	77.4					194	212.9
220	77.4	135	135.5					181	483.9

Table 15 (continued): Coastline segment orientations with segment length grouped by physiographic province.

Central Plateau		Median Valley		North-Central Highland		Northern Lowland		Southeastern Ridge	
Coast Orientation	Segment Length (m)	Coast Orientation	Segment Length (m)	Coast Orientation	Segment Length (m)	Coast Orientation	Segment Length (m)	Coast Orientation	Segment Length (m)
258	77.4	166	154.8					156	212.9
180	38.7	165	135.5					168	193.5
192	116.1	152	212.9					103	174.2
141	116.1	158	193.5					167	77.4
115	193.5	122	116.1					234	116.1
176	212.9	118	193.5					150	77.4
227	96.8							201	77.4
204	116.1							286	290.3
185	212.9							232	96.8
187	464.5							286	212.9
223	367.7							234	425.8
254	77.4							263	174.2
242	193.5							212	541.9
285	232.3							182	135.5
313	96.8							146	116.1
216	135.5							187	174.2
175	58.1							224	271.0
202	271.0							218	309.7
206	425.8							204	387.1
130	77.4							216	251.6
183	96.8							165	58.1
236	193.5							225	58.1
184	77.4							270	77.4
196	309.7							221	251.6
98	193.5							243	271.0
143	174.2							260	309.7
186	96.8							283	251.6
103	38.7							306	232.3
144	135.5							321	96.8
183	96.8							17	58.1
221	232.3							296	58.1
235	77.4							352	96.8
192	96.8							310	77.4
201	271.0							346	154.8
185	96.8							16	154.8
158	116.1							337	387.1
121	135.5							11	271.0
103	174.2								
123	96.8								
90	58.1								
50	77.4								
80	58.1								

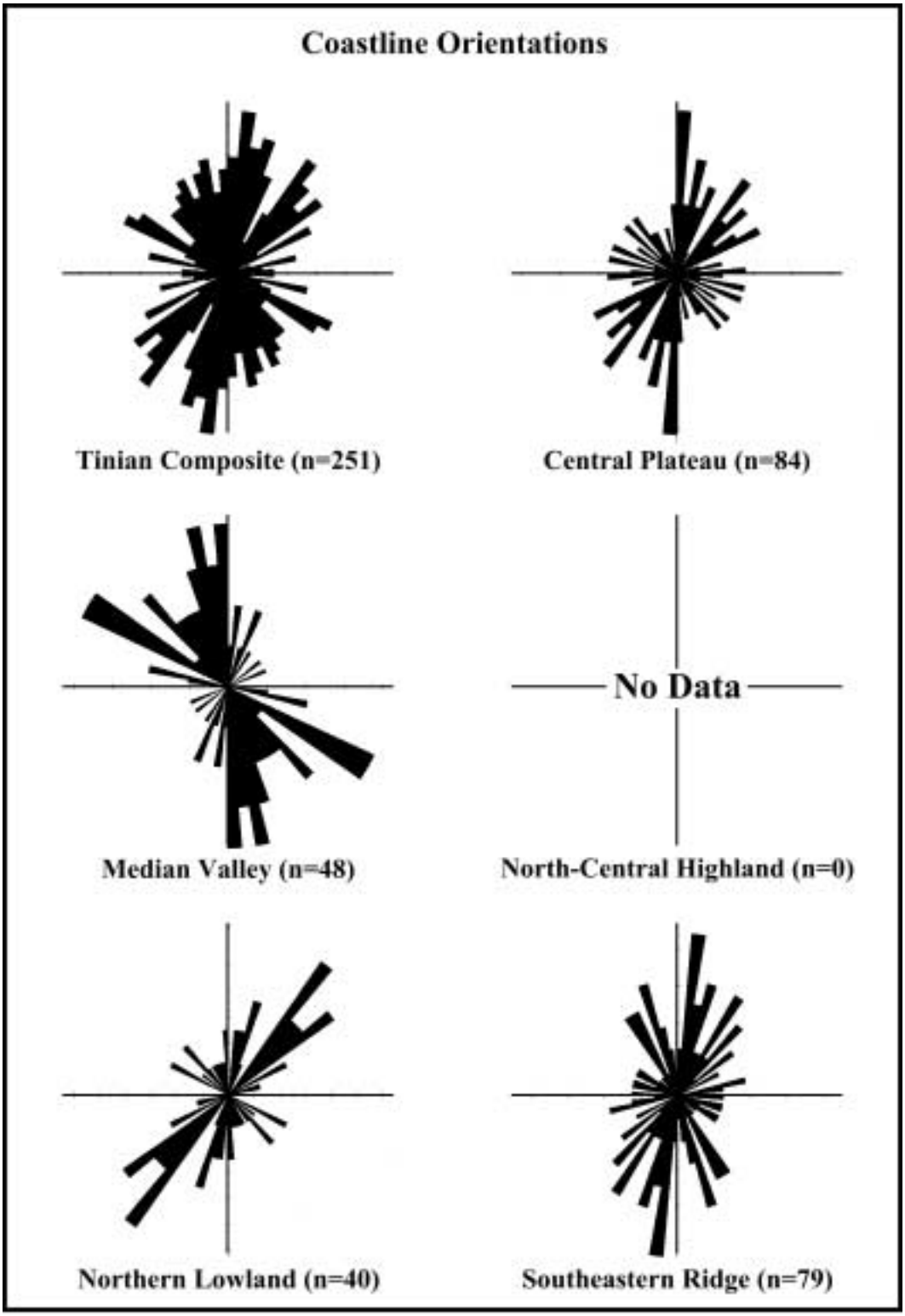

Figure 186: Rose diagrams of coastline orientations grouped by physiographic province.

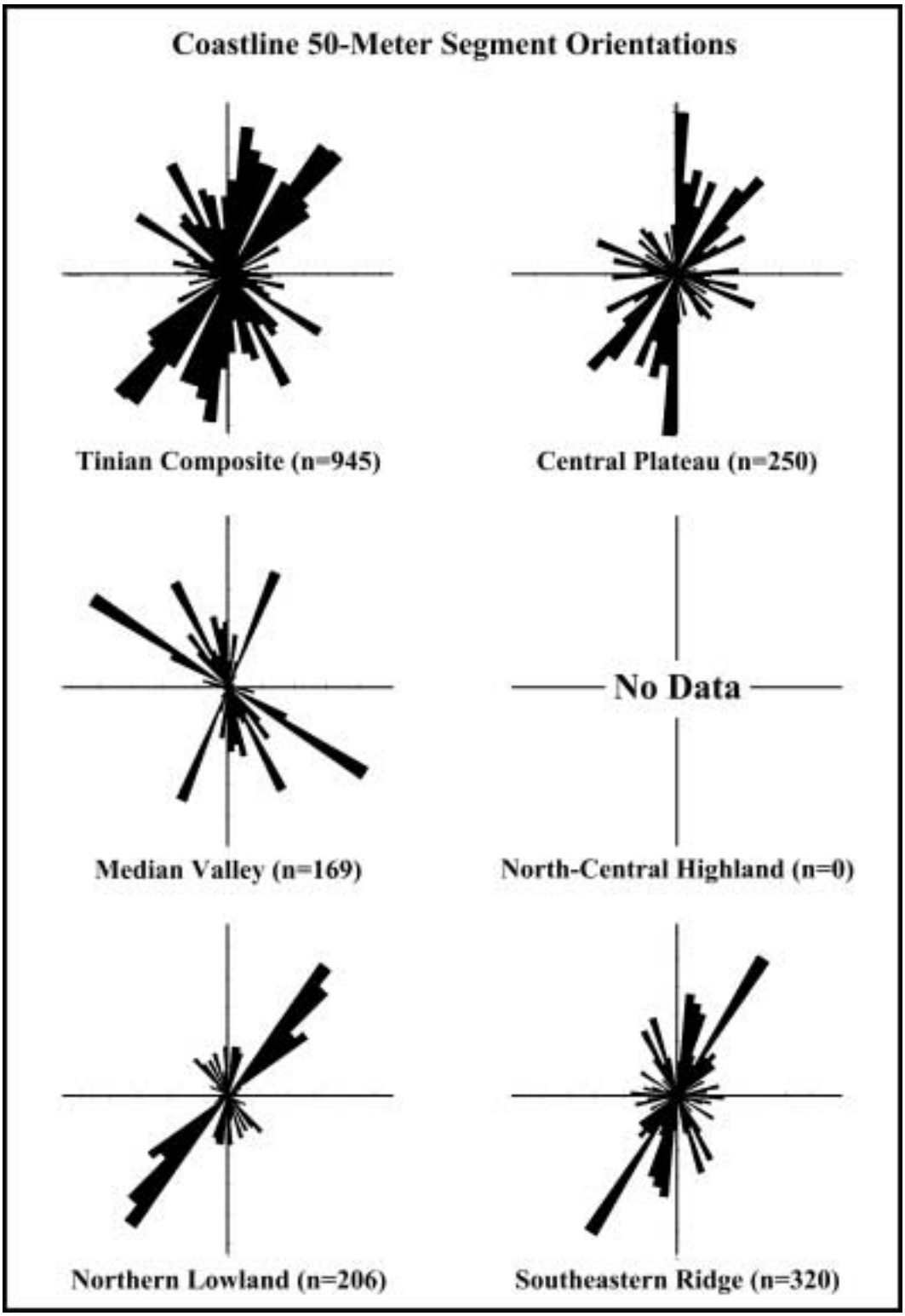

Figure 187: Rose diagrams of coastline, fifty-meter segment orientations grouped by physiographic province.

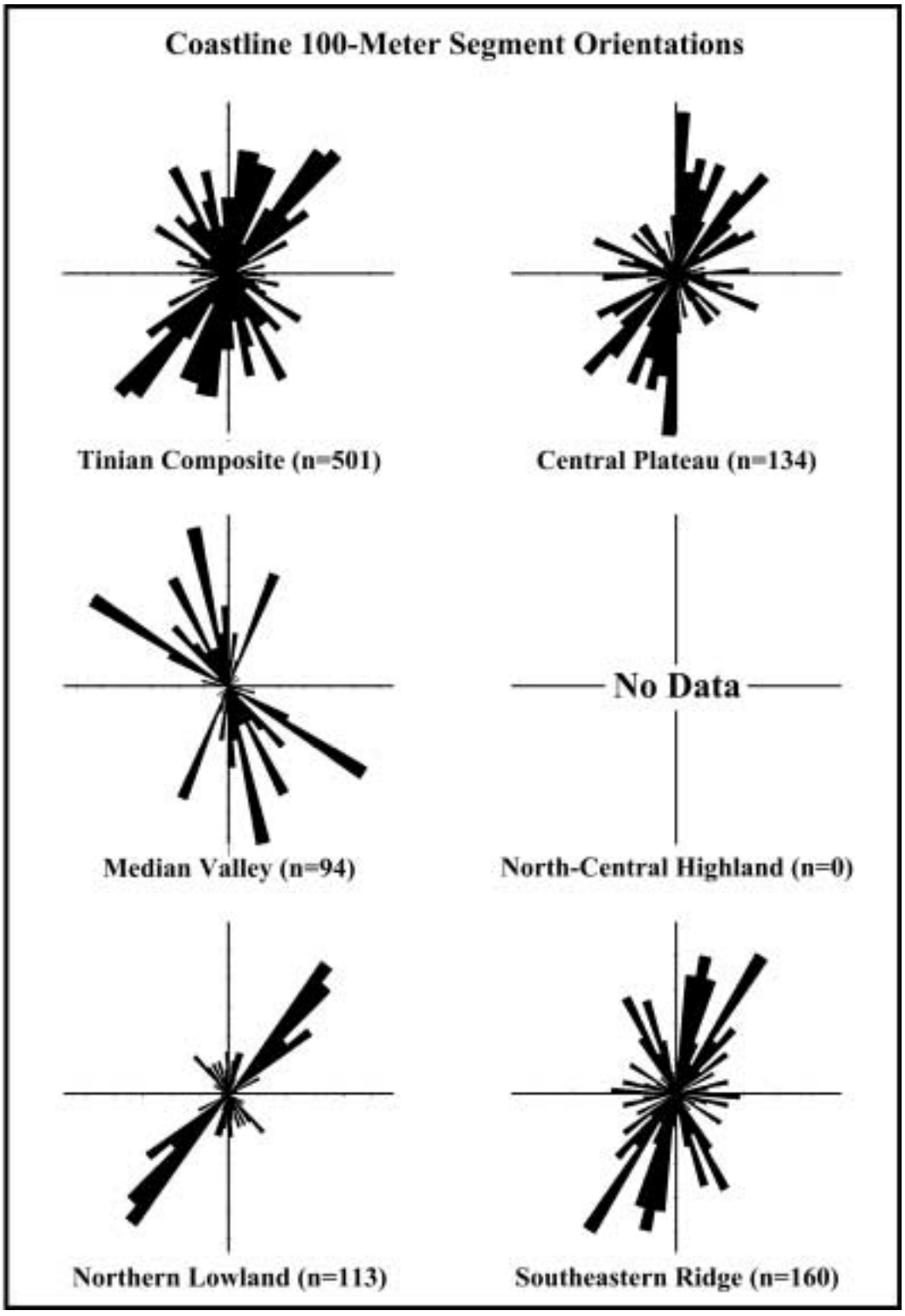

Figure 188: Rose diagrams of coastline, one hundred-meter segment orientations grouped by physiographic province.

APPENDIX D

STATISTICAL COMPARISON

Table 16: Legend for column and row headings used in statistical comparison data matrices (Tables 16 – 24).

Column and Row Headings	Category Type Used in Statitistical Comparison
1	Doan Fault Orientations
2	Doan Fault Orientations (50-meter segments)
3	Doan Fault Orientations (100-meter segments)
4	Doan Joint Orientations
5	Field Fracture Orientations
6	Inland Scarp Orientations
7	Inland Scarp Orientations (50-meter segments)
8	Inland Scarp Orientations (100-meter segments)
9	Coastal Scarp Orientations
10	Coastal Scarp Orientations (50-meter segments)
11	Coastal Scarp Orientations (100-meter segments)
12	All Scarp Orientations
13	All Scarp Orientations (50-meter segments)
14	All Scarp Orientations (50-meter segments)
15	Coastline Orientations
16	Coastline Orientation (50-meter segments)
17	Coastline Orientation (100-meter segments)
18	All Cave Types Orientations
19	All Cave Types Orientations (5-meter segments)
20	All Cave Types Orientations (10-meter segments)
21	Fissure Cave Orientations
22	Fissure Cave Orientations (5-meter segments)
23	Fissure Cave Orientations (10-meter segments)
24	Mixing Zone Cave Orientations
25	Mixing Zone Cave Orientations (5-meter segments)
26	Mixing Zone Cave Orientations (10-meter segments)
27	Cave Penetration Orientations
28	Cave Penetration Orientations (5-meter segments)
29	Cave Penetration Orientations (10-meter segments)
30	Entrance Width Orientations
31	Entrance Width Orientations (5-meter segments)
32	Entrance Width Orientations (10-meter segments)
33	Maximum Width Orientations
34	Maximum Width Orientations (5-meter segments)
35	Width Orientations (10-meter segments)

Table 17: Tinian Composite statistical comparison data matrix (see Table 16 for key to column and row headings. Bold text indicates the significantly similar comparisons ($P \leq 0.01$).

	1 n=313	2 n=3322	3 n=1661	4 n=112	5 n=345	6 n=154	7 n=725	8 n=379	9 n=147	10 n=539	11 n=266	12 n=301	13 n=1264	14 n=645	15 n=251	16 n=945	17 n=501
1	xxxx	36.660	0.716	**0.001**	**0.000**	0.356	0.073	0.231	0.121	0.019	0.430	0.175	0.176	0.297	**0.001**	0.013	0.019
2	xxxx	xxxx	1.000	**0.000**	**0.000**	0.058	**0.000**	**0.001**	**0.002**	**0.000**	**0.001**	**0.002**	**0.000**	**0.001**	**0.000**	**0.000**	**0.000**
3	xxxx	xxxx	xxxx	**0.000**	**0.000**	0.068	**0.000**	**0.003**	0.013	**0.000**	0.047	**0.004**	**0.000**	**0.002**	**0.000**	**0.000**	**0.000**
4	xxxx	xxxx	xxxx	xxxx	0.137	0.023	**0.005**	0.011	0.075	**0.000**	**0.001**	0.017	**0.000**	**0.002**	0.183	**0.002**	**0.008**
5	xxxx	xxxx	xxxx	xxxx	xxxx	0.009	**0.000**	**0.001**	0.109	**0.000**	**0.000**	0.004	**0.000**	**0.000**	0.304	**0.000**	**0.001**
6	xxxx	xxxx	xxxx	xxxx	xxxx	xxxx	1.000	1.000	0.923	0.136	0.665	1.000	0.895	0.984	0.041	0.221	0.134
7	xxxx	xxxx	xxxx	xxxx	xxxx	xxxx	xxxx	1.000	0.893	**0.001**	0.250	0.973	0.275	0.924	**0.004**	**0.000**	**0.000**
8	xxxx	xxxx	xxxx	xxxx	xxxx	xxxx	xxxx	xxxx	0.850	0.010	0.345	0.999	0.525	0.976	**0.007**	0.012	**0.008**
9	xxxx	xxxx	xxxx	xxxx	xxxx	xxxx	xxxx	xxxx	xxxx	0.220	0.860	1.000	0.720	0.849	0.297	0.778	0.624
10	xxxx	xxxx	xxxx	xxxx	xxxx	xxxx	xxxx	xxxx	xxxx	xxxx	0.964	0.038	0.106	0.052	**0.000**	**0.001**	**0.003**
11	xxxx	xxxx	xxxx	xxxx	xxxx	xxxx	xxxx	xxxx	xxxx	xxxx	xxxx	0.564	0.772	0.855	0.015	0.050	0.048
12	xxxx	xxxx	xxxx	xxxx	xxxx	xxxx	xxxx	xxxx	xxxx	xxxx	xxxx	xxxx	0.663	0.993	0.053	0.175	0.103
13	xxxx	xxxx	xxxx	xxxx	xxxx	xxxx	xxxx	xxxx	xxxx	xxxx	xxxx	xxxx	xxxx	0.995	**0.001**	**0.000**	**0.000**
14	xxxx	xxxx	xxxx	xxxx	xxxx	xxxx	xxxx	xxxx	xxxx	xxxx	xxxx	xxxx	xxxx	xxxx	**0.003**	**0.006**	**0.007**
15	xxxx	xxxx	xxxx	xxxx	xxxx	xxxx	xxxx	xxxx	xxxx	xxxx	xxxx	xxxx	xxxx	xxxx	xxxx	0.099	0.313
16	xxxx	xxxx	xxxx	xxxx	xxxx	xxxx	xxxx	xxxx	xxxx	xxxx	xxxx	xxxx	xxxx	xxxx	xxxx	xxxx	1.000
17	xxxx	xxxx	xxxx	xxxx	xxxx	xxxx	xxxx	xxxx	xxxx	xxxx	xxxx	xxxx	xxxx	xxxx	xxxx	xxxx	xxxx

	18 n=146	19 n=1277	20 n=614	21 n=18	22 n=297	23 n=135	24 n=128	25 n=980	26 n=480	27 n=118	28 n=369	29 n=190	30 n=107	31 n=324	32 n=163	33 n=118	34 n=407	35 n=208
1	**0.000**	**0.000**	**0.000**	0.030	**0.000**	**0.000**	**0.000**	**0.000**	**0.000**	**0.000**	**0.000**	**0.000**	0.148	**0.000**	**0.001**	0.016	**0.000**	**0.000**
2	**0.000**	**0.000**	**0.000**	**0.009**	**0.000**	**0.000**	**0.000**	**0.000**	**0.000**	**0.000**	**0.000**	**0.000**	0.019	**0.000**	**0.000**	**0.000**	**0.000**	**0.000**
3	**0.000**	**0.000**	**0.000**	**0.009**	**0.000**	**0.000**	**0.000**	**0.000**	**0.000**	**0.000**	**0.000**	**0.000**	0.022	**0.000**	**0.000**	**0.000**	**0.000**	**0.000**
4	0.087	0.223	0.524	0.647	0.126	0.005	0.032	0.019	0.074	0.019	**0.005**	0.021	0.291	0.132	0.201	0.689	0.179	0.262
5	0.033	**0.006**	0.011	0.536	**0.000**	**0.000**	0.043	0.023	0.106	0.182	**0.001**	0.014	0.039	0.098	0.533	0.221	0.323	0.669
6	**0.000**	**0.000**	**0.000**	0.068	**0.000**	**0.000**	**0.000**	**0.000**	**0.000**	**0.000**	**0.000**	**0.000**	0.557	0.043	0.168	0.181	0.052	0.052
7	**0.000**	**0.000**	**0.000**	0.053	**0.000**	**0.000**	**0.000**	**0.000**	**0.000**	**0.000**	**0.000**	**0.000**	0.590	**0.000**	**0.020**	0.106	**0.000**	**0.010**
8	**0.000**	**0.000**	**0.000**	0.061	**0.000**	**0.000**	**0.000**	**0.000**	**0.000**	**0.000**	**0.000**	**0.000**	0.751	**0.002**	**0.042**	0.218	**0.004**	0.014
9	**0.001**	**0.000**	**0.000**	0.137	**0.000**	**0.000**	**0.001**	**0.001**	**0.002**	**0.002**	**0.000**	**0.001**	0.869	0.123	0.340	0.508	0.215	0.317
10	**0.000**	**0.000**	**0.000**	0.017	**0.000**	**0.000**	**0.000**	**0.000**	**0.000**	**0.000**	**0.000**	**0.000**	0.040	**0.000**	**0.000**	**0.002**	**0.000**	**0.000**
11	**0.000**	**0.000**	**0.000**	0.042	**0.000**	**0.000**	**0.000**	**0.000**	**0.000**	**0.000**	**0.000**	**0.000**	0.296	**0.000**	**0.006**	0.040	**0.000**	**0.004**
12	**0.000**	**0.000**	**0.000**	0.082	**0.000**	**0.000**	**0.000**	**0.000**	**0.000**	**0.000**	**0.000**	**0.000**	0.686	0.013	0.115	0.237	0.028	0.088
13	**0.000**	**0.000**	**0.000**	0.031	**0.000**	**0.000**	**0.000**	**0.000**	**0.000**	**0.000**	**0.000**	**0.000**	0.219	**0.000**	**0.001**	0.021	**0.000**	**0.000**
14	**0.000**	**0.000**	**0.000**	0.047	**0.000**	**0.000**	**0.000**	**0.000**	**0.000**	**0.000**	**0.000**	**0.000**	0.460	**0.000**	**0.008**	0.083	**0.000**	**0.003**
15	**0.007**	**0.003**	**0.005**	0.295	**0.000**	**0.000**	**0.008**	**0.005**	0.013	0.015	**0.000**	**0.009**	0.069	0.222	0.584	0.123	0.185	0.627
16	**0.000**	**0.000**	**0.000**	0.071	**0.000**	**0.000**	**0.000**	**0.000**	**0.000**	**0.000**	**0.000**	**0.000**	**0.000**	0.123	0.018	0.052	**0.000**	**0.009**
17	**0.000**	**0.000**	**0.000**	0.083	**0.000**	**0.000**	**0.000**	**0.000**	**0.000**	**0.000**	**0.000**	**0.000**	0.092	**0.002**	0.049	0.117	**0.004**	0.031

Table 18: Central Plateau statistical comparison data matrix (see Table 16 for key to column and row headings. Bold text indicates the significantly similar comparisons ($P \leq 0.01$).

	1 n=94	2 n=944	3 n=472	4 n=38	5 n=183	6 n=27	7 n=126	8 n=68	9 n=65	10 n=209	11 n=101	12 n=92	13 n=335	14 n=169	15 n=84	16 n=250	17 n=134
1	xxxx	0.998	0.999	**0.000**	**0.000**	**0.000**	**0.000**	**0.000**	**0.005**	0.013	**0.005**	**0.000**	**0.000**	**0.000**	**0.001**	**0.000**	**0.001**
2	xxxx	xxxx	1.000	**0.000**	**0.000**	**0.000**	**0.000**	**0.000**	**0.000**	**0.000**	**0.000**	**0.000**	**0.000**	**0.000**	**0.000**	**0.000**	**0.000**
3	xxxx	xxxx	xxxx	**0.000**	**0.000**	**0.000**	**0.000**	**0.000**	**0.000**	**0.000**	**0.000**	**0.000**	**0.000**	**0.000**	**0.000**	**0.000**	**0.000**
4	xxxx	xxxx	xxxx	xxxx	0.042	0.020	**0.000**	**0.004**	0.047	**0.000**	**0.010**	0.120	0.019	0.053	0.052	**0.010**	**0.010**
5	xxxx	xxxx	xxxx	xxxx	xxxx	0.496	0.008	0.018	0.103	**0.000**	0.012	0.579	0.038	0.366	0.129	**0.003**	**0.009**
6	xxxx	xxxx	xxxx	xxxx	xxxx	xxxx	0.980	1.000	0.026	**0.000**	0.006	0.185	0.050	0.250	0.026	**0.003**	**0.005**
7	xxxx	xxxx	xxxx	xxxx	xxxx	xxxx	xxxx	0.912	**0.000**	**0.000**	**0.000**	**0.002**	**0.000**	**0.000**	**0.000**	**0.000**	**0.000**
8	xxxx	xxxx	xxxx	xxxx	xxxx	xxxx	xxxx	xxxx	**0.000**	**0.000**	**0.000**	**0.008**	**0.000**	**0.010**	**0.000**	**0.000**	**0.000**
9	xxxx	xxxx	xxxx	xxxx	xxxx	xxxx	xxxx	xxxx	xxxx	0.337	1.000	0.848	0.912	0.439	1.000	0.999	1.000
10	xxxx	xxxx	xxxx	xxxx	xxxx	xxxx	xxxx	xxxx	xxxx	xxxx	0.649	0.009	**0.002**	**0.000**	0.094	0.166	0.460
11	xxxx	xxxx	xxxx	xxxx	xxxx	xxxx	xxxx	xxxx	xxxx	xxxx	xxxx	0.385	0.378	0.085	0.941	0.984	1.000
12	xxxx	xxxx	xxxx	xxxx	xxxx	xxxx	xxxx	xxxx	xxxx	xxxx	xxxx	xxxx	0.943	1.000	0.836	0.252	0.330
13	xxxx	xxxx	xxxx	xxxx	xxxx	xxxx	xxxx	xxxx	xxxx	xxxx	xxxx	xxxx	xxxx	0.609	0.360	0.184	0.329
14	xxxx	xxxx	xxxx	xxxx	xxxx	xxxx	xxxx	xxxx	xxxx	xxxx	xxxx	xxxx	xxxx	xxxx	0.443	0.019	0.053
15	xxxx	xxxx	xxxx	xxxx	xxxx	xxxx	xxxx	xxxx	xxxx	xxxx	xxxx	xxxx	xxxx	xxxx	xxxx	0.980	0.969
16	xxxx	xxxx	xxxx	xxxx	xxxx	xxxx	xxxx	xxxx	xxxx	xxxx	xxxx	xxxx	xxxx	xxxx	xxxx	xxxx	1.000
17	xxxx	xxxx	xxxx	xxxx	xxxx	xxxx	xxxx	xxxx	xxxx	xxxx	xxxx	xxxx	xxxx	xxxx	xxxx	xxxx	xxxx

	18 n=51	19 n=326	20 n=134	21 n=5	22 n=24	23 n=12	24 n=46	25 n=302	26 n=122	27 n=42	28 n=116	29 n=54	30 n=40	31 n=105	32 n=59	33 n=42	34 n=140	35 n=72
1	**0.000**	**0.000**	**0.000**	0.120	**0.000**	**0.007**	**0.000**	**0.000**	**0.000**	**0.001**	**0.000**	**0.000**	**0.000**	**0.000**	**0.000**	**0.000**	**0.000**	**0.000**
2	**0.000**	**0.000**	**0.000**	0.098	**0.000**	**0.003**	**0.000**	**0.000**	**0.000**	**0.000**	**0.000**	**0.000**	**0.000**	**0.000**	**0.000**	**0.000**	**0.000**	**0.000**
3	**0.000**	**0.000**	**0.000**	0.099	**0.000**	**0.003**	**0.000**	**0.000**	**0.000**	**0.000**	**0.000**	**0.000**	**0.000**	**0.000**	**0.000**	**0.000**	**0.000**	**0.000**
4	0.207	**0.006**	0.023	0.895	0.037	0.449	0.173	**0.006**	0.020	0.056	**0.003**	0.014	0.037	**0.000**	**0.002**	**0.004**	**0.000**	**0.000**
5	0.961	0.725	0.851	0.733	0.110	0.898	0.993	0.746	0.875	0.659	0.396	0.784	0.788	0.185	0.458	0.314	0.055	0.159
6	0.477	0.525	0.467	0.534	0.928	0.959	0.609	0.478	0.412	0.406	0.282	0.336	0.846	0.225	0.553	0.349	0.164	0.224
7	0.028	**0.004**	0.022	0.323	0.791	0.674	0.072	**0.003**	0.024	0.020	**0.004**	0.040	0.419	**0.009**	0.156	0.089	**0.002**	0.017
8	0.190	0.019	0.045	0.586	0.791	0.890	0.187	0.014	0.047	0.053	0.018	0.053	0.513	0.028	0.185	0.123	0.012	0.038
9	0.162	0.017	0.025	0.551	0.006	0.233	0.236	0.023	0.040	0.423	0.159	0.204	0.071	**0.004**	0.079	0.021	**0.008**	0.027
10	**0.001**	**0.000**	**0.000**	0.233	**0.000**	0.032	**0.002**	**0.000**	**0.000**	0.029	**0.000**	**0.001**	**0.000**	**0.000**	**0.000**	**0.000**	**0.000**	**0.000**
11	0.040	**0.000**	**0.001**	0.412	**0.001**	0.128	0.066	**0.000**	**0.002**	0.295	0.040	0.056	0.017	**0.000**	0.014	**0.003**	**0.000**	**0.003**
12	0.435	0.156	0.245	0.734	0.040	0.502	0.573	0.192	0.270	0.330	0.081	0.349	0.360	0.018	0.185	0.110	0.006	0.028
13	0.083	**0.000**	**0.004**	0.541	**0.007**	0.252	0.119	**0.000**	**0.008**	0.148	**0.005**	0.085	0.171	**0.000**	0.056	0.033	**0.000**	**0.002**
14	0.386	0.063	0.205	0.747	0.051	0.527	0.536	0.117	0.203	0.226	0.023	0.221	0.358	**0.003**	0.111	0.061	**0.001**	**0.008**
15	0.117	0.016	0.038	0.584	**0.007**	0.310	0.182	0.021	0.045	0.723	0.150	0.150	0.101	**0.005**	0.113	0.030	**0.010**	0.038
16	0.020	**0.000**	**0.000**	0.479	**0.001**	0.157	0.039	**0.000**	**0.000**	0.267	0.011	0.031	0.015	**0.000**	**0.010**	**0.002**	**0.000**	**0.001**
17	0.018	**0.000**	**0.001**	0.414	**0.001**	0.155	0.036	**0.000**	**0.001**	0.267	0.011	0.024	0.016	**0.000**	0.013	**0.003**	**0.000**	**0.002**

Table 19: Median Valley statistical comparison data matrix (see Table 16 for key to column and row headings. Bold text indicates the significantly similar comparisons ($P \leq 0.01$).

	1	2	3	4	5	6	7	8	9	10	11	12	13	14	15	16	17
	n=50	n=686	n=343	n=25	n=106	n=12	n=46	n=24	n=3	n=10	n=5	n=15	n=56	n=29	n=48	n=169	n=94
1	xxxx	0.302	0.340	0.653	0.070	0.310	**0.001**	0.011	0.479	**0.001**	0.206	0.670	0.014	0.061	0.054	0.048	0.039
2	xxxx	xxxx	1.000	0.162	**0.000**	0.292	**0.000**	**0.001**	0.204	0.031	0.045	0.586	**0.000**	**0.007**	**0.000**	**0.000**	**0.000**
3	xxxx	xxxx	xxxx	0.177	**0.000**	0.301	**0.000**	**0.001**	0.206	**0.001**	0.046	0.600	**0.000**	**0.009**	**0.000**	**0.000**	**0.000**
4	xxxx	xxxx	xxxx	xxxx	0.382	0.274	**0.010**	0.047	0.464	0.042	0.210	0.584	0.191	0.297	0.177	0.206	0.133
5	xxxx	xxxx	xxxx	xxxx	xxxx	0.612	0.011	0.109	0.157	**0.001**	0.031	0.976	0.434	0.656	**0.000**	**0.000**	**0.000**
6	xxxx	xxxx	xxxx	xxxx	xxxx	xxxx	0.998	1.000	0.134	**0.004**	0.038	0.998	1.000	1.000	**0.005**	0.008	0.007
7	xxxx	xxxx	xxxx	xxxx	xxxx	xxxx	xxxx	1.000	0.052	**0.000**	**0.006**	0.593	0.675	0.824	**0.000**	**0.000**	**0.000**
8	xxxx	xxxx	xxxx	xxxx	xxxx	xxxx	xxxx	xxxx	0.071	**0.000**	**0.001**	0.654	0.911	0.967	**0.000**	**0.000**	**0.000**
9	xxxx	xxxx	xxxx	xxxx	xxxx	xxxx	xxxx	xxxx	xxxx	1.000	1.000	0.329	0.166	0.194	0.946	0.943	0.979
10	xxxx	xxxx	xxxx	xxxx	xxxx	xxxx	xxxx	xxxx	xxxx	xxxx	1.000	0.027	**0.001**	0.003	0.394	0.333	0.494
11	xxxx	xxxx	xxxx	xxxx	xxxx	xxxx	xxxx	xxxx	xxxx	xxxx	xxxx	0.134	0.036	0.051	0.768	0.747	0.861
12	xxxx	xxxx	xxxx	xxxx	xxxx	xxxx	xxxx	xxxx	xxxx	xxxx	xxxx	xxxx	0.998	0.999	0.041	0.074	0.059
13	xxxx	xxxx	xxxx	xxxx	xxxx	xxxx	xxxx	xxxx	xxxx	xxxx	xxxx	xxxx	xxxx	1.000	**0.000**	**0.000**	**0.000**
14	xxxx	xxxx	xxxx	xxxx	xxxx	xxxx	xxxx	xxxx	xxxx	xxxx	xxxx	xxxx	xxxx	xxxx	**0.001**	**0.001**	**0.001**
15	xxxx	xxxx	xxxx	xxxx	xxxx	xxxx	xxxx	xxxx	xxxx	xxxx	xxxx	xxxx	xxxx	xxxx	xxxx	0.917	0.999
16	xxxx	xxxx	xxxx	xxxx	xxxx	xxxx	xxxx	xxxx	xxxx	xxxx	xxxx	xxxx	xxxx	xxxx	xxxx	xxxx	1.000
17	xxxx	xxxx	xxxx	xxxx	xxxx	xxxx	xxxx	xxxx	xxxx	xxxx	xxxx	xxxx	xxxx	xxxx	xxxx	xxxx	xxxx

	18	19	20	21	22	23	24	25	26	27	28	29	30	31	32	33	34	35
	n=32	n=524	n=256	n=5	n=100	n=44	n=27	n=424	n=212	n=26	n=116	n=67	n=20	n=89	n=43	n=26	n=116	n=60
1	0.025	0.051	0.017	0.206	0.031	0.017	0.066	0.052	0.037	0.338	0.011	**0.002**	0.334	**0.002**	**0.004**	0.338	0.011	0.038
2	**0.000**	**0.000**	**0.000**	0.464	**0.001**	0.054	**0.010**	**0.000**	**0.000**	**0.004**	**0.000**	**0.000**	**0.000**	**0.000**	**0.000**	**0.004**	**0.000**	**0.000**
3	0.013	**0.000**	**0.000**	0.169	**0.003**	0.066	0.012	**0.000**	**0.000**	**0.004**	**0.000**	**0.000**	**0.006**	**0.000**	**0.000**	**0.004**	**0.000**	**0.000**
4	0.239	0.152	0.152	0.292	0.200	0.130	0.383	0.139	0.124	0.447	0.152	0.029	0.786	0.040	0.026	0.447	0.152	0.261
5	0.126	**0.000**	**0.006**	0.571	0.118	0.346	0.050	**0.000**	**0.001**	0.051	**0.000**	**0.001**	0.031	**0.000**	**0.000**	0.051	**0.000**	**0.000**
6	0.071	0.053	0.053	0.980	0.785	0.825	0.037	0.018	0.021	0.045	**0.002**	0.041	0.047	**0.000**	**0.000**	0.045	**0.002**	**0.005**
7	**0.000**	**0.000**	**0.000**	0.825	0.018	0.074	**0.000**	**0.000**	**0.000**	**0.000**	**0.000**	**0.000**	**0.000**	**0.000**	**0.000**	**0.000**	**0.000**	**0.000**
8	**0.004**	**0.000**	**0.000**	0.826	0.116	0.186	**0.001**	**0.000**	**0.000**	**0.002**	**0.000**	**0.001**	**0.002**	**0.000**	**0.000**	**0.002**	**0.000**	**0.000**
9	0.070	0.111	0.107	0.047	0.062	0.057	0.103	0.121	0.126	0.721	0.912	0.031	0.907	0.900	0.793	0.721	0.912	0.937
10	**0.000**	**0.000**	**0.000**	0.003	**0.000**	**0.000**	**0.001**	**0.000**	**0.000**	0.151	0.277	0.000	0.388	0.530	0.374	0.151	0.277	0.356
11	**0.010**	0.016	0.016	0.013	0.011	**0.007**	0.020	0.019	0.021	0.441	0.882	0.002	0.711	0.881	0.745	0.441	0.882	0.744
12	0.387	0.355	0.348	0.586	0.931	0.788	0.213	0.148	0.166	0.249	0.023	0.267	0.244	0.008	0.004	0.249	0.023	0.043
13	0.013	**0.000**	**0.000**	0.666	0.214	0.447	**0.004**	**0.000**	**0.000**	**0.008**	**0.000**	**0.000**	**0.000**	**0.008**	**0.000**	**0.008**	**0.000**	**0.000**
14	0.044	0.011	**0.009**	0.681	0.383	0.513	0.018	**0.003**	**0.003**	0.028	**0.000**	**0.007**	0.022	**0.000**	**0.000**	0.028	**0.000**	**0.001**
15	**0.000**	**0.000**	**0.000**	0.016	**0.000**	**0.000**	**0.001**	**0.000**	**0.000**	0.649	0.781	**0.000**	0.939	0.119	0.056	0.649	0.781	0.831
16	**0.000**	**0.000**	**0.000**	0.018	**0.000**	**0.000**	**0.000**	**0.000**	**0.000**	0.613	0.154	**0.000**	0.712	**0.002**	**0.002**	0.613	0.154	0.281
17	**0.000**	**0.000**	**0.000**	0.012	**0.000**	**0.000**	**0.000**	**0.000**	**0.000**	0.846	0.540	**0.000**	0.960	0.045	0.025	0.846	0.540	0.672

Table 20: Northern Lowland statistical comparison data matrix (see Table 16 for key to column and row headings. Bold text indicates the significantly similar comparisons ($P \leq 0.01$).

	1	2	3	4	5	6	7	8	9	10	11	12	13	14	15	16	17
	n=22	n=324	n=162	n=16	n=86	n=0	n=0	n=0	n=0	n=0	n=0	n=0	n=0	n=0	n=40	n=206	n=113
1	xxxx	1.000	1.000	0.027	0.029	n/a	n/a	n/a	n/a	n/a	n/a	n/a	n/a	n/a	0.025	0.972	0.982
2	xxxx	xxxx	1.000	0.000	0.000	n/a	n/a	n/a	n/a	n/a	n/a	n/a	n/a	n/a	0.100	0.005	0.050
3	xxxx	xxxx	xxxx	0.000	0.000	n/a	n/a	n/a	n/a	n/a	n/a	n/a	n/a	n/a	0.135	0.027	0.123
4	xxxx	xxxx	xxxx	xxxx	0.668	n/a	n/a	n/a	n/a	n/a	n/a	n/a	n/a	n/a	0.012	**0.000**	**0.001**
5	xxxx	xxxx	xxxx	xxxx	xxxx	n/a	n/a	n/a	n/a	n/a	n/a	n/a	n/a	n/a	**0.000**	**0.000**	**0.000**
6	xxxx	xxxx	xxxx	xxxx	xxxx	xxxx	n/a	n/a	n/a	n/a	n/a	n/a	n/a	n/a	n/a	n/a	n/a
7	xxxx	xxxx	xxxx	xxxx	xxxx	xxxx	xxxx	n/a	n/a	n/a	n/a	n/a	n/a	n/a	n/a	n/a	n/a
8	xxxx	xxxx	xxxx	xxxx	xxxx	xxxx	xxxx	xxxx	n/a	n/a	n/a	n/a	n/a	n/a	n/a	n/a	n/a
9	xxxx	xxxx	xxxx	xxxx	xxxx	xxxx	xxxx	xxxx	xxxx	n/a	n/a	n/a	n/a	n/a	n/a	n/a	n/a
10	xxxx	xxxx	xxxx	xxxx	xxxx	xxxx	xxxx	xxxx	xxxx	xxxx	n/a	n/a	n/a	n/a	n/a	n/a	n/a
11	xxxx	xxxx	xxxx	xxxx	xxxx	xxxx	xxxx	xxxx	xxxx	xxxx	xxxx	n/a	n/a	n/a	n/a	n/a	n/a
12	xxxx	xxxx	xxxx	xxxx	xxxx	xxxx	xxxx	xxxx	xxxx	xxxx	xxxx	xxxx	n/a	n/a	n/a	n/a	n/a
13	xxxx	xxxx	xxxx	xxxx	xxxx	xxxx	xxxx	xxxx	xxxx	xxxx	xxxx	xxxx	xxxx	n/a	n/a	n/a	n/a
14	xxxx	xxxx	xxxx	xxxx	xxxx	xxxx	xxxx	xxxx	xxxx	xxxx	xxxx	xxxx	xxxx	xxxx	n/a	n/a	n/a
15	xxxx	xxxx	xxxx	xxxx	xxxx	xxxx	xxxx	xxxx	xxxx	xxxx	xxxx	xxxx	xxxx	xxxx	xxxx	0.992	0.992
16	xxxx	xxxx	xxxx	xxxx	xxxx	xxxx	xxxx	xxxx	xxxx	xxxx	xxxx	xxxx	xxxx	xxxx	xxxx	xxxx	1.000
17	xxxx	xxxx	xxxx	xxxx	xxxx	xxxx	xxxx	xxxx	xxxx	xxxx	xxxx	xxxx	xxxx	xxxx	xxxx	xxxx	xxxx

	18	19	20	21	22	23	24	25	26	27	28	29	30	31	32	33	34	35
	n=2	n=13	n=11	n=1	n=2	n=2	n=1	n=11	n=9	n=1	n=16	n=8	n=1	n=22	n=11	n=1	n=22	n=11
1	0.224	**0.001**	0.097	n/a	0.362	0.362	n/a	**0.001**	0.127	n/a	**0.000**	**0.000**	n/a	**0.003**	0.025	n/a	**0.003**	0.025
2	0.126	**0.000**	**0.007**	n/a	0.269	0.269	n/a	**0.000**	0.028	n/a	**0.000**	**0.000**	n/a	**0.000**	**0.001**	n/a	**0.000**	**0.001**
3	0.129	**0.000**	**0.009**	n/a	0.272	0.272	n/a	**0.000**	0.031	n/a	**0.000**	**0.000**	n/a	**0.000**	**0.001**	n/a	**0.000**	**0.001**
4	0.131	**0.005**	0.066	n/a	0.491	0.491	n/a	0.004	0.068	n/a	0.000	0.001	n/a	0.000	0.000	n/a	0.000	0.000
5	0.200	**0.000**	0.037	n/a	0.792	0.792	n/a	0.000	0.061	n/a	0.000	0.000	n/a	0.000	0.000	n/a	0.000	0.000
6	n/a	n/a	n/a	n/a	n/a	n/a	n/a	n/a	n/a	n/a	n/a	n/a	n/a	n/a	n/a	n/a	n/a	n/a
7	n/a	n/a	n/a	n/a	n/a	n/a	n/a	n/a	n/a	n/a	n/a	n/a	n/a	n/a	n/a	n/a	n/a	n/a
8	n/a	n/a	n/a	n/a	n/a	n/a	n/a	n/a	n/a	n/a	n/a	n/a	n/a	n/a	n/a	n/a	n/a	n/a
9	n/a	n/a	n/a	n/a	n/a	n/a	n/a	n/a	n/a	n/a	n/a	n/a	n/a	n/a	n/a	n/a	n/a	n/a
10	n/a	n/a	n/a	n/a	n/a	n/a	n/a	n/a	n/a	n/a	n/a	n/a	n/a	n/a	n/a	n/a	n/a	n/a
11	n/a	n/a	n/a	n/a	n/a	n/a	n/a	n/a	n/a	n/a	n/a	n/a	n/a	n/a	n/a	n/a	n/a	n/a
12	n/a	n/a	n/a	n/a	n/a	n/a	n/a	n/a	n/a	n/a	n/a	n/a	n/a	n/a	n/a	n/a	n/a	n/a
13	n/a	n/a	n/a	n/a	n/a	n/a	n/a	n/a	n/a	n/a	n/a	n/a	n/a	n/a	n/a	n/a	n/a	n/a
14	n/a	n/a	n/a	n/a	n/a	n/a	n/a	n/a	n/a	n/a	n/a	n/a	n/a	n/a	n/a	n/a	n/a	n/a
15	0.175	**0.001**	0.030	n/a	0.351	0.351	n/a	0.101	0.098	n/a	**0.000**	**0.000**	n/a	**0.000**	**0.004**	n/a	**0.000**	**0.004**
16	0.203	**0.000**	**0.013**	n/a	0.328	0.328	n/a	**0.000**	0.059	n/a	**0.000**	**0.000**	n/a	**0.000**	**0.004**	n/a	**0.000**	**0.004**
17	0.175	**0.000**	**0.009**	n/a	0.292	0.292	n/a	**0.000**	0.045	n/a	**0.000**	**0.000**	n/a	**0.000**	**0.006**	n/a	**0.000**	**0.006**

Table 21: North-Central Highland statistical comparison data matrix (see Table 16 for key to column and row headings. Bold text indicates the significantly similar comparisons ($P \leq 0.01$).

	1 n=43	2 n=394	3 n=197	4 n=0	5 n=0	6 n=30	7 n=150	8 n=79	9 n=0	10 n=0	11 n=0	12 n=30	13 n=150	14 n=79	15 n=0	16 n=0	17 n=0
1	xxxx	0.998	0.999	n/a	n/a	0.500	0.262	0.206	n/a	n/a	n/a	0.500	0.262	0.206	n/a	n/a	n/a
2	xxxx	xxxx	1.000	n/a	n/a	0.189	**0.001**	**0.004**	n/a	n/a	n/a	0.189	**0.001**	**0.004**	n/a	n/a	n/a
3	xxxx	xxxx	xxxx	n/a	n/a	0.220	**0.004**	**0.010**	n/a	n/a	n/a	0.220	**0.004**	**0.010**	n/a	n/a	n/a
4	xxxx	xxxx	xxxx	xxxx	n/a	n/a	n/a	n/a	n/a	n/a	n/a	n/a	n/a	n/a	n/a	n/a	n/a
5	xxxx	xxxx	xxxx	xxxx	xxxx	n/a	n/a	n/a	n/a	n/a	n/a	n/a	n/a	n/a	n/a	n/a	n/a
6	xxxx	xxxx	xxxx	xxxx	xxxx	xxxx	0.999	1.000	n/a	n/a	n/a	1.000	0.999	1.000	n/a	n/a	n/a
7	xxxx	xxxx	xxxx	xxxx	xxxx	xxxx	xxxx	1.000	n/a	n/a	n/a	0.999	1.000	1.000	n/a	n/a	n/a
8	xxxx	xxxx	xxxx	xxxx	xxxx	xxxx	xxxx	xxxx	n/a	n/a	n/a	1.000	1.000	1.000	n/a	n/a	n/a
9	xxxx	xxxx	xxxx	xxxx	xxxx	xxxx	xxxx	xxxx	xxxx	n/a	n/a	n/a	n/a	n/a	n/a	n/a	n/a
10	xxxx	xxxx	xxxx	xxxx	xxxx	xxxx	xxxx	xxxx	xxxx	xxxx	n/a	n/a	n/a	n/a	n/a	n/a	n/a
11	xxxx	xxxx	xxxx	xxxx	xxxx	xxxx	xxxx	xxxx	xxxx	xxxx	xxxx	n/a	n/a	n/a	n/a	n/a	n/a
12	xxxx	xxxx	xxxx	xxxx	xxxx	xxxx	xxxx	xxxx	xxxx	xxxx	xxxx	xxxx	0.999	1.000	n/a	n/a	n/a
13	xxxx	xxxx	xxxx	xxxx	xxxx	xxxx	xxxx	xxxx	xxxx	xxxx	xxxx	xxxx	xxxx	1.000	n/a	n/a	n/a
14	xxxx	xxxx	xxxx	xxxx	xxxx	xxxx	xxxx	xxxx	xxxx	xxxx	xxxx	xxxx	xxxx	xxxx	n/a	n/a	n/a
15	xxxx	xxxx	xxxx	xxxx	xxxx	xxxx	xxxx	xxxx	xxxx	xxxx	xxxx	xxxx	xxxx	xxxx	xxxx	n/a	n/a
16	xxxx	xxxx	xxxx	xxxx	xxxx	xxxx	xxxx	xxxx	xxxx	xxxx	xxxx	xxxx	xxxx	xxxx	xxxx	xxxx	n/a
17	xxxx	xxxx	xxxx	xxxx	xxxx	xxxx	xxxx	xxxx	xxxx	xxxx	xx	xxxx	xxxx	xxxx	xxxx	xxxx	xxxx

	18 n=8	19 n=30	20 n=8	21 n=0	22 n=0	23 n=0	24 n=8	25 n=30	26 n=9	27 n=6	28 n=15	29 n=6	30 n=5	31 n=11	32 n=6	33 n=6	34 n=13	35 n=7
1	0.024	0.157	0.644	n/a	n/a	n/a	0.024	0.573	0.461	0.487	0.134	0.543	0.777	0.296	0.558	0.558	0.155	0.386
2	0.013	0.033	0.533	n/a	n/a	n/a	0.013	0.355	0.344	0.438	0.114	0.602	0.683	0.154	0.423	0.423	0.059	0.260
3	0.015	0.043	0.546	n/a	n/a	n/a	0.015	0.366	0.357	0.448	0.126	0.611	0.671	0.165	0.433	0.433	0.066	0.269
4	n/a	n/a	n/a	n/a	n/a	n/a	n/a	n/a	n/a	n/a	n/a	n/a	n/a	n/a	n/a	n/a	n/a	n/a
5	n/a	n/a	n/a	n/a	n/a	n/a	n/a	n/a	n/a	n/a	n/a	n/a	n/a	n/a	n/a	n/a	n/a	n/a
6	0.076	0.134	0.551	n/a	n/a	n/a	0.076	0.629	0.384	0.759	0.026	0.226	0.612	0.229	0.512	0.512	0.147	0.352
7	0.048	0.033	0.545	n/a	n/a	n/a	0.048	0.606	0.358	0.596	**0.003**	0.130	0.487	0.104	0.375	0.443	0.072	0.278
8	0.039	0.026	0.399	n/a	n/a	n/a	0.039	0.624	0.246	0.493	**0.002**	0.099	0.542	0.110	0.326	0.326	0.042	0.192
9	n/a	n/a	n/a	n/a	n/a	n/a	n/a	n/a	n/a	n/a	n/a	n/a	n/a	n/a	n/a	n/a	n/a	n/a
10	n/a	n/a	n/a	n/a	n/a	n/a	n/a	n/a	n/a	n/a	n/a	n/a	n/a	n/a	n/a	n/a	n/a	n/a
11	n/a	n/a	n/a	n/a	n/a	n/a	n/a	n/a	n/a	n/a	n/a	n/a	n/a	n/a	n/a	n/a	n/a	n/a
12	0.076	0.134	0.551	n/a	n/a	n/a	0.076	0.629	0.384	0.759	0.026	0.226	0.612	0.229	0.512	0.512	0.147	0.352
13	0.048	0.033	0.545	n/a	n/a	n/a	0.048	0.606	0.358	0.596	**0.003**	0.130	0.487	0.104	0.375	0.443	0.072	0.278
14	0.039	0.026	0.399	n/a	n/a	n/a	0.039	0.624	0.246	0.493	**0.002**	0.099	0.542	0.110	0.326	0.326	0.042	0.192
15	n/a	n/a	n/a	n/a	n/a	n/a	n/a	n/a	n/a	n/a	n/a	n/a	n/a	n/a	n/a	n/a	n/a	n/a
16	n/a	n/a	n/a	n/a	n/a	n/a	n/a	n/a	n/a	n/a	n/a	n/a	n/a	n/a	n/a	n/a	n/a	n/a
17	n/a	n/a	n/a	n/a	n/a	n/a	n/a	n/a	n/a	n/a	n/a	n/a	n/a	n/a	n/a	n/a	n/a	n/a

Table 22: Southeastern Ridge statistical comparison data matrix (see Table 16 for key to column and row headings. Bold text indicates the significantly similar comparisons ($P \leq 0.01$).

	1	2	3	4	5	6	7	8	9	10	11	12	13	14	15	16	17
	n=65	n=618	n=309	n=33	n=50	n=85	n=403	n=206	n=79	n=320	n=160	n=164	n=723	n=368	n=79	n=320	n=160
1	xxxx	1.000	1.000	0.209	0.772	0.242	0.149	0.314	0.609	0.281	0.543	0.674	0.208	0.424	0.609	0.281	0.543
2	xxxx	xxxx	1.000	0.106	0.679	0.032	**0.000**	**0.008**	0.169	**0.000**	0.018	**0.000**	**0.000**	0.116	0.169	**0.000**	0.217
3	xxxx	xxxx	xxxx	0.122	0.722	0.050	**0.001**	0.024	0.217	**0.001**	0.041	0.190	**0.001**	**0.010**	0.217	**0.001**	0.041
4	xxxx	xxxx	xxxx	xxxx	0.523	0.373	0.368	0.480	0.285	0.085	0.129	0.411	0.291	0.372	0.285	0.085	0.129
5	xxxx	xxxx	xxxx	xxxx	xxxx	0.112	0.057	0.099	0.783	0.083	0.259	0.240	0.054	0.114	0.783	0.083	0.259
6	xxxx	xxxx	xxxx	xxxx	xxxx	xxxx	0.995	0.996	0.477	0.367	0.793	0.978	0.999	0.985	0.477	0.367	0.793
7	xxxx	xxxx	xxxx	xxxx	xxxx	xxxx	xxxx	1.000	0.349	**0.000**	0.046	0.727	0.185	0.693	0.349	**0.000**	0.046
8	xxxx	xxxx	xxxx	xxxx	xxxx	xxxx	xxxx	xxxx	0.629	**0.003**	0.070	0.731	0.313	0.741	0.629	**0.003**	0.070
9	xxxx	xxxx	xxxx	xxxx	xxxx	xxxx	xxxx	xxxx	xxxx	0.747	0.982	0.985	0.473	0.793	1.000	0.747	0.982
10	xxxx	xxxx	xxxx	xxxx	xxxx	xxxx	xxxx	xxxx	xxxx	xxxx	1.000	0.354	0.079	0.057	0.747	1.000	1.000
11	xxxx	xxxx	xxxx	xxxx	xxxx	xxxx	xxxx	xxxx	xxxx	xxxx	xxxx	0.893	0.726	0.525	0.982	1.000	1.000
12	xxxx	xxxx	xxxx	xxxx	xxxx	xxxx	xxxx	xxxx	xxxx	xxxx	xxxx	xxxx	0.989	1.000	0.965	0.354	0.893
13	xxxx	xxxx	xxxx	xxxx	xxxx	xxxx	xxxx	xxxx	xxxx	xxxx	xxxx	xxxx	xxxx	0.989	0.473	0.079	0.726
14	xxxx	xxxx	xxxx	xxxx	xxxx	xxxx	xxxx	xxxx	xxxx	xxxx	xxxx	xxxx	xxxx	xxxx	0.793	0.057	0.525
15	xxxx	xxxx	xxxx	xxxx	xxxx	xxxx	xxxx	xxxx	xxxx	xxxx	xxxx	xxxx	xxxx	xxxx	xxxx	0.747	0.982
16	xxxx	xxxx	xxxx	xxxx	xxxx	xxxx	xxxx	xxxx	xxxx	xxxx	xxxx	xxxx	xxxx	xxxx	xxxx	xxxx	1.000
17	xxxx	xxxx	xxxx	xxxx	xxxx	xxxx	xxxx	xxxx	xxxx	xxxx	xxxx	xxxx	xxxx	xxxx	xxxx	xxxx	xxxx

	18	19	20	21	22	23	24	25	26	27	28	29	30	31	32	33	34	35
	n=53	n=384	n=205	n=7	n=171	n=77	n=46	n=213	n=126	n=43	n=106	n=55	n=42	n=97	n=44	n=43	n=116	n=58
1	**0.010**	0.041	0.069	0.191	**0.000**	**0.001**	0.016	0.634	0.695	**0.000**	**0.000**	**0.004**	0.017	**0.000**	**0.005**	0.015	**0.003**	0.030
2	**0.000**	**0.000**	**0.000**	0.148	**0.000**	**0.000**	**0.002**	0.046	0.161	**0.000**	**0.000**	**0.000**	**0.001**	**0.000**	**0.000**	**0.000**	**0.000**	**0.001**
3	**0.001**	**0.000**	**0.000**	0.152	**0.000**	**0.000**	**0.004**	0.100	0.232	**0.000**	**0.000**	**0.000**	**0.001**	**0.000**	**0.000**	**0.001**	**0.000**	**0.001**
4	0.029	0.065	0.104	0.250	**0.002**	**0.002**	0.029	0.437	0.608	**0.001**	**0.003**	0.020	0.030	**0.002**	0.011	0.075	0.015	0.103
5	0.029	0.022	0.045	0.280	**0.001**	**0.001**	0.061	0.367	0.584	0.017	**0.007**	0.041	**0.001**	**0.000**	**0.000**	**0.000**	**0.000**	**0.001**
6	**0.000**	**0.000**	**0.000**	0.027	**0.000**	**0.000**	**0.000**	0.019	0.068	**0.000**	**0.000**	**0.000**	0.093	**0.001**	0.018	0.081	**0.008**	0.110
7	**0.000**	**0.000**	**0.000**	0.028	**0.000**	**0.000**	**0.000**	**0.000**	**0.009**	**0.000**	**0.000**	**0.000**	**0.007**	**0.000**	**0.001**	**0.006**	**0.000**	**0.010**
8	**0.000**	**0.000**	**0.000**	0.039	**0.000**	**0.000**	**0.000**	**0.004**	0.047	**0.000**	**0.000**	**0.000**	**0.010**	**0.000**	**0.001**	**0.008**	**0.000**	**0.010**
9	**0.006**	**0.003**	**0.006**	0.119	**0.000**	**0.000**	0.015	0.358	0.349	**0.001**	**0.000**	**0.005**	**0.008**	**0.000**	**0.001**	**0.009**	**0.000**	0.017
10	**0.000**	**0.000**	**0.000**	0.032	**0.000**	**0.000**	**0.000**	**0.000**	**0.000**	**0.000**	**0.000**	**0.000**	0.036	**0.000**	**0.004**	0.030	**0.000**	0.057
11	**0.000**	**0.000**	**0.000**	0.050	**0.000**	**0.000**	**0.001**	**0.006**	0.011	**0.000**	**0.000**	**0.000**	0.022	**0.000**	**0.003**	0.018	**0.000**	0.035
12	**0.000**	**0.000**	**0.000**	0.050	**0.000**	**0.000**	**0.001**	0.044	0.102	**0.000**	**0.000**	**0.000**	0.018	**0.000**	**0.002**	0.014	**0.000**	0.029
13	**0.000**	**0.000**	**0.000**	0.029	**0.000**	**0.000**	**0.000**	**0.000**	**0.002**	**0.000**	**0.000**	**0.000**	0.012	**0.000**	**0.001**	0.009	**0.000**	0.016
14	**0.000**	**0.000**	**0.000**	0.041	**0.000**	**0.000**	**0.000**	**0.002**	0.013	**0.000**	**0.000**	**0.000**	**0.009**	**0.000**	**0.001**	0.007	**0.000**	0.012
15	**0.006**	**0.003**	**0.006**	0.119	**0.000**	**0.000**	0.015	0.358	0.349	**0.001**	**0.000**	**0.005**	**0.008**	**0.000**	**0.001**	**0.009**	**0.000**	0.017
16	**0.000**	**0.000**	**0.000**	0.032	**0.000**	**0.000**	**0.000**	**0.000**	**0.000**	**0.000**	**0.000**	**0.000**	0.036	**0.000**	**0.004**	0.030	**0.000**	0.057
17	**0.000**	**0.000**	**0.000**	0.050	**0.000**	**0.000**	**0.001**	**0.006**	**0.011**	**0.000**	**0.000**	**0.000**	0.022	**0.000**	**0.003**	0.018	**0.000**	0.035

Table 23: Carolinas Limestone Forest statistical comparison data matrix (see Table 16 for key to column and row headings. Bold text indicates the significantly similar comparisons ($P \leq 0.01$).

	1 n=6	2 n=53	3 n=29	4 n=0	5 n=40	6 n=10	7 n=23	8 n=15	9 n=2	10 n=9	11 n=5	12 n=12	13 n=32	14 n=20	15 n=9	16 n=24	17 n=12
1	xxxx	0.995	1.000	n / a	0.034	0.888	0.770	0.921	0.847	0.082	0.280	0.766	0.375	0.800	0.082	0.120	0.270
2	xxxx	xxxx	0.998	n / a	**0.000**	0.435	0.011	0.377	0.227	**0.002**	0.146	0.146	**0.005**	**0.005**	0.146	**0.000**	0.015
3	xxxx	xxxx	xxxx	n / a	**0.000**	0.515	0.070	0.483	0.738	**0.004**	0.093	0.302	0.013	0.237	0.042	**0.001**	0.029
4	xxxx	xxxx	xxxx	xxxx	n / a	n / a	n / a	n / a	n / a	n / a	n / a	n / a	n / a	n / a	n / a	n / a	n / a
5	xxxx	xxxx	xxxx	xxxx	xxxx	0.037	**0.000**	0.017	0.921	0.018	0.216	0.062	**0.000**	0.028	0.547	0.099	0.313
6	xxxx	xxxx	xxxx	xxxx	xxxx	xxxx	0.910	1.000	0.952	0.095	0.375	1.000	0.902	1.000	0.095	0.127	0.347
7	xxxx	xxxx	xxxx	xxxx	xxxx	xxxx	xxxx	0.923	0.747	0.048	0.325	0.725	0.921	0.717	**0.006**	**0.002**	0.039
8	xxxx	xxxx	xxxx	xxxx	xxxx	xxxx	xxxx	xxxx	0.895	0.035	0.236	1.000	0.736	0.998	0.062	0.092	0.332
9	xxxx	xxxx	xxxx	xxxx	xxxx	xxxx	xxxx	xxxx	xxxx	1.000	1.000	0.991	0.915	0.997	0.993	1.000	1.000
10	xxxx	xxxx	xxxx	xxxx	xxxx	xxxx	xxxx	xxxx	xxxx	xxxx	1.000	0.153	0.248	0.134	0.336	0.808	0.905
11	xxxx	xxxx	xxxx	xxxx	xxxx	xxxx	xxxx	xxxx	xxxx	xxxx	xxxx	0.521	0.772	0.544	0.749	0.999	0.980
12	xxxx	xxxx	xxxx	xxxx	xxxx	xxxx	xxxx	xxxx	xxxx	xxxx	xxxx	xxxx	0.947	1.000	0.153	0.211	0.518
13	xxxx	xxxx	xxxx	xxxx	xxxx	xxxx	xxxx	xxxx	xxxx	xxxx	xxxx	xxxx	xxxx	0.945	**0.020**	0.008	0.112
14	xxxx	xxxx	xxxx	xxxx	xxxx	xxxx	xxxx	xxxx	xxxx	xxxx	xxxx	xxxx	xxxx	xxxx	0.134	0.157	0.590
15	xxxx	xxxx	xxxx	xxxx	xxxx	xxxx	xxxx	xxxx	xxxx	xxxx	xxxx	xxxx	xxxx	xxxx	xxxx	0.939	0.990
16	xxxx	xxxx	xxxx	xxxx	xxxx	xxxx	xxxx	xxxx	xxxx	xxxx	xxxx	xxxx	xxxx	xxxx	xxxx	xxxx	0.979
17	xxxx	xxxx	xxxx	xxxx	xxxx	xxxx	xxxx	xxxx	xxxx	xxxx	xxxx	xxxx	xxxx	xxxx	xxxx	xxxx	xxxx

	18 n=4	19 n=91	20 n=34	21 n=3	22 n=68	23 n=24	24 n=1	25 n=23	26 n=10	27 n=1	28 n=8	29 n=4	30 n=1	31 n=3	32 n=2	33 n=1	34 n=6	35 n=3
1	0.799	0.450	0.041	0.979	0.396	0.076	n / a	0.329	0.308	n / a	0.017	0.071	n / a	0.037	0.100	n / a	**0.005**	0.037
2	0.784	**0.000**	**0.000**	0.502	**0.005**	**0.000**	n / a	**0.000**	0.030	n / a	**0.005**	0.078	n / a	**0.007**	0.042	n / a	**0.000**	**0.007**
3	0.887	**0.006**	**0.000**	0.645	**0.005**	**0.000**	n / a	0.016	0.049	n / a	**0.005**	0.071	n / a	**0.009**	0.047	n / a	**0.000**	**0.009**
4	n / a	n / a	n / a	n / a	n / a	n / a	n / a	n / a	n / a	n / a	n / a	n / a	n / a	n / a	n / a	n / a	n / a	n / a
5	0.073	**0.002**	0.021	0.130	**0.004**	0.306	n / a	0.028	0.078	n / a	**0.005**	0.073	n / a	**0.008**	0.044	n / a	**0.001**	0.035
6	0.959	0.877	0.071	0.854	0.776	0.190	n / a	0.415	0.400	n / a	0.026	0.122	n / a	0.020	0.071	n / a	**0.005**	0.048
7	0.640	**0.009**	**0.000**	0.950	0.124	**0.000**	n / a	**0.009**	0.297	n / a	**0.000**	**0.007**	n / a	**0.010**	0.050	n / a	**0.000**	**0.010**
8	0.962	0.646	0.011	0.819	0.600	0.055	n / a	0.171	0.210	n / a	**0.007**	0.067	n / a	0.013	0.059	n / a	**0.003**	0.047
9	0.893	0.911	0.732	0.925	0.716	0.745	n / a	0.878	0.799	n / a	0.819	0.893	n / a	0.181	0.270	n / a	0.100	0.181
10	0.171	0.012	**0.004**	0.270	0.173	**0.006**	n / a	**0.002**	0.187	n / a	0.046	0.171	n / a	0.022	0.076	n / a	**0.001**	0.022
11	0.400	0.205	0.067	0.509	0.070	0.102	n / a	0.419	0.375	n / a	0.216	0.400	n / a	0.047	0.115	n / a	**0.009**	0.047
12	0.893	0.988	0.074	0.799	0.939	0.211	n / a	0.284	0.300	n / a	0.028	0.139	n / a	0.016	0.065	n / a	**0.002**	0.035
13	0.600	0.018	**0.000**	0.937	0.089	**0.000**	n / a	0.018	0.162	n / a	**0.000**	0.013	n / a	**0.008**	0.046	n / a	**0.000**	**0.008**
14	0.925	0.714	**0.009**	0.796	0.567	0.053	n / a	0.064	0.134	n / a	**0.007**	0.076	n / a	0.011	0.053	n / a	**0.001**	0.029
15	0.171	0.069	0.446	0.270	0.104	0.806	n / a	0.147	0.254	n / a	0.046	0.171	n / a	0.057	0.151	n / a	0.082	0.270
16	0.267	0.051	0.015	0.414	0.169	0.031	n / a	**0.004**	0.382	n / a	0.059	0.267	n / a	**0.010**	0.050	n / a	**0.001**	0.034
17	0.441	0.235	0.092	0.586	0.058	0.124	n / a	0.555	0.579	n / a	0.181	0.441	n / a	0.035	0.112	n / a	0.022	0.134

Table 24: Puntan Diapblo statistical comparison data matrix (see Table 16 for key to column and row headings. Bold text indicates the significantly similar comparisons ($P \leq 0.01$).

	1 n=3	2 n=26	3 n=11	4 n=0	5 n=18	6 n=3	7 n=13	8 n=7	9 n=8	10 n=14	11 n=8	12 n=11	13 n=27	14 n=15	15 n=7	16 n=33	17 n=16
1	xxxx	0.997	1.000	n/a	0.938	0.518	0.061	0.091	0.969	0.947	0.969	0.914	0.375	0.476	0.921	1.000	1.000
2	xxxx	xxxx	1.000	n/a	**0.002**	0.183	**0.000**	**0.001**	0.530	0.423	0.530	0.258	**0.001**	**0.009**	0.250	**0.005**	0.035
3	xxxx	xxxx	xxxx	n/a	0.034	0.246	**0.000**	**0.004**	0.814	0.698	0.814	0.461	0.016	0.054	0.492	0.103	0.199
4	xxxx	xxxx	xxxx	xxxx	n/a	n/a	n/a	n/a	n/a	n/a	n/a	n/a	n/a	n/a	n/a	n/a	n/a
5	xxxx	xxxx	xxxx	xxxx	xxxx	0.203	**0.000**	**0.001**	0.055	**0.009**	0.055	0.020	**0.000**	**0.001**	0.137	0.027	0.070
6	xxxx	xxxx	xxxx	xxxx	xxxx	xxxx	0.997	1.000	0.843	0.886	0.843	0.982	0.993	0.994	0.612	0.387	0.449
7	xxxx	xxxx	xxxx	xxxx	xxxx	xxxx	xxxx	1.000	0.059	0.029	0.059	0.126	0.449	0.503	0.022	**0.000**	**0.001**
8	xxxx	xxxx	xxxx	xxxx	xxxx	xxxx	xxxx	xxxx	0.128	0.095	0.128	0.248	0.693	0.699	0.056	**0.004**	0.011
9	xxxx	xxxx	xxxx	xxxx	xxxx	xxxx	xxxx	xxxx	xxxx	1.000	1.000	1.000	0.612	0.766	0.921	0.140	0.139
10	xxxx	xxxx	xxxx	xxxx	xxxx	xxxx	xxxx	xxxx	xxxx	xxxx	1.000	1.000	0.513	0.766	0.841	0.034	0.048
11	xxxx	xxxx	xxxx	xxxx	xxxx	xxxx	xxxx	xxxx	xxxx	xxxx	xxxx	1.000	0.612	0.766	0.921	0.140	0.139
12	xxxx	xxxx	xxxx	xxxx	xxxx	xxxx	xxxx	xxxx	xxxx	xxxx	xxxx	xxxx	0.873	0.938	0.985	0.225	0.225
13	xxxx	xxxx	xxxx	xxxx	xxxx	xxxx	xxxx	xxxx	xxxx	xxxx	xxxx	xxxx	xxxx	1.000	0.300	**0.007**	0.048
14	xxxx	xxxx	xxxx	xxxx	xxxx	xxxx	xxxx	xxxx	xxxx	xxxx	xxxx	xxxx	xxxx	xxxx	0.461	0.060	0.109
15	xxxx	xxxx	xxxx	xxxx	xxxx	xxxx	xxxx	xxxx	xxxx	xxxx	xxxx	xxxx	xxxx	xxxx	xxxx	0.897	0.979
16	xxxx	xxxx	xxxx	xxxx	xxxx	xxxx	xxxx	xxxx	xxxx	xxxx	xxxx	xxxx	xxxx	xxxx	xxxx	xxxx	1.000
17	xxxx	xxxx	xxxx	xxxx	xxxx	xxxx	xxxx	xxxx	xxxx	xxxx	xxxx	xxxx	xxxx	xxxx	xxxx	xxxx	xxxx

	18 n=14	19 n=98	20 n=54	21 n=3	22 n=13	23 n=7	24 n=11	25 n=85	26 n=47	27 n=12	28 n=22	29 n=11	30 n=12	31 n=18	32 n=11	33 n=12	34 n=28	35 n=15
1	0.161	0.736	0.733	0.518	0.365	0.308	0.999	0.872	0.838	0.952	0.346	0.415	0.586	0.292	0.415	0.586	0.292	0.329
2	**0.000**	0.022	0.086	0.332	0.006	0.051	0.179	0.036	0.066	0.050	**0.000**	**0.001**	0.321	**0.001**	0.082	0.126	**0.002**	0.014
3	**0.004**	0.333	0.481	0.488	0.058	0.157	0.461	0.400	0.324	0.135	**0.010**	**0.006**	0.547	0.012	0.206	0.383	0.057	0.109
4	n/a	n/a	n/a	n/a	n/a	n/a	n/a	n/a	n/a	n/a	n/a	n/a	n/a	n/a	n/a	n/a	n/a	n/a
5	**0.000**	**0.002**	**0.006**	0.088	**0.001**	**0.007**	0.690	0.015	0.020	0.512	0.073	0.203	**0.001**	**0.000**	**0.000**	**0.001**	**0.000**	**0.000**
6	0.259	0.678	0.783	0.518	0.229	0.308	0.637	0.721	0.885	0.799	0.346	0.415	0.952	0.938	0.956	0.586	0.292	0.329
7	**0.008**	**0.000**	**0.002**	0.061	**0.000**	**0.003**	**0.010**	**0.001**	**0.007**	0.024	**0.000**	**0.002**	0.075	0.027	0.320	**0.006**	**0.000**	**0.000**
8	0.042	0.015	0.031	0.091	**0.002**	0.012	0.040	0.020	0.059	0.077	**0.004**	0.013	0.177	0.219	0.492	0.030	**0.002**	**0.005**
9	0.030	0.840	0.866	0.362	0.701	0.670	0.613	0.807	0.937	0.509	0.070	0.142	0.809	0.330	0.533	0.809	0.089	0.303
10	**0.006**	0.455	0.569	0.259	0.435	0.591	0.368	0.417	0.688	0.342	0.011	0.047	0.718	0.375	0.412	0.718	0.036	0.244
11	0.030	0.840	0.866	0.362	0.701	0.670	0.613	0.807	0.937	0.509	0.070	0.142	0.809	0.466	0.533	0.809	0.089	0.325
12	0.012	0.628	0.724	0.295	0.410	0.624	0.461	0.586	0.823	0.607	0.025	0.076	0.758	0.415	0.461	0.758	0.155	0.371
13	**0.001**	0.014	0.037	0.103	**0.009**	0.220	0.065	**0.010**	0.066	0.112	**0.000**	**0.003**	0.677	0.040	0.622	0.162	**0.003**	0.020
14	0.005	0.099	0.165	0.136	0.038	0.132	0.135	0.072	0.232	0.197	**0.001**	0.011	0.799	0.126	0.758	0.332	0.031	0.076
15	0.042	0.980	0.975	0.498	0.627	0.541	0.669	0.982	0.990	0.543	0.032	0.072	0.922	0.219	0.714	0.863	0.179	0.493
16	**0.000**	**0.004**	**0.009**	0.459	0.042	0.042	0.225	0.019	0.018	0.459	**0.009**	0.066	0.177	**0.007**	0.066	0.053	**0.002**	0.028
17	**0.003**	0.026	0.033	0.401	0.055	0.092	0.225	0.002	0.050	0.431	0.090	0.225	0.185	0.037	0.077	0.065	0.012	0.042

Table 25: Unai Dangkolo statistical comparison data matrix (see Table 16 for key to column and row headings. Bold text indicates the significantly similar comparisons ($P \leq 0.01$).

	1 n=3	2 n=26	3 n=11	4 n=0	5 n=44	6 n=0	7 n=0	8 n=0	9 n=0	10 n=0	11 n=0	12 n=0	13 n=0	14 n=0	15 n=4	16 n=22	17 n=9
1	xxxx	1.000	1.000	n/a	0.484	n/a	n/a	n/a	n/a	n/a	n/a	n/a	n/a	n/a	0.927	0.564	0.491
2	xxxx	xxxx	1.000	n/a	**0.001**	n/a	n/a	n/a	n/a	n/a	n/a	n/a	n/a	n/a	0.351	**0.005**	0.071
3	xxxx	xxxx	xxxx	n/a	0.016	n/a	n/a	n/a	n/a	n/a	n/a	n/a	n/a	n/a	0.347	0.025	0.105
4	xxxx	xxxx	xxxx	xxxx	n/a	n/a	n/a	n/a	n/a	n/a	n/a	n/a	n/a	n/a	n/a	n/a	n/a
5	xxxx	xxxx	xxxx	xxxx	xxxx	n/a	n/a	n/a	n/a	n/a	n/a	n/a	n/a	n/a	0.318	**0.000**	**0.004**
6	xxxx	xxxx	xxxx	xxxx	xxxx	xxxx	n/a	n/a	n/a	n/a	n/a	n/a	n/a	n/a	n/a	n/a	n/a
7	xxxx	xxxx	xxxx	xxxx	xxxx	xxxx	xxxx	n/a	n/a	n/a	n/a	n/a	n/a	n/a	n/a	n/a	n/a
8	xxxx	xxxx	xxxx	xxxx	xxxx	xxxx	xxxx	xxxx	n/a	n/a	n/a	n/a	n/a	n/a	n/a	n/a	n/a
9	xxxx	xxxx	xxxx	xxxx	xxxx	xxxx	xxxx	xxxx	xxxx	n/a	n/a	n/a	n/a	n/a	n/a	n/a	n/a
10	xxxx	xxxx	xxxx	xxxx	xxxx	xxxx	xxxx	xxxx	xxxx	xxxx	n/a	n/a	n/a	n/a	n/a	n/a	n/a
11	xxxx	xxxx	xxxx	xxxx	xxxx	xxxx	xxxx	xxxx	xxxx	xxxx	xxxx	n/a	n/a	n/a	n/a	n/a	n/a
12	xxxx	xxxx	xxxx	xxxx	xxxx	xxxx	xxxx	xxxx	xxxx	xxxx	xxxx	xxxx	n/a	n/a	n/a	n/a	n/a
13	xxxx	xxxx	xxxx	xxxx	xxxx	xxxx	xxxx	xxxx	xxxx	xxxx	xxxx	xxxx	xxxx	n/a	n/a	n/a	n/a
14	xxxx	xxxx	xxxx	xxxx	xxxx	xxxx	xxxx	xxxx	xxxx	xxxx	xxxx	xxxx	xxxx	xxxx	n/a	n/a	n/a
15	xxxx	xxxx	xxxx	xxxx	xxxx	xxxx	xxxx	xxxx	xxxx	xxxx	xxxx	xxxx	xxxx	xxxx	xxxx	1.000	1.000
16	xxxx	xxxx	xxxx	xxxx	xxxx	xxxx	xxxx	xxxx	xxxx	xxxx	xxxx	xxxx	xxxx	xxxx	xxxx	xxxx	1.000
17	xxxx	xxxx	xxxx	xxxx	xxxx	xxxx	xxxx	xxxx	xxxx	xxxx	xxxx	xxxx	xxxx	xxxx	xxxx	xxxx	xxxx

	18 n=0	19 n=263	20 n=134	21 n=1	22 n=46	23 n=23	24 n=8	25 n=217	26 n=111	27 n=5	28 n=48	29 n=24	30 n=3	31 n=21	32 n=11	33 n=5	34 n=32	35 n=17
1	0.022	0.093	0.105	n/a	0.043	0.077	0.025	0.114	0.120	0.047	**0.007**	**0.010**	0.996	0.841	0.858	0.985	0.921	0.939
2	**0.000**	**0.000**	**0.000**	n/a	**0.000**	**0.000**	**0.000**	**0.000**	**0.000**	**0.000**	**0.000**	**0.000**	0.512	**0.006**	0.042	0.245	**0.002**	0.012
3	**0.000**	**0.000**	**0.000**	n/a	**0.000**	**0.000**	**0.000**	**0.000**	**0.000**	**0.002**	**0.000**	**0.000**	0.485	0.027	0.076	0.258	0.015	0.038
4	n/a	n/a	n/a	n/a	n/a	n/a	n/a	n/a	n/a	n/a	n/a	n/a	n/a	n/a	n/a	n/a	n/a	n/a
5	0.048	0.019	0.046	n/a	**0.004**	0.074	0.068	0.021	0.033	0.212	**0.000**	**0.001**	0.147	**0.000**	**0.001**	0.658	**0.005**	0.038
6	n/a	n/a	n/a	n/a	n/a	n/a	n/a	n/a	n/a	n/a	n/a	n/a	n/a	n/a	n/a	n/a	n/a	n/a
7	n/a	n/a	n/a	n/a	n/a	n/a	n/a	n/a	n/a	n/a	n/a	n/a	n/a	n/a	n/a	n/a	n/a	n/a
8	n/a	n/a	n/a	n/a	n/a	n/a	n/a	n/a	n/a	n/a	n/a	n/a	n/a	n/a	n/a	n/a	n/a	n/a
9	n/a	n/a	n/a	n/a	n/a	n/a	n/a	n/a	n/a	n/a	n/a	n/a	n/a	n/a	n/a	n/a	n/a	n/a
10	n/a	n/a	n/a	n/a	n/a	n/a	n/a	n/a	n/a	n/a	n/a	n/a	n/a	n/a	n/a	n/a	n/a	n/a
11	n/a	n/a	n/a	n/a	n/a	n/a	n/a	n/a	n/a	n/a	n/a	n/a	n/a	n/a	n/a	n/a	n/a	n/a
12	n/a	n/a	n/a	n/a	n/a	n/a	n/a	n/a	n/a	n/a	n/a	n/a	n/a	n/a	n/a	n/a	n/a	n/a
13	n/a	n/a	n/a	n/a	n/a	n/a	n/a	n/a	n/a	n/a	n/a	n/a	n/a	n/a	n/a	n/a	n/a	n/a
14	n/a	n/a	n/a	n/a	n/a	n/a	n/a	n/a	n/a	n/a	n/a	n/a	n/a	n/a	n/a	n/a	n/a	n/a
15	**0.008**	0.039	0.047	n/a	0.013	0.031	**0.010**	0.031	0.035	0.023	**0.001**	**0.002**	0.431	0.065	0.090	0.512	0.415	0.470
16	**0.000**	**0.000**	**0.000**	n/a	**0.000**	**0.000**	**0.000**	**0.000**	**0.000**	**0.001**	**0.000**	**0.000**	0.191	**0.000**	**0.001**	0.089	**0.006**	0.029
17	**0.000**	**0.000**	**0.000**	n/a	**0.000**	**0.001**	**0.000**	**0.000**	**0.000**	**0.003**	**0.000**	**0.000**	0.270	**0.003**	**0.010**	0.095	0.091	0.148